Thomas Gamse (editor)

Book of Abstracts

ERASMUS+ BIP ESS-HPT 2025

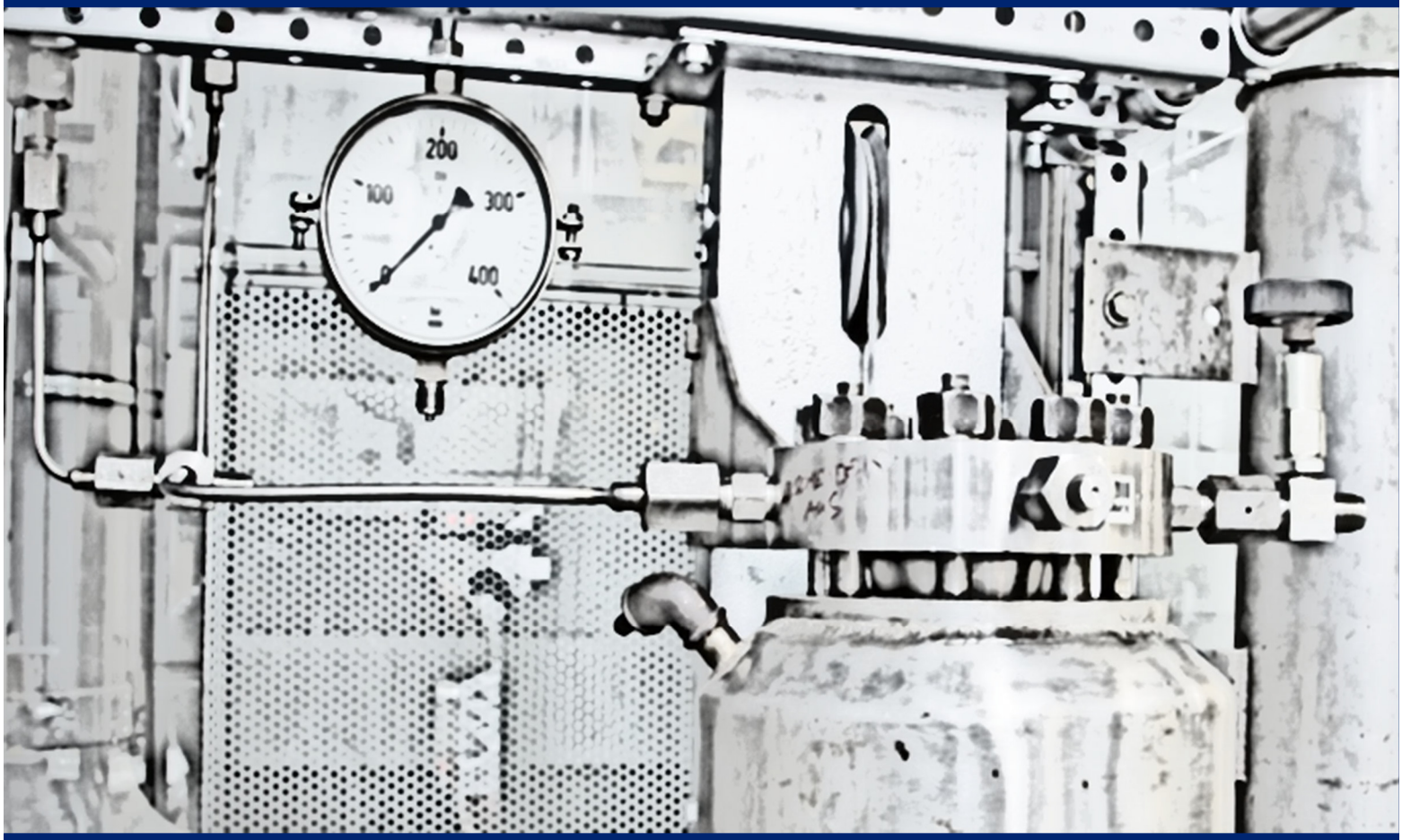

The European Summer School in
High Pressure Technology

6.7. – 19.7.2025

TU Graz
Graz University of Technology

Erasmus+

EFCE
European Federation of Chemical Engineering
Europäische Föderation für Chemie-Ingenieur-Wesen
Fédération Européenne de Génie Chimique

Imprint

Organisation: Thomas Gamse
Institute of Chemical Engineering and Environmental Technology
Graz University of Technology,
Inffeldgasse 25/C, 8010 Graz, Austria
Tel. +43 (0)316 873-7477
E-Mail: thomas.gamse@tugraz.at

Editor: Thomas Gamse
Layout: Thomas Gamse
Cover: Verlag der Technischen Universität Graz,
Thomas Gamse
Cover picture: Thomas Gamse

2025 Verlag der Technischen Universität Graz
www.tugraz-verlag.at

Book of Abstracts, ERASMUS+ BIP ESS-HPT 2025
"The European Summer School in High Pressure Technology"
6.7.-19.7.2025, Graz University of Technology

ISBN 978-3-99161-058-8

DOI 10.3217/978-3-99161-058-8

Preface

The European Summer School in High Pressure Technology (ESS-HPT) is the continuation of many years of high pressure intensive courses. The history of this very successful series of courses started in 1995, when the first intensive course took place in Monselice, Italy. Most of these Intensive Courses were supported by SOCRATES and later Life Long Learning, as shown in following overview:

SOCRATES IP "Current Trends in High Pressure Technology and Chemical Engineering"
- 1995 Monselice / Italy
- 1996 Nancy / France
- 1997 Erlangen / Germany

SOCRATES IP "High Pressure Technology in Process and Chemical Engineering"
- 1999 Abano Terme / Italy
- 2000 Valladolid / Spain
- 2001 Maribor / Slovenia and Graz / Austria

SOCRATES IP "High Pressure Chemical Engineering Processes: Basics and Applications"
- 2002 Graz / Austria and Maribor / Slovenia
- 2003 Budapest / Hungary
- 2004 Barcelona / Spain

SOCRATES IP "Basics, Developments, Research and Industrial Applications in High Pressure Chemical Engineering Processes"
- 2005 Prague / Czech Republic
- 2006 Lisbon / Portugal
- 2007 Albi / France

Life Long Learning IP "SCF- GSCE: Supercritical Fluids – Green Solvents in Chemical Engineering"
- 2008 Thessaloniki / Greece
- 2009 Istanbul / Turkey
- 2010 Budapest / Hungary

EFCE Intensive Course "High Pressure Technology - From Basics to Industrial Applications"
- 2011 Belgrade / Serbia

Life Long Learning IP "PIHPT: Process Intensification by High Pressure Technologies – Actual Strategies for Energy and Resources Conservation"
- 2012 Maribor / Slovenia and Graz / Austria
- 2013 Darmstadt / Germany
- 2014 Glasgow / Great Britain

Unfortunately, the financial support for these Intensive Programmes was cancelled within ERASMUS+. The EFCE Working Party "High Pressure Technology" decided in September 2014 to go on with this course in the form of a Summer School. The ESS-HPT takes place every year within the first 2 weeks of July at University of Maribor, Slovenia and Graz University of Technology, Austria.

EFCE ESS-HPT "The European Summer School in High Pressure Technology"

ESS-HPT 2015	Maribor / Slovenia and Graz / Austria
ESS-HPT 2016	Maribor / Slovenia and Graz / Austria
ESS-HPT 2017	Maribor / Slovenia and Graz / Austria
ESS-HPT 2018	Maribor / Slovenia and Graz / Austria
ESS-HPT 2019	Maribor / Slovenia and Graz / Austria
ESS-HPT 2021	Online Course, Graz / Austria
GEHPT and ESS-HPT 2022	Maribor / Slovenia and Graz / Austria

Since 2023 ESS-HPT is organised again as an ERASMUS+ Blended Intensive Programme (BIP). Unfortunately, there is no possibility to organise this summer school in two countries. So the whole intensive programme takes place at Graz University of Technology.

ESS-HPT 2023	Graz / Austria
ESS-HPT 2024	Graz/Austria

This year ESS-HPT 2025 will take place at Graz University of Technology in the period 6.7.2025 till 19.7.2025. Further this Summer School includes an Online Phase (21.7. till 22.8.2025) where students have to perform a project work based on the topics of the course.

All participants have to give an oral presentation and the abstracts of these presentations, which are peer-reviewed by the EFCE WP Members, are published in this book of abstracts.

The editor

Thomas Gamse
Organiser of ERASMUS+ BIP ESS-HPT 2025

Many thanks to our sponsors,

NATEX Prozesstechnologie GesmbH,

INNOWELD-Metallverarbeitung GmbH

and Tourismusverband Stadt Graz.

Time Schedule

Oral Presentations Participants

	Monday, 7 July 2025		
1	9:25 - 9:40	**A.Keßler,** M.Busch Modelling of the High-Pressure Copolymerization of Ethene and Acrylic Acid: Integrating Kinetics in Computational Fluid Dynamics Simulations	1
2	9:40 - 9:55	**B. Martín-Gómez,** A.Redondo, M.F.Montoya, A.Mangas, D.Cantero Foaming of Recycled Plastics with Water and Supercritical CO_2	7
3	9:55 - 10:10	**C.Weinzettl,** P.Demmelmayer, M.Kienberger Design and Characterization of Hydrophilic Natural Deep Eutectic Solvents for Application in Absorption Heat Pumps and Absorption Thermal Batteries	12

	Wednesday, 9 July 2025		
4	20:30 - 20:45	**M.Fermišek,** G.Hostnik, U.Bren, M.Zalara Detection of Free Amino Acids and their Oxidised Products Using HPLC Coupled with Benchtop NMR (HPLC-NMR)	17
5	20:45 - 21:00	**F. Issa,** K.Zentel Validation of a Simulation Model for Emulsion Polymerization of n- Butyl Acrylate in a Batch Reactor	23
6	21:00 - 21:15	**A.Krawiec,** M.Jackowski, A.Trusek Beer Dealcoholisation by Pervaporation Process	27
7	21:15 - 21:30	**Beatriz Monteiro,** P.Lisboa, A.Paiva, P.Simões Sustainable Valorization of Industrial Coffee By-Products Using Subcritical Water	33
8	21:30 - 21:45	**G.Araujo-Barahona,** J.García-Serna, T.Salmi Valorization of Banana Waste through Hydrothermal Extractions: Polyphenolic Compounds, Sugars and Sugar Alcohols	38
9	21:45 - 22:00	**K.Perišić** In-Depth Analysis of the Phytochemical and Bioactive Profile of Adriatic Sea Algae with an Emphasis on *Fucus virsoides*	44
10	22:00 - 22:15	**M.Hegyi,** J.Béri, Z.Morvay, E.Székely Hydrothermal Chemical Recycling of Polycondensation Polymers: Development and Deconvolution-Assisted Examination	50

	Monday, 14 July 2025		
18	20:30 - 20:45	**J.S.Castillo Gonzalez** Aerogels Based on Synthetic Polymers	97
19	20:45 - 21:00	**E.Prenzel,** M.Busch Implementation of a New Comonomer in High-Pressure Polymerization	101
20	21:00 - 21:15	**I.S.Fernandes,** R.Martins, M.J.Mendes, A.S. Reis-Machado Optimizing Porous Cathodes for CO2 Electroreduction: Computational Strategies Toward Solar Fuel Technologies	109
21	21:15 - 21:30	**A.Avdičević,** S.Lešnik, U.Bren Targeted CDK4/6 Therapy for Breast Cancer: How SNPs can Influence the Efficacy of Drugs	115
22	21:30 - 21:45	**K.Gajewska,** A.Moyseowicz, G.Gryglewicz Synthesis and Characterization of Nitrogen-Doped Graphene Materials for Supercapacitor Applications	121
23	21:45 - 22:00	**T.Goldberg,** V.Herdege Experimental Determination of Insect Fat Solubility in Dense CO_2 and Corresponding Model Description	126
24	22:00 - 22:15	**S.Sandner,** P.Kriegler, M.Kienberger Investigating the Phase Separation of GVL/Water-Mixtures by the Addition of Sugars (“Sugaring-Out”)	132

	Wednesday, 16 July 2025		
25	20:30 - 20:45	**I.Briongos-Merino,** L.Vaquerizo Ultrafast Hydrolysis of Grape Pomace in Hydrothermal Conditions: An Intensified Process for the Eco-Efficient Recovery of Lignin	137
26	20:45 - 21:00	**M.Miličič,** U.Bren, V.Furlan Antioxidative Activity of Flavonoids from *Thymus Vulgaris* and *Thymus Serpyllum*	143
27	21:00 - 21:15	**A.Boukhalaf,** A.Rott, M.Busch Deterministic Modeling of the High-Pressure Process for Ethene-Vinyl Acetate-Vinyl Neodecanoate Terpolymerization	149
28	21:15 - 21:30	**M.Körmöczi** Ammonia Production	155
29	21:30 - 21:45	**K.Aladić, K.Opačak** Ultrasound –Assisted Extraction of Phenolic Compounds from Grape Pomace Variety Pinot Noir	162
30	21:45 - 22:00	**G.Ricci,** A.Zambon Development of Antimicrobial Aerogels for Packaging	167
31	22:00 - 22:15	**J.Martinović,** M.Stamenić Supercritical CO_2 Extraction from Bilberry Fruit	173

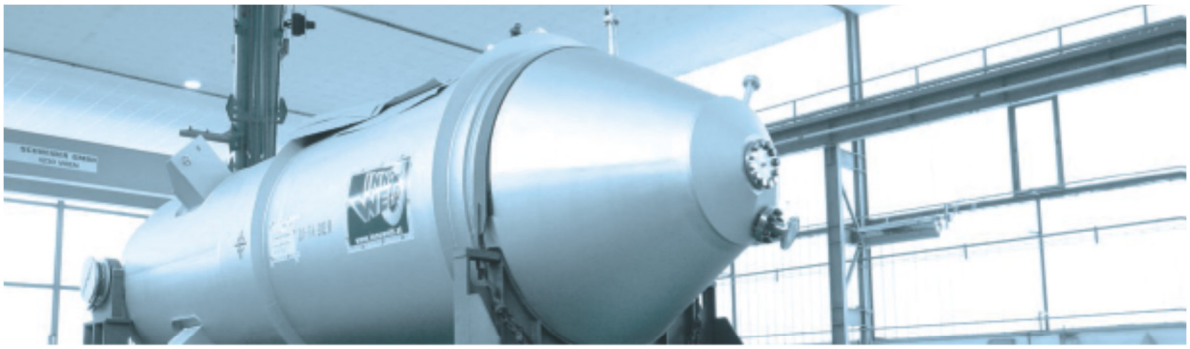

HIGH-PRESSURE VESSELS

HIGH PRESSURE VESSELS FOR VARIOUS APPLICATIONS UP TO 3.000 BAR CAN BE DESIGNED, CALCULATED, FABRICATED AND TESTED BY INNOWELD. THE POSSIBILITIES OF USING A HIGH-PRESSURE VESSEL IS NUMBERLESS. CARRYING OUT REACTIONS, SEPARATING MEDIUMS AND STORING CHEMICALS ARE ONLY A FEW OF IT. FOR INNOWELD, THE INTEREST INCREASES PROPORTIONAL TO THE PRESSURE AND THE TEMPERATURE.

With our experience from engineering and welding pressure vessels with wall thicknesses up to nearly 250mm and combining them with weld overlays out of materials like nickel, nickel chromium alloys and stainless steels, we are always looking for individual solutions for our partners with individual requirements. The core business of Innoweld starts, whenever high temperature, high pressures and dangerous acids come together.

Beside this individual solutions, we are also manufacturing high pressure and high temperature vessels according to exact specifications from our clients. With best delivery times and our high flexibility during the execution of the project, we make sure that the high pressure vessel with the best quality is ready for installation during the next scheduled shutdown.

Furthermore, our focus is also on the economical side of the project. With our weight saving designs, we make sure that the vessels is not only from the technical, but also from the financial point of view

www.innoweld.at

Modelling of the High-Pressure Copolymerization of Ethene and Acrylic Acid: Integrating Kinetics in Computational Fluid Dynamics Simulations

Alexander Keßler, Markus Busch*

Ernst-Berl-Institute of Technical and Macromolecular Chemistry, Technical University Darmstadt, *markus.busch@pre.tudarmstadt.de

Introduction

This work presents a detailed modeling approach for the high-pressure copolymerization of ethene with acrylic acid, integrating reaction kinetics into computational fluid dynamics (CFD) simulations. This integration bridges the gap between molecular-level polymerization mechanisms and reactor-scale transport phenomena. By implementing kinetic models into CFD frameworks, it becomes possible to predict the spatial distribution of species concentrations, temperature, and polymer properties within a reactor. The experiments with the corrosion resistant autoclave had previously shown unstable operational behavior in laboratory experiments, in some cases leading to flame-outs. The present study contributed to identifying the underlying causes of this instability.

Modelling

To describe the copolymerization of ethylene with acrylic acid, a complex reaction network must be implemented. Figure 1 presents the network, which includes initiation, propagation, termination, and transfer reactions. The model incorporates several simplifications, such as describing initiation with a single reaction equation instead of treating initiator decomposition and chain initiation as separate steps.

Polymerization processes can be modeled using two principal approaches: deterministic and statistical methods. Statistical approaches, such as Monte Carlo simulations, are based on probabilistic theory. While these methods are highly powerful, they often lack integration of detailed kinetic process knowledge. In contrast, deterministic modeling techniques, such as the Method of Moments, are based on kinetic approaches and typically derived from material balances. Modeling polymerization via kinetic approaches requires the formulation of material balances for all chain types and lengths, leading to an infinite set of differential equations. The Method of Moments reduces this to a smaller set

Peroxide Initiation								
Initiator Decomposition and Chain Start	I_2			$\xrightarrow{k_\mathrm{d}}$	$2 f_\mathrm{I} \mathrm{R}_1^{\mathrm{M}_i}$			
Propagation								
Propagation of Primary Radicals	$\mathrm{R}_n^{\mathrm{M}_i}$	+	M_j	$\xrightarrow{k_{\mathrm{p},ij}}$	$\mathrm{R}_{n+1}^{\mathrm{M}_j}$			
Termination								
Recombination	$\mathrm{R}_n^{\mathrm{M}_i}$	+	$\mathrm{R}_m^{\mathrm{M}_j}$	$\xrightarrow{k_{\mathrm{t,recomb}}}$	P_{n+m}			
Disproportionation	$\mathrm{R}_n^{\mathrm{M}_i}$	+	$\mathrm{R}_m^{\mathrm{M}_j}$	$\xrightarrow{k_{\mathrm{t,disp}}}$	P_n	+	$\mathrm{P}_m^{=}$	
Low-Molecular Transfer								
Transfer to Monomer	$\mathrm{R}_n^{\mathrm{M}_i}$	+	M_j	$\xrightarrow{k_{\mathrm{tr,M},ij}}$	P_n	+	$\mathrm{R}_1^{\mathrm{M}_j,=}$	
High-Molecular Transfer								
Transfer to Polymer	$\mathrm{R}_n^{\mathrm{M}_i}$	+	P_m	$\xrightarrow{m \cdot k_{\mathrm{tr,P},ij} \cdot F_j}$	P_n	+	$\mathrm{R}_{m,\mathrm{sec}}^{\mathrm{M}_j}$	
Propagation of Secondary Radicals	$\mathrm{R}_{n,\mathrm{sec}}^{\mathrm{M}_i}$	+	M_j	$\xrightarrow{k_{\mathrm{p,sec},ij}}$	$\mathrm{R}_{n+1}^{\mathrm{M}_j}$	+	LCB	
β-Scission	$\mathrm{R}_{n,\mathrm{sec}}^{\mathrm{M}_i}$			$\xrightarrow{k_{\beta,ij} \cdot F_j}$	$\mathrm{R}_{n-m}^{\mathrm{M}_j}$	+	$\mathrm{P}_m^{=}$	

Figure 1: Overview of the kinetic system for EAA copolymerization, including corresponding kinetic coefficients with simplifications. The indices $i, j \in \{1, 2\}$ denote up to four reaction steps for each reaction type. I represents the initiator, M the monomer, R the radical, and P the polymer. The indices n and m refer to the chain length. The symbol "=" indicates the formation of a terminal double bond.

of equations. However, this reduction comes at the cost of losing information about individual chains, such as the molecular weight distribution. As a result, only average polymer properties can be predicted. Nevertheless, these are often sufficient, making the Method of Moments widely applicable.[1]

In this work, the copolymerization of ethene with acrylic acid is modeled using the Method of Moments. Particular attention is given to the polymer populations of primary and secondary radicals, as well as inactive (dead) chains. Based on the calculated moments, average properties of the polymer can be predicted, including the number-average molecular weight M_n, the weight-average molecular weight M_w, and the dispersity Đ.

High-molecular-weight transfer reactions can lead to the formation of branching points, which have a significant impact on the rheological properties of the resulting polymer. Characteristics such as melt viscosity, crystallinity, and solubility are strongly affected by the formation of branching points. To account for this, so-called counter species are introduced in the model to quantify the frequency of short-chain branching (SCB, H_SCB), long-chain branching (LCB, H_LCB), and terminal double bonds (tDB, H_tDB).

The radical copolymerization of ethene with acrylic acid occurs under extreme conditions, typically at temperatures between 200 and $250\ ^{\circ}\mathrm{C}$ and pressures around $2000\ \mathrm{bar}$. Under these conditions, the reaction mixture reaches a supercritical state, allowing the polymer to dissolve completely in the monomer phase. To account for these effects, this study uses empirical correlations to describe the pressure and temperature dependence of the thermophysical properties. Mixing rules are applied to estimate the overall properties of the mixture based on the thermophysical correlations of ethene, acrylic acid, and LDPE.

In the experiments, a heating jacket is used to heat the reactor. The heat transfer from the jacket to the inner reactor wall is described by the following equation:

$$\dot{q} = k\left(T_{\mathrm{jacket}} - T_{\mathrm{wall}}\right)$$

For the simulation, the heat transfer coefficient k and the jacket temperature T_{jacket} must be specified. The implementation was validated using Predici® 11 under ideal plug-flow reactor conditions.

Summary

A residence time analysis was conducted based on the methodology described by G. Li [2], using the transport equation for steady, incompressible flow to simulate the spatial distribution of the mean residence time, as shown in Figure 2 (left). The results revealed generally efficient mixing within the reactor but also identified a backmixing effect from the autoclave body and extending into the region surrounding the stirrer shaft. To investigate this flow phenomenon in greater detail, Figure 2 (right) presents a vector plot illustrating the velocity magnitude (indicated by arrow length) and the x- and y-components of the velocity field (indicated by arrow direction). Two dominant flow patterns are observed: a flow near the inner cylinder directed towards the reactor (towards the outlet) and a flow near the outer cylinder indicating back-mixing towards the inlet. This behavior is attributed to the high stirrer speed, which forces fluid from the reactor space into the lower stirrer lens region.

In addition, pulse tracer experiments were simulated by modeling the tracer as a separate species to determine the residence time distribution (RTD).[2] Based on these simulations, time-resolved reactor images were generated to provide insight into the transient mixing behavior. The reactor images resulting from tracer injection are shown in Figure 3 for various viscosities of the fluid. Simulations were also performed at different stirrer speeds.

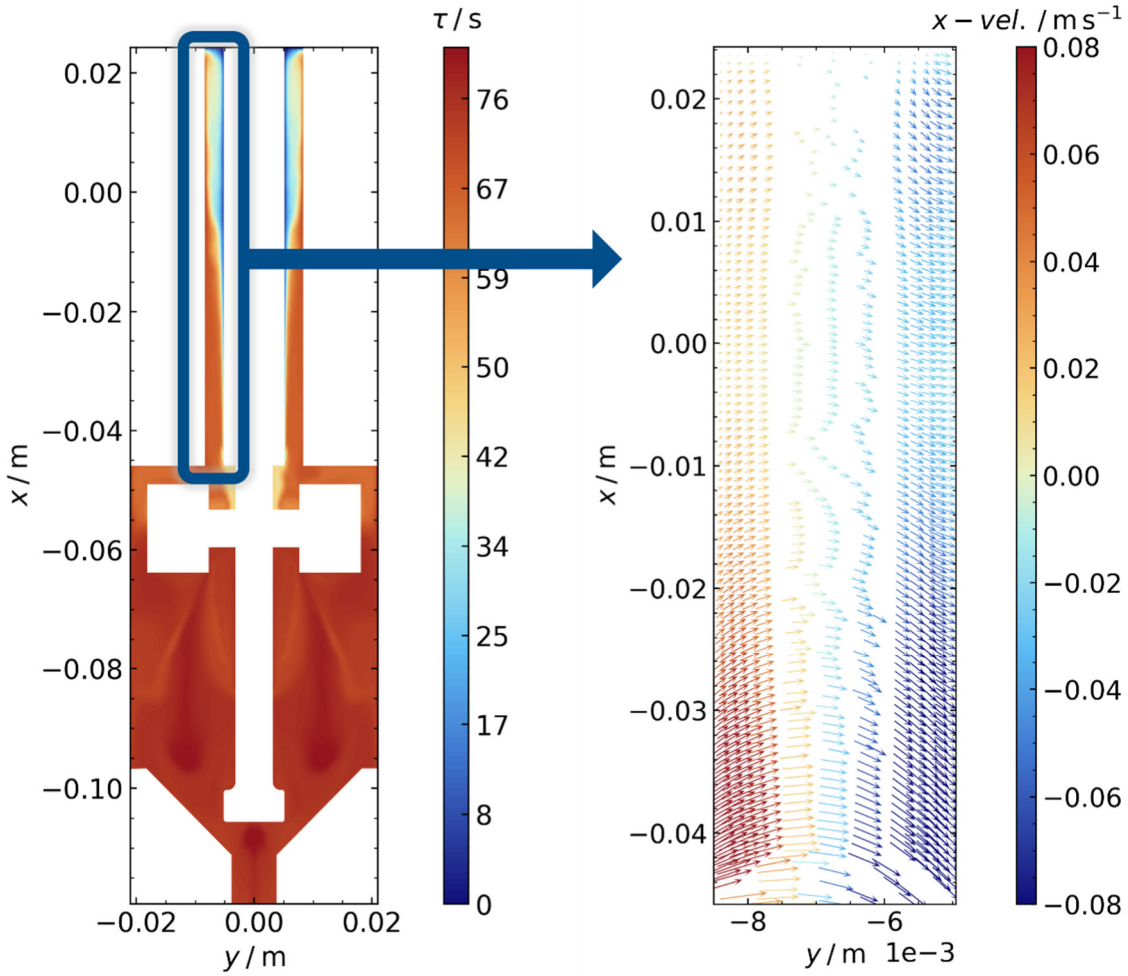

Figure 2: Contour plots of the mean residence time $\boldsymbol{\tau}$ (left) and vector plots (right) of the velocity magnitude $|v| = \sqrt{v_x^2 + v_y^2}$, derived from the x- and y-velocity components (v_x, v_y) as functions of x- and y-positions. The plots show the region around the lower stirrer lens, with the stirrer shaft on the right and the lower stirrer lens wall on the left.

The results demonstrate that the backmixing effect decreases with increasing viscosity and decreasing stirrer speed.

The implemented kinetic model was then applied to the geometry of a laboratory-scale, corrosion-resistant high-pressure autoclave. The simulation was performed using boundary conditions from an experiment at low monomer conversion. The corresponding results are shown in Figure 3.

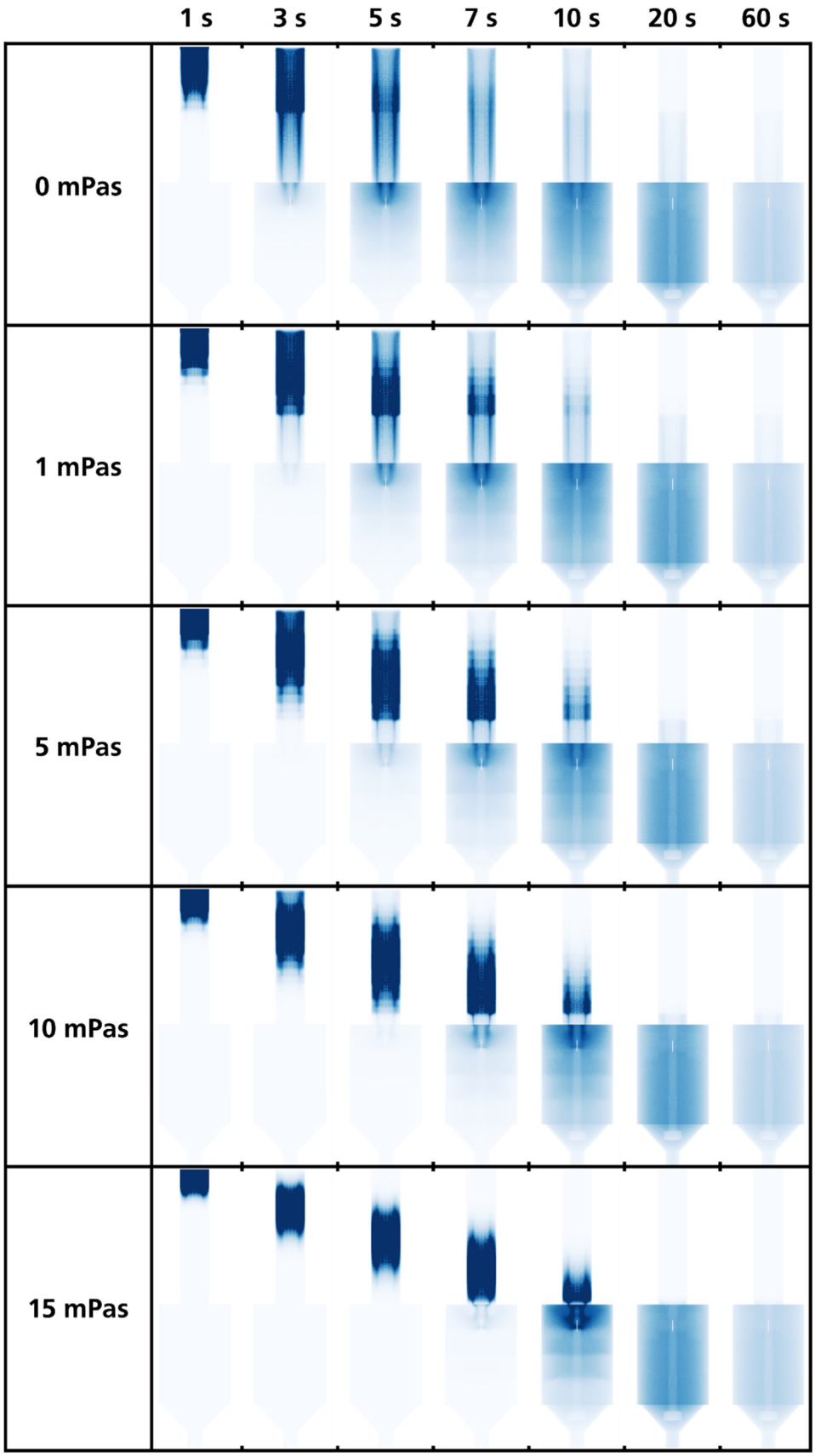

Figure 3: Reactor images of the pulse tracer injection as a function of viscosity (rows) and time (columns). The region near the outlet lens was excluded from the images.

CFD simulations incorporating the implemented kinetics revealed that the previously mentioned backmixing effect leads to a localized temperature increase near the stirrer shaft. Due to the low decomposition temperature of the initiator used, initiation occurs predominantly in this region and is already complete before the initiator reaches the main body of the autoclave. This finding highlights the need for initiators with higher decomposition temperatures in future experiments to shift the initiation into the autoclave body.

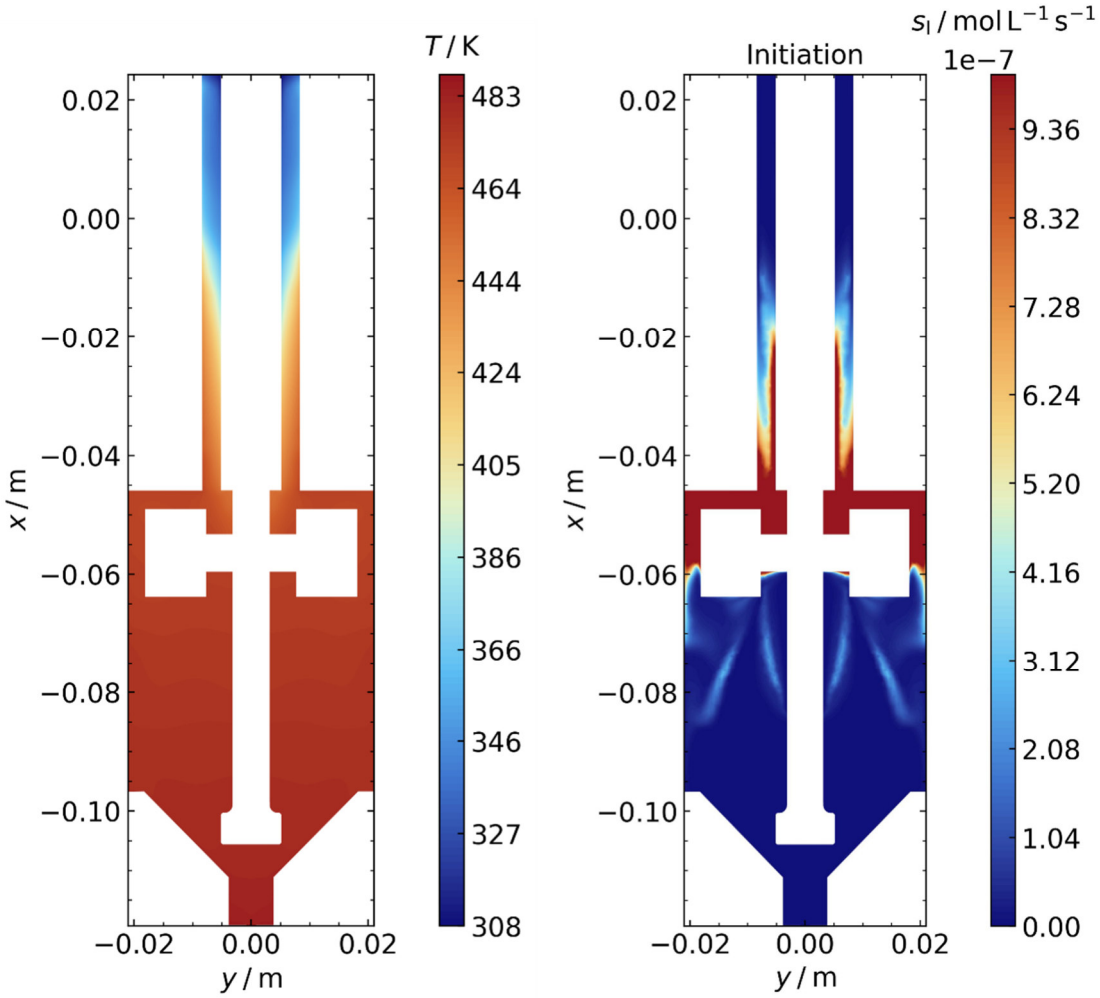

Figure 4: Contour plots of temperature T (left) and reaction rate of Initiation s_I (right).

References

[1] E. Mastan, S. Zhu, European Polymer Journal 2015, 68, 139–160.

[2] G. Li, A. Mukhopadhyay, C.-Y. Cheng, Y. Dai, In Proceedings of the ASME 2010 3rd Joint US-European Fluids Engineering Summer Meeting and 8th International Conference on Nanochannels, Microchannels, and Minichannels, ASME, 2010.

Foaming of Recycled Plastics with Water and Supercritical CO_2

Beatriz Martín-Gómez, Aránzazu Redondo, Mariana Fortunatti Montoya, Alberto Mangas, Danilo Cantero

The Institute of Bioeconomy, Department of Chemical Engineering and Environmental Technology, University of Valladolid, beatriz.martin.gomez@uva.es

Introduction

Plastics, valued for their strength, stability, and low cost, face a major environmental challenge due to their exponential production and resulting waste. Global plastic production rised exponentially from two million tonnes annually in 1950 to over 450 million tonnes per year, a number expected to increase even further in the coming decades (**Fig. 1).** These plastics predominantly end up in landfills or nature. Traditional methods to solve this accumulation, like incineration and landfilling, offer insufficient and unsustainable solutions, while mechanical recycling often leads to downcycled, lower-quality materials [1–3].

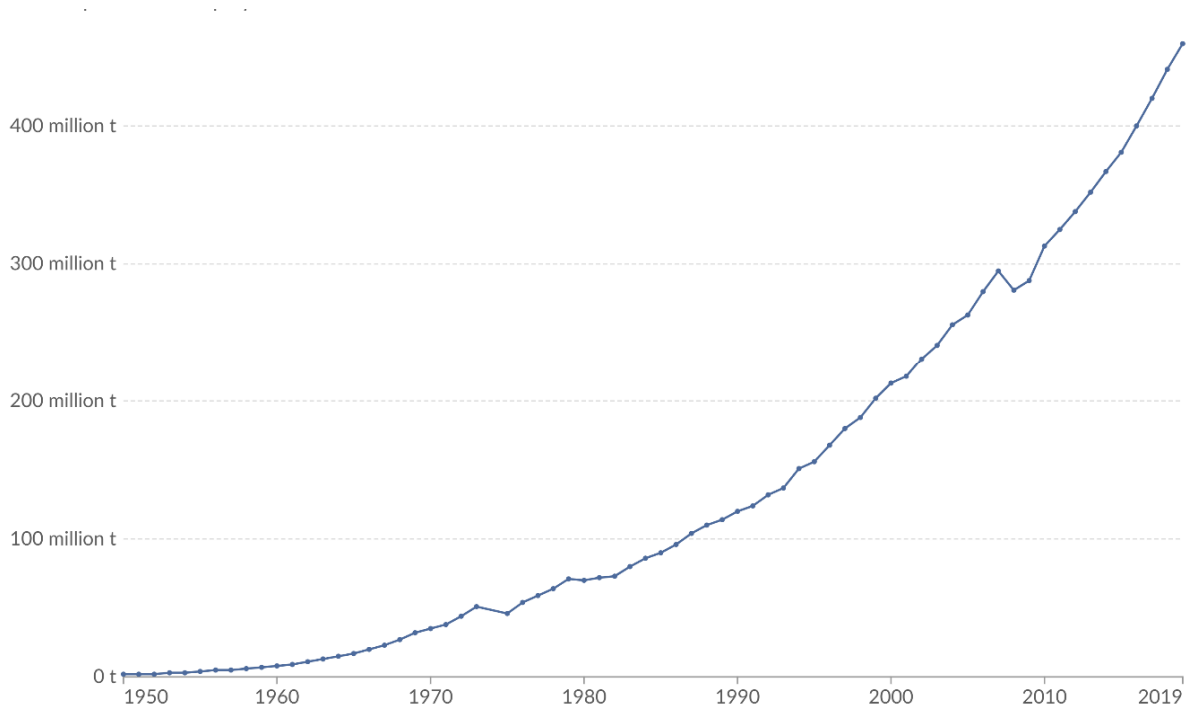

Fig. 1. Global plastic production (1950 – 2019)

Addressing this crisis requires more sustainable approaches, aligning with the Circular Economy model. This framework promotes treating plastic waste as a resource for continuous recirculation. Upcycling, in contrast to downcycling, enhances the value of waste plastics by transforming them into new, high-quality products, reducing raw material demand and boosting resource efficiency [4].

Polymer foaming stands out as a promising upcycling technology. This process introduces gas into a solid polymer, creating a porous cellular structure. The resulting foamed plastics are lightweight and can achieve high specific strength, low thermal conductivity, and excellent sound absorption. These properties make them highly useful across diverse industries, simultaneously reducing material density and plastic consumption while improving performance – an efficient solution to plastic waste [5].

While polymer foaming is typically carried out using only CO2, the incorporation of water significantly influences both the foaming process itself and the resulting foam properties. This is particularly evident in the ability to produce ultra-lightweight foams characterized by very high expansion ratios and excellent thermal insulation [6,7].

Building upon this promising approach, this work investigates the use of water and supercritical CO_2 for the foaming of high-density polyethylene (HDPE), low-density polyethylene (LDPE), polystyrene (PS), and polypropylene (PP), which constitute the majority of plastic waste streams.

Experimental

The experiments were conducted using Siphon 1, a novel batch system developed by PressTech at the University of Valladolid in collaboration with the University of Villanova. A schematic drawing of the system is shown in **Fig. 2**. This system consists of:

1. A CO_2 inlet line.
2. A heated high-pressure tubular autoclave.
3. A pneumatic valve and expansion vessel configured for rapid decompression.

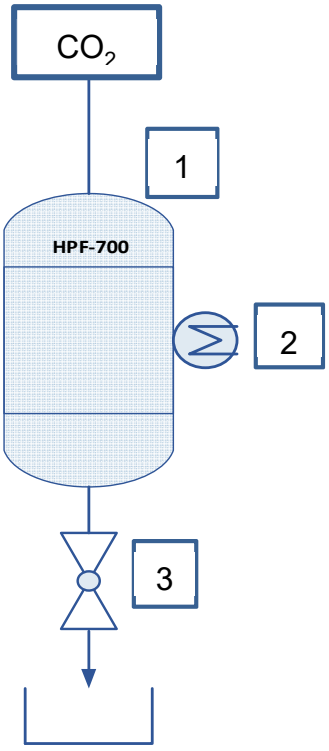

Fig. 2. Scheme of Siphon 1.

Samples of the plastic were placed in the tubular autoclave. If water was included in the trial, it was also introduced into the autoclave. The autoclave was then heated to a specific temperature and pressurized with CO_2 at a target pressure for a set time. Following this period, rapid depressurization was performed via the pneumatic valve, which resulted in the ejection of the foamed plastic into the expansion vessel for collection.

To optimize the foaming process for different plastics, the influence of saturation temperature, pressure, time, and the quantity of water addition (including trials without water) on the resulting foam's density, cell size, cell density and thermal conductivity was systematically investigated.

Summary

The experimental results indicated that the addition of water into the foaming process was found to generally lead to an observable increase in the degree of expansion obtained across the range of plastics evaluated in this study. This specific effect proved to be particularly significant and exhibited a remarkable influence in the case of HDPE. For HDPE, the presence of water not only enhanced the overall expansion achieved but also demonstrated the capability of enabling successful foaming to occur even when

processed at higher saturation temperatures than would typically be feasible with CO_2, widening the overall processing temperature window available for the foaming of HDPE, a consequence that is likely attributable to the inherent cooling effect provided by the presence of the added water within the system.

In addition, when foaming PP, it was observed that the incorporation of water within the foaming mixture led to the formation of an open-cell structure, although this specific structural characteristic was noted to occur only under certain processing conditions.

Maximum expansion ratios reached 15 for LDPE, 20 for PS and PP, and 50 for HDPE. Pore sizes across all obtained foams ranged from 1 to 100 μm.

Acknowledgments

The authors express their gratitude to the Agencia Estatal de Investigación for the financial support provided in Project PID202-119249RA-I00. Beatriz Martín-Gómez thanks the Spanish Ministry of Science, Innovation and Universities for her FPU grant (FPU22/02334).

References

[1] T.S. Athulya, J.K. Reshma, Plastic Pollution: A Global Crisis and the Overlooked Challenge of Low-Value Plastics, Copyright@ EM International 30 (n.d.) 2024–688. https://doi.org/10.53550/EEC.2024.v30i02.047.

[2] Plastics Europe, (2024). https://plasticseurope.org/ (accessed April 28, 2025).

[3] Plastic Pollution - Our World in Data, (n.d.). https://ourworldindata.org/plastic-pollution (accessed April 28, 2025).

[4] O. Horodytska, D. Kiritsis, A. Fullana, Upcycling of printed plastic films: LCA analysis and effects on the circular economy, J Clean Prod 268 (2020) 122138. https://doi.org/10.1016/J.JCLEPRO.2020.122138.

[5] M. Santiago-Calvo, A. Himmelsbach, C. Alonso, M.-T. Fernández, E. Cañibano, C. Brütting, T. Standau, H. Ruckdäschel, Enhanced Flame-retardant Performance of Undervalued Polyethylene Terephthalate Waste as a Potential use in Foamed Materials, Journal of Polymers and the Environment 2024 (2024) 1–16. https://doi.org/10.1007/S10924-024-03424-0.

[6] R. Dugad, G. Radhakrishna, A. Gandhi, Morphological evaluation of ultralow density microcellular foamed composites developed through CO2-induced solid-state batch foaming technique utilizing water as co-blowing agent, Cellular Polymers 39 (2020) 141–171. https://doi.org/10.1177/0262489319897633.

[7] Y. Yang, X. Liao, C. Lv, B. Wang, F. Zou, G. Li, Ultrasound and H2O assisted scCO2 foaming technology for preparation of PS/PMMA composite foams with ultra-lightweight and super thermal-insulation, Compos Part A Appl Sci Manuf 169 (2023) 107527. https://doi.org/10.1016/J.COMPOSITESA.2023.107527.

Design and Characterization of Hydrophilic Natural Deep Eutectic Solvents for Application in Absorption Heat Pumps and Absorption Thermal Batteries

Christoph Weinzettl, Paul Demmelmayer, Marlene Kienberger

Institute of Chemical Engineering and Environmental Technology

Graz University of Technology

c.weinzettl@tugraz.at

Introduction

Deep eutectic solvents (DESs) are a relatively novel type of solvent, first mentioned by Abbott et al. in 2003 (*1*), formed by mixing a hydrogen-bond acceptor (e.g., choline chloride) and a hydrogen-bond donor (e.g., urea). This combination results in a homogeneous liquid at room temperature (RT) by significantly lowering the melting point of the mixture compared to that of the pure substances. This melting-point depression arises from strong deviations from ideal mixing behaviour driven by van der Waals interactions, particularly hydrogen bonding. Natural deep eutectic solvents (naDESs) are defined as a subclass of DESs that, by definition, are composed solely of substances derivable from natural resources and are therefore potentially highly biodegradable and sustainable (*2, 3*). In theory, an infinite number of natural deep eutectic solvents exist, since producing one requires only a mixture containing at least one hydrogen-bond acceptor and one hydrogen-bond donor. The main properties of a naDES can be tailored to its intended application—making it, for example, hydrophobic or hydrophilic depending on its constituents—which allows for the specific design of solvents for defined applications such as absorption heat pumps (AHPs) and absorption thermal batteries (ATBs).

The state-of-the-art working medium for both AHPs and ATBs is an aqueous lithium-bromide solution. Although this salt-based medium addresses some issues, it still suffers from high corrosivity and a tendency to crystallize under certain operating conditions (*4, 5*). Using hydrophilic natural deep eutectic solvents instead of aqueous salt solutions may help overcome these problems, making them more economically feasible and increasing their sustainability. However, naDESs are relatively under-researched solvents, and hardly any data on their water-absorption capacity are available. Furthermore, most naDESs exhibit high viscosity due to strong intermolecular interactions, which can impede circulation and reduce both mass-transfer and heat-transfer rates.

Experimental and Results

For the preparation of naDESs, 37 different substances derivable from natural resources were used as precursors. All constituents are free from halides, non-oxidizing, non-harmful to humans and animals upon exposure, non-toxic, and environmentally benign. Except for one substance, based on their molecular structures, all others can act as both hydrogen-bond acceptor and hydrogen-bond donor. To determine which binary mixtures yield a homogeneous transparent liquid at RT, each potential naDES was prepared by mixing two different substances in a specific molar ratio, then heating the mixture at 80 °C and stirring for 16 h. Of 89 binary mixtures, 25 remained liquid after cooling back to RT. Of the remaining 64 mixtures, 10 were discarded because no interaction between the constituents was observed. To the other 54 mixtures, 10 wt.% water was added—since water helps to weaken the strong hydrogen-bond interactions of the precursors—yielding another 17 successfully prepared mixtures that stayed liquid at RT. When another 10 wt.% water was added to the remaining 17 mixtures, 20 more were discarded due to lack of observable interaction. The pictures in Fig. *1* show, representatively, several mixtures that resulted in homogeneous, transparent liquids at RT (Fig. *1* a), and some that showed little interaction and thus did not form homogeneous liquids at RT (Fig. *1* b).

(a) (b)

Fig. 1.: The picture on the left side (a) shows four different naDESs that remained liquid at RT. The solvents are composed of the following constituents from left to right: Betaine:Citric Acid; Betaine:Isosorbide; D-Fructose:Citric Acid; D-Glucose:Citric Acid. Each of them contains 10 wt.% water.
The picture on the right side (b) shows four different solvents that not remained liquid at room temperature. Each of them was composed of Betaine and either Tartaric Acid, Phenylacetic Acid, Pentaerythritol, or 1,2-Propanediol.

A binary mixture is not classified as a DES solely by its melting-point depression, but by the magnitude of that depression relative to the theoretical value predicted under ideal

mixing behaviour. This is visualized in the solid–liquid equilibrium diagram in Fig. 2, where the red curves show theoretical liquidus lines calculated for ideal mixing, whereas the blue curves represent the real liquidus lines of a binary mixture that forms a DES through strong deviations from ideality.

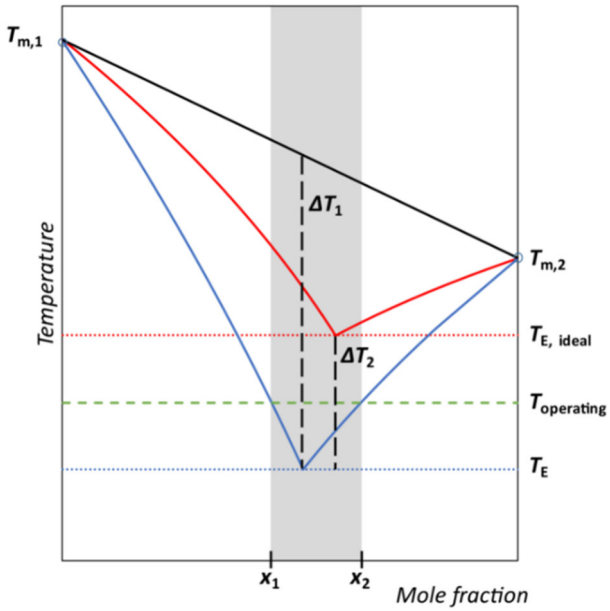

Fig. 2.: Solid-liquid equilibrium diagram of a simple eutectic mixture (continuous red line) and a deep eutectic mixture (continuous blue line), figure taken from (6).

DES tend to form undercooled liquids that exhibit a phase-transition range between solid and liquid rather than a sharp melting or solidification point, which makes the experimental construction of reliable solid–liquid equilibrium diagrams nearly impossible. Since no clear definition exists in the literature for the magnitude of melting-point depression relative to simple eutectic mixtures required for DES classification, the binary mixtures in this work were classified as deep eutectic if they remained liquid at -18 °C and stayed stable over extended periods at RT under UV protection. By this simplified criterion, 11 of the 44 solvents qualified as DES.

Mass and heat transfer are strongly influenced by liquid viscosity, so dynamic viscosities were measured at various temperatures and water loadings. At 25 °C, all investigated naDESs exhibited viscosities roughly 20 to 2 500 times greater than that of pure water. Raising the temperature to 80 °C reduced dynamic viscosities drastically, yielding values approximately 2 to 160 times higher than water at the same temperature. When each solvent was loaded with 0.25 gram of water per gram of solvent, the most viscous mixture at 80 °C proved only 19 times more viscous than pure water at 80 °C. These results are

promising for use in AHPs and ATBs, since these applications operate at elevated temperatures with continuous water uptake.

Summary

This study demonstrates that hydrophilic naDESs can specifically be designed to potentially replace a Lithium Bromide solution as working media in AHPs and ATBs. 89 binary mixtures were prepared from 37 naturally sourced, halide-free compounds, resulting in 44 mixtures that remain liquid at RT. Using a simplified criterion for the definition of eutectic mixtures as deep eutectic, remaining liquid below -18 °C and stable at RT over a period, 11 of these liquids were classified as deep-eutectic. Viscosity, often a limiting factor for applying DESs, proved manageable under real operating conditions in AHPs and ATBs. Although pseudo-pure naDESs were initially 20 to 2500 times more viscous than water at 25 °C, thermal and hydration effects drastically decreased these values. At 80 °C and 0.25 gram water per gram naDES, the most viscous mixture was only 19 times more viscous than water. Because AHP/ATB generators and absorbers operate at elevated temperatures and continuously uptake water, the effective viscosities during operation should lie well inside practical pumping and heat-transfer limits.

Overall, these results suggest naDESs are a promising, greener alternative to salt solutions in absorption systems. The straightforward preparation (80 °C, ambient pressure), flexible choice of natural components, and favourable viscosity at operating conditions make them strong candidates for further development. Next steps may include the investigation of water uptake and following desorption under operating conditions and the determination of long-time stability at elevated temperatures besides studying the probability of hydrolyses as it may lead to solvent degradation.

References

1. Abbott, A. P.; Capper, G.; Davies, D. L.; Rasheed, R. K.; Tambyrajah, V. Novel solvent properties of choline chloride/urea mixtures. *Chemical communications (Cambridge, England)* **2003** (1), 70–71. DOI: 10.1039/B210714G.
2. Płotka-Wasylka, J.; La Guardia, M. de; Andruch, V.; Vilková, M. Deep eutectic solvents vs ionic liquids: Similarities and differences. *Microchemical Journal* **2020,** *159*, 105539. DOI: 10.1016/j.microc.2020.105539.

3. Liu, Y.; Friesen, J. B.; McAlpine, J. B.; Lankin, D. C.; Chen, S.-N.; Pauli, G. F. Natural Deep Eutectic Solvents: Properties, Applications, and Perspectives. *Journal of natural products* **2018,** *81* (3), 679–690. DOI: 10.1021/acs.jnatprod.7b00945.
4. Cudok, F.; Giannetti, N.; Ciganda, J. L. C.; Aoyama, J.; Babu, P.; Coronas, A.; Fujii, T.; Inoue, N.; Saito, K.; Yamaguchi, S.; Ziegler, F. Absorption heat transformer - state-of-the-art of industrial applications. *Renewable and Sustainable Energy Reviews* **2021,** *141*, 110757. DOI: 10.1016/j.rser.2021.110757.
5. Wang, K.; Abdelaziz, O.; Kisari, P.; Vineyard, E. A. State-of-the-art review on crystallization control technologies for water/LiBr absorption heat pumps. *International Journal of Refrigeration* **2011,** *34* (6), 1325–1337. DOI: 10.1016/j.ijrefrig.2011.04.006.
6. Martins, M. A. R.; Pinho, S. P.; Coutinho, J. A. P. Insights into the Nature of Eutectic and Deep Eutectic Mixtures. *J Solution Chem* **2019,** *48* (7), 962–982. DOI: 10.1007/s10953-018-0793-1.

Detection of Free Amino Acids and their Oxidised Products Using HPLC Coupled with Benchtop NMR (HPLC-NMR)

Miha Fermišek, Gregor Hostnik, Urban Bren, Matja Zalar

Faculty of Chemistry and Chemical Engineering, University of Maribor

miha.fermisek@um.si

Introduction

Proteins have become a vital part of modern therapeutic strategies since the introduction of the first recombinant drug – insulin – into clinical use. Today it's a rapidly growing market estimated to be worth hundreds of billions of dollars. Protein therapeutics are designed to replicate natural protein mechanisms such as catalysis, signalling, transport of molecules and ions, and involvement in the immune system response, to name but a few [1]. Common classes of protein therapeutics include antibodies (e.g., monoclonal antibodies - mAbs, antibody-drug conjugates - ADCs) [1, 2], enzymes (e.g., sacrosidase, pegvaliase, laronidase [1]), coagulation factors, hormones [1, 2], cytokines [1] and others. The majority of these are used in oncology, haematology, cardiology/vascular diseases, dermatology, and gastroenterology [2].

When we evaluate the efficacy of protein therapeutics, we usually compare them to small molecule drugs (SMDs). Unlike SMDs, protein therapeutics are more selective, resulting in reduced interference with normal host biological processes and, consequently, fewer and less severe side effects. They are also more potent and can perform more complex functions [1]. However, protein therapeutics can easily undergo unwanted variations through various physical and/or chemical processes such as aggregation [1, 3, 4], degradation, denaturation [1], oxidation [1, 4, 5], deamidation [1, 5] and others. In some cases, these processes may be interrelated (e.g., oxidation followed by fragmentation or aggregation) [4]. Furthermore, these degradation processes are closely associated with poorer clearance from the body, non-specific distribution [1], immunogenicity [1, 2], and toxicity. Therefore, care must be taken when using such therapeutics, not only during manufacturing, but also in subsequent transport, storage and handling [1]. They are more difficult to produce because they require special living cell lines or organisms. They also need to undergo various post-translational modifications [2] (e.g., phosphorylation, glycosylation) to perform their optimal functions. Their instability is demonstrated by their thermal instability, reactivity in the presence of reactive oxygen species (ROS) or light,

interfaces between protein solution and container material, variations in pH value, and changes in buffer solution [1, 5]. ROS (e.g., $HO^{\cdot}$, $ROO^{\cdot}$, $^1O_2$, O_3) induce oxidative stress on proteins, altering their structure and consequently their biological activity [3, 4]. Amino acids which are known to be susceptible to oxidation induced by ROS are cysteine (Cys), methionine (Met), tryptophan (Trp) [3–5], tyrosine (Tyr), histidine (His) [4, 5], and phenylalanine (Phe) [4].

A variety of analytical techniques are available to assess protein damage caused by oxidative stress. Commonly employed methods include 1D or 2D electrophoresis, ELISA test, HPLC-MS, circular dichroism (CD), light scattering, small-angle neutron scattering SANS), small-angle X-ray scattering, turbidity methods, X-ray crystallography, and NMR spectroscopy. These methods can be used for detection of chemical modification, quantification, mass and particle size observation, and solubility changes. Despite the broad range of analytical tools, most methods are optimized for the analysis of purified proteins rather than complex biological samples. Typically, two or more methods must be used to characterize samples (coupled methods are also possible). But still the main technique for amino acid analysis is performed with HPLC/UPLC (ultra high-performance liquid chromatography) as separation, which is followed by quantification with MS, fluorescence, UV absorption, or by other electrochemical methods. Separating amino acids often requires the addition of ion-pairing reagents such as heptafluorobutyric acid (HFBA). This reagent artificially increases the hydrophobicity of the molecules in our samples, enabling the amino acids to bind more effectively to the stationary phase. This increases the elution time of more polar amino acids, preventing them from eluting immediately after column dead time (t_D) [4].

Experimental

Protein modifications mainly occur on amino acid residues, which are bonded together by a polypeptide chain to form a molecule with specific functions and properties. As previously mentioned, several amino acids are more susceptible to oxidation and form the basis of the experimental work. These are Cys, Met, His, Trp, and Tyr. In the presence of an oxidising agent, Met converts to methionine sulfoxide (MetO). If a strong oxidant is present, further oxidation occurs, forming methionine sulfone ($MetO_2$). Figure 1 describes the entire oxidation process of Met.

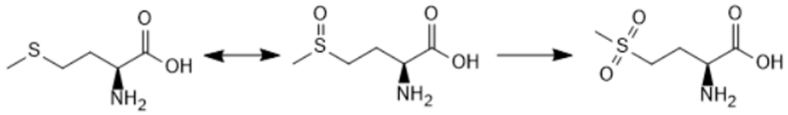

Figure 1: The oxidation of the amino acid Met to MetO. If a stronger oxidant is present, then MetO undergoes further oxidation and converts into $MetO_2$.

Oxidation involves more than just the addition of atoms or functional groups (e.g., -OH). It can also involve two or more amino acids combining to form aggregates. This process is well known for Cys, where linking of two amino acids by a disulphide bridge (-S-S-) is a common occurrence in proteins that stabilises their structures against thermal stress. However, in this case disulphide bridges form intermolecularly, and later aggregation occurs. A formed dimer of two molecules of free Cys is known as cystine. The formation of dimer cystine is represented in Figure 2.

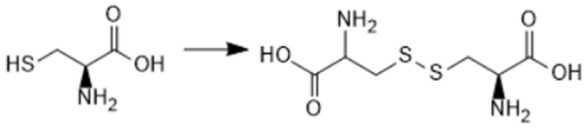

Figure 2: Oxidation of Cys to cystine.

Any oxidation product can alter the biological activity of proteins, including protein therapeutics. Therefore, it is important to be aware of any potential changes. In some cases, unwanted chemical modifications lead into formation of aggregates and can be detected by looking for turbidity in the protein solutions. However, the vast majority of degradations are not so easily observed. Therefore, other approaches must be considered. In our experimental work we used high-performance liquid chromatography (HPLC) (Vanquish Core, Thermo Scientific, USA) to separate amino acids (L-Met, L-Cys, L-His, L-Trp, and L-Tyr) from their oxidised products (L-MetO, L-$MetO_2$, L-Cystine, L-Asparagine (L-Asn), L-Aspartic acid (L-Asp), L-Kynurenine (L-Kyn), and 3-(3,4-dihydroxyphenyl)-L-alanine (L-DOPA)). L-Met, L-Cys (Sigma Aldrich, Japan), L-Kyn (TCI, Japan), L-Asn, L-His (Sigma Aldrich, USA), L-Trp (Sigma Aldrich, China), L-DOPA (ThermoFisher Scientific, China), L-$MetO_2$ (Sigma Aldrich, Germany), L-Asp (Sigma Aldrich, France), L-Tyrosine (Carlo Erba, France), L-Cystine (Sigma Aldrich, India), and L-MetO (Sigma Aldrich, Switzerland), were all commercially available.

Since not all amino acids are easily and in large quantities soluble in MiliQ water (Adrona, Latvia), we had to prepare them in 0.1 M or 1M HCl (HoneyWell Fluka, Austria) solution, depending on their solubility. Primarily we prepared individual standards and mix

standard with concentrations of amino acids above 0.1 mg/ml so that their absorbance at 221 nm during separation remained constant. We prepared standard samples for every amino acid and their oxidised product, as well as the standard which contained all of the amino acids. Crafts *et al.* [6] provided a method for separating amino acids. We later modified this method due to the presence of several other compounds that were not present in the initial study. The steps of the gradient mode were also altered because the column does not possess the same parameters. Amount of volume that was injected on to the column was set on 10 µl, and the temperature of both column and sample chamber was 20 °C. We used as a solvent A MiliQ water with 0.4% heptafluorobutyric acid - HFBA (Sigma Aldrich, Switzerland), and as solvent B acetonitrile - ACN with 0.4% HFBA. We used Acclaim Polar Advantage II HPLC Column (150×4.6 mm; 3 µm) (ThermoFisher Scientific™, USA) with polar embedded stationary phase. We used reversed-phase high-performance liquid chromatography (RP-HPLC) method, where we began using polar solvents and later slowly adding more non-polar solvent, before repeating the method for another separation. Changing the polarity of solvent greatly influences the separation of amino acids. At the beginning more polar amino acids elute, but when we increase the ratio of ACN the more non-polar amino acids start to elute through the column. The flow rate was set on 0.500 ml/min. Measured chromatographic peaks were analysed using software Chromeleon 7 (Thermo Scientific Dionex Chomeleon 7 Chromatography Data System, USA). When separation method was fully developed, we continued our experimental work on coupling HPLC with X-Pulse benchtop NMR (Oxford Instruments, United Kingdom).

NMR spectroscopy is an established method in protein analysis. Sample is placed in a strong, constant magnetic field in which we apply radio frequency (RF) pulses to detect specific nuclei (e.g., ^{1}H, ^{13}C, ^{15}N, ^{31}P). Here we focused on the flow-through method where we use the flow from HPLC to transfer the separated amino acids and their oxidised products through the NMR probe and measure their NMR spectra over time. To successfully measure NMR signals we must properly increase the concentration of previously prepared amino acid samples, so that the NMR probe can in short time detect the compounds passing through. As we have been using Water type I (and later ACN) as the mobile phase during the separation, we have also measured the NMR peak(s) for the mobile phase. To avoid solvent peak we used solvent suppression pulse sequence. Every NMR spectrum was analysed and optimized using software MestReNova x64 (Mestrelab Research, Spain). The goal was to couple together HPLC-benchtop NMR for early

detection of degraded amino acids. This provides a better resolution of chemicals for their detection ad quantification. Figure 3 describes the entire procedure, from the separation of amino acids and their oxidised products to their detection using a UV/VIS detector and an NMR spectrometer.

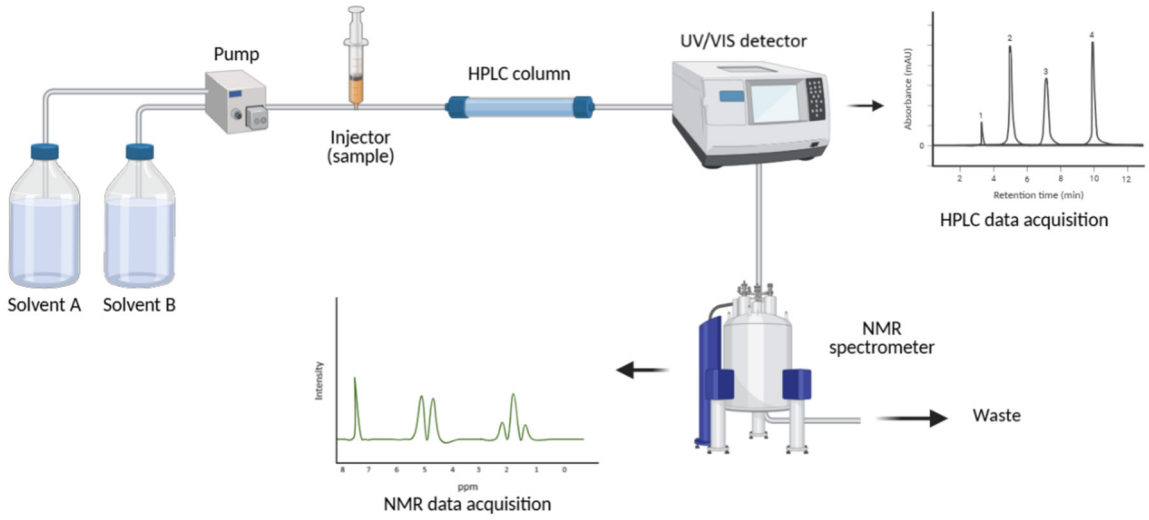

Figure 3: Scheme representing separation of amino acids and their oxidised products using HPLC, followed by the detection of compounds using benchtop NMR spectroscopy.

A major advantage of using NMR coupled to HPLC is that in many cases the separated chromatographic peaks on HPLC could contain two or more undetectable compounds. This problem is usually neglected when mass spectrometry (MS) is used to measure the weights of molecular fragments. NMR can also be used in a similar way, where we do not detect specific molecular fragments, but rather specific fingerprints, or better still, specific NMR peaks that are assigned to specific amino acids. This allows us to analyse samples that are not sufficiently separated but can still indicate if oxidation has taken place. Experimental work did not consider any pre-separation modifications of amino acids.

Summary

Despite being used to treat many diseases, protein therapeutics still exhibit several disadvantages. The biggest risk is their ability to trigger a life-threatening immune response due to presence of aggregates. This is primarily due to their size, whether native or resulting from improper management and degradation over time. Therefore, it is important to develop precise and accurate analytical techniques for screening them to prevent toxic proteins from being administered to the patients. One such method could be

HPLC coupled to benchtop NMR. By adding an ion-pairing reagent (HFBA) to the mobile phase, we were able to separate free amino acids from their oxidised products. We then coupled the HPLC to the benchtop NMR, and by using the flow-through method, we were able to detect the separated compounds in the NMR probe using the flow formed by the HPLC pump. As a result, we obtained many NMR spectra, enabling us to detect and quantify separated components.

Acknowledgment

The authors thank the Slovenian Research and Innovation Agency (ARIS) for their financial support of research project J4-4633.

References

[1] Ebrahimi, S. B.; Samanta, D. Engineering Protein-Based Therapeutics through Structural and Chemical Design. *Nat Commun*, 2023, *14* (1), 2411. https://doi.org/10.1038/s41467-023-38039-x.

[2] Lagassé, H. A. D.; Alexaki, A.; Simhadri, V. L.; Katagiri, N. H.; Jankowski, W.; Sauna, Z. E.; Kimchi-Sarfaty, C. Recent Advances in (Therapeutic Protein) Drug Development. *F1000Res*, 2017, *6*, 113. https://doi.org/10.12688/f1000research.9970.1.

[3] Lévy, E.; El Banna, N.; Baïlle, D.; Heneman-Masurel, A.; Truchet, S.; Rezaei, H.; Huang, M.-E.; Béringue, V.; Martin, D.; Vernis, L. Causative Links between Protein Aggregation and Oxidative Stress: A Review. *Int J Mol Sci*, 2019, *20* (16), 3896. https://doi.org/10.3390/ijms20163896.

[4] Hawkins, C. L.; Davies, M. J. Detection, Identification, and Quantification of Oxidative Protein Modifications. *Journal of Biological Chemistry*, 2019, *294* (51), 19683–19708. https://doi.org/10.1074/jbc.REV119.006217.

[5] Li, S.; Schöneich, C.; Borchardt, R. T. Chemical Instability of Protein Pharmaceuticals: Mechanisms of Oxidation and Strategies for Stabilization. *Biotechnol Bioeng*, 1995, *48* (5), 490–500. https://doi.org/10.1002/bit.260480511.

[6] Crafts, C.; Plante, M.; Bailey, B.; Acworth, I. Sensitive Analysis of Underivatized Amino Acids Using UHPLC with Charged Aerosol Detection https://assets.thermofisher.com/TFS-Assets/CMD/posters/PN-70038-Analysis-Underivatized-Amino-Acids-UHPLC-CAD-PN70038-EN.pdf (accessed May 13, 2025).

Validation of a Simulation Model for Emulsion Polymerization of n-Butyl Acrylate in a Batch Reactor

Ferel Issa, Kristina Zentel

Ernst-Berl-Institute /department of chemistry, Technical University Darmstadt,
kristina.zentel@pre.tu-darmstadt.de

Introduction

Polymerisation is a fundamental chemical process that plays a crucial role in a wide range of everyday applications and industrial processes.[1] A specialised form of polymerisation is emulsion polymerisation, which has many advantages and a broad scope of applicable uses. Unlike conventional methods such as bulk or solution polymerisation, emulsion polymerisation occurs in an aqueous phase, with the monomers dispersed as small droplets stabilised by surfactants.[2] This technique provides superior control over the exothermic reaction and allows for high scalability. In radical polymerisation, the reaction takes place in nanoscale particles, resulting in high polymerisation rates and the formation of high-molecular-weight polymers that can be processed without significant viscosity issues. These benefits make emulsion polymerisation the preferred method for producing synthetic textiles, coatings, and adhesives, among other materials.[3]

However, emulsion polymerisation is inherently complex, involving three main phases: the polymer phase, the droplet phase, and the aqueous phase. Given the multiphase nature of the system, advanced simulation tools such as Predici[4] offer an efficient means of analysing the process kinetics and thus speeding up the development of new products. Nevertheless, accurate experimental data are essential for validating these simulation models prior to their application to process development.

Overview of the Simulation Model

In this work a kinetic simulation model in Predici 11[4] developed in the Zentel research group[5] is to be validated. This model can predict monomer conversions in homo- and copolymerizations, as well as the number and size of particles formed during the reaction. The model uses the masses of the reaction mixture as input. For initiator decay reactions, the Arrhenius equation is employed. Scripts containing the reaction temperature measured during the experiments are also incorporated into the model for simulation purposes.

Previous work in the Zentel research group[5] investigated the ability to predict conversion and diameter with the redox-initiating system in both styrene homopolymerization and copolymerisation systems composed of styrene and BA in a batch reactor. In addition, reactions were carried out in a continuous 3D-printed tubular reactor and the results were compared with simulations. The results of this comparison showed good agreement with the simulations.

The focus of this work was the validation of the model in batch reactor for homopolymerization of n-BA with two different initiating systems.

Experimental

Experimental validation was performed in a 1 L double-jacketed glass reactor. Sodium dodecyl benzenesulfonate (SDBS) was used as the emulsifier, n-BA as the monomer, and water as the continuous phase. Two initiation systems were studied: a redox system containing tert-butyl hydroperoxide (TBHP) and ascorbic acid (AsAc), as well as an iron-based catalyst (Ammonium iron (III) sulfate- dodecahydrate, Fe-cat). A simplified reaction scheme for this system is shown in Figure 1.

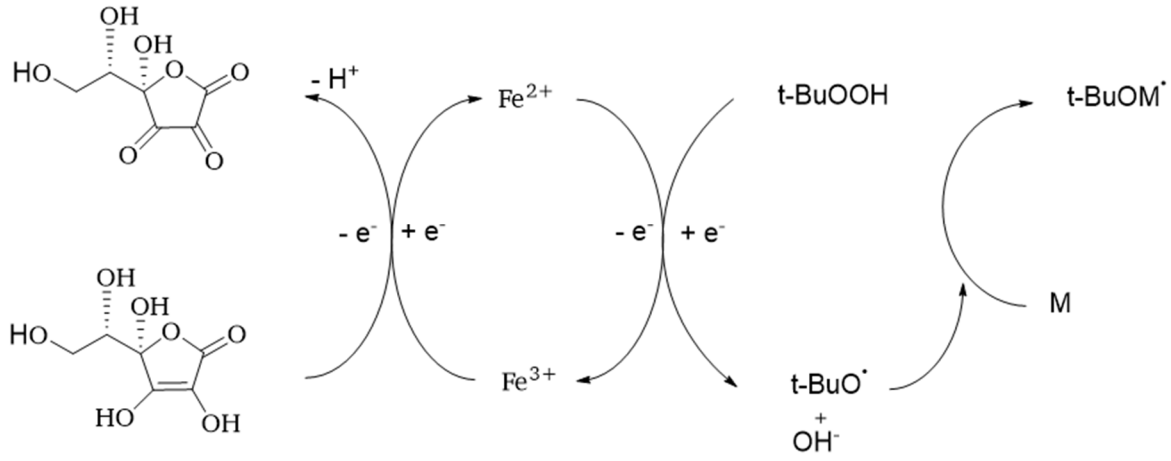

Figure 1: Simplified rection mechanism of the used redox system consisting of TBHP/AsAc/Fe-Cat.[6]

In addition to the redox system also the behaviour of the thermal azo initiator 2,2'-Azobis[N-(2-carboxyethyl)-2-methylpropionamidin] tetrahydrate (VA-057) was also investigated. The decay reaction of this azo initiator is shown in Figure 2.

Figure 2: Decay reaction of the thermal azo initiator VA-057.

Throughout the reactions, numerous samples were collected and analysed to track the progression of the reactions. For this gravimetric analysis of the solid content of each sample were performed, and the particle size was also measured using dynamic light scattering (DLS). The experimentally collected results were then compared with the simulation results. Figure 3 shows the comparison results for both initiating systems.

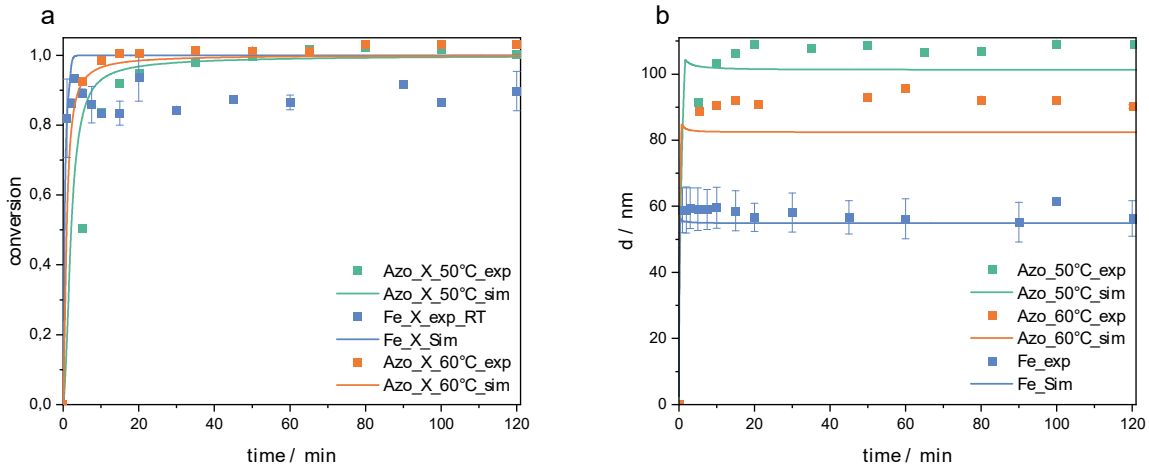

Figure 3: a) Comparison of experimentally determined monomer conversion with simulation results. b) comparison of measured hydrodynamic diameter of particles with simulated values.

Comparing experimental and simulated data showed that the model accurately predicts monomer conversion and particle size evolution. The results confirm the model's efficacy in describing radical distribution and polymer growth under various initiation conditions.

The model's ability to simulate the emulsion kinetics of n-BA at different temperatures and with different initiators is also evident.

Summary and outlook

With the aim of validating a Predici 11 simulation model, a number of n-BA homopolymerisations were carried out using two different initiators. The temperature was

measured continuously during the reaction, and this data was used as input for the simulation model alongside the weighted reaction components. The results were then compared with those collected experimentally and showed good agreement. This proves that the simulation model is able to predict the reaction kinetics and correctly calculate the distribution of radicals on particles, thus determining the number and size of particles formed during polymerisation.

Building on these results, our next step is to expand our setup to include semi-batch reactions and validate the model using these experiments. Furthermore, we seek to enhance our understanding of n-BA behaviour in both one-phase and multi-phase reactions, laying the groundwork for n-BA copolymerisations with ethylene at moderate pressures.

Acknowledgment

Part of this research was funded by DFG under the project number: 537707035

References

[1] R. J. Crawford, P. J. Martin, Plastics engineering, 4. Aufl., Butterworth-Heinemann, Amsterdam.

[2] M. D. Lechner, K. Gehrke, E. H. Nordmeier, Makromolekulare Chemie. Ein Lehrbuch für Chemiker, Physiker, Materialwissenschaftler und Verfahrenstechniker, 4. Aufl., Birkhäuser, Basel, Boston, 2010.

[3] M. Aguirre, N. Ballard, E. Gonzalez, S. Hamzehlou, H. Sardon, M. Calderon, M. Paulis, R. Tomovska, D. Dupin, R. H. Bean et al., Macromolecules 2023, 56, 2579.

[4] Dr. M. Wulkow Computing in Technology GmbH. (2020). Predici (11) [Software].

[5] Nachwuchsgruppe Dr. K. Zentel, Internetseite: https://www.chemie.tu-darmstadt.de/zentel/index.de.jsp

[6] B. Schroeter, S. Bettermann, H. Semken, T. Melchin, H.-P. Weitzel, W. Pauer, *Ind. Eng. Chem. Res.* **2019**, *58*, 12939

Beer Dealcoholisation by Pervaporation Process

Aneta Krawiec, Mateusz Jackowski, Anna Trusek

Faculty of Chemistry, Wroclaw University of Science and Technology,

258934@student.pwr.edu.pl

Introduction

Beers with an alcohol content not exceeding 0.5% alcohol by volume (ABV) are typically called non-alcoholic beers. Recently, consumer interest in non-alcoholic beer has been increasing, and it is estimated that between 2024 and 2029, it will reach a growth rate of 10.01% (Brewers Journal, 2025).

Low-alcohol beers usually have worse sensory qualities, such as taste, unwanted wort-like aromas, or too much sweetness. The lower the alcohol content, the stronger these problems become. These issues are related to the production methods of non-alcoholic beer, where not only alcohol but also other volatile compounds are removed (Pater & Frączek, 2024).

Pervaporation is a membrane process used for the separation of liquid mixtures. It is a highly effective technique for separating ethanol and water, making it suitable for the dealcoholization of beverages. The feed solution is applied to the membrane under atmospheric pressure, while the opposite side is kept under reduced pressure or vacuum. In these conditions, the permeating components evaporate, are collected in the gas phase, and then condensed in a receiver tank outside the system, from which they can be removed. The separation of components is based on their affinity for the membrane material (Bodzek Michał, 1997; Konieczny & Rychlewska, 2016; Van der Bruggen & Luis, 2015).

Pervaporation is a technology with great potential for beer dealcoholization, but it requires precise adjustment of operating conditions to avoid aroma loss and low selectivity. Therefore, it is necessary to study how the efficiency of ethanol removal from beer is affected by specific membranes and process conditions. Another challenge is the transfer of volatile compounds through the membrane, which can negatively impact the sensory profile of the beer (Castro-Muñoz, 2019).

Experimental

The study used a dark beer produced at the University Brewery. Before pervaporation, the beer was degassed and micro-filtered to remove solid particles. Its alcohol content by volume and density was determined using the "FermentoFlash" beer analyzer (Fluke Gerber, Germany).

Tab. 1.: Parameters of the beer sample.

Alcohol content [% v/v]	4.39
Alcohol content [% w/w]	3.46
Density [g/cm^3]	1.0054

Pervaporation was carried out using the setup schematically shown in Fig. 1, applying a PERVAP 4155-40 membrane (Sulzer Chemtech, Switzerland) with a surface area of A = 200 cm². The process was conducted in two temperature ranges: 40–45 °C and 50–55 °C, with a beer flow rate of 30 L/h.

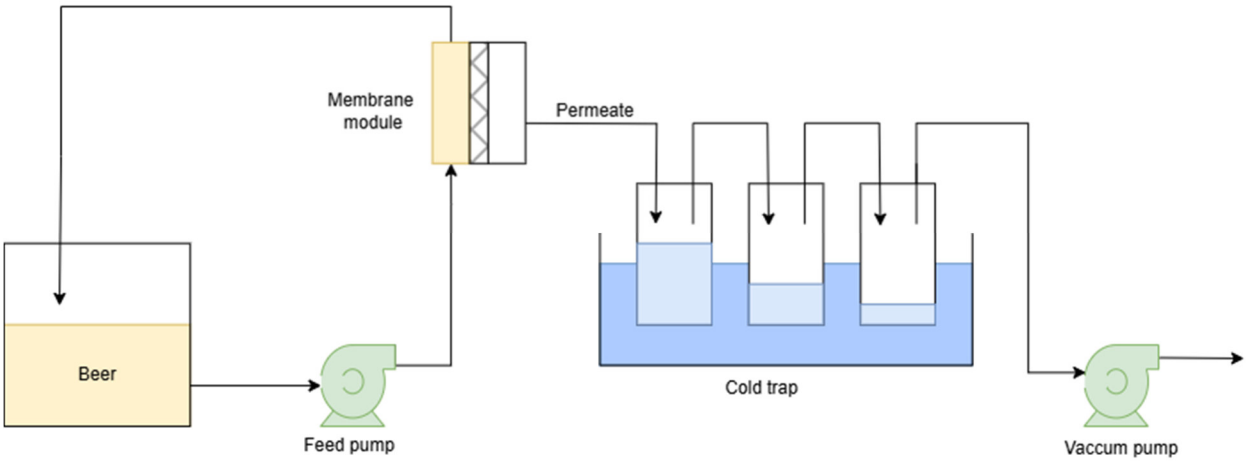

Fig. 1.: Scheme of the pervaporation setup.

1L of beer was placed in a jacketed feed tank, the feed pump was activated, and the heating temperature was set. Simultaneously, the cold trap tank was filled with an ice-water mixture to ensure a low temperature in the permeate collectors, enabling vapor condensation. Effective cooling was maintained by regularly adding ice or replacing the water. Once the beer reached the target temperature, the vacuum pump was switched on. During the process, the pressure on the permeate side of the membrane was kept between 50 and 130 mbar.

Pervaporation was continuous, and permeate samples were withdrawn from the collectors during the process. Fig. 2 presents the permeate flow rate throughout pervaporation.

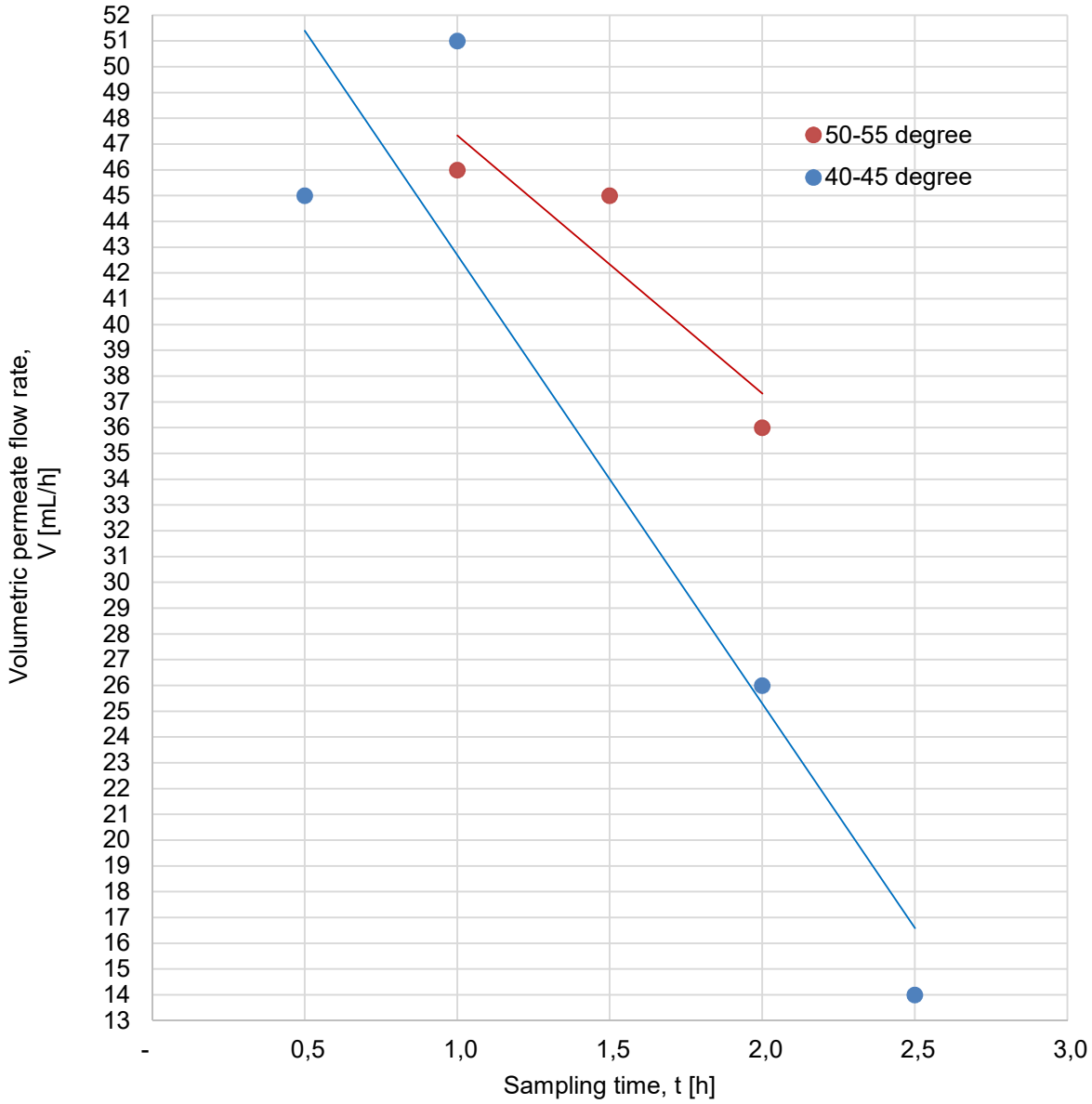

Fig. 2.: Comparison of volumetric permeate flux at 40-45 °C and 50-55 °C.

The density of the collected permeate samples was measured using a DMA 38 density meter (Anton Paar, Austria). Based on these measurements and with the use of a densimetric table for aqueous ethanol mixtures, the approximate alcohol content in the tested samples was estimated.

Tab. 2.: Density of permeate samples collected during pervaporation using the PV 4155-40 membrane.

Sample No.	Density [g/cm³]	Alcohol [% v/v]	Process duration [h]	Temperature [°C]
1A	0.9975	<1%	1.0	50
2A	0.9979	0%	1.5	50
3A	0.9979	0%	1.9	50
1B	0.9973	<1%	0.5	40
2B	0.9974	<1%	1.0	40
3B	0.9979	0%	1.5	40
4B	0.9980	0%	2.0	40
5B	0.9979	0%	2.5	40

The permeate was also subjected to chromatographic analysis using a GC-2014 gas chromatograph (Shimadzu, Japan) equipped with a flame ionization detector (FID) and an automated injection port (AOC-20). Data acquisition was carried out using the ChromaX1 2007 software (ver. 1.0b), and the results were processed with the Chr-mod1 2007 software (ver. 1.0). The column used for compound separation was a Zebron ZB-WAX plus (30 m length, 0.25 mm inner diameter).

The chromatograph operating parameters were as follows: injection port temperature – 250 °C, detector temperature – 250 °C, injection volume – 1 µL, split ratio – 2:1, helium as the carrier gas with a flow rate of 2 mL/min. The temperature program started at 40 °C (held for 2 minutes), followed by an increase to 60 °C at 5 °C/min, then to 240 °C at 15 °C/min, with a final hold at 240 °C for 5 minutes.

For each sample, chromatographic peaks with the highest areas were identified and are presented in Table 3.

Tab. 3.: Chromatographic analysis.

Peak No.	Retention time [min]	Compound	Peak area [µV·1/100 min]	Peak height [µV]	Peak width [min]	Calculated amount	Unit
SAMPLE NO. 1A							
A/1	1.913	Acetaldehyde	502727	52327	0.075	2.1613	mg/ml
A/2	2.513	Etanol	189269	14899	0.07	0.8137	mg/ml
A/3	2.932	Etanol	737908	54913	0.077	3.1724	mg/ml
A/4	3.253	Etanol	168305	8503	0.113	0.7236	mg/ml
SUMA			1598209	130642		6.871	0
SAMPLE NO. 2A							
A/1	2.502	Etanol	4218	530	0.058	0.0181	mg/ml
A/2	2.908	Etanol	230524	19212	0.065	0.9911	mg/ml
A/3	3.345	Etanol	57203	1703	0.308	0.2459	mg/ml
SUMA			291945	21445		1.255	0
SAMPLE NO. 3A							
A/1	1.908	Acetaldehyde	21637	2775	0.06	0.093	mg/ml
A/2	2.503	Etanol	44382	4226	0.06	0.1908	mg/ml
A/3	2.907	Etanol	192730	11737	0.065	0.8286	mg/ml
SUMA			258749	18738		1,112	0
SAMPLE NO. 1B							
A/1	2.507	Etanol	18038	1695	0.067	0.0775	mg/ml
A/2	2.933	Etanol	872804	73397	0.072	3.7524	mg/ml
A/3	3.328	Etanol	179221	5767	0.282	0.7705	mg/ml
SUMA			1070063	80859		4.6	0
SAMPLE NO. 2B							
A/1	1.905	Acetaldehyde	43116	12156	0.053	0.1854	mg/ml
A/2	2.503	Etanol	-22487	3388	0.043	-0.0967	mg/ml
A/3	2.922	Etanol	386593	48363	0.06	1.662	mg/ml
SUMA			407222	63907		1.751	0
SAMPLE NO. 3B							
A/1	1.9	Acetaldehyde	45946	6234	0.055	0.1975	mg/ml
A/2	2.498	Etanol	43438	6066	0.055	0.1868	mg/ml
A/3	2.905	Etanol	229618	19344	0.06	0.9872	mg/ml
SUMA			319002	31644		1.372	0
SAMPLE NO. 4B							
A/1	1.903	Acetaldehyde	955183	121757	0.06	4.1065	mg/ml
A/2	2.502	Etanol	257327	23883	0.06	1.1063	mg/ml
A/3	2.908	Etanol	411584	26656	0.07	1.7695	mg/ml
SUMA			1624094	172296		6.982	0
SAMPLE NO. 5B							
A/1	1.898	Acetaldehyde	187489	26058	0.052	0.8061	mg/ml
A/2	2.492	Etanol	95613	9474	0.053	0.4111	mg/ml
A/3	2.897	Etanol	281314	19835	0.063	1.2094	mg/ml
SUMA			564416	55367		2.427	0

Summary

Fig. 2 shows a trend: the volume of permeate collected during pervaporation decreases over time for both temperature ranges, 40–45 °C and 50–55 °C. When the process was carried out at the higher temperature range (50–55 °C), the permeate flow rate was greater compared to the lower temperature range (40–45 °C).

The density of the permeate collected in both temperature ranges was similar, with differences between samples remaining below 0.1%. The first collected samples contained a small amount of ethanol in both cases.

The gas chromatography results showed only a few peaks per sample, which may indicate that only a limited number of compounds passed into the permeate. Based on the retention time analysis, ethanol was identified, as the observed peaks had retention times close to that of the ethanol standard, which was 3.132 min under the applied chromatographic conditions.

References

[1] Brewers Journal. (2025, February 10). *Rising health consciousness fuels non-alcoholic beer industry growth projected to reach USD 43.9 billion by 2034*.

[2] Pater, A., & Frączek, D. (2024). *Biological methods for production of low alcohol beers*. Przemysł Fermentacyjny i Owocowo-Warzywny, 5(2024), 8–11.

[3] Castro-Muñoz, R. (2019). Pervaporation-based membrane processes for the production of non-alcoholic beverages. *Journal of Food Science and Technology, 56*, 2333–2344.

[4] Bodzek, M., & Konieczny, K. (1997). *Techniki membranowe w ochronie środowiska*. Wydawnictwo Politechniki Śląskiej.

[5] Konieczny, K., & Rychlewska, K. (2016). *MEMBRANE TECHNIQUES FOR THE SEPARATION OF VOCS AQUEOUS SOLUTIONS – PERVAPORATION.* Water Supply and Water Quality *(*pp. 583–604).

[6] Van der Bruggen, B., & Luis, P. (2015). Pervaporation. In *Progress in Filtration and Separation* (pp. 101–154). Elsevier. https://doi.org/10.1016/B978-0-12-384746-1.00004-5

Sustainable Valorization of Industrial Coffee By-Products Using Subcritical Water

Beatriz Monteiro[a], Pedro Lisboa[b], Alexandre Paiva[a], Pedro Simões[a]

[a]LAQV-REQUIMTE, Departamento de Química, Faculdade de Ciências e Tecnologia, Universidade Nova de Lisboa, 2829-516 Caparica, Portugal.

[b]Mocoffee Europe S.A., Rua da Logística Nº7, 2050-542 Vila Nova da Rainha, Portugal.

bg.monteiro@campus.fct.unl.pt

Introduction

Nowadays, there is growing interest in the valorization of waste and by-products from agrifood industries, not only by using them as alternative raw materials for different processes, but also to reduce their environmental impact. Most of these by-products are disposed or degraded, thus creating a pollution problem, yet these feedstocks hold large potential to produce added-value materials with applications in pharmaceutical, cosmetic and nutraceutical industries [1].

In the European coffee sector, the primary by-product generated during the roasting process is coffee silverskin (CS), a thin layer that covers the green coffee bean and detaches during roasting [2-3]. As Europe imports and roasts already-processed green coffee beans, silverskin is the main solid residue produced at this stage of the value chain.

In Portugal, coffee production reached 46 thousand tons in 2023. This volume of roasting generated an estimated 465 tons of coffee silverskin, which are typically discarded as waste, highlighting the potential of this by-product for valorization.[4]

Coffee silverskin is mainly composed by dietary fiber (cellulose, hemicellulose, and lignin), lipids, proteins and minerals [5-8]. Despite its promising composition, most chemical processes used to decompose lignocellulosic materials and extract polyphenols are time consuming, require the use of significant amounts of acid, alkali, and organic solvents, raising environmental concerns [9-10].

A promising alternative to these conventional methods is the use of subcritical water (SBW), i.e., liquid water at temperatures above 100°C and pressures above its vapor pressure [11-12]. Subcritical water presents interesting properties such as extraction and reaction solvent medium: it dissolves less polar compounds since its dielectric constant decreases as temperature increases (78 to 20 decrease from 20 to 300°C) [12]. Simultaneously, its ionic product increases significantly (pKw drops from 14 to 11.1

between 25°C and 259°C at 25 MPa), enhancing its ability to promote both acid- and base-catalyzed reactions [13].

It is an environmentally safer alternative process as it does not require the use and further disposal of added chemicals, is relatively fast, and has moderate energy requirements (water stays at liquid state so no vaporization occurs).[12]

Extraction of water-soluble extractives is efficiently achieved at low temperature range 100 - 140°C but further increase in temperature may lead to degradation of polyphenols. At temperatures ranging 140 - 230°C, SBW hydrolyses carbohydrates to monosaccharides, lignin to monolignols, lipids to fatty acids, and proteins to aminoacids [12].

Given its potential to treat and value agri-food residues, subcritical water emerges as a promising green technology for sustainable processing. This work focuses on assessing the sustainability of valorizing by-products from the coffee industry, particularly coffee silverskin, using subcritical water as an environmentally friendly solvent. In addition, it aims to develop a mathematical model of the subcritical water process, grounded in both experimental data and theoretical analysis.

Experimental

Initially, coffee silverskin was characterized in terms of its main compositional components, including lipids, carbohydrates, lignin, and ash content. SBW experiments were then carried out in a batch reactor system (Figure 1). The objective was to selectively extract and/or hydrolyze the biomass into distinct fractions by leveraging the tunable properties of subcritical water, and thus to evaluate the influence of key process parameters, such as temperature, residence time, and water-to-biomass ratio, on the composition and yield of the resulting hydrolysates. A first approach focused on extractions performed at temperatures ranging from 120°C to 280°C, with a fixed residence time of 10 minutes and a solid-to-liquid ratio of 1:10.

Fig. 1.: Lab-scale batch apparatus.

Summary

At this initial stage, subcritical water extraction proved to be an effective and environmentally friendly method for recovering bioactive compounds from coffee silverskin, with particularly high efficiency in extracting carbohydrate-rich fractions. Even with a short residence time of only 10 minutes, the process yielded favorable extraction results. These findings also revealed the transition point at which subcritical water shifts from functioning primarily as an extraction solvent to exhibiting hydrolytic and catalytic activity, demonstrating its tunable nature and broad applicability.

Following these initial results, the study will focus on a more detailed exploration of process conditions, such as residence time and solid-to-liquid ratio, to further optimize the extraction and hydrolysis of key components.

Acknowledgment

The authors would like to acknowledge the support from Associate Laboratory for Green Chemistry- LAQV which is financed by national funds from FCT/MCTES (UID/QUI/50006/2019). This work is supported by Fundação para a Ciência e a Tecnologia (FCT) through PhD grant 2024.01895.BDANA. The authors would also like to acknowledge Mocoffee Europe S.A. for kindly providing the coffee silverskin used in this study.

References

[1] M. Arshadi, T.M. Attard, R.M. Lukasik, M. Brncic, A.M. Da Costa Lopes, M. Finell, et al., Pre-treatment and extraction techniques for recovery of added value compounds from wastes throughout the agri-food chain, Green Chem. 18 (2016) 6160. Doi:10.1039/c6gc01389a

[2] Y. Narita and K. Inouye, “Review on utilization and composition of coffee silverskin,” 2014, Elsevier Ltd. doi: 10.1016/j.foodres.2014.01.023.

[3] S. M. F. Bessada, R. C. Alves, and M. B. P. P. Oliveira, “Coffee silverskin: A review on potential cosmetic applications,” Mar. 01, 2018, MDPI AG. doi: 10.3390/cosmetics5010005.

[4] European Coffee Federation, “European Coffee Report 2023-2024”.

[5] M. Machado et al., “Prebiotic potential of a coffee silverskin extract obtained by ultrasound-assisted extraction on Lacticaseibacillus paracasei subsp. paracasei,” J Funct Foods, vol. 120, Sep. 2024, doi: 10.1016/j.jff.2024.106378.

[6] M. Machado et al., “Bioactive Potential and Chemical Composition of Coffee By-Products: From Pulp to Silverskin,” Foods, vol. 12, no. 12, Jun. 2023, doi: 10.3390/foods12122354.

[7] V. Gottstein et al., “Coffee silver skin: Chemical characterization with special consideration of dietary fiber and heat-induced contaminants,” Foods, vol. 10, no. 8, Aug. 2021, doi: 10.3390/foods10081705.

[8] T. G. Toschi, V. Cardenia, G. Bonaga, M. Mandrioli, and M. T. Rodriguez-Estrada, “Coffee silverskin: Characterization, possible uses, and safety aspects,” J Agric Food Chem, vol. 62, no. 44, pp. 10836–10844, Nov. 2014, doi: 10.1021/jf503200z.

[9] M. Galbe, O. Wallberg, Pretreatment for biorefineries: A review of common methods for efficient utilisation of lignocellulosic materials, Biotechnol. Biofuels 12 (2019) 294. Doi:10.1186/s13068-019-1634-1.

[10] S.H. Mood, A.H. Golfeshan, M. Tabatabaeib, G.S. Jouzani, G.H. Najafi, M. Gholami, M. Ardjmand, Lignocellulosic biomass to bioethanol, a comprehensive review with a focus on pretreatment, Renew. Sustainable Energy Rev. 27 (2013) 77. Doi:10.1016/j.rser.2013.06.033.

[11] J. Zhanga, C. Wena, H. Zhanga, Y. Duana, H. Maa, Recent advances in the extraction of bioactive compounds with subcritical water: A review, Trends in Food Science & Technology 95 (2020) 183. Doi:10.1016/j.tifs.2019.11.018

[12] G. Ischia, H. Sudibyo, A. Miotello, J.W. Tester, L. Fiori, J.L. Goldfarb, Identifying the Transition from Hydrothermal Carbonization to Liquefaction of Biomass in a Batch System, ACS Sustainable Chemistry & Engineering 12 (2024) 11, 4539. Doi:10.1021/acssuschemeng.3c07731

[13] Martins-Vieira, J. C., Torres-Mayanga, P. C., & Lachos-Perez, D. (2023). Hydrothermal Processing of Lignocellulosic Biomass: an Overview of Subcritical and Supercritical Water Hydrolysis. In Bioenergy Research (Vol. 16, Issue 3, pp. 1296–1317). Springer. https://doi.org/10.1007/s12155-022-10553-8

Valorization of Banana Waste through Hydrothermal Extractions: Polyphenolic Compounds, Sugars and Sugar Alcohols

German Araujo-Barahona, Juan García-Serna, Tapio Salmi

Laboratory of Industrial Chemistry and Reaction Engineering, Åbo Akademi University,

Pressure Technologies group (PressTech), University of Valladolid,

german.araujobarahona@abo.fi

Introduction

Banana peels, a major by-product representing approximately 35% of the fruit's weight, account for over 40 million tons of waste annually worldwide, often discarded despite their richness in bioactive compounds such as phenolics, catecholamines (e.g., dopamine), dietary fibers, and free sugars [1.2]. In recent years, growing interest in sustainable valorization of agro-industrial residues has motivated research on the recovery of high-value compounds from banana peel for use in food, pharmaceutical, and materials applications [3,4].

This work explores a systematic strategy to valorize banana peels using hydrothermal and solvent-based extraction techniques on pilot scale. The study focuses on extracting and characterizing target molecules such as dopamine, L-Dopa, phenolic compounds, soluble sugars, and hemicelluloses under controlled conditions in a pilot-scale reactor. Particular attention is given to the influence of temperature, extraction time, and solvent composition on the yield and stability of the bioactive compounds.

Experimental

Bananas (*Musa acuminata Colla*) from discarded production were supplied by Fruta Viva Valladolid. The fruits were harvested on January 16, 2024, in Puntallana, Gran Canaria, Spain, and classified at ripening stage 4–5 according to the standard scale. A sequential approach was adopted to valorise the entire discarded fruit. The bananas were manually peeled, and the peels were cut into rectangular pieces (approx. 4 × 3 cm). These were loaded into a pilot plant equipped with five batch-operated reactors (2 L each), which were used to investigate the influence of process parameters on compound extraction. Initially, a 1:1 ethanol–water mixture was used to extract polyphenolic compounds at temperatures ranging from 45 to 75 °C. After this step, the reactors were emptied, and the solvent was replaced with water to perform hydrothermal extraction at 120 to 160 °C. In all cases, the

solvent-to-biomass ratio was approximately 2 (w/w). Liquid samples were collected at various time intervals to monitor extraction kinetics.

In parallel, part of the banana pulp was homogenised and mixed with an appropriate amount of water to prepare a slurry containing 10.57 wt.% total solids. This slurry was processed in a continuous Sudden Expansion Reactor (SER). The feed was pumped at an average flow rate of 10 kg/h through the SER, which had a length of 2 m and an internal diameter of 3.05 mm. Inside the reactor, the slurry was contacted with hot water to reach reaction temperatures of 280 °C, 340 °C, and 360 °C, under corresponding pressures of 170, 170, and 340 bar, respectively. Depressurisation was achieved using a needle valve, which induced a rapid pressure drop and cooling via the Joule–Thomson effect, effectively quenching the reaction and preventing thermal degradation.

The extract obtained from the 1:1 ethanol–water extraction at 65 °C was concentrated by rotary evaporation to a total solids content of 4 wt.%. It was then blended with equal amounts of maltodextrin and gum arabic to achieve a final mixture containing 15 wt.% total solids. This formulation was spray-dried using a GEA Mobile Minor™ (model MM Basic, Düsseldorf, Germany) equipped with a rotary atomizer. The atomization pressure was set at 0.6 MPa, with an air flow rate of 30 kg/h. Drying was performed at an inlet air temperature of 200 °C and an outlet temperature of 95 °C, using a feed rate of 1 kg/h.

The hydrothermal extract obtained at 140 °C and the processed pulp treated at 360 °C were subjected to a sequential ultrafiltration process. Four ultrafiltration membranes were employed: three Pellicon 2 Mini Biomax polymeric membranes (flat-sheet configuration, polyethersulfone material) with molecular weight cut-offs (MWCO) of 30, 10, and 5 kDa, each with a filtration area of 0.1 m²; and one Prep Scale-TFF membrane (spiral-wound configuration, regenerated cellulose) with a MWCO of 1 kDa and a filtration area of 0.23 m².

The extracts were analysed via high-performance liquid chromatograph (Hitachi Chromaster HPLC) equipped with a Bio-Rad HPX-87C carbohydrate column and a refractive index (RI) detector (Hitachi 5450 RI Detector). The injection volume was 10 µL, and the mobile phase consisted of a 1.2 mM calcium sulphate solution at a flow rate of 0.6 mL/min while the column temperature was maintained at 50 °C. The total phenolic compounds of the extracts were estimated using the Follin-Ciucalteou method, using gallic acid as reference. The molecular weight of the extraction solutions was assessed using size exclusion chromatography (HPLC-SEC). A GPC column (SB-803 HQ; Shodex) with a guard column (SB-G; Shodex) was maintained at 35 °C. The mobile phase comprised

NaNO3 0.1 M + NaN3 0.02% in Milli-Q water, with a flow rate of 0.5 mL/min. A Waters IR 2414 detector was used. Polyethylene glycol of different molecular weight was dissolved in Milli-Q water, covering a weight-average molecular weight range from 0.4 to 20 kDa. For the quantification of dopamine, L-Dopa, and α-tocopherol, a known quantity of extract was diluted in methanol and filtered through a 0.22 µm nylon syringe filter prior to chromatographic analysis. Analyses were carried out using an HPLC system equipped with a UV detector and a Daicel ChiralPak IB column. Methanol was used as the mobile phase, at a flow rate of 1 mL/min. The column was maintained at 42 °C.

Summary

The yield profile of total extracted compounds from the processed banana peels using the ethanol–water mixture is shown in Fig. 1(a), together with the corresponding temperature profiles. The distribution of the compounds detected in the experiment conducted at an average temperature of 80 °C is presented in Fig. 1(b). Overall, the extraction process is clearly enhanced by increasing the temperature, as reflected by higher concentrations of solubilised material in the liquid phase. High-performance liquid chromatography (HPLC) revealed the presence of several soluble sugars, including fructose, glucose, sucrose, and cellobiose, which are likely released from both the residual pulp and hemicellulosic fractions of the banana peel.

The total phenolic content followed an increasing trend with extraction time (Fig. 1(c)), with no evidence of degradation under the tested conditions, suggesting that the phenolic compounds present in the peel matrix exhibit thermal stability within the studied temperature range. This observation is further supported by the monotonic relationship between phenolic content and total extractives shown in Fig. 1(d). Additionally, bioactive compounds in the ethanol–water extract obtained at 65 °C confirmed the presence of dopamine (1089.85 ppm), L-Dopa (75.17 ppm), and α-tocopherol (57.39 ppm).

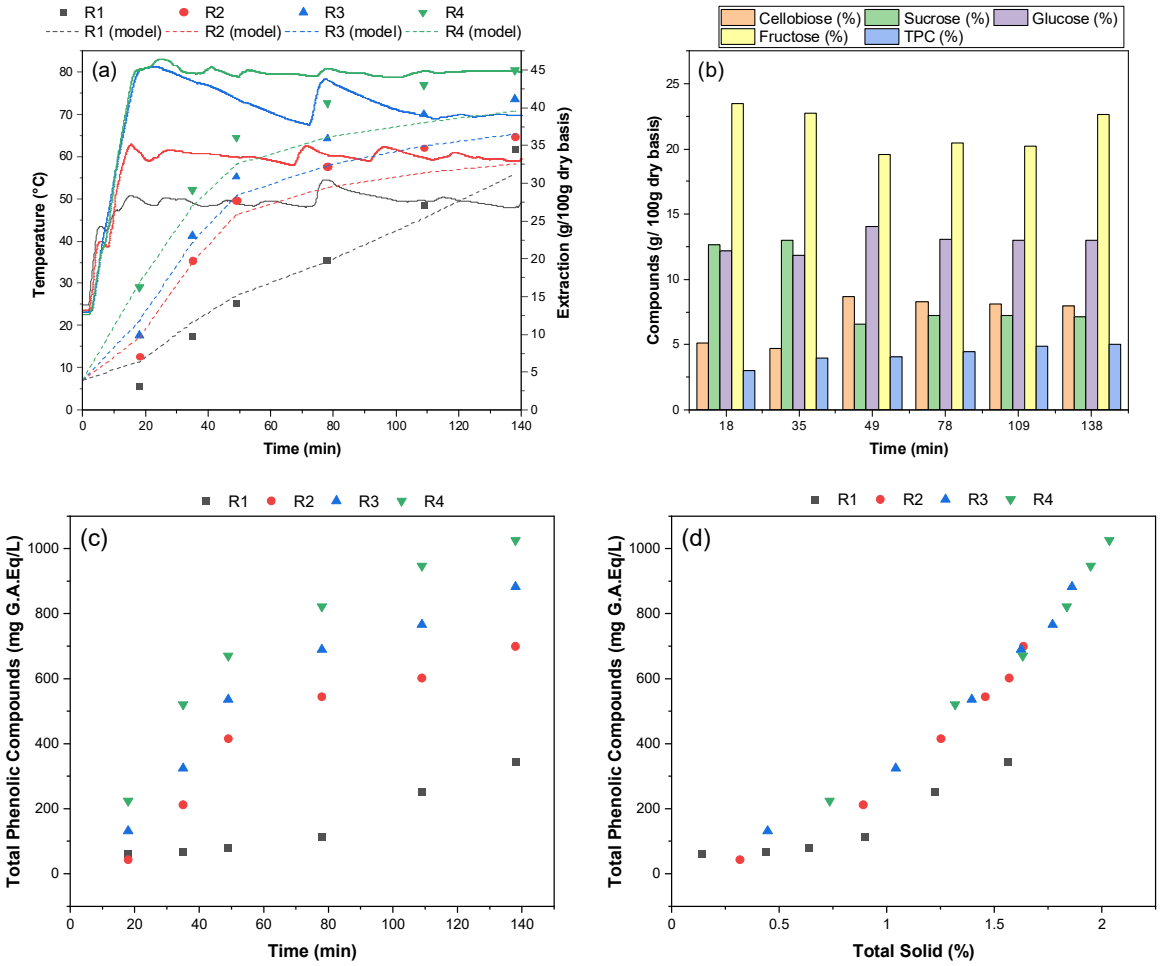

Fig. 1.: Extraction experiments carried with banana peels using 1:1 ethanol/water mixture in batch extractions: (a) profile of extractives in the liquid phase and temperature profile, (b) distribution of detected compounds as a function of time for experiment at 80°C, (c) evolution of total phenolic compounds, (d) total phenolic compounds vs total solids.

Fig. 2 shows the scanning electron microscopy (SEM) image of the microcapsules obtained from the spray-drying of the ethanol–water extract at 65 °C. The microcapsules exhibited a predominantly spherical morphology, with minimal deformation and a smooth surface, indicating good encapsulation conditions and structural integrity. The stability of total phenolic compounds (TPC) during storage at 4 °C was evaluated over time and compared with the non-encapsulated extract. As shown in Fig. 2(b), the encapsulated polyphenols demonstrated good stability throughout the monitored shelf-life, while the liquid extract experienced a significant degradation, losing approximately 40% of its TPC after 57 days.

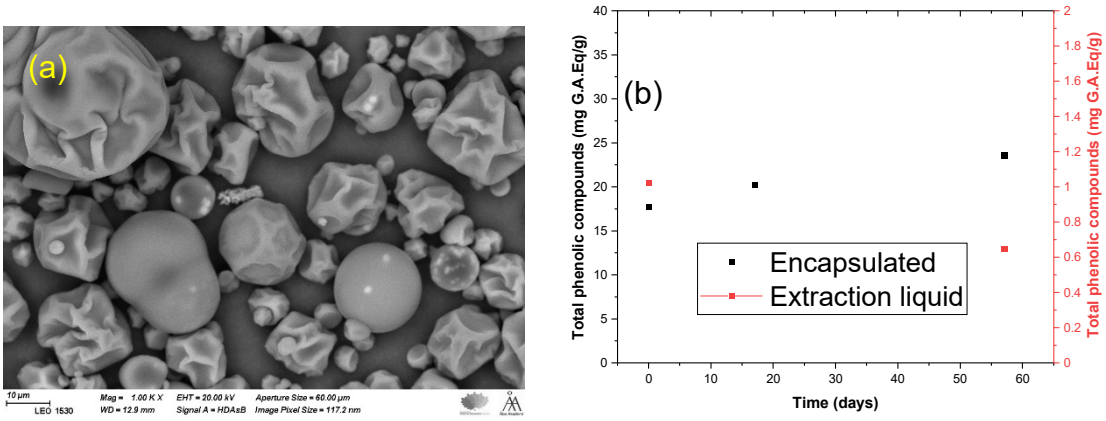

Fig. 2: scanning electron microscopy (SEM) image of the microcapsules obtained from the spray-drying of the ethanol–water extract at 65 °C

The results of the hydrothermal extraction of banana peels are shown in Fig 3. As observed, the process is highly temperature-dependent, with significant hydrolysis only occurring at 160 °C within the screened time window—particularly after 2 hours of exposure. At this temperature, partial degradation of the released sugars was also observed, as illustrated in Fig. 3(b), indicating that prolonged exposure to high temperatures may compromise the integrity of the extracted compounds. For applications that require the preservation of hemicelluloses and pectins, milder thermal conditions (e.g., around 140 °C) and extended extraction times are recommended.

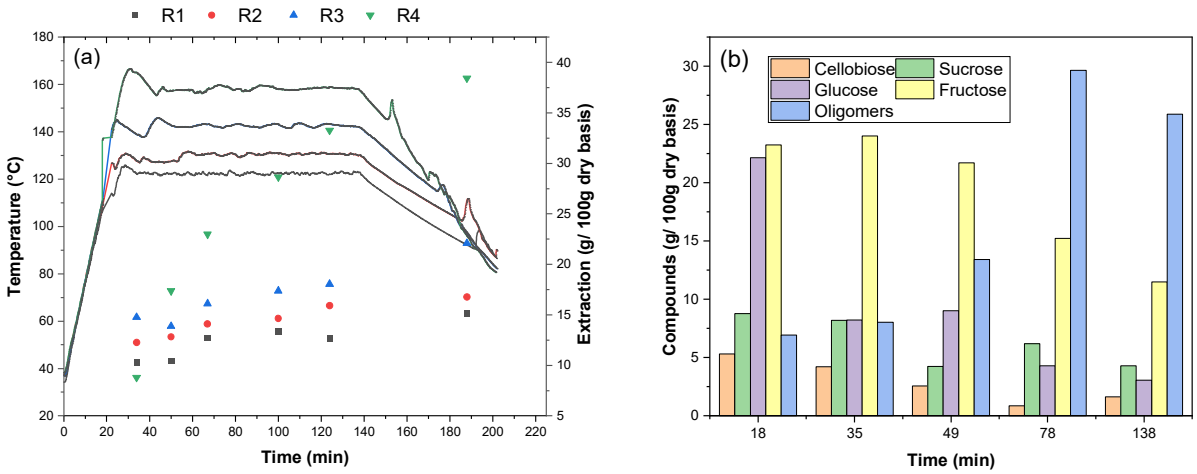

Fig. 3.: Hydrothermal extraction of banana peels: (a) profile of extractives in the liquid phase and temperature profile, (b) distribution of detected compounds as a function of time for experiment at 160°C.

The extraction performed with banana pulp under continuous operation resulted in significantly more concentrated extracts. This is attributed to the ability of the technology to process the biomass as a slurry, enabling effective contact with the solvent and achieving a higher degree of hydrolysis. Importantly, this was accomplished with minimal

formation of undesired by-products, owing to the short residence time characteristic of the system. Following the extraction, ultrafiltration allowed for the separation of low-molecular-weight fractions, yielding a solution primarily composed of monomeric and dimeric sugars. These fractions are of particular interest for future production of sugar alcohols, which are valuable in the pharmaceutical and food industries. The molecular weight distribution of the extracted compounds. was assessed by size exclusion chromatography (SEC), clearly showing the removal of high-molecular-weight compounds (Fig. 4).

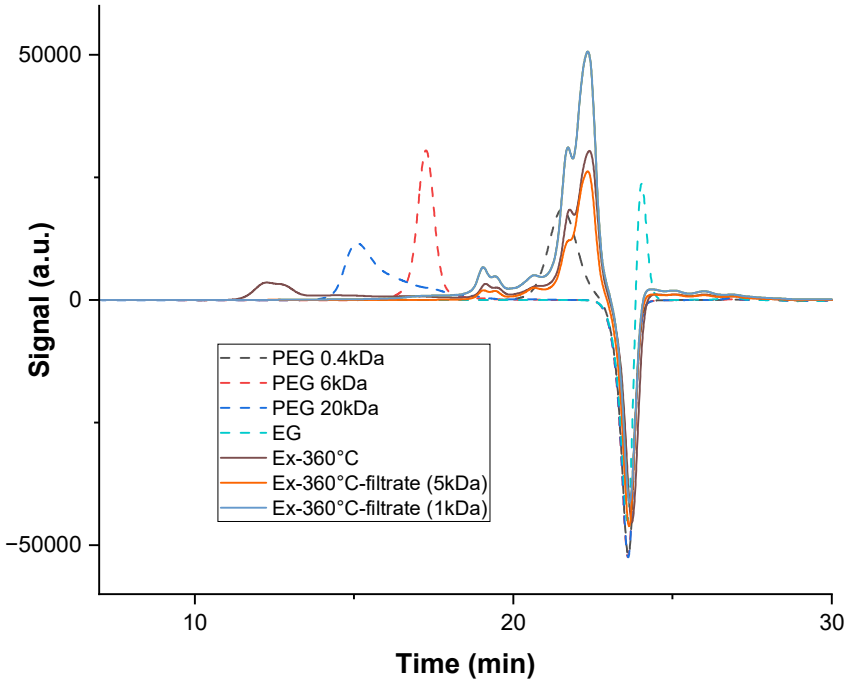

Fig. 4. Size exclusion chromatography (SEC) profiles of the extract obtained from banana pulp processed at 360 °C and 340 bar under continuous operation, and corresponding permeates from the sequential ultrafiltration steps.

Acknowledgment

The research visit to the University of Valladolid, which made this research possible, was financed by the Åbo Akademi Graduate School through the Finland Talent Boost program (German Araujo Barahona).

References

[1] Sidhu, J. S., & Zafar, T. A. (2018).. Food Quality and Safety, 2(4), 183–188.

[2] Kabir, M. R., et al. (2021). J. Food Process. Preserv., 45(3), e15191.

[3] Cegledi, E., et al. (2024). Molecules, 29(15), 3672.

[4] Pereira, M. A. F., et al. (2021). Bioprocess Biosyst. Eng., 44, 297–306.

In-Depth Analysis of the Phytochemical and Bioactive Profile of Adriatic Sea Algae with an Emphasis on *Fucus virsoides*

Kristina Perišić

Faculty of Food Technology Osijek, Josip Juraj Strossmayer University of Osijek,

kperisic@ptfos.hr

Introduction

The significant relationship between the algal phytochemical profile and the habitat conditions is well known. Salinity changes, high solar radiation levels, and adverse climatic conditions induce the release of bioactive compounds by these macro-organisms. In this context, the Adriatic Sea is notable for its high solar irradiance, a high salinity gradient, and for being a hotspot in terms of multiple climatic hazards. Thus, although a relevant concentration of the phytochemical arsenal of macroalgae inhabiting the Adriatic Sea can be assumed, the characterisation of its diverse species has been little explored. In this context, 12 Adriatic Sea algal species are explored, including 7 brown algae (*Ericaria amentacea,* ***Fucus virsoides****, Cutleria multifida, Cystoseira compressa, Cystoseira corniculata, Gongolaria barbata*, and *Padina pavonica*), 3 green algae (*Codium adhaerens, Codium vermilara,* and *Ulva lactuca*) and 2 species of red algae of the genus *Asparagopsis* catalogued as invasive, but with an important bioactive potential, so their use in industrial applications could be a suitable strategy to reduce their population. The species are shown in Fig. 1.

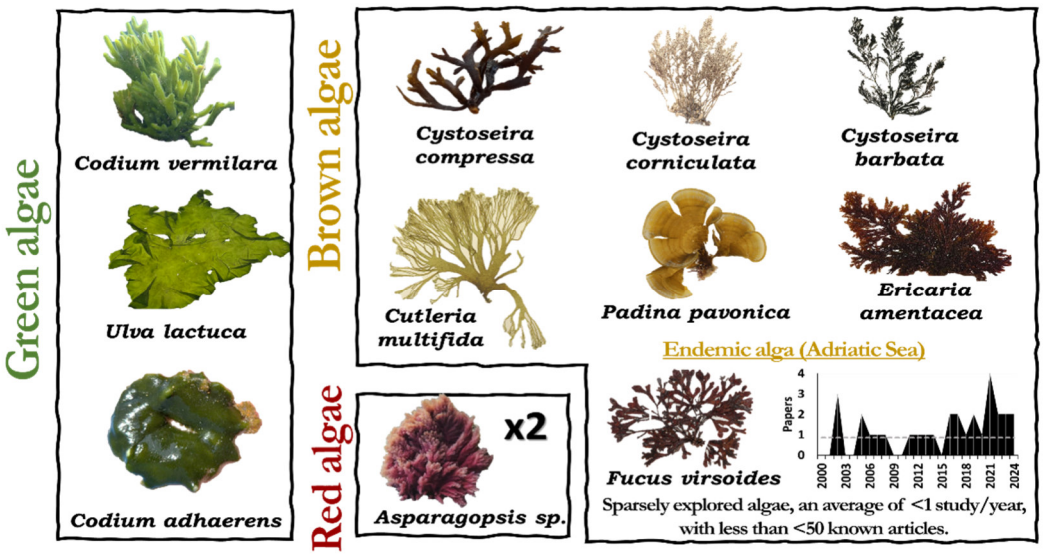

Fig. 1: Twelve Adriatic Sea algae Species

Experimental

In accordance with previous research, matrix solid phase dispersion (MSPD) is proposed as an extraction technique, using solvents generally recognised as safe (GRAS) to obtain algal extracts without prior drying pre-treatments. In addition to that, this technique is considered environmentally friendly based on its greenness degree (Castillo et al. 2023).

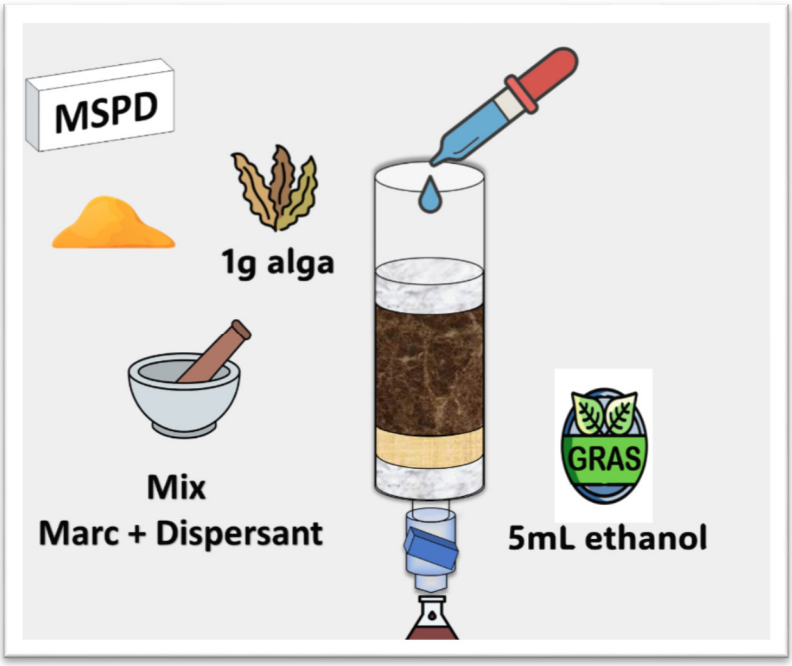

Fig. 2: Matrix Solid Phase Dispersion

The extracts were analysed by quantifying their total polyphenolic content TPC and antioxidant activity using ABTS method. A bioactive response of these 12 species is shown for the first time, revealing a significant response of the polyphenolic content.

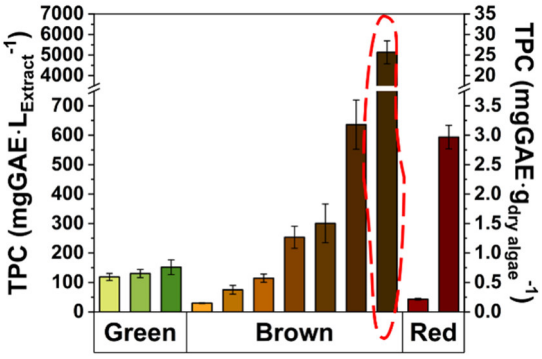

Fig. 3: Total Phenolic Content (TPC) of 12 Algal Species

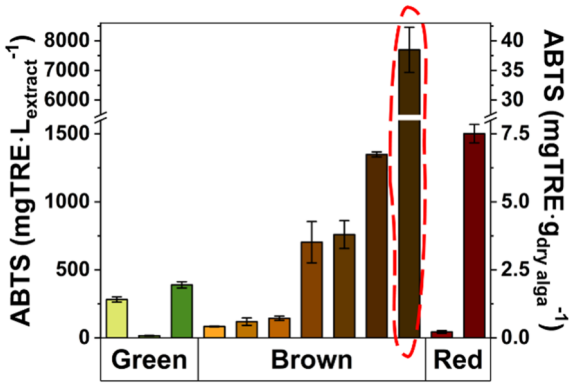

Fig. 4: Antioxidant Activity (AA) of 12 Algal Species

A proportional response of polyphenolic content (TPC) and antioxidant activity (AA) is detailed, assuming this antiradical activity to the content of phenolic compounds in the algae. *Fucus virsoides* is shown to be far superior. This alga, endemic to the Atlantic Sea, shows an order of magnitude higher than the other species evaluated with a TPC of 26 mgGAE·g -1 (2.6%) and AA 38.5 mgTRE·g -1 (3.8%).

Furthermore, a targeted analysis of more than 50 phenolic compounds was performed using LC-MS/MS, detecting 19 of them, with 7-hydroxycoumarin, narigenin and hydroxybenzoaldehyde derivatives being the most present in the green algae, in the brown algae hydroxybenzoic, chlorogenic and rosmarinic acid derivatives, and in the red algae myricetin and quercetin as shown in Fig. 5.

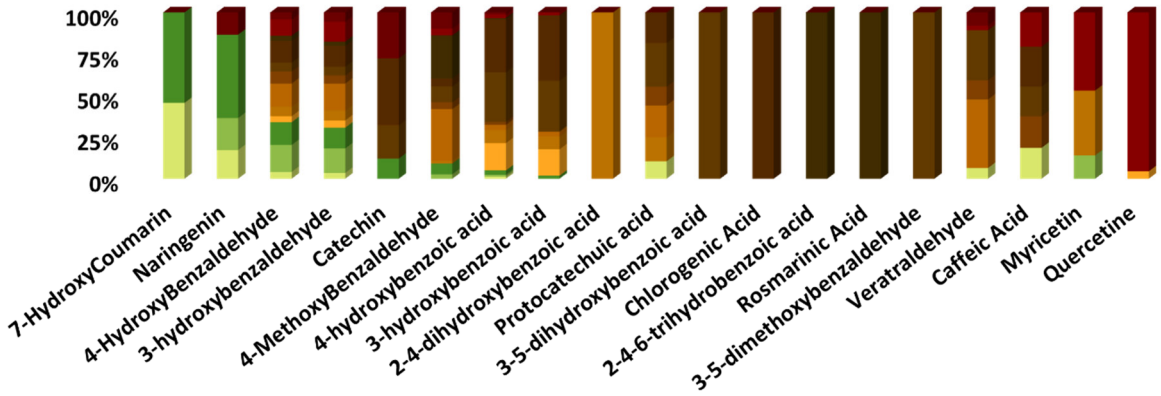

Fig. 5: Polyphenolic Profile of 12 Green, Brown and Red Algal Species

As *Fucus virsoides* demonstrated the strongest bioactivity, it was selected for further in-depth analysis aimed at evaluating its suitability for pharmaceutical or nutraceutical development. In addition to the MSPD method, the ultrasound-assisted extraction method (UAE) was also used for obtaining extracts rich in polyphenolic compounds. The effectiveness of these two extraction methods was evaluated based on the TPC and AA results shown in Fig. 6.

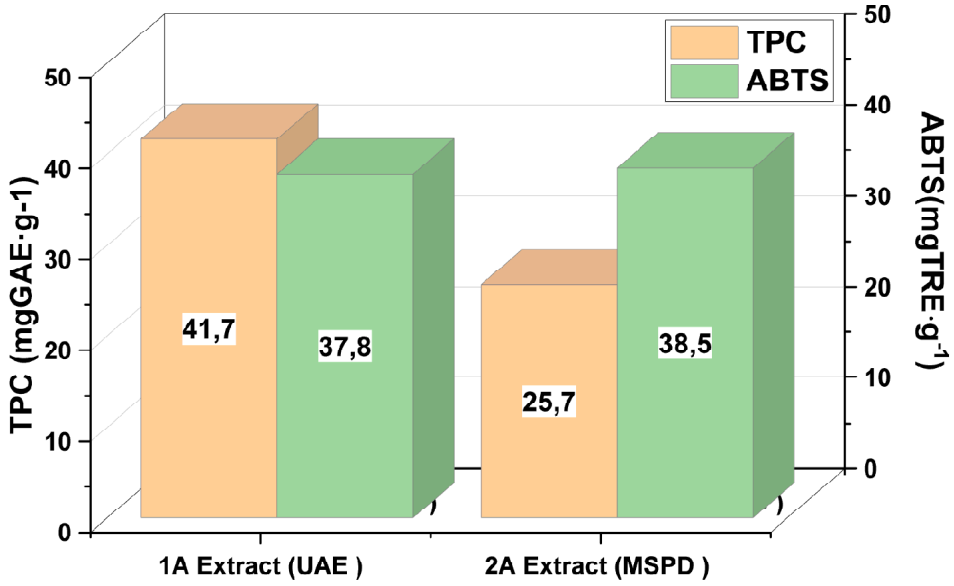

Fig. 6: Comparison of Ultrasound-assisted and Matrix Solid Phase Dispersion Extraction Methods

While the antioxidant activity was comparable between both extracts, the total phenolic content (TPC) obtained via MSPD was significantly lower than that of the UAE extract. Nevertheless, this suggests that MSPD may be more efficient at selectively extracting phenolic compounds with high antioxidant activity, despite the lower overall phenolic yield.

To determine the polyphenolic profile of *Fucus virsoides* LC-MS/MS technique was used once again. Since 4-methoxybenzaldehyde was the most present compound in *Fucus virsoides*, relative concentrations of the polyphenols present in relation to 4-methoxybenzaldehyde are shown in Fig. 7. The next compound present in significant concentrations was 4-hydroxybenzaldehyde followed by 2-4-6-trihydroxybenzoic acid.

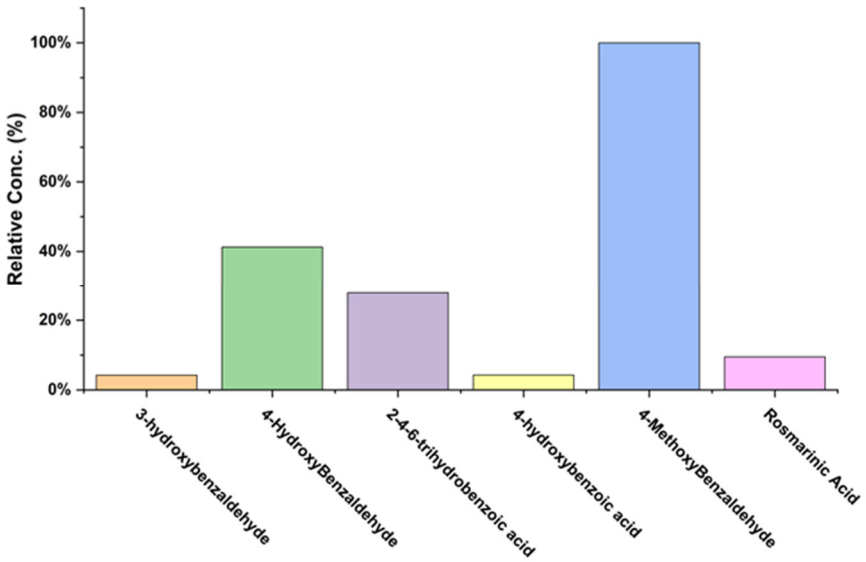

Fig. 7: Polyphenolic Profile of *Fucus virsoides*

Additionally, an untargeted analysis was performed using ultra-high-performance liquid chromatography quadrupole time-of-flight (UHPLC-QToF) revealing compounds highly specific to sea algae as can be seen in Fig. 8.

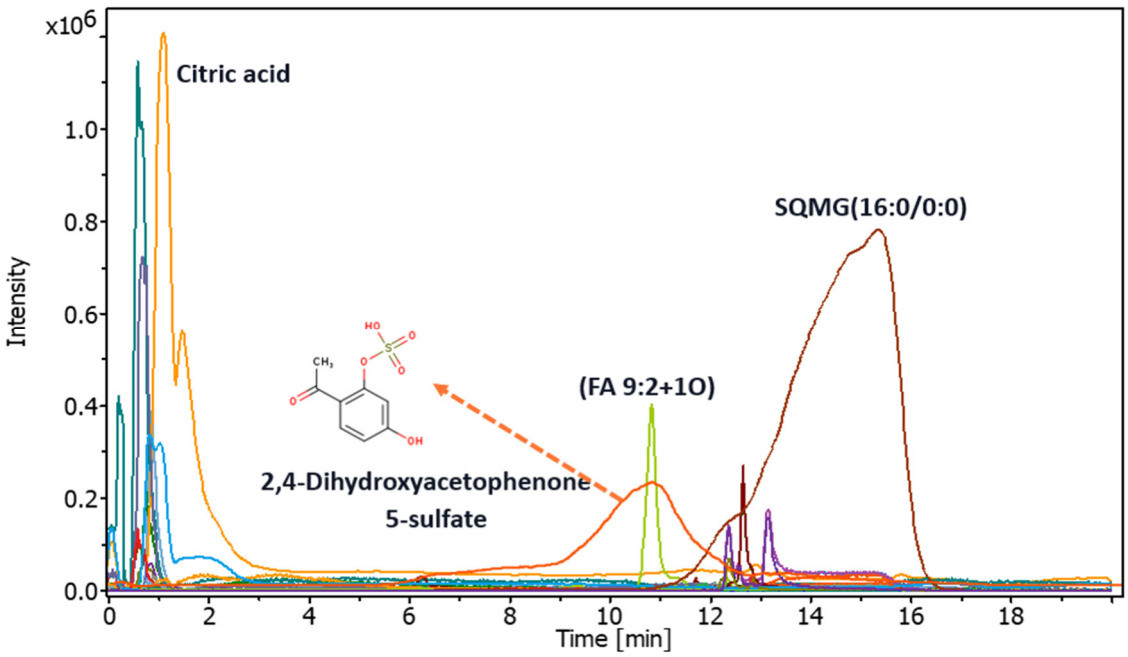

Fig. 8: Compound Profile from Untargeted Analysis of *Fucus virsoides*

Summary

This study focuses on the Adriatic Sea macroalgae, with an emphasis on *Fucus virsoides*, which, despite its biological value, remains insufficiently studied. As a representative of brown algae, it is a rich source of bioactive compounds, including complex polysaccharides, polyphenols, fatty acids, and vitamins, which may have significant health benefits. For the isolation of bioactive compounds, a green solvent ethanol/water in a 1:1 volume ratio was used, as well as two environmentally friendly extraction methods: ultrasound assisted extraction (UAE) and matrix solid phase dispersion (MSPD Spectrophotometric methods TPC, DPPH, and ABTS were used to determine the total phenolic content and antioxidant activity of the extracts. The phenolic profile was analysed using liquid chromatography coupled with tandem mass spectrometry (LC-MS/MS). Furthermore, UHPLC-QToF was used to identify new compounds, which provided detailed insight into the chemical composition of the algae. The results obtained as part of this research can be used as a database on the bioactivity and analytical profile of these mostly understudied algae, showing their potential as a natural source of functional compounds.

Acknowledgment

We would like to thank Croatian Government and the European Union through the European Regional Development Fund - the Competitiveness and Cohesion Operational Programme (KK.01.1.1.01) for funding The Scientific Centre of Excellence for Marine Bioprospecting - BioProCro.

References

Castillo, Aly, Maria Celeiro, Marta Lores, Kristina Grgić, Marija Banožić, Igor Jerković, i Stela Jokić. 2023. „Bioprospecting of Targeted Phenolic Compounds of Dictyota Dichotoma, Gongolaria Barbata, Ericaria Amentacea, Sargassum Hornschuchii and Ellisolandia Elongata from the Adriatic Sea Extracted by Two Green Methods“. *Marine Drugs* 21 (2): 97. https://doi.org/10.3390/md21020097.

Hydrothermal Chemical Recycling of Polycondensation Polymers: Development and Deconvolution-Assisted Examination

Mihály Hegyi, János Béri, Zsigmond Morvay, Edit Székely

Department of Environmental and Chemical Process Engineering, Faculty of Chemical Technology and Biotechnology, Budapest University of Technology and Economics,

edit.szekely@edu.bme.hu

Introduction

Hydrothermal processes are a collection of technologies where water is used as a solvent at temperatures beyond the atmospheric boiling point. At elevated temperature, increased pressure ensures that water remains in the liquid state. Water is most commonly used under subcritical conditions, which refers to the loosely defined temperature and pressure range slightly below supercritical conditions. While water is in its liquid state under subcritical conditions, its important physical-physicochemical parameters such as density, polarity or rate of autoprotolysis change significantly as a function of temperature and pressure. This means that hydrothermal systems are suitable for a wide variety of processes ranging from synthesis of nanostructured materials to waste conversion. [1–3] Along with unique hydrothermal processes, the benefits of the hydrothermal environment can be exploited in already existing technologies to substitute harmful, toxic, costly or otherwise problematic solvent systems.

Waste conversion is a rapidly broadening field for hydrothermal processes. As the many issues caused by the overuse of natural resources gain increasing recognition, the need to lessen impact on the environment drives interest in waste conversion technologies, ranging from utilisation of agricultural waste to efforts to recover material from plastic waste.[4,5]

The most common way of recovering polymeric material is physical recycling, which usually is based on the remelting of the polymer. While it is relatively simple and, in some cases, even economically competitive, both the recyclable waste streams and the quality of the recovered material are severely limited. This led to a surge in the development of chemical recycling processes to obtain valuable material streams, substances by the decomposition of the end-of-life polymers. Controlled decomposition and high selectivity result in better efficiency in recycling, which is both crucial for waste reduction and economic viability.

Controlled decomposition is a viable strategy when dealing with polycondensation polymers, as the heteroatoms of the main chain provide an opportunity for selective cleavage to yield the monomers, which in turn can be intensively purified and then directly used to synthesize new polymers of virtually any quality.

This process, the chemolytic recycling of polycondensation polymers is most commonly performed in organic solvents such as methanol or ethylene glycol. While this means decomposition at milder conditions (as low as 180-240°C in case of polyethylene terephthalate[6] and 80-150°C in case of poly(bisphenol A carbonate)[7]), it also necessitates the usage of high amounts of organic, fossile-based solvents, which raises environmental concerns and operational hazards alike. In contrast, in hydrothermal recycling, the used solvent is water. The main challenge in the development of hydrothermal chemical recycling processes is to develop technologies that can be considered competitive in comparison with organic solvent-based chemolysis.

In this work, we present how properly designed non-stationary processes such as decomposition in semi-continuous reactors can overcome many of the challenges present in the field of hydrothermal chemical recycling. We present a uniquely designed semi-continuous reactor system that can be used for the rapid, efficient, and selective monomer recovery from polycondensation polymers such as polyethylene terephthalate (PET) or poly(bisphenol A carbonate) (PC).

A significant challenge when developing such processes is that for hydrothermal decomposition, most kinetic studies are based on batch reactor experiments. While it can be used to design flow systems to some extent, the overall decomposition process usually incorporates mass transfer steps, that are reflective of the experimental setup, which is usually highly unique. For both design of such systems, and correct interpretation of the experimental results, we must strive for reported data as indifferent of the exact setup as possible. This is especially true for complex setups with coolers, mixers and other following units characteristic for hydrothermal reactors. These units usually does not influence the hydrothermal reactions directly as they are usually located downstream in relation to the reactor. On the other hand, their presence significantly influence product concentration profiles at the end of the whole system and in turn the behaviour and measurable performance of the setup. For the sake of increasing interpretability and usability of results acquired by ex-situ measurements in hydrothermal flow systems, the effects of the follow-up units must be minimised on the experimental results.

In this work, we present how residence time distribution (RTD) measurements coupled with deconvolution can aid the recovery of information on concentration in a hydrothermal reactor from ex-situ results. As no established universal method exists for the mathematical operation of deconvolution, an algorithm and software were developed for the task.

Experimental

First, an in-house developed reactor system is presented, with which the controlled hydrothermal decomposition of some polyesters is examined. (Fig. 1.)

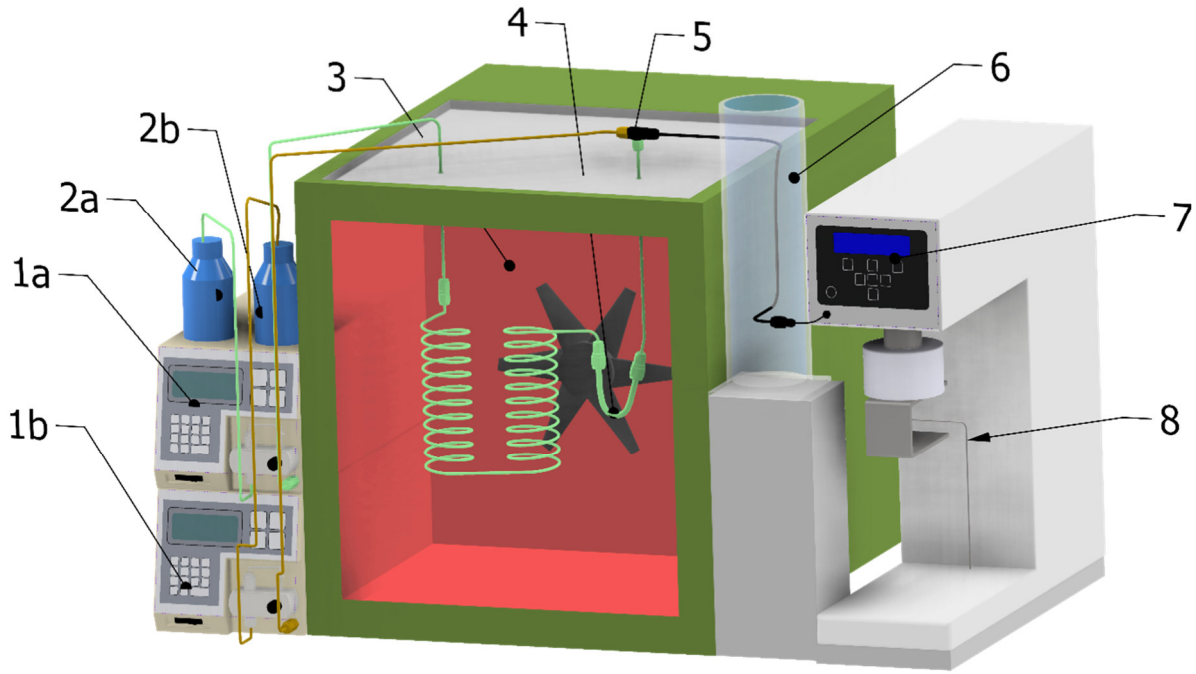

Fig. 1. Schematic of the experimental setup. 1a, 1b: HPLC pumps, 2a, 2b: reservoirs of main stream (water) and sidestream (NaOH solution) respectively, 3: air thermostat, 4: reactor, 5: mixing point of sidestream, 6: cooler, 7: back pressure regulator, 8: exit point. Based on Ref. 8.[8]

During chemical recycling of PET, the otherwise untreateable waste PET streams are selectively hydrolysed to yield the monomers terephthalic acid (TPA) and ethylene glycol (EG). At the temperature range of 250-300°C and pressures between 10-30 MPa, PET chains are rapidly hydrolysed, with the time of total conversion falling between 15-30 minutes without the aid of catalysts. The parameter range is set so that both products are stable and as such high recovery with good purity can be achieved. The main challenge

of the work besides finding optimal parameters for efficient chemolysis lies in the consequences of the semi-continuous setup. While the constant exchange of water in the reactor enhances the decomposition reaction, it also creates a potential operational instability, as the main product TPA's solubility diminishes while the product solution cools to room temperature from hydrothermal conditions. To allow stable operation, an alkaline side-stream is used to stabilise the products in salt form. With the presented setup, total conversion and preparative yields above 92% in respect to TPA content were achieved at 300°C and 12 MPa under less than 20 minutes of total reaction time and approximately 1 minute average water residence time in the hydrothermal section. The purity of the recovered TPA exceeds 99% without additional purification steps.[9]

The same semi-continuous hydrolysis process was successfully applied to the more challenging chemical recycling of PC. In case of PC, the main target monomer, the Bisphenol A (BPA), itself is unstable under the conditions of the decomposition. The semi-continuous setup therefore presents an advantage to batch reactors: constant solvent flow means the constant removal of the unstable product from the reactive environment, as BPA is dissolved in water at hydrothermal conditions. Using already available kinetic data[10], the system could be planned in such a way, that the decomposition of the product was limited without having to compromise total decomposition time and as such conversion of the polymeric feedstock. As BPA, similarly to TPA, has poor solubility in ambient water, solution-stabilisation is also necessary. In the designed reactor system, total conversion of PC was achieved under 70 min at 300°C, with the obtained BPA crystals having a purity of 94% with phenol as the only identifiable contaminant, showcasing the effective control on the decomposition achieved by controlling the residence time in the reactor.[8]

In case of both polyesters, it was found that semi-continuous hydrolysis coupled with alkaline solvent stabilisation resulted in simple and efficient product recovery, stable operation, and in most cases faster reaction than any of the batch hydrothermal systems. The non-catalytic route is also beneficial as it permits the utilisation of possibly contaminated waste plastic as feedstock, which is one of the most important tasks for chemical recycling. Both studies highlight that pressure in the region of 10-30 MPa does not influence the progress of decomposition significantly, and its role practically exhausted by keeping water in the liquid state.

Further investigation of these decomposition reactions required us to gather time-related information on the product concentrations in the system. While the most relevant to the

reaction itself would be the development of product concentration in the reactor, or at the end of the hydrothermal section of the system, direct measurement in the hydrothermal environment is difficult. In contrast, ex-situ measurement of concentration is easy, however, data gathered from ex-situ measurements must be correlated to conditions in the reactor.

With properly designed experimental conditions, the connection between concentrations in the reactor and data gained by ex-situ measurements can be drawn with the aid of the residence time distribution of various segments of the setup. With the measurement of these distributions, approximate concentration profiles in the reactor can be calculated by the mathematical method of deconvolution. As there is no obvious or established best process for deconvolution, a calculation algorithm suitable for this task, and its implementation in Python was developed, with which a better understanding of the hydrothermal system can be reached. With deconvolution, the residence time distribution of the reactive segment was approximated without the need to directly measure in the hydrothermal environment. Moreover, investigation on the plausibility of approximating RTDs of hydrothermal system components from ex-situ measurements was investigated via tracer-based experiments. The proposed deconvolution method, while not suitable to calculate the perfectly accurate concentration profiles, is able to approximate concentration profiles in the reactor with acceptable accuracy.

Summary

Hydrothermal decomposition as a way of chemical recycling of polymers presents unique issues and opportunities. Hydrolytic decomposition creates the opportunity to effectively and selectively regain monomers from polycondensation polymers such as PET or PC without the need for organic solvents or catalysts. While the problematic feeding of polymers, especially contaminated streams, to elevated pressures renders a continuous setup problematic, semi-continuous reactors are a suitable compromise between the advantages and drawbacks of batch and continuous reactors. Studies on PET and PC showed that the continuous exchange of water over the polymer accelerates decomposition reactions, as the products are sufficiently soluble in subcritical water and as such can be carried out from the reactor. The recovery of unstable intermediers is also possible since the residence time of these molecules can be effectively controlled in a semi-continuous reactor by the appropriate choice of flowrates. Our experiments on the hydrothermal decomposition of PET and PC yielded above 90% conversion, excellent

yield, and above 94% purity in the recovered crystals for the target monomers. Under 300°C and 10-30 MPa pressure PET and PC can be completely hydrolysed under 16 and 70 minutes respectively, which are both competitive with already existing, organic solvent-based and catalytic methods.

The deeper understanding of semi-continuous flow reactors is aided by residence time measurements, and subsequent deconvolution of these RTDs from the end-of-pipe concentration profiles. An algorithm and software were developed, with which the special case of deconvolution representative of this case can be effectively calculated.

The presented methods are a promising way to develop hydrothermal chemical recycling technologies for polycondensation polymers, which would prove invaluable in the effort of reducing plastic waste and improving the circular economy of fossil-based materials.

Acknowledgment

Project no. TKP2021-EGA-02 has been implemented with the support financed the research under the TKP2021-EGA funding scheme. Research of Mihály Hegyi was supported by the Doctoral Excellence Fellowship Programme (DCEP) is funded by the National Research Development and Innovation Fund of the Ministry of Culture and Innovation and the Budapest University of Technology and Economics. Participation of Mihály Hegyi at the ERASMUS+ BIP ESS-HPT 2025 "The European Summer School in High Pressure Technology" was financed by the ERASMUS+ program of the European Union.

References

1 E. Galiwango, M. Beaulne, J. Butler, W. Ma, K. Austin and S. Lotfi, *Int. J. Hydrogen Energy*, 2024, **87**, 1389–1403.

2 C. Wang, Z. Wang, X. Wang, N. Li, J. Tao, W. Zheng, B. Yan, X. Cui, Z. Cheng and G. Chen, *Processes*, DOI:10.3390/pr10112439.

3 D. A. Peixoto, S. C. Silva, P. H. S. Borges, R. C. Lima and E. Nossol, *J. Mater. Sci.*, 2023, **58**, 2993–3024.

4 A. Moustafa, K. Abdelrahman, A. Abdelhaleem and I. S. Fahim, *J. Anal. Appl. Pyrolysis*, DOI:10.1016/j.jaap.2025.107112.

5 M. H. Marzbali, S. Kundu, P. Halder, S. Patel, I. G. Hakeem, J. Paz-Ferreiro, S. Madapusi, A. Surapaneni and K. Shah, *Chemosphere*, 2021, **279**, 130557.

6 L. Umdagas, R. Orozco, K. Heeley, W. Thom and B. Al-Duri, *Polym. Degrad. Stab.*, 2025, **234**, 111246.

7 R. Piñero, J. García and M. J. Cocero, *Green Chem.*, 2005, **7**, 380–387.

8 J. Béri, M. Hegyi, B. Tóth and E. Székely, *J. Supercrit. Fluids*, 2025, 106610.

9 J. Béri, M. Hegyi, A. Menyhárd and E. Székely, *Chem. Eng. J.*, DOI:10.1016/j.cej.2024.154601.

10 S. E. Hunter and P. E. Savage, *J. Org. Chem.*, 2004, **69**, 4724–4731.

UPea Project – Upcycling Pea Waste Side Streams for Developing Future Food Ingredients

Davide Bonaldo[1]*, Stella Plazzotta[2], Francesca Bot[3], Alessandro Zambon[1]**

[1] Department of Civil, Chemical, Environmental and Materials Engineering (DICAM), University of Bologna, Via Umberto Terracini 28, 40131, Bologna, Italy

[2] Department of Agricultural, Food, Environmental and Animal Sciences University of Udine, Via Sondrio 2/A, 33100, Udine, Italy

[3] Department of Food and Drug, University of Parma, Parco Area delle Scienze 27/A, 43124, Parma, Italy

*davide.bonaldo2@studio.unibo.it **alessandro.zambon2@unibo.it

Introduction

Each year in the European Union, 15% of processed peas are discharted due to damage and imperfections, resulting in approximately 135‘000 tons of pea waste annually. The current method of managing damaged peas, anaerobic digestion, leads to the loss of valuable components such as proteins, carbohydrates, and fibers, which still have nutritional values and functional properties comparable to those of fresh peas.

The main challenges which are nowadays hindering the development of a biorefinery process for the recovery of pea waste have been identified as i) raw material challenge (low storage stability of fresh pea waste), ii) technological challenge (absence of process optimization aiming at obtaining value ingredients like flours and proteins) and iii) feasibility challenge (lack of information on process scalability and applicability of the new ingredients in foods).

In this contest, UPea is going to investigate the use of innovative technologies to stabilize fresh peas and enhance protein extraction. A feasibility study will determine potential obstacles related to process efficiency, scalability, food safety and regulatory compliance. Ultimately, UPea will provide innovative and sustainable alternative solutions to the current pea waste management, which will pave the way for the definition of industrial cascade bio-refinery processes aiming at exploiting pea waste into a source of value ingredients for the food industry.

Experimental

Pea is an agricultural commodity belonging to the *Leguminosae* family which is commercialized as fresh or canned green peas, or yellow dried peas. The world production amounts for more than 35 million tons [1] and in EU about 0,9 million tons of green peas are processed yearly [2].

Peas reach the processing site without leaves and pods and after the preliminary cleaning and grading, damaged peas (yellowish, stained, sub-standard dimension peas) are discarded and mainly subjected to anaerobic digestion [2]. This waste management results in the loss of valuable compounds contained in pea waste (5% of fresh weight is made of proteins, 14% of carbohydrates and 5% of fibres) [3]. Since this type of waste is highly perishable and deteriorates within just a few days due to microbial and enzymatic activity, extending its shelf life is crucial for any industrial valorisation.

Conventional high-temperature thermal treatments (e.g blanching above 80°C) is used as stabilization process for fresh food, however the high temperature may reduce the nutritional and functional properties of the valuable compounds in peas. Therefore, UPea investigated new strategies for the stabilization of raw peas like supercritical CO_2 ($ScCO_2$). Stabilization was performed using $ScCO_2$ at lab-scale and the results were compared with conventional thermal treatments [4].

The efficiency of the treatment was investigated on the inactivation of the total bacteria count (TBC) and by challenge tests with surrogate microorganism (i.e. *E. coli*). Process optimization was carried out to determine the effects of the main process parameters (e.g. temperature, pressure and treatment time).

$ScCO_2$ was also investigated as drying technology alone and in combination with High Power Ultrasound (HPU) [5]. The combination of the processes led to the highest reduction in weight and achieved the lowest levels of moisture and water activity, indicating improved product stability compared to using $ScCO_2$ alone. Results demonstrated the efficacy of the technology to reduce the microbial load on the samples and, when the technology is used for drying, the capacity to dry peas at lab scale in less than 8 hours.

Once dried, peas were valorised by two strategies: the development of whole flour and the production of protein powders which were characterized and used for the preparation of food prototypes. An example of application of pea derivatives is the production of food powders with specific functional and sensory qualities. For this purpose, ethanol solvent exchange and supercritical CO_2 drying (SE + SCD) were investigated as innovative

production processes [6]. This processing method produces a pea-based powder with excellent rehydration and oil absorption capabilities, thanks to its low density, highly porous microstructure, and conformational changes in the biopolymers. Additionally, the SE + SCD treatment yields a powder that is neutral in colour, taste, and smell, so it effectively removes the characteristic sensory traits of green peas, which are often undesirable in various food applications. These distinctive functional and sensory properties make the powder a promising high-protein, high-fiber ingredient for use in diverse food formulations. Another application of pea-based proteins is the development of novel microaerogel particles and their implementation as ingredient for low-saturated fat cocoa spreads [7].

No data are currently available on regulatory issues potentially associated with novel ingredients derived from legume waste. Furthermore, valorisation strategies for legume waste are mostly limited to the laboratory scale, highlighting the need for scalability data to support the practical feasibility of the proposed approaches.

For this reason, the last objective of the project is to assess the feasibility of the proposed processes and products for the industrial exploitation of pea waste. The aim is to collect preliminary data to support the scalability of these valorised strategies. A workflow for the new processes was developed and an estimate of the implementation cost was carried out by scaling up laboratory data and performing preliminary design of necessary components, including estimates of energy and labour cost at larger scale. These data were then used to conduct predictive environmental and economical sustainability assessment using Life Cycle Assessment (LCA) and Life Cycle Costing (LCC) methodologies.

A risk characterization was conducted across the entire process workflow to identify potential hazards such as chemical contaminants, pesticide residues, allergens, and pathogens and to evaluate the associated risks related to the future consumption of the newly developed ingredients. This analysis serves as a foundation for future, more detailed risk assessment studies.

In conclusion, UPea’s outcomes could pave the way for future initiatives aimed at implementing a zero-waste approach to legume by-products, transforming them into raw materials for sustainable food ingredient production. The identification and development of new processes for converting pea waste into innovative ingredients, along with feasibility data, are expected to support industrial development and implementation of legume valorisation strategies.

Summary

Every year millions of tons of peas are wasted, resulting in the loss of valuable compounds. The UPea project aims to develop and optimize innovative, environmentally sustainable processing technologies for the valorisation of pea by-products, with the goal of producing high-value functional food ingredients. The current increasing market demand of pea flours and protein extracts [8] supports the recovery of pea waste into these dried ingredients. The results achieved by the UPea project are expected to provide a foundation for the development of sustainable food prototypes incorporating ingredients not only from pea waste valorisation but also from other legume by-products. Furthermore, this approach could deliver significant economic and environmental benefits by promoting circular economy strategies that reduce food waste and enable the creation of new, economically valuable food products.

Acknowledgment

The project is financed by the Italian Ministry of University and Research (MUR) through the Next Generation EU, PNRR M4C2I1.1, for the funded Project PRIN 2022 [Grant No. 2022P5C3E – CUP C53D23004980006] titled "Upcycling pea waste side streams for developing future food ingredients" (UPea).

References

[1] FAOSTAT, “Food and Agriculture data,” 2017. [Online]. Available: http://www.fao.org/faostat/en/#home. [Accessed: 28-Mar-2022].

[2] A. Tassoni et al., “State-of-the-art production chains for peas, beans and chickpeas-valorization of agro-industrial residues and applications of derived extracts,” Molecules, vol. 25, no. 1383, pp. 1–21, 2020.

[3] USDA Food Data Center, “Peas, green, raw,” 2017. [Online]. Available: https://fdc.nal.usda.gov/fdc-app.html#/food-details/170419/nutrients. [Accessed: 28-Mar 2022].

[4] G. Ferrentino and S. Spilimbergo, “High pressure carbon dioxide pasteurization of solid foods: Current knowledge and future outlooks,” Trends Food Sci. Technol., vol. 22, no. 8, pp. 427–441, Aug. 2011, doi: 10.1016/J.TIFS.2011.04.009.

[5] Marco Cardina, Riccardo Zullia, Fabio Santia, Pietro Andrigoa, Elisa Lincettia, Davide Colinia, Sara Spilimbergoa, Alessandro Zambon, “Exploring Novel Supercritical CO2

Drying Combined with High Power Ultrasounds: a Case on Peas and Apples", Chemical Engineering Transactions, Volume 110, 2024.

[6] Lara Manzocco, Lorenzo Barozzi, Stella Plazzotta, Yanjun Sun, Song Miao, Sonia Calligaris, "Feasibility of water-to-ethanol solvent exchange combined with supercritical CO_2 drying to turn pea waste into food powders with target technological and sensory properties", LWT, Volume 194, 15 February 2024, 115778.

[7] Stella Plazzotta, Lorenzo De Berardinis, Baldur Schroeter, Lara Manzocco, "Development of novel microaerogel particles from pea protein and their application as ingredient for low-saturated fat cocoa spreads", Journal of Food Engineering, Volume 391, May 2025, 112413.

[8] Market Research, "Pea Protein Market by Type (Pea Protein Isolate, Pea Protein Concentrate, Pea Flour), Source (Yellow Pea, Green Pea), Source Process (Conventional, Organic), Application (Nutritional Supplements, Meat Alternatives) - Global Forecast to 2028," 2022. [Online]. Available: https://www.marketresearch.com/Meticulous-Research-v4061/Pea-Protein-Type-Isolate-Concentrate-30992020/. [Accessed: 29-Mar-2022].

Phase Behavior and Hydrogenation of Plastic Pyrolysis Oil under Supercritical Conditions: Simulation and Experimental Perspectives

Iván Navarro-Cárdenas, Andreas Kilzer, Marcus Petermann

Chair of Particle Technology, Ruhr-University Bochum, navarro@fvt.rub.de

Introduction

Every year, millions of tons of plastic waste are generated, yet only a small fraction is recycled, while a significant portion accumulates in landfills or the natural environment [1]. As plastic pollution escalates into a critical global concern, developing efficient recycling strategies is increasingly urgent. Among these, pyrolysis stands out as a promising approach that converts plastic waste into oil and gas, potentially serving as feedstock for industrial applications. However, upgrading techniques such as hydrogenation must be further investigated and optimized to render pyrolysis oil viable for integration into existing systems.

While hydrogenation processes have been extensively studied for biological feedstocks, such as vegetable oils, fatty acids, triglycerides, and esters [2-6], comparatively little attention has been paid to the hydrogenation of pyrolysis oil derived specifically from plastic waste. Although some studies address the treatment of bio-oil, coal tar, and other heavy oils, focused research on plastic-derived pyrolysis oils remains limited. This gap presents a valuable opportunity to contribute to a growing field of industrial significance. For instance, Adamou et al. have highlighted the need for effective catalysts in the hydrotreatment of polyethylene-derived pyrolysis oil [7], while others note the hydrogenation of plastic oils remains largely unexplored [8].

A key challenge in conventional hydrogenation is the limited solubility of hydrogen in the oil phase, which hinders reaction efficiency. The use of supercritical propane as a co-solvent offers a promising solution, as it improves miscibility between hydrogen and the oil, thereby facilitating more effective hydrogenation [6, 9].

Plastic pyrolysis oils are generally unsuitable for direct industrial use due to their low stability, high acidity, and the presence of oxygenated compounds such as aldehydes, acids, and ketones. These compounds, along with unsaturated hydrocarbons and high aromatic content, compromise fuel quality and increase corrosiveness. According to Belbessai**,** hydrotreating has been identified as a viable method to improve oil properties

by reducing olefins and aromatics and eliminating heteroatoms such as nitrogen, oxygen, sulfur, and chlorine [10].

Methodology

A model mixture representing typical components of plastic-derived pyrolysis oil was defined based on the literature. According to the work of Budsaereechai and colleagues [11], the five most common compounds in catalytically derived polypropylene (PP) pyrolysis oils, detected by GC-MS analysis, are listed in Table 1.

Table 1. Five main compounds in oil from catalytic pyrolysis of polypropylene (PP) waste

Component	%mole
2,4 Dimethyl-1-heptene (C_9H_{18})	15.71
1-Tricosene ($C_{23}H_{46}$)	7.87
1-Nonadecene ($C_{19}H_{38}$)	7.38
1-Hexadecene ($C_{16}H_{32}$)	7.27
3-Eicosene ($C_{20}H_{40}$)	7.11

A simplified hydrogenation mixture model is shown in Table 2. The composition presented in Table 2 was obtained using the same proportion of hydrocarbons as in Table 1, but adding propane and hydrogen according to the oil/hydrogen/propane ratio proposed by Pereda et al. (2002) [2] and Rovetto et al. (2003) [5].

Table 2. Composition of a simplified pyrolysis oil model from polypropylene (PP) waste, hydrogen, and propane.

Component	%mole
Hydrogen (H_2)	2.6
Propane (C_3H_8)	94.1
2,4 Dimethyl-1-heptene (C_9H_{18})	1.2
1-Tricosene ($C_{23}H_{46}$)	0.5
1-Nonadecene ($C_{19}H_{38}$)	0.5
1-Hexadecene ($C_{16}H_{32}$)	0.5
3-Eicosene ($C_{20}H_{40}$)	0.6

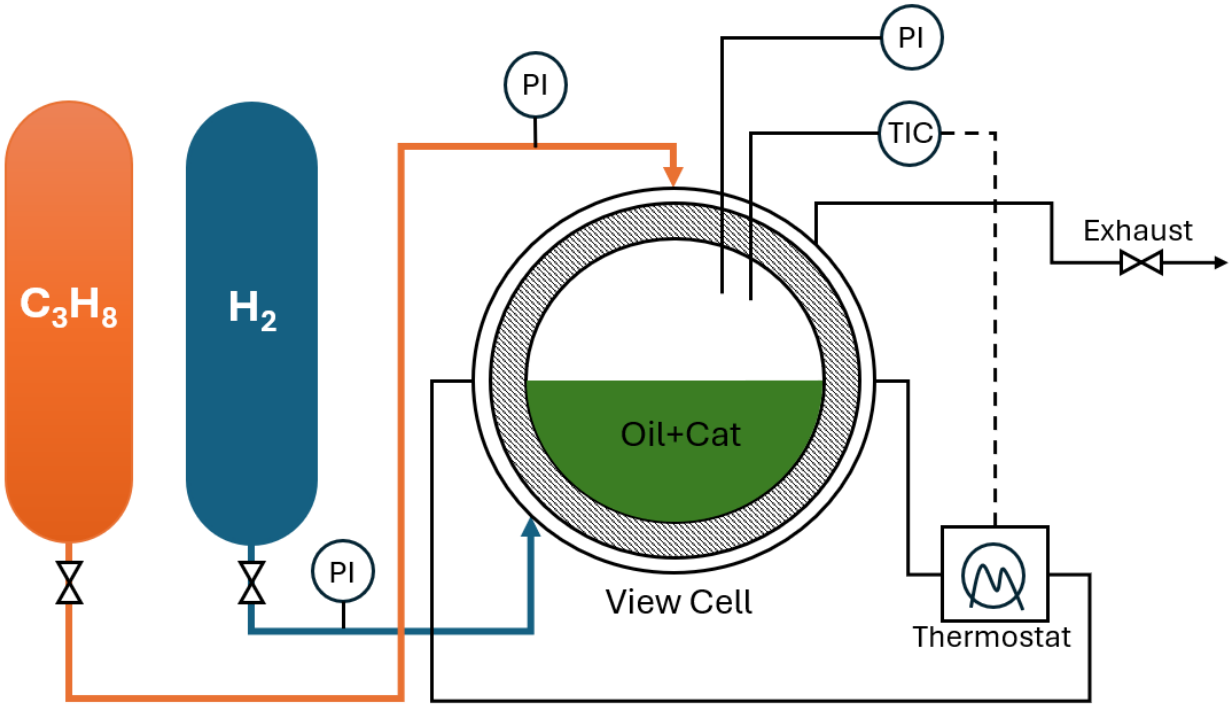

Figure 1. Process flow diagram of the experimental set-up.

Figure 1 shows the proposed setup for the hydrogenation process. The system consists of a high-pressure and high-temperature view cell reactor to observe the phase changes. The catalyst selected is palladium on Al_2O_3 [3, 12]. The composition of the mixture will be analyzed using Gas Chromatography (GC) before and after the reaction to measure the yield.

The key experiments and simulations objectives include:

- Mapping phase behavior (1-phase vs. 2-phase regions) under varying operating conditions.
- Identifying critical points and determination of the pT-envelopes of the mixtures.
- Studying the influence of temperature, pressure, and feed ratios on the system's phase stability.
- Studying the effect of supercritical fluids on the hydrogenation of pyrolysis oil from plastic.

The experimental results will also be used to validate simulations in Aspen Plus. All simulations will be conducted using the Peng–Robinson equation of state (PR EOS) for phase behavior modeling, due to its ability to accurately represent systems involving hydrocarbons [13].

Summary

This research explores the phase behavior of pyrolysis oil, hydrogen, and propane in catalytic hydrogenation under supercritical conditions through experimentation and Aspen simulations. By focusing on the phase behavior of the system, the study aims to identify optimal process conditions for the process to reintegrate plastic waste into the production cycle as a sustainable raw material for industrial applications. Therefore, this research aligns with the principles of sustainability and circular economy, contributing to the development of green technologies and reducing environmental waste.

Acknowledgment

I would like to thank the Chair of Particle Technology at Ruhr University Bochum for funding the project.

References

1. Geyer, R., J.R. Jambeck, and K.L. Law, *Production, use, and fate of all plastics ever made.* Science Advances, 2017. **3**(7): p. e1700782.
2. Pereda, S., S.B. Bottini, and E.A. Brignole, *Gas–liquid reactions under supercritical conditions—phase equilibria and thermodynamic modeling.* Fluid Phase Equilibria, 2002. **194-197**: p. 493-499.
3. Pereda, S., S.B. Bottini, and E.A. Brignole, *Supercritical fluids and phase behavior in heterogeneous gas–liquid catalytic reactions.* Applied Catalysis A: General, 2005. **281**(1): p. 129-137.
4. Pereda, S., et al., *Phase-equilibrium modeling in the hydrogenation of vegetable oils and derivatives.* Journal of the American Oil Chemists' Society, 2006. **83**(5): p. 461-467.
5. Rovetto, L.J., et al., *Supercritical hydrogenation processes: Experimental results on the fluid phase behavior of binary and ternary mixtures of hydrogen, propane and tripalmitin.* The Journal of Supercritical Fluids, 2003. **25**(2): p. 165-176.
6. Ramírez, E., et al., *Fatty oil hydrogenation in supercritical solvents: Process design and safety issues.* The Journal of Supercritical Fluids, 2011. **57**(2): p. 143-154.
7. Adamou, P., et al., *Effect of Polyethylene Pyrolysis Oil Hydrotreatment on the Pt/Al(2)O(3) Catalyst: Experimental Characterization.* ACS Omega, 2024. **9**(17): p. 19057-19062.
8. Catizane, C., Y. Jiang, and J. Sumner, *Improving plastic pyrolysis oil quality via an electrochemical process for polymer recycling: a review.* Energy Advances, 2024. **3**(2): p. 366-388.
9. Pereda, S., E.A. Brignole, and S.B. Bottini, *Advances in phase equilibrium engineering of supercritical reactors.* The Journal of Supercritical Fluids, 2009. **47**(3): p. 336-343.
10. Belbessai, S., A. Azara, and N. Abatzoglou *Recent Advances in the Decontamination and Upgrading of Waste Plastic Pyrolysis Products: An Overview*. Processes, 2022. **10**, DOI: **10.3390/pr10040733**.

11. Budsaereechai, S., A.J. Hunt, and Y. Ngernyen, *Catalytic pyrolysis of plastic waste for the production of liquid fuels for engines.* RSC Advances, 2019. **9**(10): p. 5844-5857.
12. Weidner, E., C. Brake, and D. Richter, *Chapter 1.11 - Thermo- and fluiddynamic aspects of the hydrogenation of triglycerides and esters in presence of supercritical fluids*, in *Supercritical Fluids as Solvents and Reaction Media*, G. Brunner, Editor. 2004, Elsevier: Amsterdam. p. 269-294.
13. Brunner, G., *Calculation of phase equilibria and their relation to separation with supercritical fluids.* The Journal of Supercritical Fluids, 2018. **134**: p. 2-11.

Visualisation of Combined Relief and Decomposition Events of Ethylene and Comonomer Mixtures

Jarne Berning, Markus Busch*

Ernst-Berl-Institute of Technical and Macromolecular Chemistry, Technical University Darmstadt, *markus.busch@pre.tudarmstadt.de

Introduction

In the LDPE-Process, ethene is used under harsh temperature and pressure conditions. These conditions make a decomposition of ethene into methane, hydrogen and soot possible. The exothermic decomposition increases the pressure and temperature, which can cause severe damages in the plant. To prevent the damage, pressure relief devices such as rupture disk and safety valves are used to reduce the pressure in the system. An important fact is that the decreasing pressure and temperature affect the decomposition reaction vice versa. Normally the decomposition experiments are recorded with pressure sensors and thermocouples. This gives information about the pressure and temperature rise in the reactor, but less information about the flame front which moves through the reactor. With more thermocouples, the flame front geometry can be assumed. [1] With a view cell and a high-speed camera the flame front can be directly observed.

Experimental

The volume of the view cell is 34 mL or 70 mL depending on the setup and the experiment. A stirrer can also be implemented. This is shown in Fig. *1*. As in other experiments, the pressure and temperature are also recorded with a fast-measuring system. Additionally, the decomposition is also recorded with a high-speed camera, which is placed on the right. The decomposition is started with a direct current pulse and an ignition coil, which is made of a tungsten wire. A capillary and a pneumatic valve simulate the relief facilities, which are attached at a top bore in view cell, and the opening and closing pressure of the valve can be set differently. The visual examination is done with the TRACKER © software. This software enables to measure the position and the speed of the flame front. With this set-up, decompositions at reactor and at high-pressure separator conditions are examined especially the flame front behaviour.

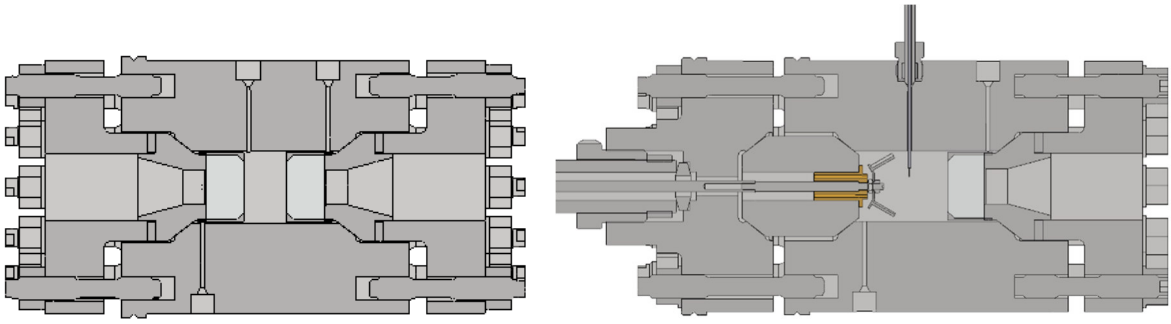

Fig. 1.: view cell for decomposition experiments without (left) and with stirrer (right)

On the one hand, experiments at reactor conditions were executed. At 2000 bar the flame front propagates differently compared experiments with lower inital pressures. At high pressure conditions the flame front is more spherical, which is shown in the following figure. The reason for this is the higher density and higher viscosity at higher pressure conditions. [2]

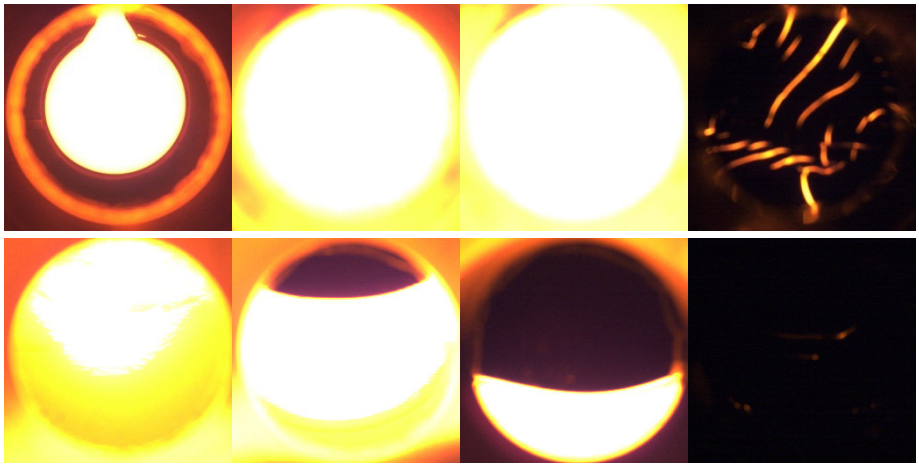

Fig. 2.: Flame front at 2000 bar (top) and 450 bar (bottom) 0.5 s, 1.0 s, 1.5 s, 2.0 s after the ignition.

On the other hand, experiments with vinyl acetate were executed. Vinyl acetate has a larger thermal conductivity and a larger density then ethene, which influences the flame front propagation. PRENZEL assumes, that through the higher density, vinyl acetate accumulates at the bottom of the view cell at first. [3] The mixture is homogenized with the stirrer before the decomposition is ignited. The stirrer was stopped 30 seconds before the ignition to keep sure, that no rotational moving of the mixture has an influence on the

decomposition or the relief. The mixing especially influences the relief during the decomposition, which indicates that the homogeneity is not reached without stirring. This is shown in the following Figure.

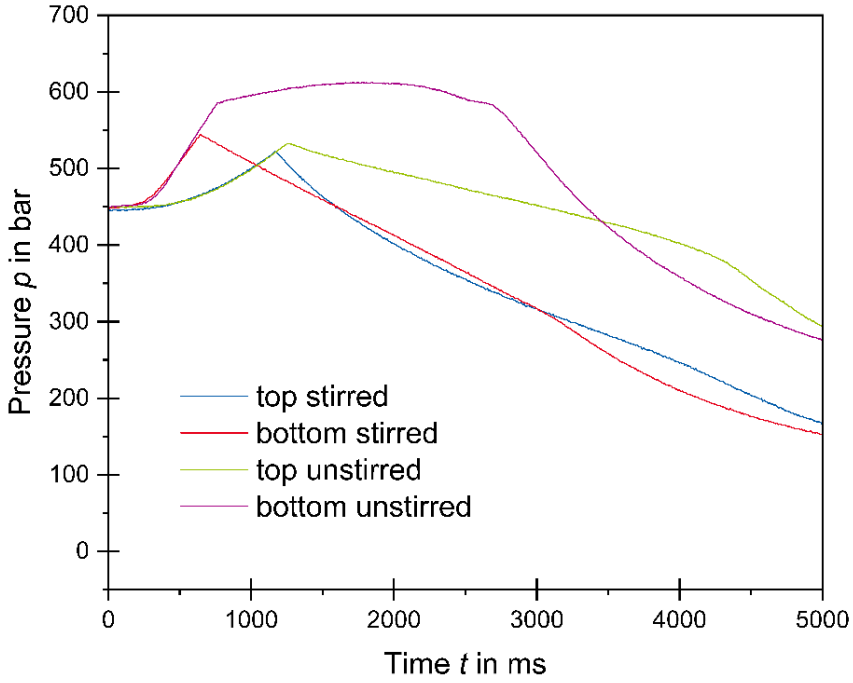

Fig. 3.: Pressure profile of stirred and unstirred decomposition experiments with the ignition coil at the top or bottom of the view cell.

At first during the decomposition and before the relief, the pressure rises quite similarly, but if the relief starts, the pressure falls faster in stirred experiments than in unstirred experiments. In the experiment with ignition at the bottom, pressure rises slightly even the valve has open completely. That could become critical if the pressure still rises. To prevent that, a shorter nozzle or a nozzle with a larger diameter can be used. The stirring has only a small influence on the flame front behaviour, which is shown in the Figure 4. The flame front is a little bit faster in the unstirred experiment because at top there is a lesser concentration of vinyl acetate than in the stirred experiment.

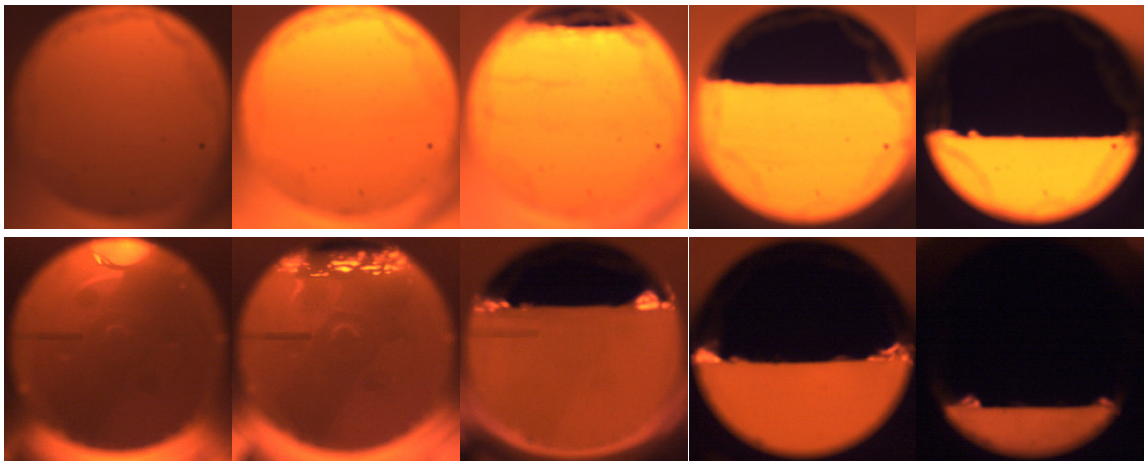

Fig. 4.: Flame fronts in experiments with 30% vinyl acetate at 450 bar and 250°C unstirred (top) and stirred before the decomposition (bottom) at 1.0 s, 1.5 s,2.0 s,2.5 s and 3.0 s after the ignition.

Summary

In this work, the influence of the initial pressure at reactor conditions is examined. Therefore, the pressure and temperature profile and the flame front behaviour is studied. PRENZEL assumes that the vinyl acetate is not homogeneously distributed in the view cell at high-pressure separator because vinyl acetate has a higher density. [3] Therefore a stirrer is implemented to homogenesis the mixture.

References

[1] Ö. Delibalta, Dissertation, Technical University Darmstadt, Darmstadt, 2022.

[2] A. Röblitz, Visualization of the Decomposition and Relief Process in High-Pressure Systems, Proceedings of the . Volume 4: High Pressure Technology, Atlanta, 2023

[3] E. Prenzel, Bachelorthesis, Technical University Darmstadt, Darmstadt, 2023

Particle Size Reduction with Supercritical Fluids

David Hvalec

Laboratory for Separation Processes and Product Technology, University of Maribor,
david.hvalec@um.si

Introduction

High-pressure technologies employing subcritical and supercritical fluids (SCFs) represent advanced approaches for the development of novel products characterized by distinctive physical properties, minimal toxic residues, and reduced energy requirements, all within an environmentally sustainable framework. In particular, supercritical fluids exhibit considerable potential as alternative solvents in green chemistry, offering a viable replacement for conventional organic solvents that are detrimental to the environment. The selection of an appropriate SCF for industrial or chemical applications requires consideration of multiple practical factors. Carbon dioxide (CO_2) is the most widely used SCF due to its favorable critical constants, non-toxic and non-flammable nature, and chemical inertness. Additionally, CO_2 is inexpensive and readily available, making it the second most economical solvent after water. SCFs are well-established as environmentally friendly processing solvents in a variety of polymer-related applications, including polymer modification, composite formation, polymer blending, microcellular foaming, polymerization, and particle production. Of particular interest is the application of SCFs in the micronization of biodegradable polymers for pharmaceutical purposes, especially in the context of controlled drug delivery systems. Among the most commonly utilized biodegradable polymers in such processes is polyethylene glycol (PEG), which is a water-soluble, biocompatible polymer that is generally recognized as physiologically acceptable, making it highly suitable for biomedical and pharmaceutical applications (Budisa & Schulze-Makuch, 2014; Knez et al., 2014, 2015).

I focused on the production of fine particles using supercritical fluid (SCF) technologies. Various SCF-based techniques were employed, including Rapid Expansion of Supercritical Solutions (RESS), the Gas Antisolvent processes (Supercritical Antisolvent precipitation (SAS), Solution Enhanced Dispersion by Supercritical fluids (SEDS), Aerosol Solvent Extraction Systems (ASES)), Supercritical Fluid Extraction of Emulsions (SFEE), and Particles from Gas-Saturated Solutions (PGSS™). The PGSS™ process involves the transformation of the target polymer into a sprayable form through melting or dissolution.

The resulting melt or solution is then saturated with gas under pressure. Upon expansion through a nozzle, fine particles are formed due to the combined effects of reduced interfacial tension and low viscosity, facilitating efficient atomization (Knez et al., 2015).

Experimental

In this summary, I will present two projects where we performed micronization using supercritical fluids. In the first project, the PGSS™ process was applied to the biodegradable polymer material polyethylene glycol (PEG 4000) and Brij S100 for embedding water-insoluble substances. In another project, we performed micronization of PEG 4000 with an emulsion made from beetroot extract.

Before starting particle precipitation, preliminary thermodynamic data of water-soluble carrier polyethylene glycol and Brij were carried out. The diffusion coefficient, density, interfacial tension, melting points and solubility of CO_2 saturated PEG 4000 were studied at different pressure and temperature process parameters. In my research work, I dealt with determining the solubility of supercritical gas in the investigated materials, determining diffusion coefficients and melting points of substances at different pressures and temperatures.

Modified capillary method for determination of melting points

The melting interval of the CBD and PEG in contact with dense CO_2 was determined using a modified glass capillary method. The initial and final melting points were recorded, indicating the onset and completion of melting. The sample, placed in a glass capillary, was inserted into an optical cell with sapphire windows. To determine the melting point, we used a view cell, that operates up to 2 500 bar and 300°C, and a cell that operates up to 7 000 bar and 200°C were used. Dense CO_2 was introduced into the cell using a high-pressure pump, and the temperature was gradually increased by 1°C until the sample was fully melted. The results were subsequently presented as a pressure-temperature (P-T) graph. A high-pressure cell is shown schematically in Fig. 1. a, and a cell that can operate at a maximum pressure of 2 500 bar is shown in Fig. 1. b. (Knez et al., 2010).

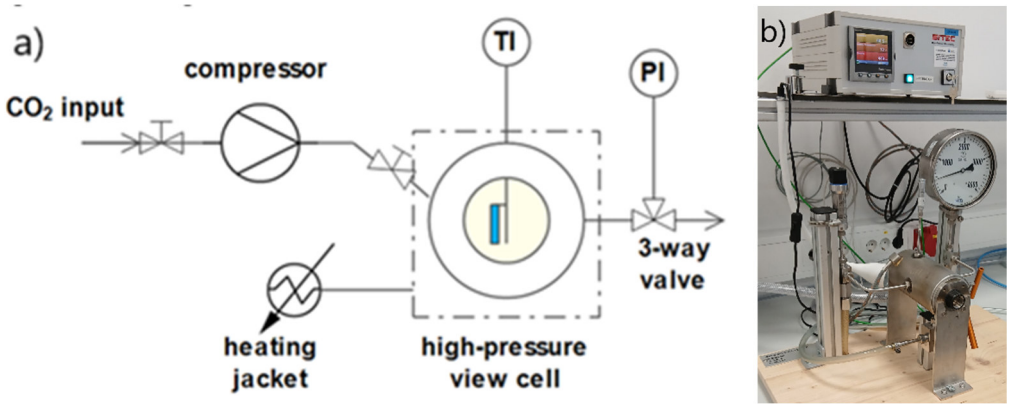

Fig. 1.: a) A sheme of a high-pressure optical cell and, b) picture of a high pressure cell (Kravanja et al., 2018).

Fig. 2. shows a diagram of the variation of the average melting point for the example of PEG 1500. As can be seen from the graph, the slope of dP/dT is negative, and the average melting point decreases almost linearly. This can be explained by the high solubility of CO_2 in the melt. Later the melting point is constant for a short temperature interval, after which the melting point starts to increase again. This method also allows us to determine the minimum melting point, which is crucial for planning and optimizing high-pressure micronisation processes. Specifically, systems with a negative dP/dT slope on the solid-liquid-gas (S-L-G) minimum temperature curve are particularly advantageous for PGSS™ processes.

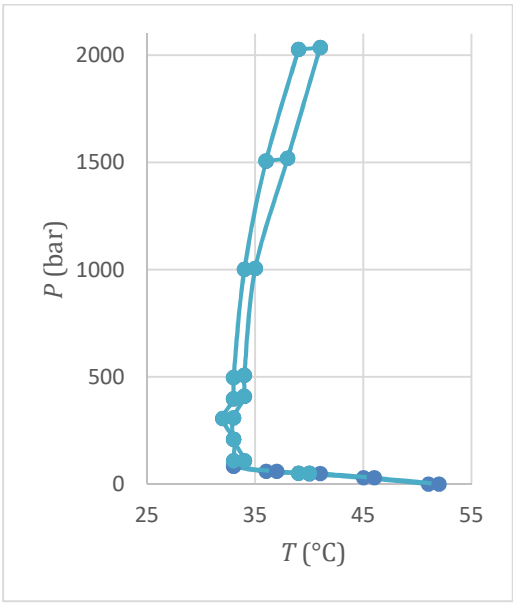

Fig. 2.: P-T diagram for PEG 1500-CO_2 systems.

Mass transfer data

Diffusion coefficients, density and solubility of the CO_2 saturated solutions of molten PEG were measured by a gravimetric method using magnetic suspension balance (MSB). The applied MSB is designed for the maximum operating pressure of 350 bar and operating temperature of 250°C. The measuring force is transmitted contactless from the measuring chamber to microbalance by magnetic suspension coupling. The measuring cell of MSB is also provided with a window, which allows observation of the sample and estimation of volume modifications during the sorption measurements (Fig. 3.).

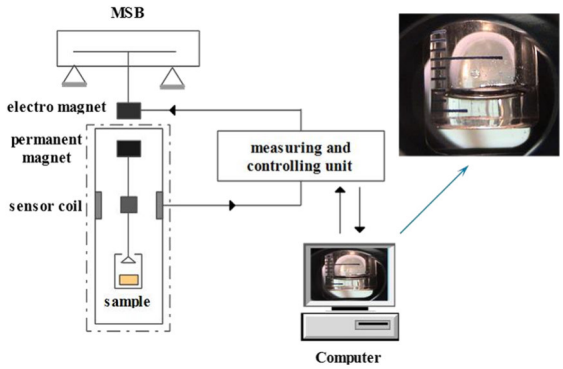

Fig. 3.: A scheme of measuring density and solubility by a gravimetric method involving MSB (Kravanja et al., 2018).

In the present work, density, solubility, and diffusion coefficients were measured for investigated binary system by increasing the pressure step by step from 0 bar up to 300 bar at constant temperatures. Before applying next pressure step, the software recorded conditions (mass temperature, pressure) inside measuring cell. After a period of time, the equilibrium was reached and the volume of the sample could be analyzed by digital photo camera. Fig. 4. shows an example where molten PEG was exposed to certain pressure and temperature.

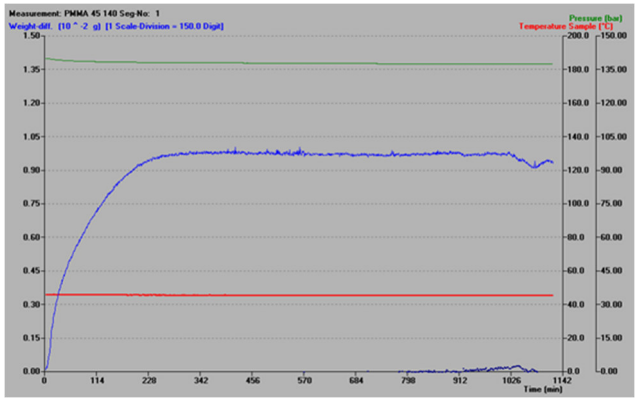

Fig. 4.: Monitoring the change in mass of the molten sample over time in MSB.

In Figure 4, it is shown that the absorption of CO_2 into the molten sample starts off high, but after a period of time, an equilibrium is reached, at which point the mass of the sample remains constant. By applying a mathematical model based on Fick's law, the diffusion coefficient can be calculated from the data on mass changes measured under specific pressure and temperature conditions. The obtained diffusion coefficients and solubilities can be shown on a graph, where the abscissa shows the pressure. In Fig. 5. the results of determination of solubility and diffusion coefficients for systems with PEG of different molecular masses are shown.

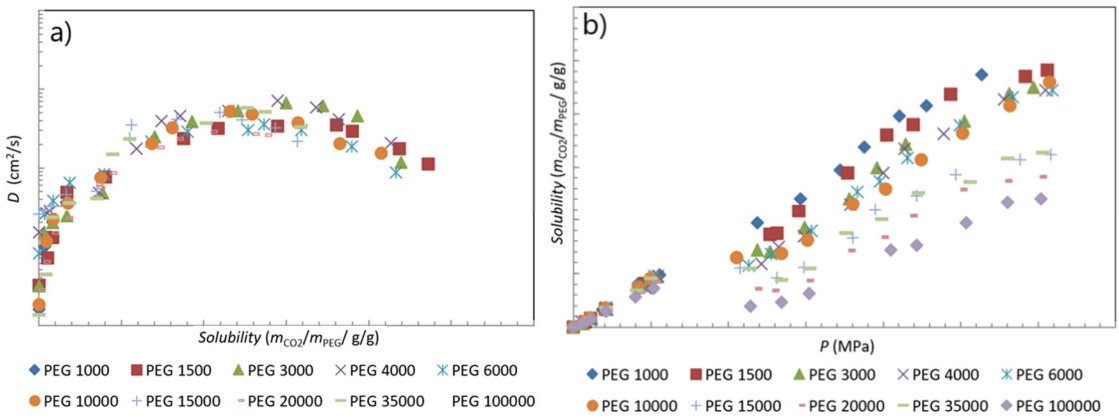

Fig. 5.: a) Diffusion coefficients for the system CO_2 /polyethylene glycol of different molecular mass at constant temperature, b) solubility of CO_2 in polyethylene glycol of different molecular mass at constant temperature (Hrnčič et al., 2014).

Micronization Processes

The morphology, size, and size distribution of particles are becoming increasingly important in the food and pharmaceutical industries, as consumers demand specific properties in the products they purchase. Traditionally, solid particle size reduction has been achieved using mills or organic solvents, which can damage the material or leave undesirable residues in the final product. This is particularly unacceptable in the food and pharmaceutical sectors. In the PGSS^{TM} process, a polymer carrier with active ingredients is mixed with supercritical CO_2 in a high-pressure autoclave. Heating melts the polymer, forming a CO_2-saturated solution. When this expands through a nozzle, the CO_2 evaporates, cooling the melt via the Joule-Thomson effect. This temperature drop leads to polymer crystallization and the formation of uniformly sized particles. Particle size and morphology depend on factors such as pressure, temperature, nozzle size, input material, and SCF type.

Formulation of pure components with PEG 4000 and Brij S100 using the PGSS™ method

In the research work, we micronized CBD and the drugs nifedipine, felodipine, fenofibrate, nimodipine and o-vanillin. Fig. 6 shows a schematic of the PGSS™ batch process. PEG and Brij were used as polymer carriers.

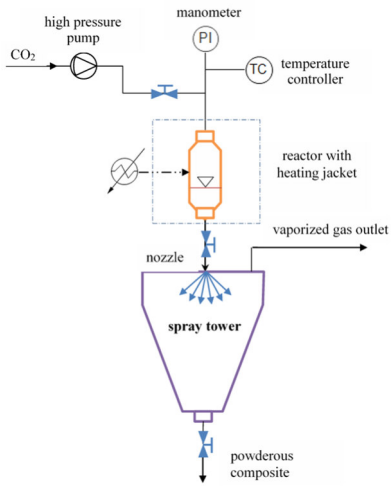

Fig. 6.: Scheme of a batch PGSS™ process (Kravanja et al., 2018).

The Fig. 7 shows an example of the dissolution rate of pure nifedipine compared to micronized formulations at a pressure of 120, 160 and 190 bar. The graph shows that the absorption of nifedipine is greater in the formulations than in the original sample.

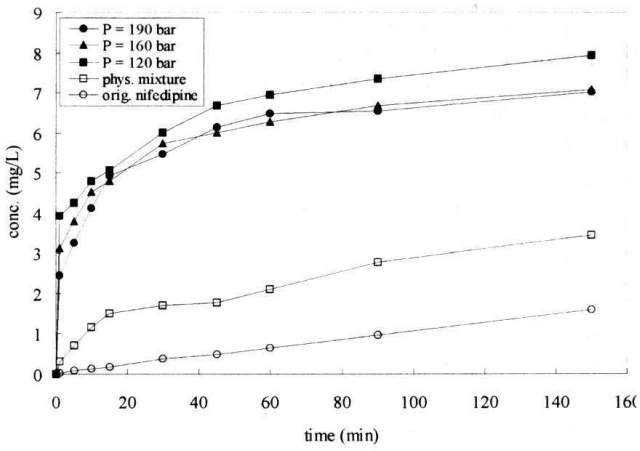

Fig. 7.: Dissolution rate for nifedipine and its formulations, which were micronized using the PGSS™ method (Senčar-Božič et al., 1997).

Formulation of beetroot extracts with biodegradable polymers

Beetroot has gained attention in recent years for its rich content of bioactive compounds, particularly betalains. These pigments offer antioxidant, anti-inflammatory, anticancer,

antimicrobial, and cardiovascular benefits, making them valuable in the food and pharmaceutical industries. However, betalains are highly unstable and sensitive to factors like pH, temperature, oxygen, enzymes, and condensation reactions. Further research is needed to find new sources and improve stabilization methods to develop cost-effective, stable, and vibrant natural colorants. We investigated the applicability of the high-pressure micronization technique using supercritical CO_2 for the formulation of composites and stabilization of beetroot betalain extracts. In this technique, an emulsion with an aqueous beetroot extract, a melted carrier, and supercritical CO_2 are mixed in a static mixer. The process is schematically shown in Fig. 8. At the end of the experiment, a fine red powder of uniform size was obtained.

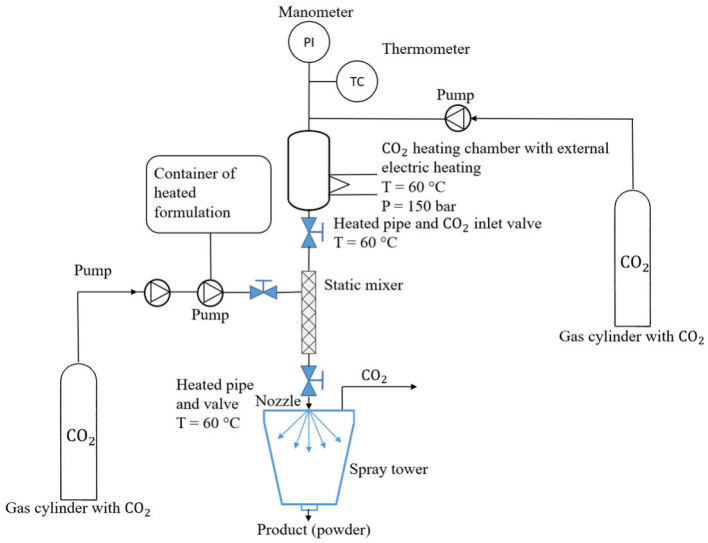

Fig. 8.: Scheme of a batch micronization process.

Summary

I investigate the basic thermodynamic and transport properties of systems and substances involving subcritical and supercritical fluids under moderate to ultra-high pressures. these data are essential for planning and optimizing high-pressure processes. As part of this research, we experimentally determine phase equilibria for multicomponent systems at elevated pressures and temperatures. Based on the experimentally determined data, we utilize thermodynamic and empirical models for further modelling efforts. A primary focus of my research is the development of high-pressure processes for particle size reduction. The products generated through these methods exhibit high stability and rapid release characteristics. Additionally, I am involved in developing various HPLC methods for identifying antioxidant compounds in natural extracts and products produced by these high-pressure processes.

References

Budisa, N., & Schulze-Makuch, D. (2014). Supercritical Carbon Dioxide and Its Potential as a Life-Sustaining Solvent in a Planetary Environment. *Life*, *4*(3), 331–340. https://doi.org/10.3390/life4030331

Hrnčič, M. K., Markočič, E., Trupej, N., Škerget, M., & Knez, Ž. (2014). Investigation of thermodynamic properties of the binary system polyethylene glycol/CO2 using new methods. *The Journal of Supercritical Fluids*, *87*, 50–58. https://doi.org/10.1016/j.supflu.2013.12.021

Knez, Ž., Knez Hrnčič, M., & Škerget, M. (2015). Particle Formation and Product Formulation Using Supercritical Fluids. *Annual Review of Chemical and Biomolecular Engineering*, *6*(1), 379–407. https://doi.org/10.1146/annurev-chembioeng-061114-123317

Knez, Ž., Markočič, E., Leitgeb, M., Primožič, M., Knez Hrnčič, M., & Škerget, M. (2014). Industrial applications of supercritical fluids: A review. *Energy*, *77*, 235–243. https://doi.org/10.1016/j.energy.2014.07.044

Knez, Ž., Škerget, M., & Mandžuka, Z. (2010). Determination of S–L phase transitions under gas pressure. *The Journal of Supercritical Fluids*, *55*(2), 648–652. https://doi.org/10.1016/j.supflu.2010.09.016

Kravanja, G., Knez, Ž., Kotnik, P., Ljubec, B., & Knez Hrnčič, M. (2018). Formulation of nimodipine, fenofibrate, and o-vanillin with Brij S100 and PEG 4000 using the PGSS^{TM} process. *The Journal of Supercritical Fluids*, *135*, 245–253. https://doi.org/10.1016/j.supflu.2018.01.021

Senčar-Božič, P., Srčič, S., Knez, Z., & Kerč, J. (1997). Improvement of nifedipine dissolution characteristics using supercritical CO2. *International Journal of Pharmaceutics*, *148*(2), 123–130. https://doi.org/10.1016/S0378-5173(96)04838-7

Advancing Olive Pomace Valorization through Supercritical CO_2 Technology

Ricardo Hipólito [a], C.I. Daniel [b] , M. Nunes da Ponte [b] , A.V.M. Nunes [a]

a) LAQV-REQUIMTE, Departamento de Química, Faculdade de Ciências e Tecnologia, Universidade Nova de Lisboa, 2829-516 Caparica, Portugal
b) Zeyton Nutraceuticals, Parque Industrial do Penique, Estrada Nacional 2, Km 585 Odivelas - Ferreira do Alentejo, Portugal
r.hipolito@campus.fct.unl.pt

Introduction

In recent years, the valorization of agricultural by-products has emerged as a key strategy to promote sustainable development, reduce environmental burdens, and create novel economic opportunities [1]. This shift is particularly relevant in the context of the olive oil industry, one of the most emblematic sectors in Mediterranean countries [1]. Olive oil production generates substantial amounts of waste, including olive pomace, leaves, and olive mill wastewater which, if left untreated, can result in significant environmental problems due to their high organic content and phytotoxicity [2]. However, these by-products are also rich in bioactive compounds, particularly phenolic compounds such as tyrosol and hydroxytyrosol, which are known for their antioxidant, anti-inflammatory, and antimicrobial properties [2][3]. Their recovery and reintegration into the food, cosmetic, and pharmaceutical sectors as natural preservatives or nutraceuticals represent an important opportunity for circular bioeconomy approaches [4][5].

Among these by-products, concentrated polyphenol streams obtained from prior treatments, such as nanofiltration and reverse osmosis, offer a valuable yet underexploited intermediate for further purification [6]. Despite initial removal of large molecular weight compounds and suspended solids, these concentrates often retain significant quantities of carbohydrates, organic acids, and mineral salts. These residual components hinder the usability of the extracts, as they compromise both stability and organoleptic quality of final formulations [7]. Furthermore, their presence complicates downstream purification strategies due to overlapping polarity and solubility characteristics with the target phenolics [8].

Conventional methods for phenolic recovery from olive matrices typically rely on adsorption/desorption processes using polymeric resins due to their simplicity, reusability, and relatively low cost [9][10]. Macroporous resins have been extensively studied for this

purpose, offering selective retention of phenolic compounds through physical interactions (e.g., hydrogen bonding, π–π stacking, and van der Waals forces) [10]. However, challenges still remain in optimizing these processes for both selectivity and energy efficiency, particularly in the desorption step, where aqueous ethanol is traditionally employed to release adsorbed phenolics [11]. Although effective, this method introduces additional solvent recovery steps, increases operational costs, and reduces the overall greenness of the process due to the energy demand associated with ethanol separation and recycling [11].

To overcome these limitations, this work investigates the application of supercritical carbon dioxide ($scCO_2$) as an alternative desorbing agent for phenolic compounds [12]. Supercritical CO_2 is a well-established green solvent known for its low critical temperature and pressure (31.1°C, 73.8 bar), non-toxicity, inertness, and easy removal post-process by simple depressurization, leaving no solvent residues [12]. While traditionally used for nonpolar or moderately polar compounds (e.g., caffeine, essential oils, lipids), its tunability, especially when combined with co-solvents such as ethanol, has expanded its potential to extract a broader range of compounds, including moderately polar phenolics [13][14]. The use of ethanol-modified $scCO_2$ may therefore provide a selective, cleaner, and more sustainable route to recover hydroxytyrosol-rich fractions from complex olive-based matrices without the drawbacks of conventional solvent use [14][15].

This study is part of a broader effort to enhance the technological and environmental performance of phenolic recovery processes from olive pomace, contributing to the development of more sustainable and scalable strategies for by-product valorization. The research begins by optimizing adsorption and desorption steps using commercial resins under conventional conditions and then transitions into evaluating the feasibility of supercritical CO_2 as a desorbing fluid. The goal is not only to assess its desorption potential but also to explore how selectivity, recovery, and energy efficiency compare to existing techniques. Ultimately, this work aims to support the creation of a green, efficient purification route for high-value olive phenolics, aligned with circular economy and clean technology principles.

Experimental

Initially, olive pomace was characterized with a focus on its content of phenolic compounds (mainly hydroxytyrosol and tyrosol), as well as sugars and organic acids, which are relevant co-extracted compounds in the downstream process. The first stage of the experimental work involved a comparative study of adsorption efficiency using a selection of Amberlite™ polymeric resins (XAD-4, XAD-7, and XAD-16). These tests aimed to optimize the choice of resin for effective capture of phenolics from olive pomace extracts.

After determining the best-performing resin, desorption experiments were carried out under conventional conditions using ethanol:water mixtures at different ratios. This provided a reference for evaluating the performance of a greener and potentially more selective alternative: supercritical CO_2 extraction. For this stage, a high-pressure extraction system equipped with a CO_2 pump, thermostated extraction cell, and back-pressure regulator was used.

Supercritical CO_2 experiments were conducted at a fixed pressure of 200 bar and temperature of 40°C, for extraction times of 1, 2, 3, and 5 hours. These time points were chosen to establish the desorption profile and determine the optimal extraction duration for maximal recovery of phenolics. Selected assays also included the use of ethanol as a co-solvent to assess its role in enhancing desorption efficiency. All extracts were collected in a fractionated manner to monitor the kinetic release of compounds and were analyzed by HPLC for quantification of hydroxytyrosol, tyrosol, sugars, and organic acids. The goal was to compare the desorption capacity, selectivity, and environmental impact of supercritical CO_2 with that of conventional solvents, within the context of developing a sustainable recovery process for bioactive compounds from olive pomace.

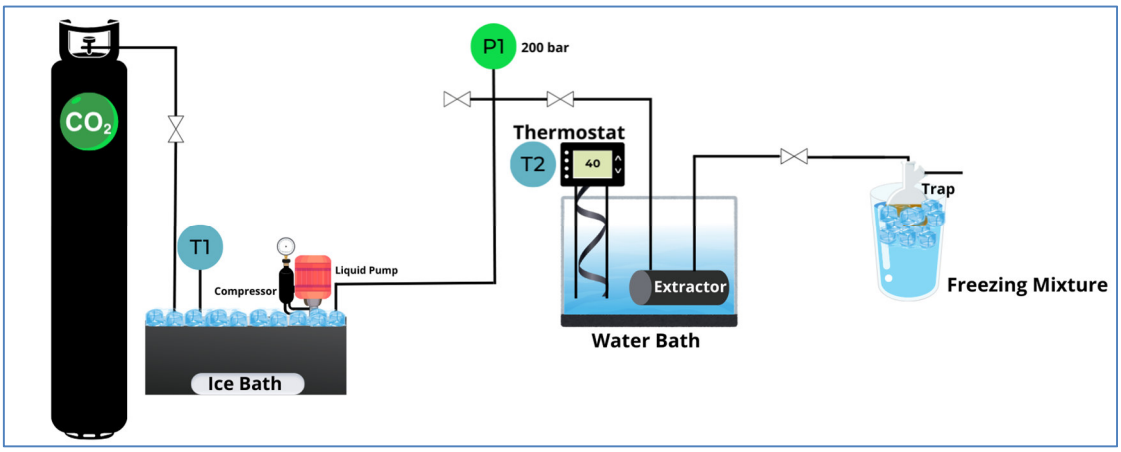

Fig. 1: Schematic of the Supercritical CO_2 extraction setup.

Summary

In the initial phase of this study, various polymeric resins were screened to identify the most effective material for the selective adsorption of phenolic compounds from olive pomace extracts. Among the tested resins, Amberlite XAD-4 was selected due to its superior performance, exhibiting a high adsorption capacity for hydroxytyrosol (55 mg/g resin) and notable selectivity. These properties are attributed to its relatively small pore size and non-polar character, which favor interactions with hydroxytyrosol, one of the key bioactive targets.

In the conventional extraction step, multiple ethanol:water mixtures were evaluated. The 60:40 (v/v) solution yielded the highest recovery of total phenolic content while maintaining favorable selectivity. This solvent system was therefore established as a benchmark for subsequent comparisons.

During the supercritical fluid desorption phase, experiments were conducted at 200 bar and 40°C, using residence times of 1, 2, 3, and 5 hours to investigate the kinetic profile of phenolic recovery. Results demonstrated a clear time-dependent desorption behavior, with longer contact times enhancing the recovery of target phenolics. Despite the intrinsic limitations of pure CO_2 in desorbing highly polar compounds due to its non-polar nature, the process effectively removed low molecular weight organic acids, particularly butyric acid, 65% of which was recovered, compared to only 1% of hydroxytyrosol. This selective removal is noteworthy, as butyric acid impairs extract quality due to its pungent odor. The findings highlight the potential of supercritical CO_2 as a pre-purification strategy, improving the overall quality of phenolic-rich extracts.

Moreover, the addition of ethanol as a co-solvent significantly enhanced the desorption efficiency of hydroxytyrosol and tyrosol. This underscores the importance of solvent polarity modulation in optimizing supercritical extraction systems for bioactive compound recovery.

Acknowledgments

The authors would like to acknowledge the financial support from Fundação para a Ciência e a Tecnologia, Ministério da Ciência, Tecnologia e Ensino Superior (FCT/MCTES), Portugal, through projects PTDC/EQU-EQU/32473/2017 and LA/P/0008/2020. R.F.Hipólito acknowledges FCT/MCTES for his PhD Grant

(UI/BD/154490/2022). The Associate Laboratory Research Unit for Green Chemistry–Clean Technologies and Processes–LAQV-REQUIMTE is financed by national funds from FCT/MCTES (UIDB/50006/2020, UIDP/50006/2020, and UID/QUI/50006/2020) and cofinanced by the ERDF under the PT2020 Partnership Agreement (POCI-01-0145-FEDER–007265).

References

[1] Covas, M. I., Ruiz-Guitérrez, V., de la Torre, R., Kafatos, A., Lamuela-Raventós, R. M., Osada, J., Owen, R. W., & Visioli, F. (2006). Nutrition reviews, 64, S20–S30. https://doi.org/10.1111/j.1753-4887.2006.tb00260.x

[2] Romani, A., Pinelli, P., Ieri, F., & Bernini, R. (2016). Sustainability, innovation, and green chemistry in the production and valorization of phenolic extracts from Olea europaea L. Sustainability, 8(10), 1002. https://doi.org/10.3390/su8101002

[3] EFSA Panel on Dietetic Products, Nutrition and Allergies (NDA). (2011).

[4] Romeu, M. F. C., Bernardo, J., Daniel, C. I., Costa, N., Crespo, J. G., Pinto, L. S., Nunes da Ponte, M., & Nunes, A. V. M. (2024). Journal of Food Science and Technology, 61, 161–168.

[5] Madureira, J., Margaça, F. M. A., Santos-Buelga, C., Ferreira, I. C. F. R., Verde, S. C., & Barros, L. (2022). Applications of bioactive compounds extracted from olive industry wastes: A review. Comprehensive Reviews in Food Science and Food Safety, 21(1), 453–476. https://doi.org/10.1111/1541-4337.12785

[6] Nunes da Ponte, M., Santos, J. L. C., Matias, A., Nunes, A. V. M., Duarte, C. M. M., & Crespo, J. G. Method of obtaining a hydroxytyrosol-rich extract from olive tree residues and sub-products using clean technologies. US Patent 8066881B2.

[7] Wang, S., Liu, H., Zhao, J., Dong, Z., Li, J., & Shao, T. (2023). Influences of organic acid salts and bacterial additives on fermentation profile, aerobic stability, and in vitro digestibility of total mixed ration silage prepared with wet hulless barley distillers' grains. Agronomy, 13(3), 672. https://doi.org/10.3390/agronomy13030672

[8] Lama-Muñoz, A., & Contreras, M. d. M. (2022). Extraction systems and analytical techniques for food phenolic compounds: A review. Foods, 11(22), 3671. https://doi.org/10.3390/foods11223671

[9] Johnson, R., & Mitchell, A. E. (2019). Use of Amberlite macroporous resins to reduce bitterness in whole olives for improved processing sustainability. Journal of

Agricultural and Food Chemistry, 67(5), 1546–1553. https://doi.org/10.1021/acs.jafc.8b06014

[10] Tapia-Quirós, P., Montenegro-Landívar, M. F., Reig, M., Vecino, X., Cortina, J. L., Saurina, J., & Granados, M. (2022). Recovery of polyphenols from agri-food by-products: The olive oil and winery industries cases. Foods, 11(3), 362. https://doi.org/10.3390/foods11030362

[11] Cifuentes-Cabezas, M., Sánchez Arévalo, C. M., Mendoza-Roca, J. A., Vincent Vela, M. C., & Álvarez Blanco, S. (2022). Recovery of phenolic compounds from olive oil washing wastewater by adsorption/desorption process. Separation and Purification Technology, 302, 121562. https://doi.org/10.1016/j.seppur.2022.121562

[12] Díaz-Reinoso, B., Moure, A., Domínguez, H., & Parajó, J. C. (2006). Supercritical CO_2 extraction and purification of compounds with antioxidant activity. Journal of Agricultural and Food Chemistry, 54(7), 2441–2469. https://doi.org/10.1021/jf052858j

[13] Yousefi, M., Rahimi-Nasrabadi, M., Pourmortazavi, S. M., Wysokowski, M., Jesionowski, T., Ehrlich, H., & Mirsadeghi, S. (2019). Supercritical fluid extraction of essential oils. TrAC Trends in Analytical Chemistry, 118, 182–193. https://doi.org/10.1016/j.trac.2019.05.038

[14] Chemat, F., et al. (2020). Bioactive phenolic compounds from agri-food wastes: An update on green and sustainable extraction methodologies. Frontiers in Nutrition, 7, 60.

[15] Cvetanović, A., et al. (2024). An eco-friendly supercritical CO_2 recovery of value-added extracts from Olea europaea leaves. Foods, 13(12), 1836. https://doi.org/10.3390/foods13121836

Flame Retardant Treatment of Wood Using Supercritical CO_2

Dumschat, Lara[1,2*], Liebner, Falk[1], Hansmann, Christian[2]

[1] BOKU University Vienna, Institute of Chemistry of Renewable Resources, Konrad-Lorenz-Strasse 24, 3430 Tulln an der Donau, Austria

[2] Wood K plus - Kompetenzzentrum Holz GmbH, Altenberger Strasse 69, 4040 Linz, Austria

* Corresponding author: l.dumschat@wood-kplus.at

Introduction

The increasing awareness for the finite availability of fossil resources has recently moved renewable raw materials much stronger into the awareness of our society. This development is strongly fostered by Austria's current bioeconomy strategy which put strong emphasis on a better material usage of biomass in general with wood being one of the most prominent pillars. Beyond its use as construction material, wood is highly valued in furniture production as well as for a broad variety of indoor and outdoor applications. In the mobility sector wood is increasingly desired for decorative elements as it has an aesthetic appearance, warm perception on a touch, is durable, and sustainable. Even though such decorative technical wood veneers are very thin (<1.5 mm), legislation requests these combustible materials to meet high fire safety standards. Fire protection is hitherto accomplished using mainly inorganic compounds like sodium carbonates, aluminum hydroxide or ammonium chloride. Since inorganic fire retardants (FR) tend to migrate and crystallize on the surface of the treated materials under the impact of elevated humidity, commercial organohalogen and organophosphorus compounds are frequently used to maintain the aesthetics of wooden surfaces. While the introduction of phosphorous groups is well-known to promote formation of charred thermal insulating surface layers, also other efficient hetero-organic FRs containing silicon, nitrogen, or sulfur atoms have recently emerged [1]. However, since impregnation with organic FRs commonly requires organic solvents, alterations in visual (removal of extractives), textural (swelling) or olfactory perception (solvent residues) of wood are likely.

In wood construction, large cross-sections of load-bearing structures provide a natural fire resistance as thermally-insulating, thus protective char layers can be formed in the case of a fire [2]. However, relying on natural fire protection is not feasible for veneers due to their low thickness, which is insufficient for the formation of a protective char layer. Thus,

addition of highly efficient FRs is required, which is commonly accomplished through protective coatings or (pressure) impregnation [3, 4]. An important advantage of paint and varnish coatings is that they are applied at the surface, which is most vulnerable to ignition. The opportunity of adding FR coatings post-production represents an additional advantage, offering enhanced protection against mechanical damage and moisture absorption. However, surface coatings provide only an initial barrier against fire; once the coating is compromised, the underlying material remains susceptible to thermal degradation and ignition. Another disadvantage is the common loss of decorative appearance caused by the opaqueness of most fire-protective coatings [3, 5]. In contrast, impregnation offers the advantage of protecting (almost) the entire cross-section of wooden parts, including veneers. This allows subsequent processing, such as drilling, sanding, or cutting, without significant loss of fire protection. However, this process requires time-consuming and costly post-impregnation drying, which can lead to alteration of color, dimensional stability, and crack formation. Supercritical fluids (SFs) have proven to be highly effective media for impregnation of (even highly fragile) porous materials and should be established as an alternative to traditional impregnation to overcome some of the above obstacles [6].

The supercritical state is reached when a fluid has arrived at its critical point, characterized by its critical temperature and pressure. Beyond this point, phase boundaries no longer exist, and the fluid acquires properties that lie between that of gases and liquids. In this state, a fluid can easily diffuse through solids, similar to gases, while maintaining a solubilization performance that is comparable to that of conventional liquids [7, 8]. This phenomenon is harnessed in multiple applications, such as in pharmacy (e.g., extraction of bioactive compounds from mixtures [9]), food technology (e.g., de-caffeination of coffee [10]) and material applications (e.g., foaming, particle formation [11]). In the field of fire protection, supercritical fluids are hitherto mainly used for FR extraction and recycling from electronic devices or polymers [12, 13].

In this work, we investigate the impregnation of technical veneers with high-performance (reactive) flame retardants using CO_2. Due to its moderate critical temperature (31.1°C), critical pressure (7.4 MPa), non-toxic nature, and cost-effectiveness, CO_2 is a promising green solvent for this application [14, 15]. A preliminary literature search aiming to narrow the field of potential flame retardants for this study – specifically, high-performance hetero-organic synthetic or biobased compounds compatible with both wood and supercritical

CO_2 – indicated that 9,10-dihydro-9-oxa-10-phosphaphenanthrene-10-oxide (DOPO) could be a suitable candidate to consider as a starting point.

Using DOPO as a promising, hetero-araliphatic FR for veneer protection, we investigated its pressure/temperature-dependent solubilization behavior in $scCO_2$ and compared it with data calculated using the mathematical Chrastil model. The Chrastil model was chosen as it essentially connects the density of a given SF with its (positively correlated) solubilization performance. Pressure and temperature are, however, non-linear inversely correlated with density. The latter increases with pressure but decreases with temperature, respective changes are most pronounced in the low-pressure range. The solubility of a given compound in an SF is furthermore governed by its molecular features in terms of size, spatial arrangement, and polarity, all affecting the interactions among and between solvent and solute molecules, as well as entropy changes upon dissolution [16, 17].

Experimental

Experiments on DOPO solubility in $scCO_2$ were performed at both laboratory and pilot scale using high-pressure stainless-steel equipment and loading chambers of different volume (0.2 and 4.4 liters). Figure 1 shows the schematic diagram of the smaller SF working station.

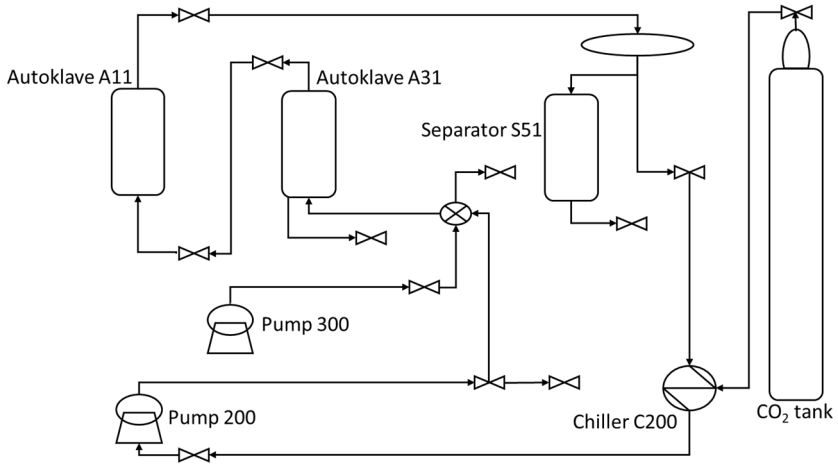

Figure 1: Schematic diagram of the experimental setup used to determine the solubility of DOPO in supercritical CO_2.

CO_2 (22°C, 4.5-7.0 MPa) exits the storage tank, is cooled to for liquefaction (0-5°C, chiller C 200) and subsequently pressurized to 10-30 MPa (piston pump P 200). If required, a co-solvent can be added (pump P 300) before the CO_2 enters autoclave A31, where it is

heated to the desired temperature to reach the target pressure. The preheated, pressurized CO_2 then flows into autoclave A11 (200 mL), where it gets in contact with the flame retardant and wood veneers. Excess flame retardant is precipitated in the separator S 51 (50°C, 6 MPa) from where it can be collected, while CO_2 is recycled through C 200 and P 200. Please note that all experiments were performed in static mode.

The solubility of DOPO was determined gravimetrically using a SI-234 microbalance (Denver Instruments, CO, USA). A defined amount of DOPO was transferred in an open pan into the autoclave. After closing the lid, the loading chamber was heated and pressurized with CO_2 (0.43 MPa/min) until the target conditions were reached. Pressure and temperature (p/T) were then kept constant for one hour before pressure was released at a rate of 0.1 MPa min^{-1} and the residual weight of DOPO in the pan was determined.

A mathematical prediction of the solubility of DOPO in $scCO_2$ was attempted using the Chrastil model (Equation 1). The respective input parameters and constants required to solve this equation were taken from the respective literature [18], i.e. density ρ of the pure solvent at given p/T conditions, average equilibrium association number *k*, constant a (summarizing the gas constant with the enthalpies of vaporization and solvation), absolute temperature *T*, and *b* (the quotient of the molecular weights of solvent and solute).

$$ln\,C = k\,ln\,p + \frac{a}{T} + b \qquad \text{Equation 1}$$

It is worth noting that the Chrastil model can be expanded by additional parameters or combined with other equations for further refinement, potentially improving prediction accuracy especially at low supercritical CO_2 densities [19-21].

A comparison of the calculated values with experimental data confirms the suitability of the Chrastil model to predict the solubility of DOPO in $scCO_2$ for the temperature range of 45-65°C and a pressure of 10-35 MPa (Figure 2). In this p/T range, the calculated and experimental data show that the solubility of DOPO in general increases with pressure and, hence, $scCO_2$ density. This effect was most pronounced at the lowest temperature studied (45°C) and the pressure range of 10-20 MPa. Across the entire pressure range (10-35 MPa), the highest solubility was achieved at the lowest temperature (45°C).

This, however, contrasts the findings by Liu, Han [18], who reported that an increase of both pressure (16-24 MPa) and temperature (40-110°C) improved solubility of DOPO in CO_2. This specific result, however, deviates from the general consent that the solubility of rather non-polar substances like DOPO decreases with $scCO_2$ density. Further studies of

the solubilization behavior of DOPO in $scCO_2$ are scarce and focused rather on technical applications and their economic aspects. Thus, $scCO_2$ impregnation of PET fibers (120°C, 25 MPa) was recently studied aiming to reach DOPO contents of 1-9 wt.%. The data calculated and experimentally determined exhibited considerable deviations, at lower pressures, an observation that was also made by other studies. This suggests the need for further model refinement to predict solubility values in this p/T region more precisely.

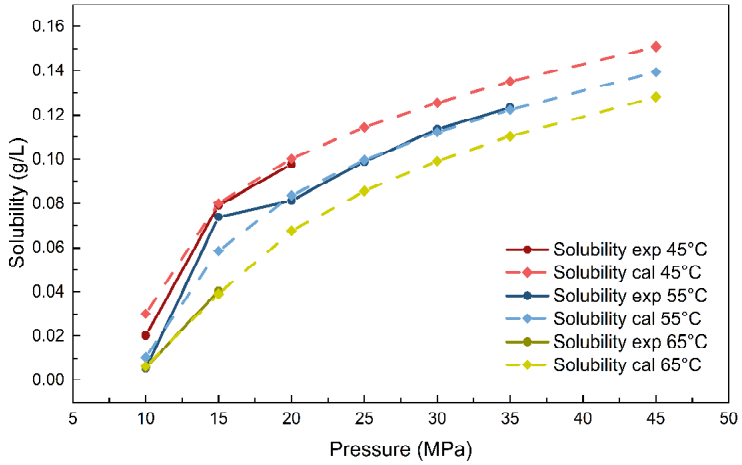

Figure 2: Calculated and experimental p/T-dependence of DOPO solubility in $scCO_2$.

Summary

This study investigated the solubilization behavior of DOPO, a potent organophosphorus alternative to halogenated FRs, in $scCO_2$ under static conditions. It has been shown that the solubility of DOPO increases with pressure but is inversely correlated with temperature. Furthermore, the applicability of the mathematical Chrastil model for predicting DOPO solubility has been confirmed, since good agreement between experimental data and calculated values could be obtained. Based on this preliminary work, we have started our work on $scCO_2$-assisted impregnation of technical veneers with heterorganic FRs hoping to meet the stringent regulatory requirements for respective materials in the automotive, aviation or nautical sector.

Acknowledgment

This work was part of the Bridge Project FO999903628 “Fire Protection of Wood Using $scCO_2$” (2023–2026) funded by the Austrian Research Promotion Agency. The authors are very grateful to their project partners Natex Prozesstechnologie GesmbH (Ternitz,

Austria) and Fritz Kohl GmbH & Co. KG (Karlstadt am Main, Germany) for co-funding and the generous support of this project.

References

1. Morgan, A.B. and A.Z. Worku, *Flame Retardants: Overview*, in *Kirk-Othmer Encyclopedia of Chemical Technology*. 2015. p. 1-28.
2. Pettersson, C., *Fire Safety in Timber Buildings - A review of existing knowledge*. 2020, Brandforsk. p. 80.
3. Lee, Y.X., et al., *Flame-retardant coatings for wooden structures.* Progress in Organic Coatings, 2025. **198**.
4. Acker, J.V., et al., *Wood Preservation and Wood Finishing*, in *Handbook of Wood Science and Technology*, P. Niemz;, A. Teischinger;, and D. Sandberg, Editors. 2023, Springer International Publishing. p. 793-871.
5. Mali, P., et al., *Morphology of wood degradation and flame retardants wood coating technology: An overview.* International Wood Products Journal, 2022. **13**(1): p. 21-40.
6. Kjellowa, A.W. and O. Henriksen, *Supercritical wood impregnation.* The Journal of Supercritical Fluids, 2009. **50**: p. 297-304.
7. Abdullah, S.A., *Solubility in supercritical carbon dioxide*, in *New Jersey Institute of Technology*. 2006, New Jersey's Science Technology University. p. 221.
8. Goñi, M.L., N.A. Gañán, and R.E. Martini, *Supercritical CO2-assisted dyeing and functionalization of polymeric materials: A review of recent advances (2015–2020).* Journal of CO2 Utilization, 2021. **54**: p. 101760.
9. Sánchez-Camargo, A.d.P., et al., *Supercritical fluid extraction.* Reference Module in Chemistry, Molecular Sciences and Chemical Engineering, 2014.
10. Zosel, K., *Process for the decaffeination of coffee* 1981, Studiengesellschaft Kohle MBH. p. 5.
11. Dahmen, N., et al., *Überkritische Fluide zur Behandlung und Herstellung komplexer Werktsoffe und Oberflöchenstrukturen*, I.f.T.C. Forschungszentrum Karlsruhe GmbH, Institut für Materialforschung, Editor. 2001: Karlsruhe. p. 111.
12. Gripon, L., et al., *Brominated flame retardants extraction from waste electrical and electronic equipment-derived ABS using supercritical carbon dioxide.* Waste Manag, 2021. **131**: p. 313-322.
13. Preetam, A., et al., *Supercritical fluid technology - an eco-friendly approach for resource recovery from e-waste and plastic waste: A review.* Separation and Purification Technology, 2023. **304**.
14. Weidner, E., *Impregnation via supercritical CO2–What we know and what we need to know.* The Journal of Supercritical Fluids, 2018. **134**: p. 220-227.
15. Zhang, J., L. Yang, and H. Liu, *Green and Efficient Processing of Wood with Supercritical CO2: A Review.* Applied Science 2021. **11**.
16. Uquiche, E., I. Leal, and C. Marillán, *Effect of process parameters on the extraction kinetics of Leptocarpha rivularis DC. in a packed bed extractor using supercritical carbon dioxide.* The Journal of Supercritical Fluids, 2024. **211**.
17. Peach, J. and J. Eastoe, *Supercritical carbon dioxide: a solvent like no other.* Beilstein J Org Chem, 2014. **10**: p. 1878-95.

18. Liu, G., et al., *Development of CO2 utilized flame retardant finishing: Solubility measurements of flame retardants and application of the process to cotton.* Journal of CO2 Utilization, 2020. **37**: p. 222-229.
19. García-Samino, C., E.M. del Valle, and A. Tabernero, *Predicting the solubility of solids in supercritical carbon dioxide using the Chrastil equation with parameters estimated from a group contribution method.* Journal of Molecular Liquids, 2024. **403**.
20. Sparks, D.L., R. Hernandez, and L.A. Estévez, *Evaluation of density-based models for the solubility of solids in supercritical carbon dioxide and formulation of a new model.* Chemical Engineering Science, 2008. **63**(17): p. 4292-4301.
21. Saldaña, M.D.A., et al., *Determination of vapor pressure and solubility correlation of phenolic compounds in supercritical CO2.* The Journal of Supercritical Fluids, 2007. **40**(1): p. 7-19.

Integrated Process of Supercritical Extraction from Bilberry Fruit and Impregnation of Extract onto Starch Aerogels

Jana Stamenović, Marko Stamenić

Department of Organic Chemical Technology, Faculty of Technology and Metallurgy, University of Belgrade, E-mail: 20243026@estudent.tmf.bg.ac.rs

Introduction

A process involving supercritical fluid technology that has been extensively investigated and industrially applied is the supercritical fluid extraction (SFE), in which a supercritical fluid (SCF), mainly supercritical carbon dioxide (SC CO_2), is used as a solvent for extractables within the plant matrix. Plant extracts have been used in traditional medicine for centuries and are known to have a variety of properties, such as antioxidant, anti-inflammatory and/or antimicrobial, suitable for various applications in food, pharmaceutical and cosmetic industries, among others. SFE offers several advantages over the conventional extraction procedures, such as organic solvent extraction and distillation, among which the most significant are obtaining product without the traces of a solvent and processing under mild conditions [1, 2]. In order to obtain a functional product, extracts can be incorporated into a matrix that serves as a carrier and can generally be in a form of a film or a tablet. One way to perform the incorporation is the supercritical solvent impregnation (SSI) process, in which a SCF, again mainly SC CO_2, is used firstly to dissolve the extract, and then to impregnate it into the desirable carrier [3]. Particularly suitable carriers are natural polysaccharide based aerogels, biocompatible and biodegradable highly porous materials with large specific surface area [4].

In this work the integrated process of SFE from bilberry fruit and SSI into starch aerogel (SFE-SSI process) is performed. Bilberry fruit was found to have a high amount of phenolic compounds, including anthocyanins, which have been proved to have a positive effect on human health [5]. Among the suitable natural polysaccharides, starch is favourable due to its low toxicity, renewability, stability, availability and low cost [6].

Experimental

Starch aerogel in the form of tablets was obtained by supercritical drying at 10 MPa and 45 ºC, as these conditions were previously shown to be optimal [7].

The integrated SFE-SSI process was performed in the apparatus shown in Figure 1. Bilberry fruit was dried and ground in a coffee mill for 30 s before the extraction process. The material (20±0.1 g) was mixed with glass beads, placed into the stainless-steel tube, and covered with a porous net and filter paper. Tablets of starch aerogel were placed in a mesh basket which was put at the top of the stainless-steel tube, above the plant material. At start the desired temperature was reached, and subsequently CO_2 was introduced into the system. When desired process pressure was reached, circulation of the solution (CO_2 + extract) through the extraction column was provided for four hours using the high pressure gear pump.

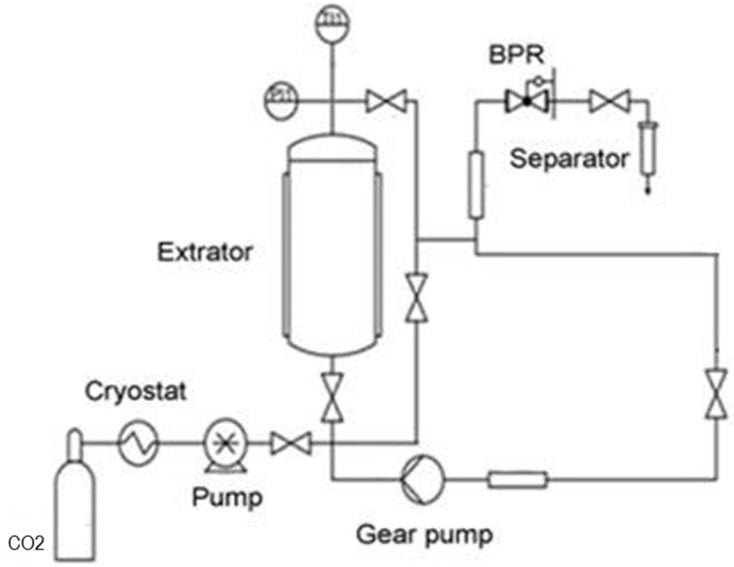

Fig 1. Scheme of the apparatus for integrated SFE-SSI process.

Experiments were carried out at several process conditions. Temperature was 70 °C in all experiments, while pressures of 15 and 30 MPa were applied. Additionally, ethanol as cosolvent in the amount of 20wt% (based on the plant material) was introduced to the two sets of experimental conditions. The process ended with decompression at the rate of 2 MPa/min. The extract loading yields were determined gravimetrically as the percentage of mass ratio of extract loading and the loaded aerogel.

The results of SFE-SSI experiments are shown in Figure 2 for all sets of experimental conditions. Clearly, pressure had a significant influence on the impregnation of the starch aerogels. Without the cosolvent, increase in pressure from 15 to 30 MPa led to an increase in loading yield from around 2% to 32%. Higher pressure implies higher solubility of the extract in the SC CO_2, and thus, higher availability of the extract for impregnation into the carrier. On the other hand, the addition of ethanol as a cosolvent had different impact on

the loading yield, depending on the pressure. At lower pressure, ethanol significantly improved the impregnation, while at higher pressure the yield was somewhat decreased. In general, ethanol, as a polar substance, improves the extraction of polar components. On the other hand, the impact of ethanol addition on impregnation is not straightforward, as it includes complicated interactions between SC CO_2, extract and ethanol, which include the phase behaviour and competitive solubility in this multicomponent system. Besides, the affinity of compounds in the extract towards solvent mixture with enhanced solvating power can be higher than the partition coefficient in favour of the carrier, which can negatively affect impregnation efficiency.

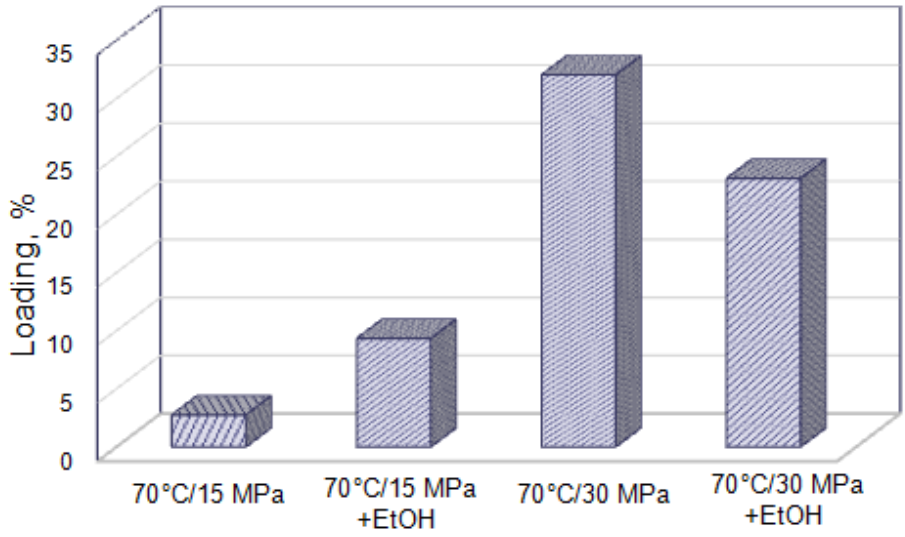

Fig. 2. Loading yields for SFE-SSI of bilberry extracts into starch aerogels.

In order to assess the quality of the impregnation in the performed experiments, re-extraction from obtained impregnated materials was performed. The bilberry extract was re-extracted from the impregnated aerogels employing an ultrasound extraction with a $CHCl_3$:MeOH (7:3) mixture. The samples were crushed into smaller pieces and rinsed in an appropriate volume of $CHCl_3$:MeOH mixture to obtain the final extract concentration of approximately 30 mg/mL. The samples were sonicated using an ultrasonic bath in five cycles, each lasting for 30 min. In this way, re-extracts were prepared for HPLC analyses. The results of HPLC analysis of the re-extracts are shown in Table 1.

Tab.1: Results of the HPLC analysis of the obtained e-extracts.

Name	70°C/15MPa	70°C/15 MPa + EtOH	70°C/30 MPa	70°C/30 MPa + EtOH
	mg/g re-extract			
Protocatechuic acid	0.63	2.46	0.23	3.00
Procyanidin B1	62.79	75.61	26.94	42.97
Vanillic acid	/	0.36	0.18	0.21
Syringic acid	0.68	0.45	0.22	0.32
p-Coumaric acid	/	0.49	0.12	0.5
Ellagic acid	0.12	/	0.01	0.02
Chrysin	0.68	1.30	0.04	0.09
trans-Ferulic acid	/	0.86	/	/

Summary

In this work the results of the integrated process of supercritical fluid extraction from bilberry fruit and extract impregnation on starch aerogels are presented. Experiments were performed at pressures of 15 and 30 MPa, with and without the addition of ethanol as cosolvent, at the temperature of 70 °C. The results show the strong influence of pressure on the impregnation, as increase in pressure brought significant increase in the loading yield. The influence of ethanol addition on the impregnation was quantitatively positive on lower pressure, while the opposite effect was observed at higher pressure. Qualitatively, ethanol contributed to the increase in the content of the main extract constituent, Procyanidin B1.

References

[1] Knez, Ž., Markočič, E., Leitgeb, M., Primožič, M., Knez Hrnčič, M., & Škerget, M. (2014). Industrial applications of supercritical fluids: A review. *Energy*, *77*, 235–243. https://doi.org/https://doi.org/10.1016/j.energy.2014.07.044

[2] Reverchon, E., & de Marco, I. (2006). Supercritical fluid extraction and fractionation of natural matter. *The Journal of Supercritical Fluids*, *38*(2), 146–166. https://doi.org/https://doi.org/10.1016/j.supflu.2006.03.020

[3] Weidner, E. (2018). Impregnation via supercritical CO2–What we know and what we need to know. *The Journal of Supercritical Fluids*, *134*, 220–227. https://doi.org/https://doi.org/10.1016/j.supflu.2017.12.024

[4] García-González, C. A., Alnaief, M., & Smirnova, I. (2011). Polysaccharide-based aerogels—Promising biodegradable carriers for drug delivery systems. *Carbohydrate Polymers*, *86*(4), 1425–1438.
https://doi.org/https://doi.org/10.1016/j.carbpol.2011.06.066

[5] Giovanelli, G., & Buratti, S. (2009). Comparison of polyphenolic composition and antioxidant activity of wild Italian blueberries and some cultivated varieties. *Food Chemistry*, *112*(4), 903–908.
https://doi.org/https://doi.org/10.1016/j.foodchem.2008.06.066

[6] Malafaya, P. B., Stappers, F., & Reis, R. L. (2006). Starch-based microspheres produced by emulsion crosslinking with a potential media dependent responsive behavior to be used as drug delivery carriers. *Journal of Materials Science: Materials in Medicine*, *17*(4), 371–377.
https://doi.org/10.1007/s10856-006-8240-z

[7] Lukic, I., Pajnik, J., Tadic, V., & Milovanovic, S. (2022). Supercritical CO2-assisted processes for development of added-value materials: Optimization of starch aerogels preparation and hemp seed extracts impregnation. *Journal of CO2 Utilization*, *61*, 102036.
https://doi.org/https://doi.org/10.1016/j.jcou.2022.102036

Aerogels Based on Synthetic Polymers

Juan Sebastian Castillo Gonzalez

Institute of Thermal Separation Processes, Hamburg University of Technology,
sebastian.castillo@tuhh.de

Introduction

Aerogels are highly porous materials known for their low density, high surface area (100–1200 m²/g), and excellent thermal and acoustic insulation properties [1]. First-generation aerogels, primarily silica-based, offered strong performance but suffered from brittleness and poor mechanical flexibility. To address these drawbacks and promote sustainability, second-generation aerogels made from biopolymers like cellulose, chitosan, and alginate have been developed. These renewable, biodegradable materials offer greener alternatives but often lack the mechanical and thermal performance needed for advanced applications [2]. To enhance structural properties, synthetic polymer aerogels have been introduced, particularly those based on high-performance polymers such as polyimide, polyamide, and polyurea [3]. However, the range of polymers used remains narrow and typically excludes commodity plastics like polypropylene and polystyrene, which contribute significantly to plastic pollution. Thermally induced phase separation (TIPS) has emerged as a promising method for processing these widely available polymers into aerogels, enabling the formation of nanostructured porous materials with improved mechanical stability [4]. This research aims to explore the fabrication of aerogels from commonly used synthetic polymers—such as polypropylene (PP), polystyrene (PS), and polyethylene terephthalate (PET)—via the TIPS method. By focusing on these high-volume, widely discarded materials, particularly from post-consumer and industrial plastic waste, the study seeks to develop high-value, sustainable aerogels and contribute to circular economy strategies for polymer upcycling

Experimental

Polypropylene gels were successfully obtained via thermally induced phase separation (TIPS) using solvents such as hexane, heptane, and octane. The dissolution temperature strongly influenced the gel morphology: lower temperatures favored monoliths, while higher ones led to particulate structures. Polymer molecular weight and concentration also affected the macroscopic shape. As is possible to see on figure 1, different macroscopic shapes can be obtained.

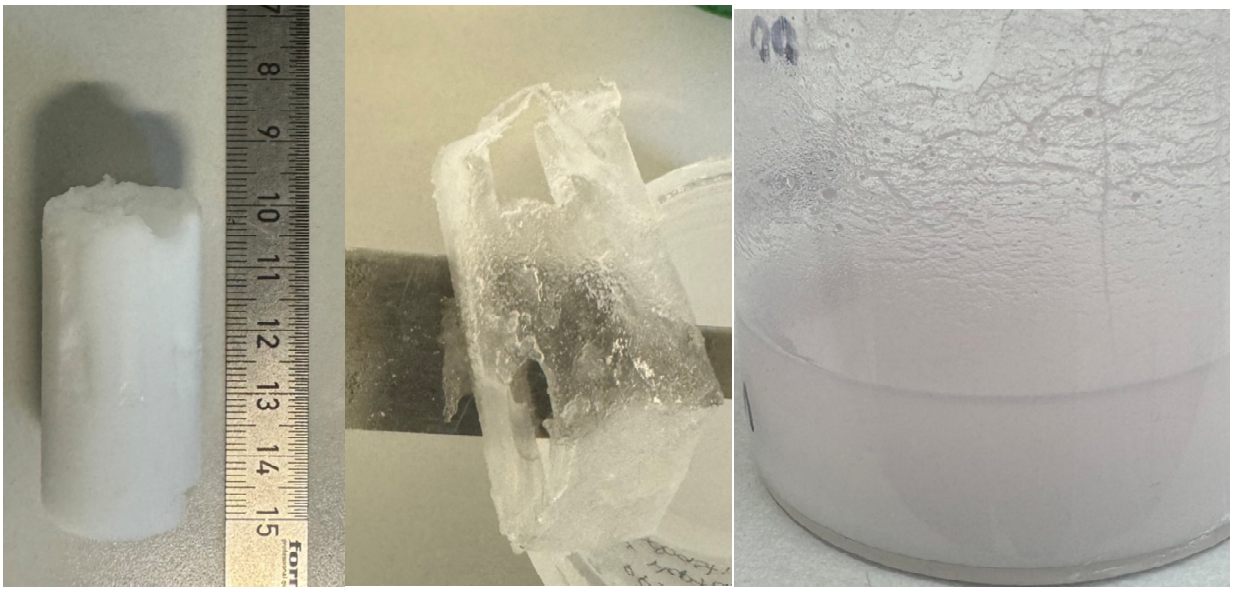

Figure 1. Macroscopic shapes of polypropylene gels monolith, film and powder

A major advantage of this system is that the organogels can be directly supercritically dried without solvent exchange, as the solvents are CO_2-soluble. BET surface area and pore size analysis (Table 1) show promising values, indicating the feasibility of producing porous polypropylene aerogels via TIPS. The process demonstrated good reproducibility and robustness, providing a solid foundation for future development.

Table 1. Surface area and pore size distribution of polypropylene aerogels obtained via TIPS with different solvents

	Hexane	Heptane	Octane
BET surface area (m2/g)	226	228	220
R2	0,9999	0,9999	0,9999
C-Constant	21	20	23
Pore volume (cc/g)	1,3	1,2	1,2
Average pore diameter (nm)	23,3	22,2	21,2

Scanning electron microscopy (Figure 2) clearly reveals a well-developed pore network. One notable benefit of polypropylene aerogels is their intrinsic hydrophobicity, which may enable their use in hydrophobization applications. However, this work represents only an initial step, and further optimization is needed to improve performance and expand functionality.

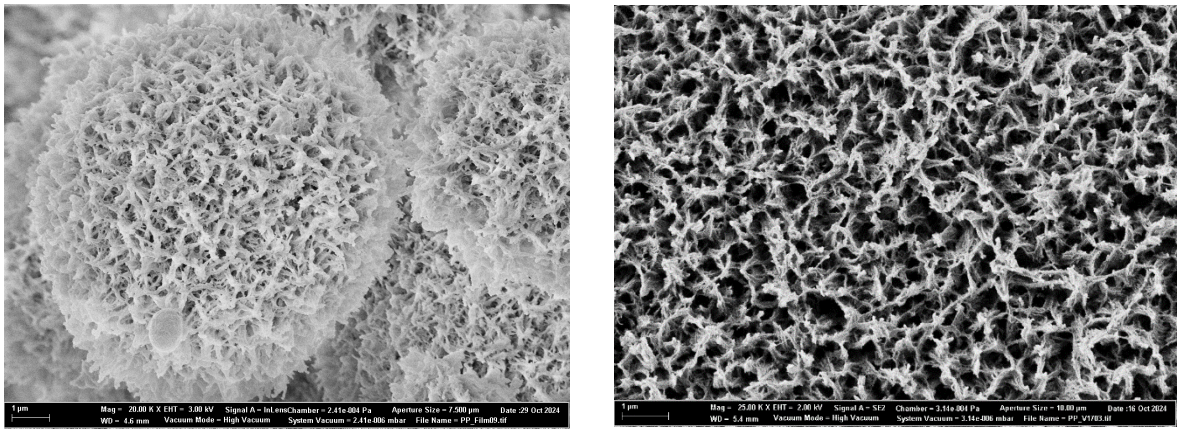

Figure 2. Scanning electron microscope pictures of polypropylene aerogels. showing well developed porous structure.

Summary

Polypropylene aerogels were successfully produced via TIPS, showing good reproducibility, direct compatibility with supercritical drying, and promising porous structures. Their hydrophobicity and process simplicity make them attractive for further development, though optimization is still needed to enhance performance and expand applications.

Acknowledgment

The author thanks the Ingeborg Gross foundation for funding this research.

References

[1] M. A. Aegerter, N. Leventis, and M. M. Koebel, Aerogels Handbook. New York, NY, USA: Springer, 2011. [Online]. Available: https://link.springer.com/book/10.1007/978-1-4419-7589-8

[2] A. Muhammad, D. Lee, Y. Shin, and J. Park, “Recent Progress in Polysaccharide Aerogels: Their Synthesis, Application, and Future Outlook,” Polymers, vol. 13, no. 8, p. 1347, Apr. 2021. [Online]. Available: https://www.mdpi.com/2073-4360/13/8/1347

[3] B. N. Nguyen, D. A. Scheiman, M. A. B. Meador, J. Guo, B. Hamilton, and L. S. McCorkle, “Effect of Urea Links in the Backbone of Polyimide Aerogels,” ACS Applied Polymer Materials, vol. 3, no. 4, pp. 2027–2037, Apr. 2021. [Online]. Available: https://doi.org/10.1021/acsapm.1c00085

[4] H. Ma, B. Wang, J. Qi, Y. Pan, and C. Chen, “Fabrication of Mechanically Strong Silica Aerogels with the Thermally Induced Phase Separation (TIPS) Method of Poly(methyl methacrylate),” Materials, vol. 16, no. 10, p. 3778, May 2023. [Online]. Available: https://www.mdpi.com/1996-1944/16/10/3778

Implementation of a New Comonomer in High-Pressure Polymerization

Erik Prenzel, Markus Busch*

Ernst-Berl-Institute of Technical and Macromolecular Chemistry, Technical University Darmstadt, *markus.busch@pre.tu-darmstadt.de

Introduction

We encounter plastics in a wide variety of areas in everyday life. Plastic surrounds us in the form of packaging, textiles, and automotive interiors.[1] Over the past decades, plastics have gained increasing importance as a high-performance material.[2] As a result, global annual production has grown steadily, reaching approximately 400 million tons. Approximately 26 % of the global plastic production consists of polyethylene.[3,4]

Low-density polyethylene is synthesized through a radical polymerization process at temperatures ranging from 150 to 300°C and pressures of up to 3 000 bar. This process creates both short- and long-chain branching.[1,2] Despite the more cost-intensive high-pressure synthesis, polymers with various properties can be produced by using comonomers. The properties include molar mass distribution, branching densities, density, and crystallinity, which allows for a wide range of applications. To enable the implementation of new comonomers in the high-pressure polymerization process, several experiments are conducted within our research group beforehand. Thermophysical properties are determined using transitiometry, phase behavior is investigated, decomposition temperatures are measured, and batch polymerization experiments are performed.

Differential thermal analysis (DTA)

To introduce a new comonomer into the high-pressure polymerization process, the initial step involves assessing the thermal stability of the substance using differential thermal analysis (DTA). DTA is a valuable technique for investigating both endothermic and exothermic processes of a substance, in an ethylene or nitrogen atmosphere under high-pressure conditions. DTA predominantly yields qualitative and semi-quantitative data.[5]

As illustrated in Figure 1, DTA employs the twin principle, where the temperature profiles for both the sample and reference are identical. Consequently, thermal events are observed as temperature differences between the two. When ethylene is used as the

pressure medium, the DTA allows for the precise determination of the decomposition temperature of the sample.[5]

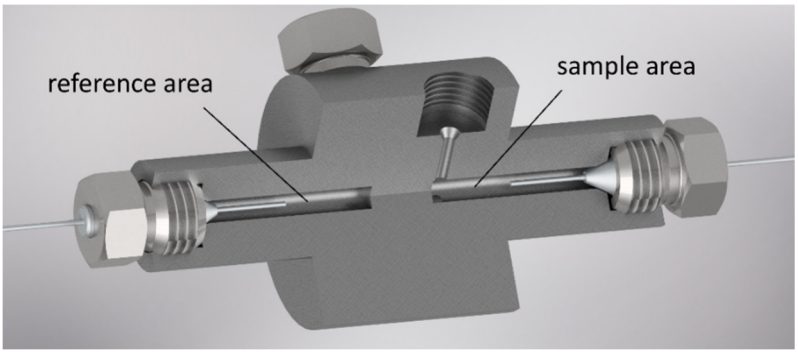

Fig. 1.: Computer aided design of the DTA.

To perform a DTA measurement, approximately 0.3 mg of a solid sample or 0.3 mL of a liquid sample is added into the DTA sample-chamber, which is subsequently sealed. The DTA device is then connected to the high-pressure infrastructure inside the oven. Prior to the measurement, a pressure test is conducted. The sample-chamber is purged with ethylene to eliminate contaminants. Once purging is complete, the temperature program is initiated.[5]

Figure 2 shows the results of the DTA of vinyl acetate VA, using ethene as the pressure medium. The temperature difference between the sample and the reference is plotted as a function of the reference temperature. Up to approximately 260°C, no significant temperature difference between the two chambers is observed. Beyond this temperature, the temperature of the sample chamber increases drastically, as the decomposition temperature of vinyl acetate is reached, which subsequently leads to the decomposition of ethene.

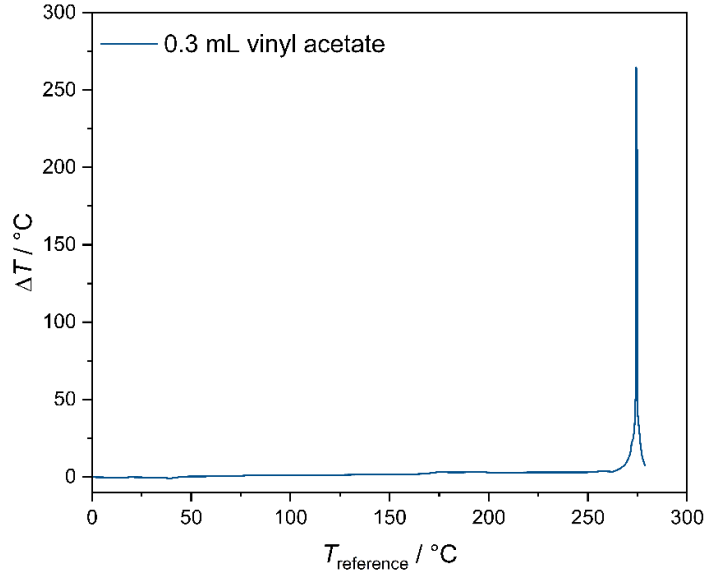

Fig. 2.: DTA measurement with vinyl acetate and ethene as pressure medium.[5]

Thermophysical properties

Transitiometry is an analytical technique used to precisely determine thermophysical properties under conditions of high pressure. The thermophysical properties include density, compressibility, thermal expansion coefficient and heat capacity. These properties form the foundation for accurate simulations and process upscaling. To obtain these measurements, the method involves controlling the three fundamental thermodynamic variables pressure, temperature, and volume. In each experimental setup, one of these variables is maintained constant while another is temporarily varied, allowing for the calculation of the respective property.[6]

As illustrated in Figure 3, the calorimetric block consists of two independent measuring cells, the sample crucible and the reference crucible. The reference crucible is filled with air, while the sample crucible contains the substance of interest. The pressure and volume within the measuring cells are precisely regulated by using nearly incompressible mercury and a step motor. The calorimetric block is equipped with 672 thermocouples, arranged in a cylindrical configuration around the crucibles according to the Tian-Calvet principle, ensuring accurate thermal measurements.[6]

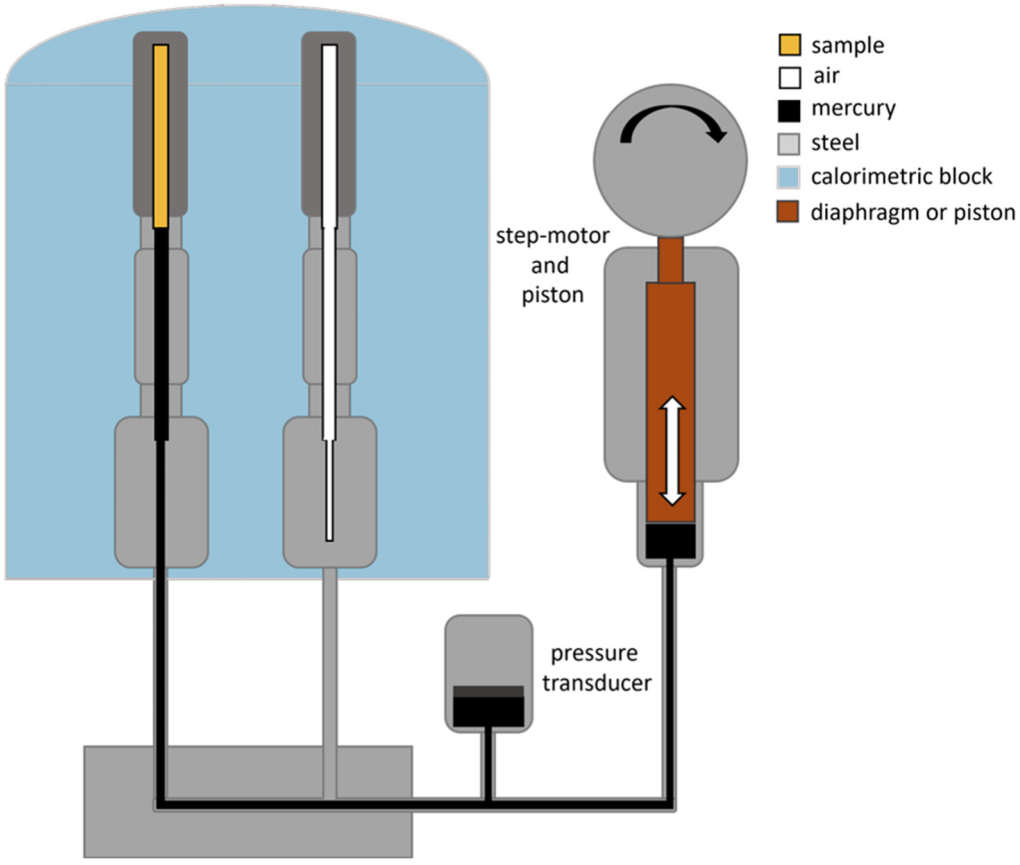

Fig. 3.: Schematic representation of the standard unit transitiometer from BGR TECH.[7]

Phase behavior

To feed comonomers using compressors and pumps, it is crucial to know the phase behavior to prevent equipment damage. Additionally, the phase behavior of the reaction mixture within the autoclave is of importance to ensure product quality and maintain process safety.[5]

To investigate the phase behavior of a substance, a view cell, as depicted in Figure 4, is used. During the assembly process, solid samples are introduced directly into the cell. Subsequently, a pressure test is performed to verify the tightness of the system.

In the case of a liquid sample, it is first drawn into a syringe within a glove box to ensure an oxygen-free environment. The syringe contents are then transferred into the view cell through a lateral bore hole while maintaining an ethylene counterflow.[5]

To achieve the desired pressure or composition, ethylene is supplied via the ethylene line. The temperature within the view cell is regulated using two heating jackets, while pressure variation is accomplished by adjusting the position of a movable piston. The piston changes its position by changing the pressure on the opposite side of the sample using two syringe pumps.[5]

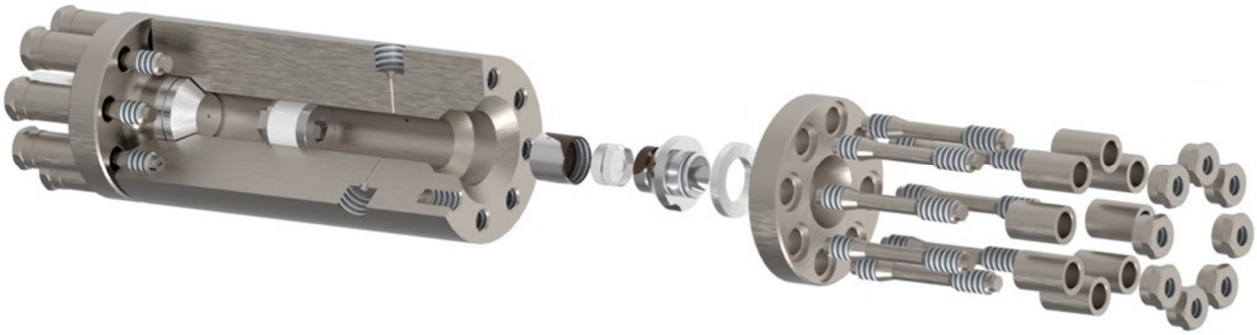

Fig. 4.: Computer aided design of the view cell.[8]

Different types of phase transitions occur during the experiment. A distinction is made between bubble point and dew point. The type of transition is influenced by the proportion of the light and heavy phase and their properties. Typically, when the heavy phase predominates, a bubble point transition occurs, characterized by the formation of gas bubbles during depressurization, as illustrated in Figure 5 (left). In contrast, when the light phase is more abundant and the temperature is higher, the system undergoes a dew point transition (Figure 5, right).[5]

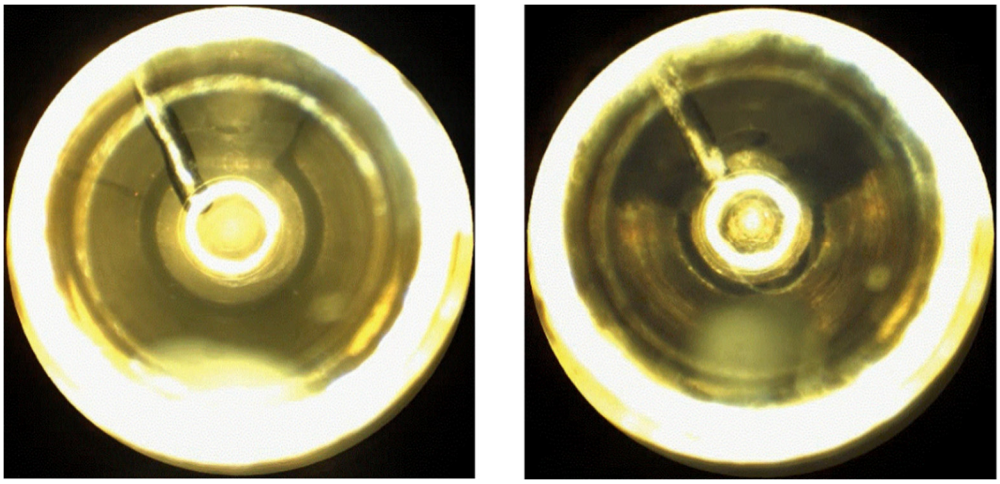

Fig. 5.: Bubble point like transition (left) and dew point like transition (right).[5]

Figure 6 shows the phase diagram of ethene and vinyl acetate as a function of the mass fraction of vinyl acetate and the pressure at 80°C and 150°C. The dew points are represented by squares, while bubble points are indicated by dots.

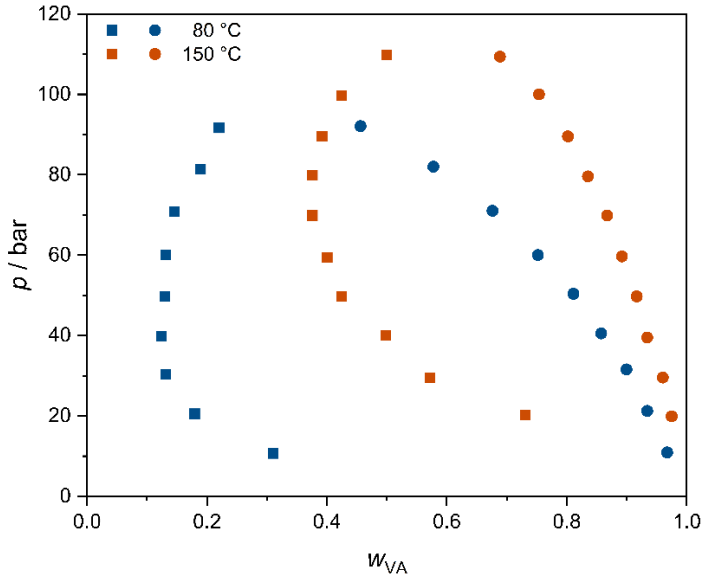

Fig. 6.: Phase diagram of the vinyl acetate–ethene system at 80°C and 150°C.[9]

Batch experiments

In addition to phase behavior studies, batch experiments can also be conducted. The configuration of the view cell, depicted in Figure 7, is adapted for batch experiments by removing the piston and connecting an ethene pipe to a lateral bore hole. After a pressure test the view cell is subsequently flushed with ethylene to eliminate residual oxygen, thereby creating an oxygen-free environment within the autoclave.

Simultaneously, the injection mixture is prepared in the glove box by drawing it into a Hamilton syringe and then transferring it into the evacuated injection tube. The ethylene pressure within the viewing cell and the injection tube is adjusted using a piston compressor. Upon opening the valve, the injection mixture is released into the autoclave, initiating the polymerization process.[5]

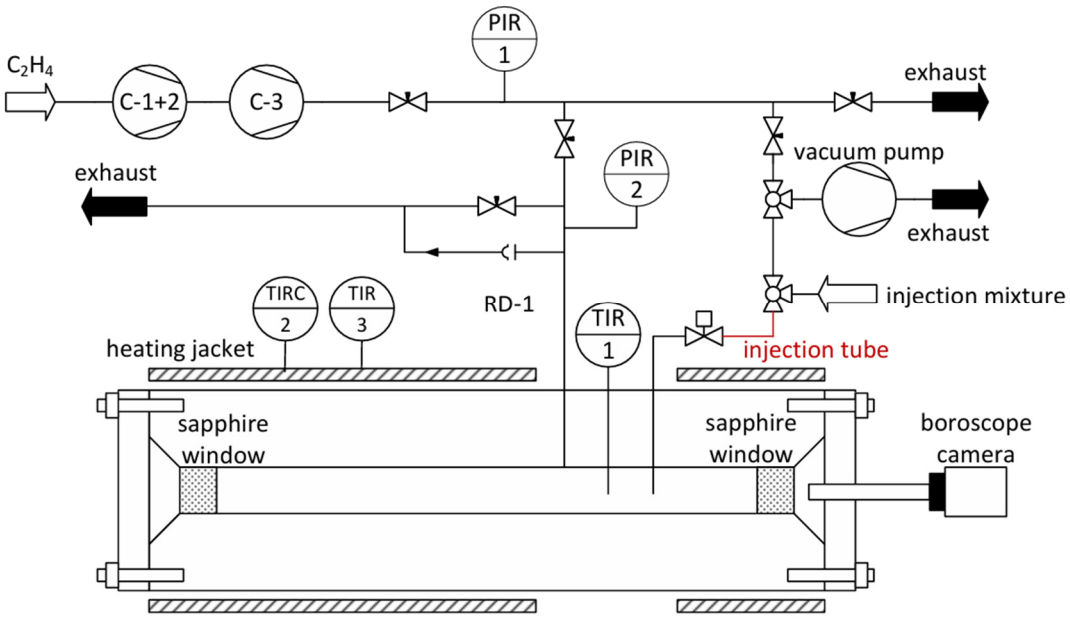

Fig. 7.: Simplified flow sheet of the batch experiment setup.[5]

Batch experiments enable the efficient performance of copolymerization reactions of small polymer samples while minimizing comonomer consumption. However, due to the temporal variation in reactant concentrations throughout the process, a steady state is not attained.

Continuous experiments

To conduct experiments under continuous operation, preliminary batch polymerization and phase behavior are necessary.

The working group has access to several autoclaves designed for high-pressure polymerization, including a 15 mL autoclave, a 100 mL autoclave, and a 300 mL multi-zone autoclave, which is shown in Figure 8.

The 15 mL autoclave is particularly suitable for synthesizing small sample quantities with rare or expensive chemicals. The 100 mL autoclave serves as the standard apparatus and is also suitable for preparing larger sample quantities. The 300 mL multi-zone

autoclave allows for the introduction of chemicals into individual zones, thereby increasing the number of process variables available for polymer synthesis. In general, a wide range of experimental conditions can be achieved by adjusting parameters such as temperature, pressure, and the controlled feed of initiator, chain transfer agent, and comonomer.

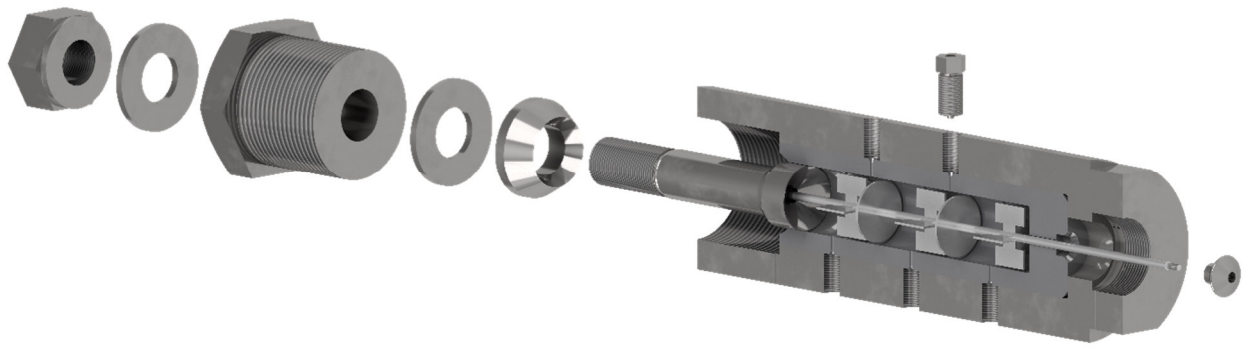

Fig. 8.: Computer aided design of the 300 mL multi-zone autoclave [10]

Summary

In order to implement a new comonomer in the high-pressure process, it is essential to first collect comprehensive data on the comonomer's properties. This includes thermophysical data, which can be determined using a transitiometer, as such data is crucial for process simulation and scale-up. Additionally, understanding endothermic and exothermic processes (e.g., decomposition) is important, and these can be qualitatively and semi-quantitatively assessed using differential thermal analysis (DTA).

Investigating the phase behavior is also important to ensure the safe and efficient feeding of the comonomer using compressors and pumps, thereby preventing equipment damage and maintaining a homogeneous reaction mixture within the reactor.

Batch experiments are useful for synthesizing small quantities of polymer with little effort, allowing for first investigations. In contrast, continuous experiments enable the production of larger polymer quantities while offering the advantage of controlling numerous process variables such as pressure, temperature, chain transfer agent (CTA) concentration, and comonomer feed rate to fine-tune the polymer properties.

References

[1] D. Eckes, PhD thesis, Technische Universität Darmstadt, **2017**.

[2] I. Neuhaus, PhD thesis, Technische Universität Darmstadt, **2014**.

[3] Statista (2024), https://de.statista.com/statistik/daten/studie/167099/umfrage/weltproduktion-von-kunststoff-seit-1950/, last accessed: 30.03.2025.

[4] Plastics Europe (2024), https://plasticseurope.org/knowledge-hub/plastics-the fast-facts-2024/, last accessed: 30.03.2025.

[5] S. Hintenlang, PhD thesis, Technische Universität Darmstadt, **unpublished**.

[6] S. Albus, Master's thesis, Technische Universität Darmstadt, **2021**.

[7] S. Albus, J. Nowottny, J. Sartorius, M. Busch, *Journal of Solution Chemistry* 2023, 53, 43-59.

[8] L. Dietrich, Master's thesis, Technische Universität Darmstadt, **2023**.

[9] B. Folie, C. Gregg, G. Luft, M.Rasdosz, *Fluid phase equilibria* **1996**, 120, 11-37.

[10] C. Weigel, M. Busch, *ASME Press. Vessels Pip. Div.* **unpublished**.

Optimizing Porous Cathodes for CO_2 Electroreduction: Computational Strategies Toward Solar Fuel Technologies

Inês S. Fernandes [a], Rodrigo Martins [a], Manuel J. Mendes [a], Ana S. Reis-Machado [a,b,*]

[a] i3N/CENIMAT, Department of Materials Science, NOVA School of Science and Technology, NOVA University Lisbon, CEMOP/UNINOVA, 2829-516 Caparica, Portugal

[b] LAQV, REQUIMTE, Department of Chemistry, NOVA School of Science and Technology, NOVA University Lisbon, 2829-516 Caparica, Portugal

Corresponding author: ams.machado@fct.unl.pt

Introduction

Carbon dioxide (CO_2) electroreduction (CO_2R) represents a promising carbon capture and utilization (CCU) strategy, potentially enabling the transformation of waste CO_2 into value-added fuels and chemicals. This technology is particularly relevant in the context of the global climate crisis, where sustainable energy solutions are imperative. Among the various CO_2R platforms, aqueous-phase electrochemical systems stand out for their modularity and compatibility with renewable electricity sources.

Porous electrodes have garnered attention due to their enhanced surface areas, which support higher reaction rates. This research presents a detailed computational study on the optimization of porous zinc cathodes using finite-element modeling. The goal is to design cathodes capable of high current density operation under realistic conditions suitable for industrial upscaling including conditions at pressures higher than atmospheric pressure.

Figure 1 illustrates the general concept of the solar fuels cycle and the electrochemical reduction cell architecture, showing the integration of photovoltaic power with CO_2R and H_2O electrolysis to produce syngas.

Experimental/Methodology

A 2D finite-element method (FEM) model was developed using COMSOL Multiphysics® to simulate porous zinc cathodes for CO_2R. The model incorporates modules for secondary current distribution, species transport, and creeping flow, reflecting the electrochemical environment. The simulated domain accounts for geometric

characteristics such as pore length, fiber diameter, and porosity. Electrochemical kinetics are described using the Butler-Volmer equation.

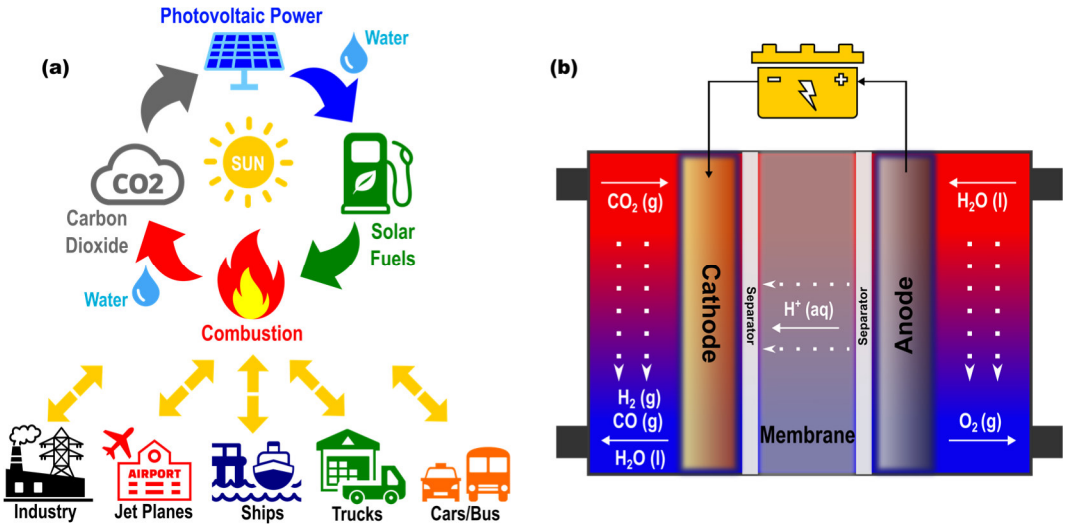

Fig. 1.: (a) Solar fuels concept. (b) MEA electrolyzer for CO_2 reduction and water splitting in a zero-gap setup (not to scale). Reproduced from [1].

Table 1 summarizes key electrochemical and physical parameters used in the model.

Tab. 1.: Species transport and electrochemical parameters from model [1].

Designation	Symbol	Value	Units	Source
Electrode Conductivity	σ_s	16.6 x 10^6	S/m	[2]
CO_2R Standard Equilibrium Potential (vs. RHE)	E_0	-0.10	V	[3,4]
CO_2R Exchange Current Density	i_0	8.7488	mA/cm^2	[5]
CO_2R Cathodic Transfer Coefficient	α_c	0.5	---	[6]
CO_2R Anodic Transfer Coefficient	α_a	0.5	---	[6]
Electrolyte Density	ρ	1000	g/L	[6]
Electrolyte Kinematic Viscosity	μ	600	g/(cm.min)	[6]
Reference Temperature	T_{ref}	25.0	°C	NTP
Reference Pressure	P_{ref}	1.0133	bar	NTP

To identify optimal operational parameters, the Nelder-Mead optimization algorithm was applied. Variables included cathode porosity, number of fibers per side, fiber shape, inlet pressure, temperature, and flow rate. Boundary conditions replicate realistic electrolyzer environments, including stationary flow, non-gravity fluid behaviour, and pressurized CO_2 entry.

Figure 2 shows the 2D geometry of the porous electrode and validation of the model against experimental data, achieving strong agreement and verifying simulation reliability.

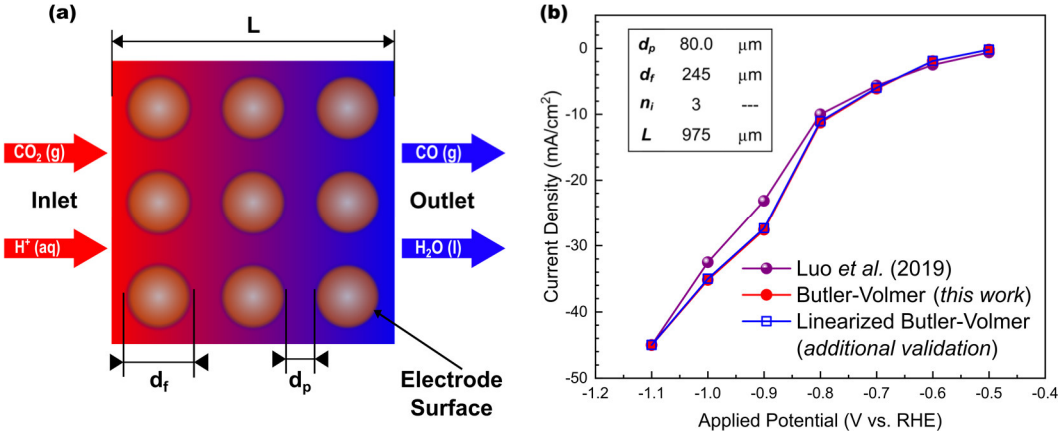

Fig. 2.: (a) 2D porous cathode model with infinite cylindrical fibers. Key parameters: side length (L), fiber diameter (d_f), pore length (d_p), number of fibers per side (n_i = 3), and electrode surface area (S). (b) Simulated vs. experimental current–voltage curves (Luo *et al.* [5]), using validation parameters shown in the inset. Reproduced from [1].

Summary

The study explored the impact of cathode morphology and operational parameters on local current density (i_{loc}). Simulations revealed that fiber shape significantly affects performance. Equilateral triangular fiber geometry, for example, achieved i_{loc} values up to 128.2 mA/cm^2, while further optimization with the Nelder-Mead method yielded 263.6 mA/cm^2 at −1.1 V vs. RHE (Figure 3).

Lower catholyte flow rates, particularly at 1.0 mL/min, also enhanced iloc by up to 171% relative to baseline. Meanwhile, increased inlet pressure and optimal temperature tuning (34 °C at 20 bar) provided up to 486% performance improvement, highlighting the critical role of thermodynamic and transport conditions.

Figure 4 presents the final comparison of optimized configurations across morphological and operational scenarios, validating the approach's effectiveness.

This research underscores the power of FEM modeling and computational optimization in designing efficient, scalable cathodes for CO_2 electroreduction. The outcomes serve as a theoretical basis for experimental electrode fabrication and suggest paths toward practical deployment of solar fuel technologies.

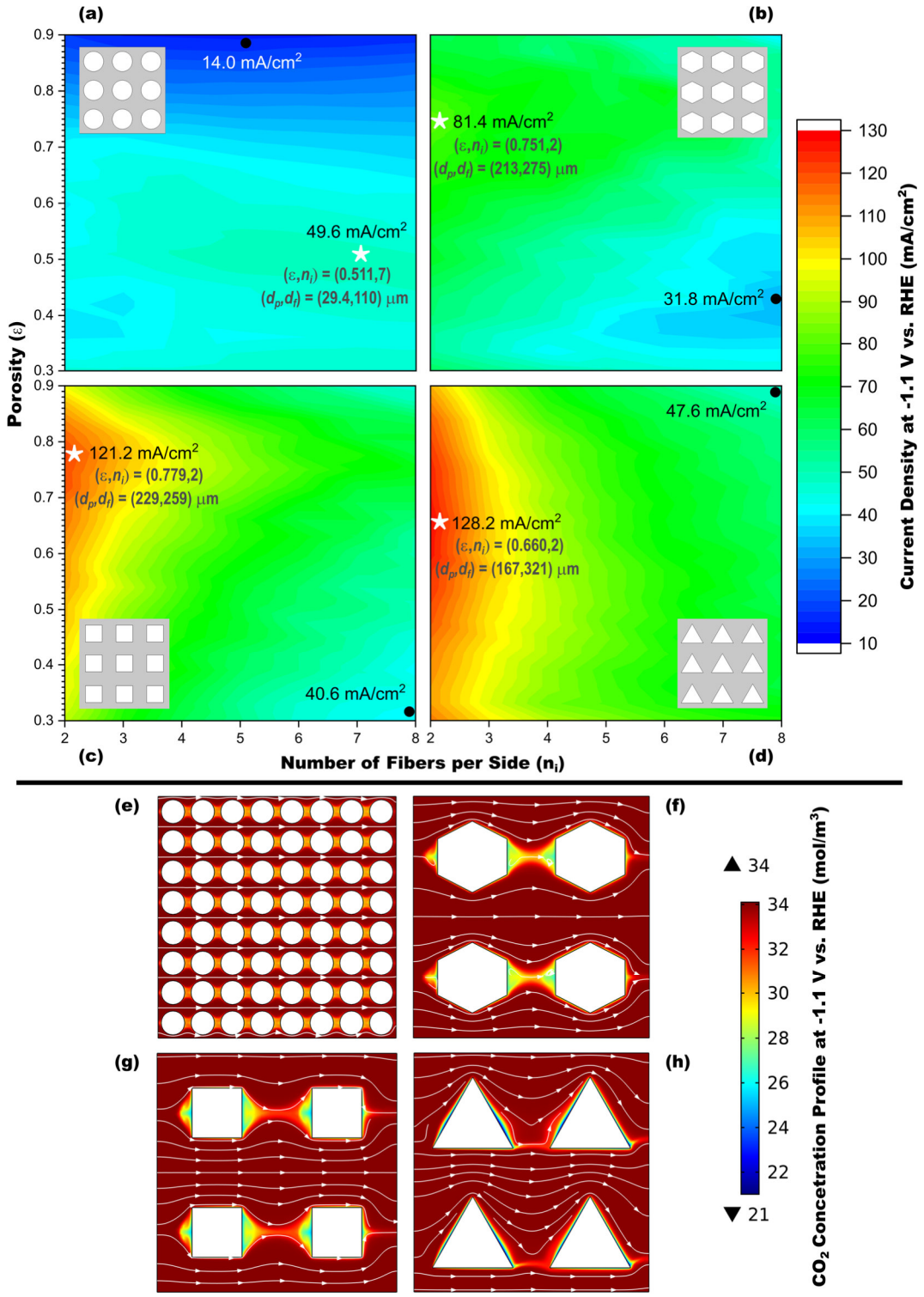

Fig. 3.: (a–d) Contour plots of current density (i_{loc}) vs. number of fibers per side (n_i) and porosity (ε). (e–h) Corresponding CO_2 concentration profiles and flux streamlines for fiber shapes: (a, e) circle; (b, f) hexagon; (c, g) square; (d, h) triangle. Operating conditions: -1.1 V vs. RHE, 22 °C, 1 atm, Q_{out} = 21 mL/min. White stars: maxima i_{loc}; black dots: minima i_{loc}. Reproduced from [1].

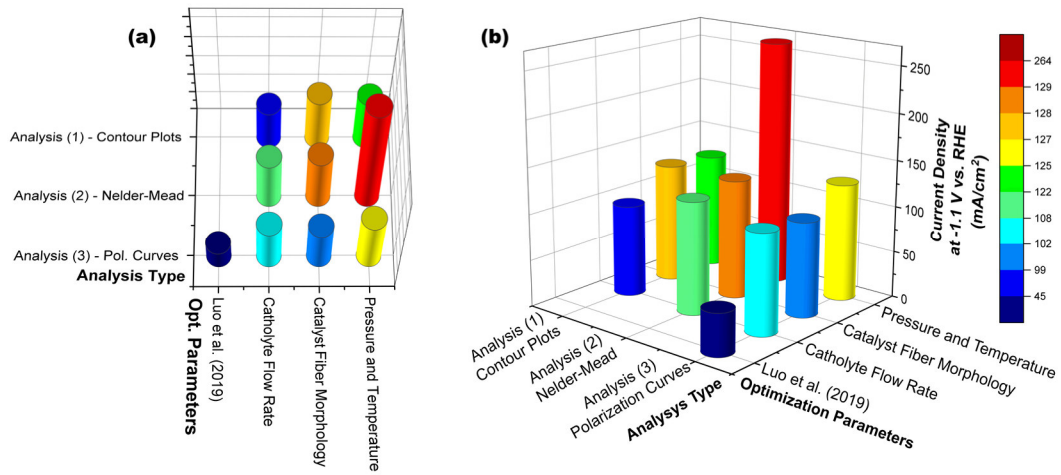

Fig. 4.: (a) Top view and (b) side view of simulated current density at –1.1 V vs. RHE from the porous cathode model, comparing three analysis types – (1) Contour Plots, (2) Nelder-Mead, (3) Polarization Curves – across optimization categories: flow rate, fiber morphology, and pressure/temperature, vs. experimental data from Luo *et al.* [5]. Reproduced from [1].

Acknowledgment

This work received funding from FCT (Fundação para a Ciência e a Tecnologia, I.P.) under the projects LA/P/0037/2020, UIDP/50025/2020 and UIDB/50025/2020 of the Associate Laboratory Institute of Nanostructures, Nanomodelling and Nanofabrication – i3N, and by the project CO2RED (DOI 10.54499/PTDC/EQU-EPQ/2195/2021). The work was also supported by the project M-ECO2 – Industrial cluster for advanced biofuel production, Ref. C644930471-00000041, co-financed by PRR - Recovery and Resilience Plan of the European Union (Next Generation EU).

The authors also acknowledge funding from the European Union via the projects X-STREAM (Horizon EU, ERC CoG, No. 101124803), SolarWay (HORIZON-MSCA-2023-PF-01, No. 101148726), and a grant for participation in the ERASMUS+ Blended Intensive Program (BIP) course: “ERASMUS 2024-1-AT01-KA131-HED-000201666”.

Views and opinions expressed are, however, those of the authors only and do not necessarily reflect those of the European Union or the European Research Council. Neither the European Union nor the granting authority can be held responsible for them.

References

[1] I. S. Fernandes, D. Antunes, R. Martins, M.J. Mendes, A.S. Reis-Machado, Solar fuels design: Porous cathodes modeling for electrochemical carbon dioxide reduction in aqueous electrolytes, Heliyon 10 (2024) e26442. https://doi.org/10.1016/j.heliyon.2024.e26442.

[2] A. Desalvo, P. Gondi, F.A. Levi, F. Zignani, Electrical conductivity of high-purity zinc, Il Nuovo Cimento 1955-1965 31 (1964) 904–913. https://doi.org/10.1007/BF02733804.

[3] K. Wu, E. Birgersson, B. Kim, P.J.A. Kenis, I.A. Karimi, Modeling and Experimental Validation of Electrochemical Reduction of CO2 to CO in a Microfluidic Cell, J. Electrochem. Soc. 162 (2014) F23. https://doi.org/10.1149/2.1021414jes.

[4] S. Nitopi, E. Bertheussen, S.B. Scott, X. Liu, A.K. Engstfeld, S. Horch, B. Seger, I.E.L. Stephens, K. Chan, C. Hahn, J.K. Nørskov, T.F. Jaramillo, I. Chorkendorff, Progress and Perspectives of Electrochemical CO2 Reduction on Copper in Aqueous Electrolyte, Chem. Rev. 119 (2019) 7610–7672. https://doi.org/10.1021/acs.chemrev.8b00705.

[5] W. Luo, J. Zhang, M. Li, A. Züttel, Boosting CO Production in Electrocatalytic CO2 Reduction on Highly Porous Zn Catalysts, ACS Catal. 9 (2019) 3783–3791. https://doi.org/10.1021/acscatal.8b05109.

[6] R. Chang, K. Goldsby, Chemistry, 12th ed., McGraw-Hill Education, 2015.

[7] C. Ma, X. Li, L. Lin, L. Chen, M. Wang, J. Zhou, A two-dimensional porous electrode model for designing pore structure in a quinone-based flow cell, J. Energy Storage 18 (2018) 16–25. https://doi.org/10.1016/j.est.2018.04.007.

Targeted CDK4/6 Therapy for Breast Cancer: How SNPs can Influence the Efficacy of Drugs

Adela Avdičević[a], Samo Lešnik[a,b], Urban Bren[a, b, c]

a Faculty of Chemistry and Chemical Engineering, University of Maribor, Smetanova 17, 2000 Maribor, Slovenia

b Institute of Environmental Protection and Sensors, Beloruska 7, 2000 Maribor, Slovenia

c Faculty of Mathematics, Natural Sciences and Information Technologies, University of Primorska, Glagoljaška 8, 6000 Koper, Slovenia

adela.avdicevic@um.si

Introduction

Breast cancer is the most frequently diagnosed type of cancer worldwide and the most common cause of cancer-related death in women[1]. The most common subtype is the hormone receptor-positive (HR+) and HER2-negative breast cancer, the growth of which depends on the activity of cyclin-dependent kinases 4 and 6 (CDK4/6), whose threedimensional structure is represented in Figure 1(a)[2]. These kinases regulate the cell cycle by phosphorylating the retinoblastoma protein (Rb), thus enabling the transition of cells from G1 to S phase and initiating their proliferation[3]. Disruptions to this strictly regulated process can lead to uncontrolled cell division, which contributes significantly to the development and progression of this type of cancer[4].

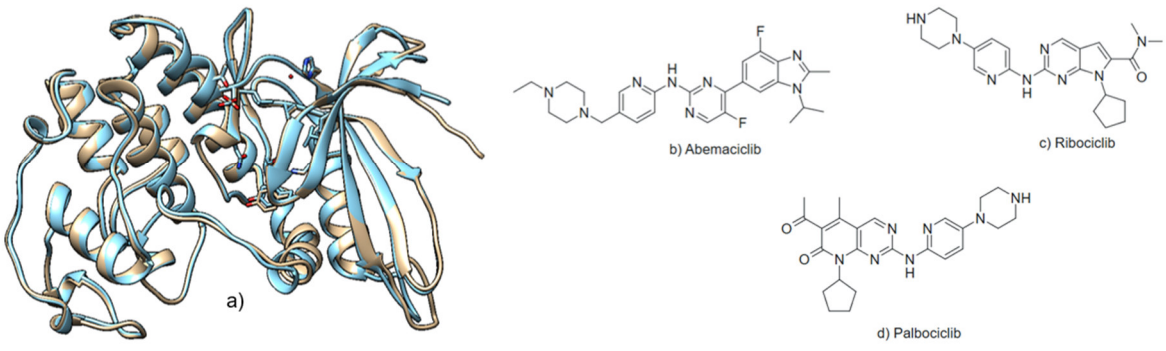

Figure 1: a) CDK4/6 structure (CDK4 in brown, CDK6 in blue); b) Abemaciclib, c) Ribociclib, d) Palbociclib – chemical structures.

An important advance in the treatment of HR+/HER2− breast cancer subtype is the introduction of selective CDK4/6 inhibitors such as palbociclib, ribociclib and abemaciclib

(Figure 1b–d), which, in combination with endocrine therapy, significantly improve clinical outcomes in patients with advanced disease[5].

However, the occurrence of congenital or acquired resistance to treatment remains a major therapeutic challenge. In this context, genetic differences between individuals, in particular single nucleotide polymorphisms (SNPs), play an important role as they can influence the individual response to medication and contribute to the development of resistance[6].

Computer-aided drug design is becoming an important tool in the search for effective therapeutic compounds, as it enables faster, cheaper and more accurate identification of molecules with the desired properties. By using methods such as molecular docking, molecular dynamics simulations and linear interaction energy (LIE) calculations, researchers can predict the binding modes of drugs to target proteins, monitor their structural changes and quantitatively assess the effects of sequence variations on binding affinity. These approaches not only bridge the gap between theoretical models and experimental data, but also provide deeper insights into the complexity of biological systems[7].

Such understanding is particularly valuable in the context of personalized medicine, where genetic differences between individuals significantly influence treatment outcomes. By integrating computational methods with genomic data, therapies can be tailored to an individual's biological background, leading to more targeted approaches, higher efficacy and better clinical outcomes[8].

Experimental

The results of the molecular dynamics simulations show the stability of the CDK4/6–abemaciclib complexes over the entire simulation period. Root mean square deviation (RMSD) analysis, which represents the average deviation of atomic positions from the initial structure over time, shows that both CDK4 and CDK6 largely maintained a stable conformation during the simulation (Figure 2). The RMSD values for CDK4/6 remained approximately between 2 and 3 Å after initial stabilization, indicating good structural conservation of the proteins, while the values for the ligand abemaciclib were higher and more scattered, especially in the case of CDK6, which could indicate greater flexibility of the molecule in the binding site or transient changes in the binding interactions.

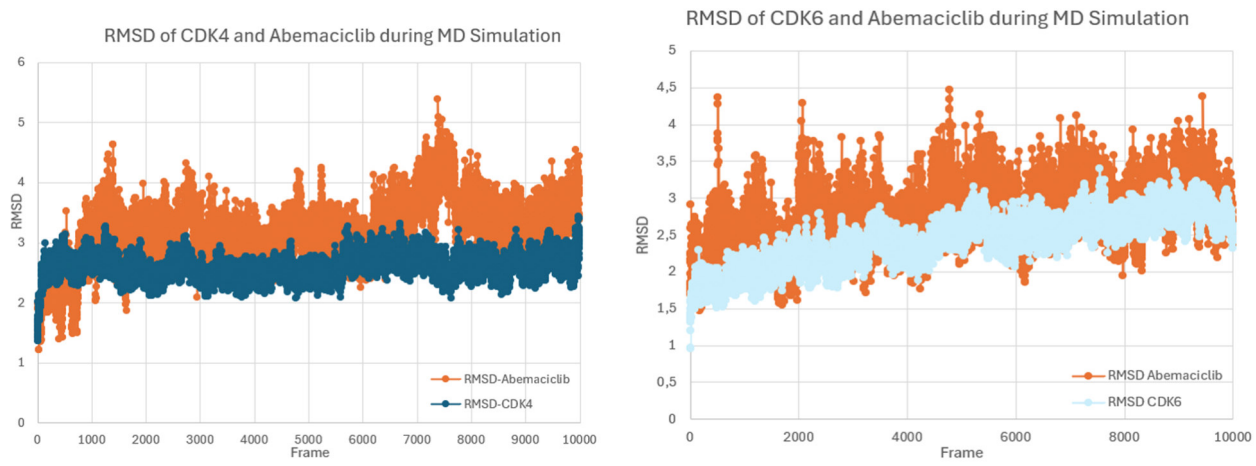

Figure 2: RMSD profiles for the CDK4–abemaciclib complex (left) and the CDK6–abemaciclib complex (right). In both diagrams, the RMSD values of abemaciclib are shown in orange, while the RMSD values of the proteins for CDK4 (left) are shown in blue and for CDK6 (right) in light blue.

The RMSF (Root Mean Square Fluctuation), which reflects the local flexibility of individual amino acid residues, revealed different fluctuation patterns for CDK4 and CDK6 (Figure 3). For CDK4, the highest flexibility was observed in the N-terminal region (residues 1–10), followed by two loop regions around residues 40–60 and 240–260. For CDK6, the highest fluctuation also occurred at the N-terminus, albeit with a lower amplitude than for CDK4, and several additional peaks were observed at regular intervals in the sequence. Although RMSF amplitudes were generally lower in CDK6, the broader and more regular distribution of peaks suggests greater dynamic mobility throughout the protein structure.

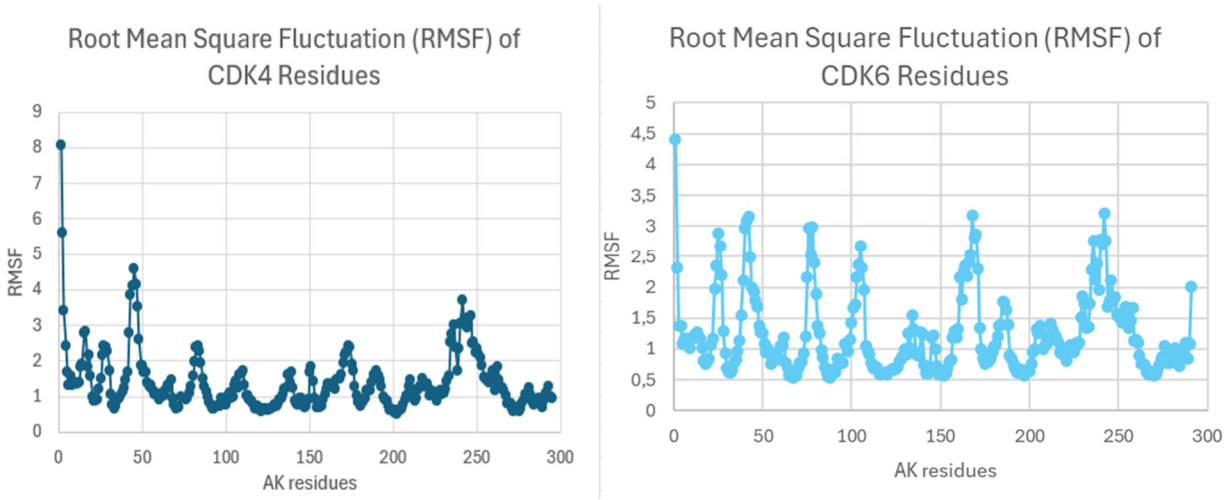

Figure 3: RMSF profiles of individual amino acid residues in CDK4 (left, dark blue) and CDK6 (right, light blue).

To quantitatively evaluate the binding affinity between the ligand and the target proteins, we used the linear interaction energy (LIE) method, which estimates the binding energy based on the average of the van der Waals and electrostatic interactions (Figure 4). The total interaction energy remained relatively stable for both complexes during the simulation. Although slightly larger structural changes were observed in the CDK6–abemaciclib complex during the simulation, the calculated binding energies for CDK4 and CDK6 were comparable, indicating a similar interaction profile for both complexes.

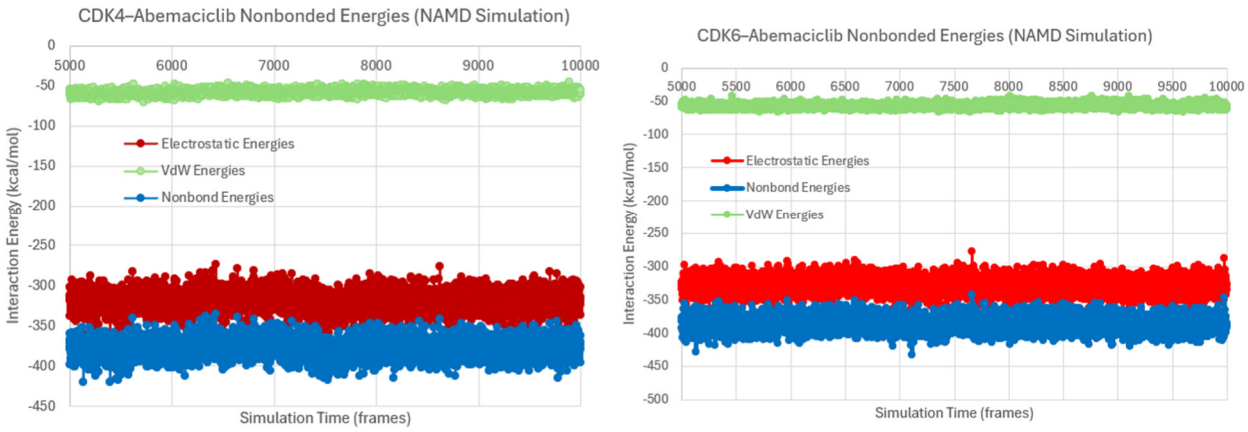

Figure 4: shows the non-covalent interaction energies between abemaciclib and CDK4 (left) and CDK6 (right), calculated from NAMD simulations. Three components of the interaction energies are shown: electrostatic energy (red), van der Waals (VdW) energy (green) and total non-covalent energy (blue).

All the analyzes described were also performed for the CDK4/6 complexes with palbociclib and ribociclib; however, only the interactions of the abemaciclib complex are presented here as a representative example of selective CDK4/6 inhibitors.

The initial analysis of the complexes with the wild-type proteins enabled the creation of a reference binding model that serves as a basis for investigating the effects of genetic variations on treatment efficacy. The interactions between the drugs palbociclib, abemaciclib (Figure 5) and ribociclib with the target proteins CDK4 and CDK6 were analyzed in detail using the PLIP tool.

Based on these results, we will select SNPs from the dbSNP database (NIH) that lead to amino acid substitutions within the binding pocket, especially at positions critical for stable hydrophobic, hydrogen bonding or ionic interactions. To assess the functional impact of these changes, we will perform molecular dynamics simulations of the mutant complexes and compare them to the reference systems.

Such analysis will provide a detailed understanding of how genetic alterations affect inhibitor binding, which is essential for explaining differences in therapeutic response and for developing approaches tailored to the genetic profile of individual patients.

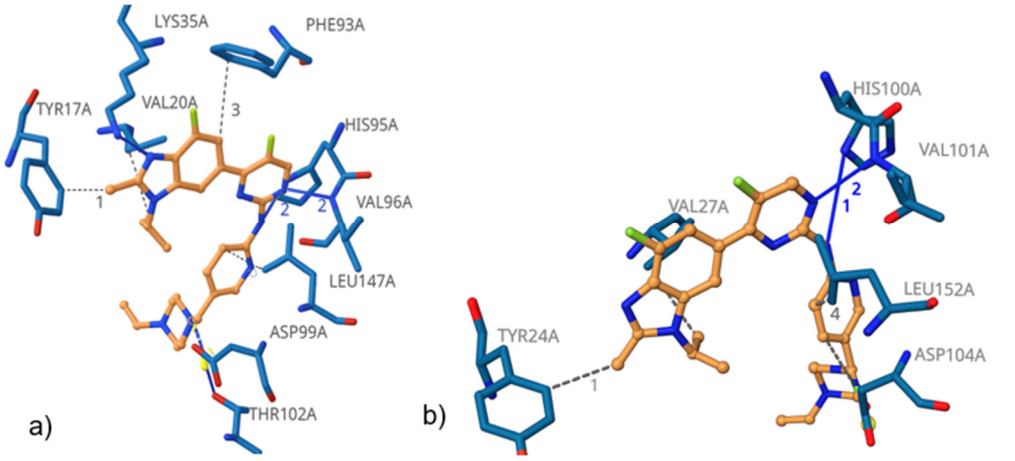

Figure 5: Interactions between the inhibitor Abemaciclib and a) CDK4 and b) CDK6, obtained with PLIP[9]. Dashed grey lines represent hydrophobic interactions, solid blue lines represent hydrogen bonds and yellow lines represent salt bridges. Abemaciclib is shown in orange, while the protein residue carbons are shown in blue.

Summary

In the treatment of hormone-dependent breast cancer with CDK4/6 inhibitors (palbociclib, ribociclib, abemaciclib), certain SNP mutations can influence therapeutic efficacy. Using extensive molecular dynamics simulations and LIE (linear interaction energy) calculations, we have investigated the stability of the complexes and the interactions between the drugs and the CDK4/6 proteins. In the next phase, we will investigate the effects of common SNPs on the binding affinity to contribute to the development of more personalized therapies.

Acknowledgment

The authors thank the Slovenian Research and Innovation Agency (ARIS) for the financial support through project and programme grants P2-0438, I0-E015, J1-4398, J1-60001, J1-50034, and L7-60161.

References

(1) Houghton, S. C.; Hankinson, S. E. Cancer Progress and Priorities: Breast Cancer. *Cancer Epidemiol. Biomarkers Prev.* **2021**, *30* (5), 822–844. https://doi.org/10.1158/1055-9965.EPI-20-1193.

(2) Hamilton, E.; Infante, J. R. Targeting CDK4/6 in Patients with Cancer. *Cancer Treat. Rev.* **2016**, *45*, 129–138. https://doi.org/10.1016/j.ctrv.2016.03.002.

(3) Piezzo, M.; Cocco, S.; Caputo, R.; Cianniello, D.; Gioia, G. D.; Lauro, V. D.; Fusco, G.; Martinelli, C.; Nuzzo, F.; Pensabene, M.; Laurentiis, M. D. Targeting Cell Cycle in Breast Cancer: CDK4/6 Inhibitors. *Int. J. Mol. Sci.* **2020**, *21* (18), 6479. https://doi.org/10.3390/ijms21186479.

(4) Xu, H.; Yu, S.; Liu, Q.; Yuan, X.; Mani, S.; Pestell, R. G.; Wu, K. Recent Advances of Highly Selective CDK4/6 Inhibitors in Breast Cancer. *J. Hematol. Oncol.J Hematol Oncol* **2017**, *10* (1), 97. https://doi.org/10.1186/s13045-017-0467-2.

(5) Pandey, K.; An, H.-J.; Kim, S. K.; Lee, S. A.; Kim, S.; Lim, S. M.; Kim, G. M.; Sohn, J.; Moon, Y. W. Molecular Mechanisms of Resistance to CDK4/6 Inhibitors in Breast Cancer: A Review. *Int. J. Cancer* **2019**, *145* (5), 1179–1188. https://doi.org/10.1002/ijc.32020.

(6) Islam, R.; Rahaman, M.; Hoque, H.; Hasan, N.; Prodhan, S. H.; Ruhama, A.; Jewel, N. A. Computational and Structural Based Approach to Identify Malignant Nonsynonymous Single Nucleotide Polymorphisms Associated with CDK4 Gene. *PLOS ONE* **2021**, *16* (11), e0259691. https://doi.org/10.1371/journal.pone.0259691.

(7) Oselusi, S. O.; Dube, P.; Odugbemi, A. I.; Akinyede, K. A.; Ilori, T. L.; Egieyeh, E.; Sibuyi, N. RS.; Meyer, M.; Madiehe, A. M.; Wyckoff, G. J.; Egieyeh, S. A. The Role and Potential of Computer-Aided Drug Discovery Strategies in the Discovery of Novel Antimicrobials. *Comput. Biol. Med.* **2024**, *169*, 107927. https://doi.org/10.1016/j.compbiomed.2024.107927.

(8) Collin, C. B.; Gebhardt, T.; Golebiewski, M.; Karaderi, T.; Hillemanns, M.; Khan, F. M.; Salehzadeh-Yazdi, A.; Kirschner, M.; Krobitsch, S.; Kuepfer, L. Computational Models for Clinical Applications in Personalized Medicine—Guidelines and Recommendations for Data Integration and Model Validation. *J. Pers. Med.* **2022**, *12* (2), 166. https://doi.org/10.3390/jpm12020166.

(9) Salentin, S.; Schreiber, S.; Haupt, V. J.; Adasme, M. F.; Schroeder, M. PLIP: Fully Automated Protein–Ligand Interaction Profiler. *Nucleic Acids Res.* **2015**, *43* (Web Server issue), W443–W447. https://doi.org/10.1093/nar/gkv315.

Synthesis and Characterization of Nitrogen-Doped Graphene Materials for Supercapacitor Applications

Katarzyna Gajewska, Adam Moyseowicz, Grażyna Gryglewicz

Department of Process Engineering and Technology of Polymer and Carbon Materials,
Wrocław University of Science and Technology,

grazyna.gryglewicz@pwr.edu.pl

Introduction

As the demand for energy continues to grow, it is important to find ways to store it that are both efficient and environmentally friendly. The European Union expects renewable energy sources to supply about 69% of electricity by 2030 and around 80% by 2050 [1]. However, solar and wind power depend on weather conditions, which makes their energy output unpredictable. These solutions must provide flexibility, stability, and reliability for both homes and industry. To manage this, we need effective energy storage systems based on batteries and supercapacitors. These systems should store extra energy when production is high (like on sunny or windy days) and release it when demand increases or production drops.

Supercapacitors can store significantly more energy than conventional capacitors while achieving power densities typical of capacitors, which are unattainable for batteries. Unlike traditional batteries, supercapacitors can be charged and discharged in mere seconds, making them ideal for applications that require rapid energy delivery. However, due to their lower energy density—limited by the theoretical potential of water decomposition—supercapacitors are unlikely to replace batteries in most applications. Instead, they can be used in conjunction with batteries to enhance efficiency and extend the lifespan of these devices. Scientists aim to identify suitable electrode materials and electrolytes to achieve high capacitance values and a broad operating potential window leading to high energy density of the device [2].

Reduced graphene oxide (rGO) has gained significant attention as an electrode material for supercapacitors, particularly for aqueous systems due to its excellent electrical conductivity, high surface area, good cyclic stability, and mechanical strength. However, to overcome its limitations in terms of capacitance and pseudocapacitance, doping with heteroatoms like nitrogen atoms can significantly enhance the electrochemical performance of rGO. These dopants provide additional active sites for charge storage,

improve conductivity and modify the interaction between the electrode surface and the electrolyte, all of which contribute to higher energy and power densities [3].

rGO is typically obtained by reducing graphene oxide (GO) dispersion using chemical, thermal, or electrochemical reduction methods. Each of these methods has distinct advantages and disadvantages in terms of cost, scalability, efficiency, and the quality of the resulting rGO material. One of the most promising methods to obtain rGO is hydrothermal reduction, a process where GO is reduced in a sealed, high-temperature water-based solution, typically under autogenous pressure (~10 bar). This method involves placing GO in a water dispersion and heating it to temperatures up to 200°C in a high-pressure autoclave. Hydrothermal reduction stands out for its simplicity, scalability, and the high quality of fewer defects and good electrochemical properties. The process is environmentally friendly and can be scaled up for industrial production. Hydrothermal reduction remains one of the most promising techniques for producing high-performance rGO, particularly for energy storage applications such as supercapacitors [4].

Combining hydrothermal synthesis with an appropriate drying method, such as freeze-drying, provides several distinct advantages for enhancing graphene material properties, particularly for energy storage devices like supercapacitors. Freeze-drying, also known as lyophilization, is a process that involves the removal of water from a material by freezing it and then reducing the surrounding pressure to allow the frozen water to sublimate directly from the solid phase to the gas phase. Freeze-drying offers significant advantages when preparing rGO for supercapacitor applications, particularly in terms of enhancing the material's structural integrity, porosity, conductivity, and electrochemical performance. By preserving a high surface area and preventing agglomeration of graphene sheets, freeze-drying results in rGO with superior charge storage capacity and improved rate capability [5].

Experimental

Graphene oxide (GO) was prepared via modified Hummers' method [4]. 3D N-doped and undoped rGO aerogels (N-rGO aero and rGO aero, respectively) were obtained via hydrothermal treatment (at autogenous pressure 10.2 and 10.1 bar, respectively) followed by purification and freeze-drying (Fig. 1).

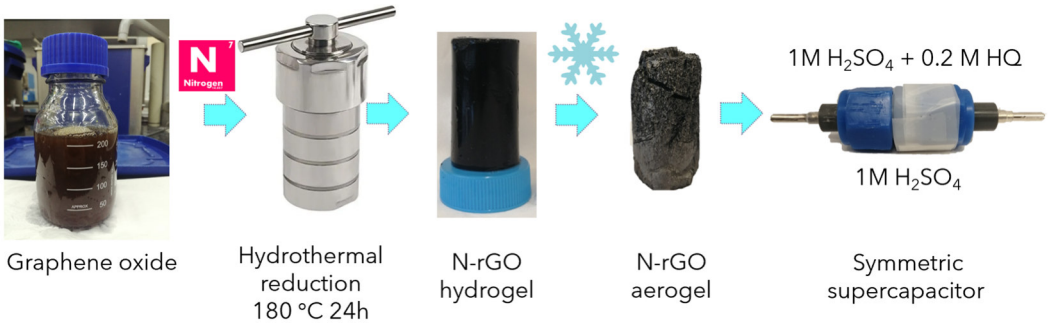

Fig. 1. Synthesis of N-rGO aero and its application in supercapacitors.

The morphology, structure, chemical composition, surface area, and thermal stability of the graphene-based samples were analyzed using FESEM, HRTEM, XRD, XPS, N_2 sorption and TGA techniques.

Electrochemical tests were performed in a symmetric setup using acidic and redox-active electrolytes. Aerogel-based electrodes were prepared as compressed tablets and tested via CV, GCD, and EIS to evaluate supercapacitors electrochemical performance.

The XRD patterns (Fig. 2a) of rGO aero and N-rGO aero materials show a strong diffraction peak at 2θ = 23.3° and 24.8°, respectively, along with a weaker peak at 2θ = 43.1°. These peaks correspond to the (002) and (100) lattice planes of graphite-like crystallites. The absence of the (001) peak, which is typical for GO, confirms the successful reduction to graphene-based aerogels through the hydrothermal process.

To further examine the porous structure of the aerogels, they were analyzed using N_2 sorption at 77 K. Fig. 2b presents the N_2 adsorption–desorption isotherms of rGO aero and N-rGO aero. Both aerogels show a type IV isotherm according to the IUPAC classification, with a hysteresis loop in the 0.4–0.9 p/p_0 range, indicating the presence of mesopores. The BET surface area of N-rGO aero is notably higher than that of rGO aero (586 vs. 495 $m^2\ g^{-1}$).

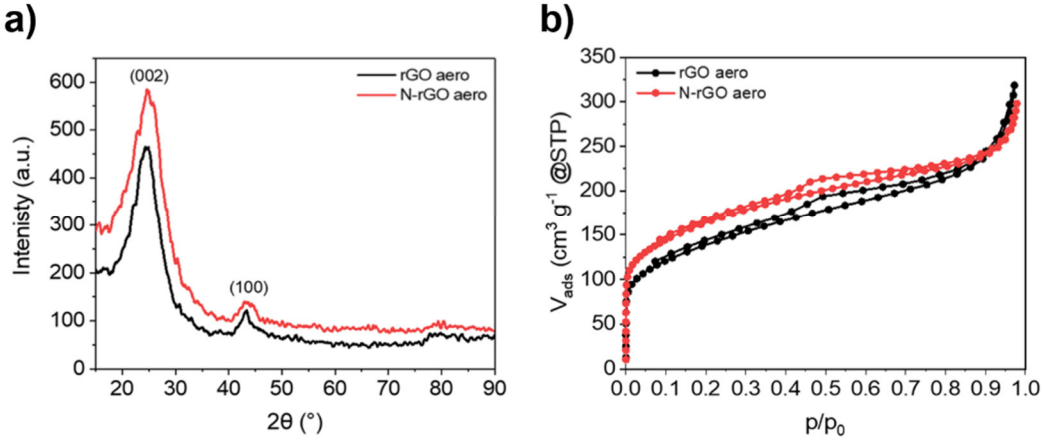

Fig. 2. The XRD patterns (a) and N_2 adsorption–desorption isotherms (b) of rGO aero and N-rGO aero.

The synthesized aerogels were used as active materials in aqueous symmetric supercapacitors. Fig. 3a presents the CV curves of rGO aero and N-rGO aero devices at a scan rate of 10 mV s^{-1} within a voltage range of 0–1.4 V in both 1 M H_2SO_4 and 1 M H_2SO_4 + 0.2 M hydroquinone (HQ) electrolytes. All devices operate above the theoretical potential of water decomposition (1.23 V), which typically limits energy density in supercapacitors. The comparison of CV curves shows improved electrochemical performance for N-rGO aero, attributed to its higher electrical conductivity and the contribution of pseudocapacitive effects related to the presence of nitrogen functionalities [3].

The Ragone plots (Fig. 3b) show the energy and power densities of symmetric devices in various electrolytes. Adding 0.2M HQ to the acidic electrolyte significantly improves the supercapacitor charge storage ability, allowing the rGO aero device to reach an energy density of 19.5 Wh kg^{-1} at 0.072 kW kg^{-1}. Notably, the N-rGO aero device in the same electrolyte achieves an energy density as high as 29.3 Wh kg^{-1} at 0.076 kW kg^{-1}. These values exceed those typically reported for symmetric supercapacitors based on graphene aerogels.

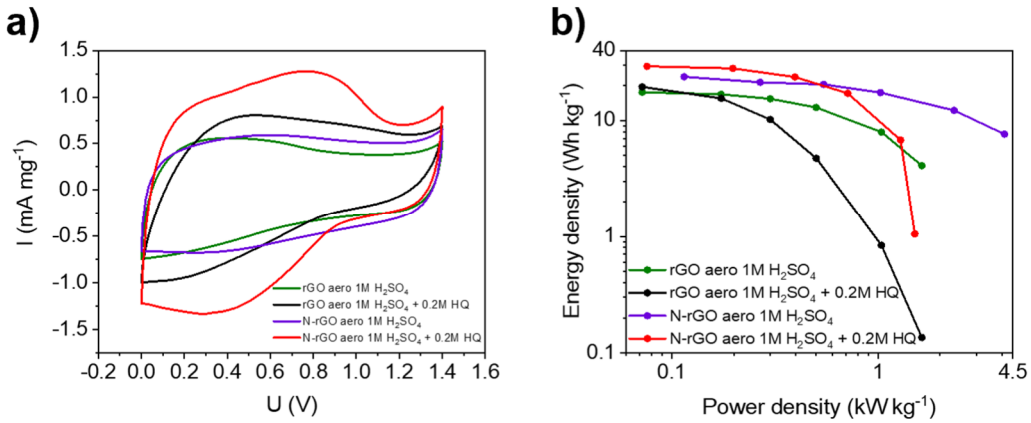

Fig. 3. CV curves recorded at 10 mV s^{-1} (a) and Ragone plot (b) of rGO and N-rGO aero in 1M H_2SO_4 and 1M H_2SO_4 + 0.2M HQ.

Summary

The unique 3D porous structure of N-rGO aero, formed through hydrothermal synthesis, effectively prevents graphene sheet aggregation and provides a large surface area for electrochemical reactions, contributing to improved device performance. This study shows that N-rGO aerogels can significantly enhance the electrochemical performance of aqueous symmetric supercapacitors. This improvement results from the

combined effects of nitrogen functional groups, which are introduced during the hydrothermal process and boost pseudocapacitive behavior through the redox-active HQ species that supply additional charge via reversible Faradaic redox reactions.

Acknowledgment

The following research was financially supported by a statutory activity subsidy from the Polish Ministry of Education and Science for the Faculty of Chemistry of Wrocław University of Science and Technology.

References

[1] European Commission, *Commission recommendations on how to exploit the potential of energy storage*, 2023

[2] B.E. Conway, Electrochemical Supercapacitors, Springer US, Boston, MA, 1999, 10.1007/978-1-4757-3058-6.

[3] A. Chenwittayakhachon, K. Jitapunkul, B. Nakpalad, P. Worrayotkovit, S. Namuangruk, P. Sirisinudomkit, P. Iamprasertkun, Machine learning approach to understanding the ‘synergistic’ pseudocapacitive effects of heteroatom doped graphene, 2D Mater 10, 2023, 10.1088/2053-1583/acaf8d.

[4] N. Díez, A. Śliwak, S. Gryglewicz, B. Grzyb, G. Gryglewicz, Enhanced reduction of graphene oxide by high-pressure hydrothermal treatment, RSC Adv 5, 2015, 10.1039/C5RA14461B.

[5] J.S. Shaikh, N.S. Shaikh, Y.K. Mishra, S.S. Pawar, N. Parveen, P.M. Shewale, S. Sabale, P. Kanjanaboos, S. Praserthdam, C.D. Lokhande, The implementation of graphene-based aerogel in the field of supercapacitor, Nanotechnology 32, 2021, 10.1088/1361-6528/ac0190.

Experimental Determination of Insect Fat Solubility in Dense CO_2 and Corresponding Model Description

Tom Goldberg*, Volker Herdegen

Institute of Thermal-, Environmental- and Resources' Process Engineering,

Technische Universität Bergakademie Freiberg, 09599 Freiberg, Germany

* Corresponding author: Tom.Goldberg@tun.tu-freiberg.de

Introduction

The relatively low critical temperature of carbon dioxide (CO_2) allows high-pressure extraction processes under mild conditions to preserve physiological and high valuable ingredients in natural feedstocks [1]. Moreover, important solvent properties, such as density, viscosity and diffusivity, are easily tunable by changing temperature and pressure conditions [1, 2]. Therefore, high-pressure CO_2 extraction provides advantages, especially for foods, pharmaceuticals and cosmetics [2], where extracts of high quality need to be processed.

Natural fats and oils play a crucial role in these industries, and dense CO_2 is an effective solvent for the purification of lipid compounds due to its rather non-polar character [3]. An emerging renewable and regionally available resource is the fat residue from protein meal production from black soldier fly (*Hermetia illucens*) larvae [4, 5]. This fat provides a fatty acid (FA) profile very similar to that of tropical fats and oils, e.g., palm kernel or coconut [6], making it a potential candidate for industrial applications after purification in accordance with regulatory framework considerations [7].

In this work, the obtained insect fat is analyzed with respect to important physico-chemical properties and the solubility in dense CO_2 is extensively studied. As a basis for prospective process design, suitable thermodynamic models should be identified to describe the measured solubility behavior.

Experimental

Crude insect fat was purchased from Madebymade (German company), where the fat is obtained as a by-product of protein meal production after the rearing, drying and pressing of black soldier fly larvae.

The insect fat is solid at room temperature, with a mean melting point of 306.5 K coming from DSC measurements. The crude fat is mainly composed of triglycerides with a high portion of saturated FA (75 % of total FA) and lauric acid (C12:0) being the most abundant (55 % of total FA), which is typical for insect fat obtained from black soldier fly larvae [8, 9]. Apart from triglycerides and small fractions of fat-accompanying compounds (e.g., waxes, vitamins, colorants or free FA), the crude fat contains proteins and remains of the larval shells as impurities. To investigate the impact of these impurities and free FA, the solubilities in dense CO_2 were measured for both, the crude insect fat and a pre-cleaned fat obtained by liquid-liquid extraction with hexane and water. Fig. 1 shows the exemplary appearance of both feed materials and the resulting fat extracted with dense CO_2.

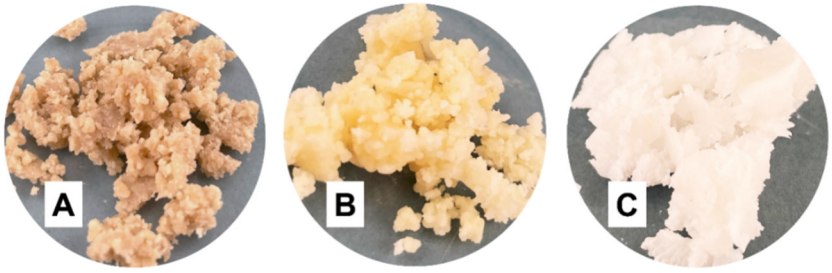

Fig. 1: Exemplary appearance of (A) crude and (B) pre-cleaned insect fat as feedstocks for the solubility measurements and (C) purified CO_2 extracted fat.

The pre-cleaned fat is much lighter in color than the crude insect fat, which comes mainly from separating the larval residues. A significantly brighter extract is obtained from both feed materials using dense CO_2, which is a promising indicator of successful purification. However, the specific compositions of the extracts have not yet been determined.

The equilibrium solubilities S_2 of the fat (2) in dense CO_2 (1) were measured at 4 set temperatures (298 to 353 K) over a wide range of different pressures (15 to 60 MPa) using the gravimetric static-analytical method. The detailed description of the applied methodology for the measurements can be found elsewhere [10]. For all test points, the solubilities were measured at least twice and the equilibration waiting time was set to 3 h after preliminary trails. The variation in all measured solubilities, determined in duplicates, was less than 10 % relative to their mean value. Moreover, no significant differences between the solubilities of the crude and the pre-cleaned fat were observed within the range of experimental reproducibility, so that the examined data may also stand for the behavior of the crude fat. The solubilities were therefore extensively determined for the pre-cleaned fat.

The measured solubility behavior of the insect fat is in agreement with the expectations – increasing solubility with CO_2 density at constant temperature, and with increasing temperature at constant density due to higher solute vapor pressure (cf. Fig. 2). This led to measured solubilities ranging from 0.15 to 167 g_{fat}/kg_{CO_2}. Especially at elevated pressures, the solubility was relatively high, because of the high content of rather short-chain lauric acid. However, the results are quite similar to the solubilities that have been reported for other natural fats and oils with a similar fatty acid profile (e.g., babassu oil) [11].

Modeling

Semi-empirical density-based models are widely used to describe experimental solubility data as a function of CO_2 density, temperature, and pressure. These models do not require any physical or chemical properties of the solute, but still provide a basic thermodynamic background. Two main density-based approaches exist in the literature, upon which numerous extensions have been developed: The solvato-complex formation approach developed by Chrastil [12] and the enhancement factor approach, first introduced by Bartle et al. [13].

In our study 8 common density-based models with up to 5 fitting parameters were examined, covering both approaches. Within all models investigated, the heterogeneous insect fat was considered as one pseudo-compound with mean physico-chemical properties. Based on thermodynamic considerations, we also developed an improved density-based model. The results of the fitted Chrastil and Bartle model – as the two elementary models of both approaches – and of our proposed model [10] are exemplary illustrated in Fig. 2, left.

Furthermore, the measured solubility data were modeled based on the Expanded liquid theory by fitting the solute's activity coefficient at infinite dilution by applying two modifications of the Wilson model proposed by Nasri [14] and Su et al. [15]. The results are reported in Fig. 2, right.

The solubility behavior of the insect fat is well described by fitting density-based models under considering the fat as one pseudo-compound. In particular, the investigated range of pressure and temperature is excessively large compared to other studies [11]. However, the investigated transition from subcritical to supercritical CO_2 and the exceeding of the melting point of the fat do not appear to cause any challenges in model fitting. Common Chrastil-type models investigated in our work only led to a slightly better

solubility description with a minimum Absolute Average Relative Deviation ($AARD$) of 10.0 %. From thermodynamic framework, our proposed model allows data representation with the best goodness of fit (R^2_{adj} = 0.91, $AARD$ = 9.8 %) of all investigated models in our study. Since the model deviations are in the same order of magnitude as the experimental errors, a significant better description could not be expected. The adjusted coefficients of determination R^2_{adj} of all models were in the range of 0.85 to 0.91, indicating no overdetermination of the model equations.

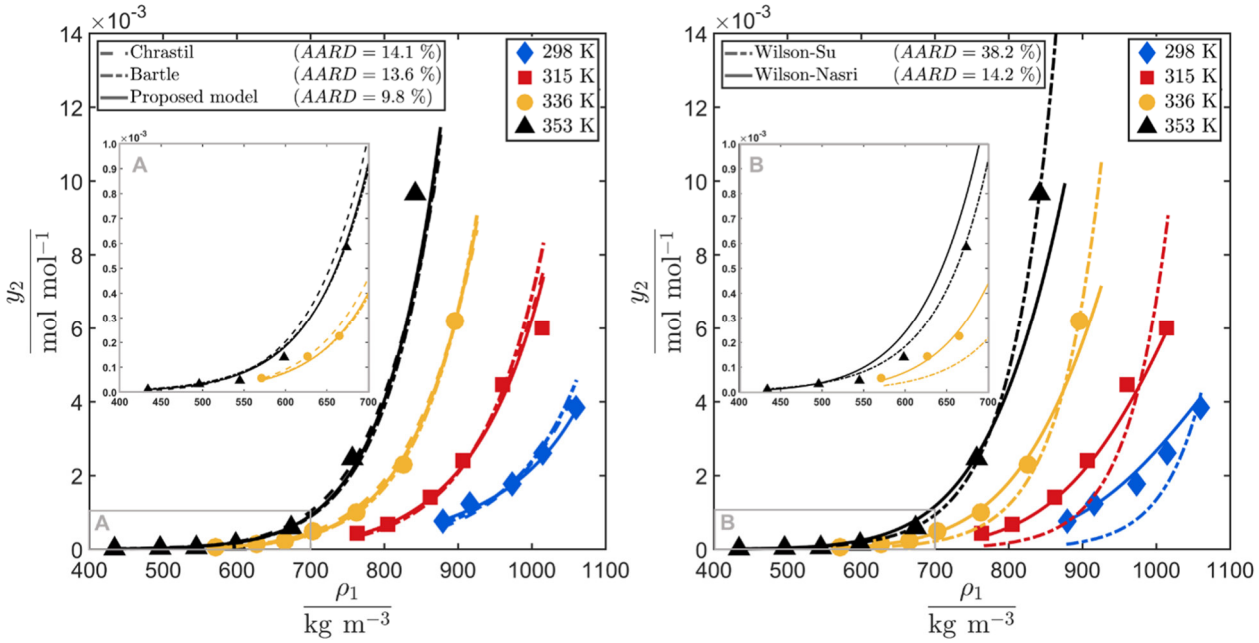

Fig. 2: Solubility (mole fraction) of insect fat (2) in dense CO_2 (1): Points indicate the experimental data and the lines indicate the fit of three exemplary semi-empirical density-based models (left) and of two activity-based models derived from expanded liquid theory using modified Wilson equations (right).

The activity-based models, derived from Expanded liquid theory, were expected to provide a physically better description of the measured solubility behavior compared to the density-based models. However, both modifications of the Wilson model involve an empirical structure, which shows a massive impact on the solubility description (cf. Fig. 2, right) and, therefore, negates the advantage of this more fundamental approach. Nevertheless, the modified Wilson model according to Nasri [14] also seems to be suitable for describing the solubility behavior of the insect fat in dense CO_2.

Summary

In this work, the solubility of insect fat from black soldier fly larvae in dense CO_2 was determined using the gravimetric static-analytical method across a wide range of set temperatures and pressures. The obtained solubility data were successfully modeled by fitting common semi-empirical density-based models. Based on thermodynamic considerations, an improved density-based model was developed, providing the best goodness of fit of all models investigated and within experimental error. Activity-based models derived from Expanded liquid theory using two modifications of the Wilson model have also been considered. These models provide a good representation of the solubility behavior, but the empiricism of the applied modifications reduces the expected advantage over the density-based models. A more physically-based modification to describe the pure molar solute volume under high pressure would be desirable, e.g., in relation to its density at standard conditions. However, in terms of thermodynamic fundamental modeling, the description of the solubility behavior using equations of state is to be considered next by splitting the natural fat into several pseudo-compounds with individual properties.

Acknowledgment

We appreciate Professor Andreas S. Bräuer, Director of ITUN, TU Bergakademie Freiberg for his valuable feedback and support. We thank the TUBAF Innovation Fond (TIF) of the TU Bergakademie Freiberg for the financial support of this study.

References

[1] S. Machmudah, Wahyudiono, H. Kanda, M. Goto, Supercritical Fluid Extraction and Fractionation, In: RA Meyers (Ed.), Encyclopedia of Sustainability Science and Technology. Springer New York, New York, NY, 2018, pp. 1–40

[2] T. Wu, B. Han, Supercritical Carbon Dioxide (CO2) as Green Solvent, In: RA Meyers (Ed.), Encyclopedia of Sustainability Science and Technology. Springer New York, New York, NY, 2018, pp. 1–25

[3] P. Maheshwari, Z.L. Nikolov, T.M. White, R. Hartel, Solubility of fatty acids in supercritical carbon dioxide, J Americ Oil Chem Soc. 69 (1992) 1069–1076. https://doi.org/10.1007/BF02541039

[4] R. Muangrat, S. Pannasai, Exploring the potential of black soldier fly larvae oil: Supercritical CO2 extraction, physicochemical analysis, antioxidant properties, shelf life, and keratinocyte growth inhibition, Journal of Agriculture and Food Research. 15 (2024) 101008. https://doi.org/10.1016/j.jafr.2024.101008

[5] T. Suryati, E. Julaeha, K. Farabi, H. Ambarsari, A.T. Hidayat, Lauric Acid from the Black Soldier Fly (Hermetia illucens) and Its Potential Applications, Sustainability. 15 (2023) 10383. https://doi.org/10.3390/su151310383

[6] A.Q. Alves, V.A. Da Silva, A.J.S. Góes, M.S. Silva, G.G. de Oliveira, I.V.G.A. Bastos, A.G. de Castro Neto, A.J. Alves, The Fatty Acid Composition of Vegetable Oils and Their Potential Use in Wound Care, Adv Skin Wound Care. 32 (2019) 1–8. https://doi.org/10.1097/01.ASW.0000557832.86268.64

[7] Commission Implementing Regulation (EU) 2017/2470 of 20 December 2017 establishing the Union list of novel foods in accordance with Regulation (EU) 2015/2283 of the European Parliament and of the Council on novel foods: Commission Implementing Regulation (EU) 2017/2470

[8] R. Smets, B. Verbinnen, I. van de Voorde, G. Aerts, J. Claes, M. van der Borght, Sequential Extraction and Characterisation of Lipids, Proteins, and Chitin from Black Soldier Fly (Hermetia illucens) Larvae, Prepupae, and Pupae, Waste Biomass Valor. 11 (2020) 6455–6466. https://doi.org/10.1007/s12649-019-00924-2

[9] M.D. Alifian, M.M. Sholikin, D. Evvyernie, Nahrowi, Potential Fatty Acid Composition of Hermetia illucens Oil Reared on Different Substrates, IOP Conf Ser.: Mater Sci Eng. 546 (2019) 62002. https://doi.org/10.1088/1757-899X/546/6/062002

[10] T. Goldberg, V. Herdegen, Solubility of insect fat in compressed CO2: Experiments and density- as well as activity-based modeling, The Journal of Supercritical Fluids. Under Review (26/05/2025)

[11] B. Soares, F. Gamarra, L.C. Paviani, L. Gonçalves, F.A. Cabral, Solubility of triacylglycerols in supercritical carbon dioxide, The Journal of Supercritical Fluids. 43 (2007) 25–31. https://doi.org/10.1016/j.supflu.2007.03.013

[12] J. Chrastil, Solubility of solids and liquids in supercritical gases, J Phys Chem. 86 (1982) 3016–3021. https://doi.org/10.1021/j100212a041

[13] K.D. Bartle, A.A. Clifford, S.A. Jafar, G.F. Shilstone, Solubilities of Solids and Liquids of Low Volatility in Supercritical Carbon Dioxide, Journal of Physical and Chemical Reference Data. 20 (1991) 713–756. https://doi.org/10.1063/1.555893

[14] L. Nasri, Modified Wilson's Model for Correlating Solubilities in Supercritical Fluids of Some Polycyclic Aromatic Solutes, Polycyclic Aromatic Compounds. 38 (2018) 244–256. https://doi.org/10.1080/10406638.2016.1200636

[15] C.-S. Su, Y.-M. Chen, Y.-P. Chen, Correlation of solid solubilities for phenolic compounds and steroids in supercritical carbon dioxide using the solution model, Journal of the Taiwan Institute of Chemical Engineers. 42 (2011) 608–615. https://doi.org/10.1016/j.jtice.2010.11.005

Investigating the Phase Separation of GVL/Water-Mixtures by the Addition of Sugars ("Sugaring-Out")

Sebastian Sandner, Paul Kriegler, Marlene Kienberger

Institute of Chemical Engineering and Environmental Technology

Graz University of Technology

sandner@tugraz.at

Introduction

Replacing hazardous solvents is essential to reduce human and environmental impact. A promising green solvent is γ-valerolactone (GVL). GVL is made from biomass and is non-toxic (*1*). However, due to its comparatively high vapor pressure it is energy intensive to separate it from water using distillation. Therefore, alternative methods for the separation of water and GVL need to be investigated.

Certain molecules become less soluble in a solution of high ionic strength. This phenomenon, also called "salting out", can be used to separate otherwise miscible substances (*2*). The newly formed phases can be separated energy efficiently using decantation. In addition to some salts, sugars can also cause phase separation ("sugaring out") (*3*). However, the mechanisms of this phenomenon are not fully understood (*4*). Therefore, the behavior of the organic solvent/water/salt, and organic solvent/water/sugar systems need to be investigated experimentally. Sugars have the advantage over salts, that they are cheap, eco-friendly, non-corrosive to equipment and do not affect the pH of the resulting solution (*5*).

The goal of this work was to screen five sugars (glucose, sucrose, xylose, maltose, fructose) on their suitability to induce phase separation in mixtures of GVL and water, at a ratio of 80 % (v/v) GVL, and 20 % (v/v) water.

Experimental

All experiments were performed in duplicate. 40 g of 80 % (v/v) GVL solutions were prepared in 100 ml laboratory bottles. The bottles were then placed in a laboratory shaker, set to 25°C. Then the sugar was added stepwise. After the sugar was fully dissolved, solution was settled for 10 minutes. The point at which a second phase first appeared was noted, and an image taken of the two bottles. Further sugar was then added and a picture

taken after every addition. The experiment was finished once sugar addition did not cause an increase in the organic phase size. The phases where then separated in separatory funnels. The two liquid phases where then weight. The water content in the organic phase was determined using Karl-Fischer's titration. The sugar content was determined gravimetrically after drying at 50°C and 20 mbar, to prevent caramelization. The GVL and sugar content in the organic phase, and the GVL and water concentration in the aqueous phase was then determined by solving the mass balance under the assumption, that the losses were split evenly between all substances.

Results

A second liquid phase was detected for all sugars except maltose. 1.0 g of sucrose and glucose was needed to form a second phase, 1.5 g of fructose, and 2.4 g of xylose. The 0.5 g of maltose added in the first step already did not dissolve fully, without forming a second liquid phase. Figure *1* shows the image of the settled mixtures of GVL, water, and the respective sugar after the addition of 3.5 g of sugar. Addition of glucose and fructose lead to the largest aqueous layer, followed by sucrose. The second phase formed through the addition of xylose was smaller than the phases formed by the other sugars. For 3.5 g of each sugar, the corresponding molar amounts are: glucose – 19.4 mmol, xylose – 23.3 mmol, sucrose – 10.2 mmol, and fructose – 19.4 mmol. Although xylose yields the highest number of molecules at this mass, it shows the worst phase separation, producing the smallest second phase. Additionally, the second phase induced by the addition of sucrose was only slightly lower than that of fructose and glucose even though only about half the number of moles was present in the solution.

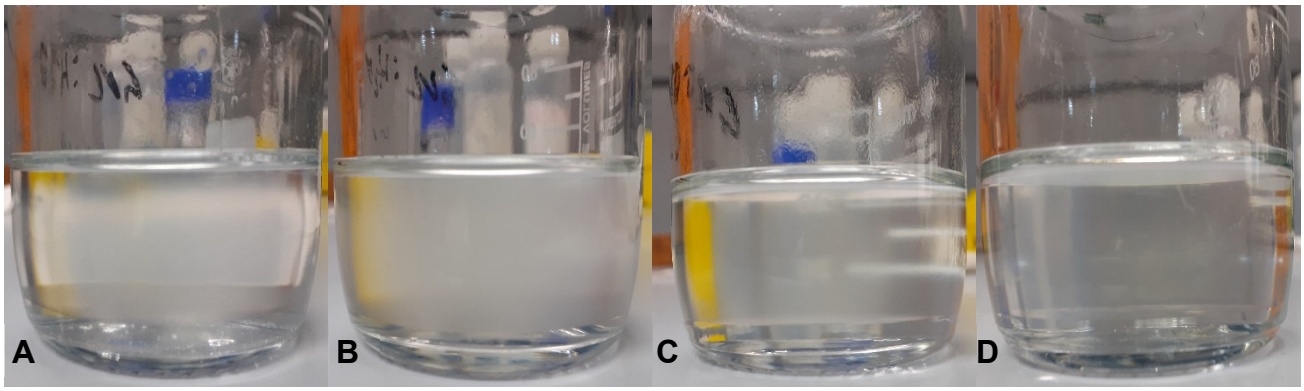

Figure 1 Separated phases of mixtures of GVL and water (80:20 v/v%) after adding 3.5 g of the respective sugar with the organic phase on the top and the aqueous phase in the bottom at 25°C. The sugars are: A) glucose, B) xylose, C) sucrose and D) fructose.

For additional comparison of the influence of mole number on the resulting phases solutions of similar numbers of molecules (~19.3 mmol) are compared in Figure *2*. It is clearly visible, that sucrose caused the largest aqueous phase, followed by glucose and fructose with comparable phase sizes. The addition of xylose caused the smallest aqueous phase. This indicates, that for sugars the number of hydroxy groups is a predictor for the sugaring out performance of the sugar, as they enable hydrogen bonding. This relationship has also been reported for other solvent systems (*6, 7*). Sucrose is a disaccharide, and as such has eight hydroxy groups. Glucose and fructose are hexoses, with five hydroxy groups. Pentoses, such as xylose have four hydroxy groups.

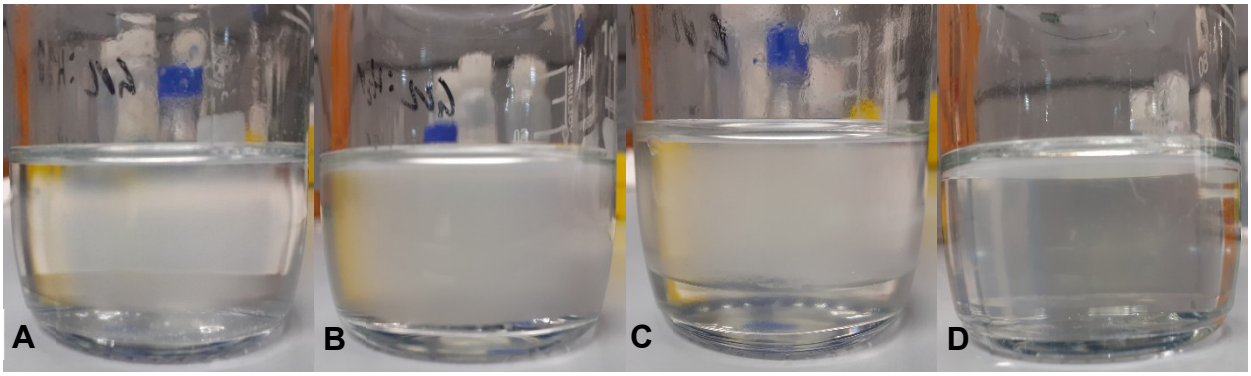

Figure 2 Separated phases of mixtures of GVL and water (80:20 v/v%) after adding A) 3.5 g glucose (19.4 mmol), B) 2.9 g xylose 19.3 mmol), C) 6.5 g sucrose (19.0 mmol) and D) 3.5 g fructose (19.4 mmol) with the organic phase on the top and the aqueous phase in the bottom at 25°C.

The resulting compositions in the respective phases are given in Figure *3*. Only very low amounts of sugar could be detected in the organic phases, which is an important metric for process design. Additionally, only a relatively low amount of water (~10 wt.%) remains in the organic phase. Notably, the water content in organic phase of the fructose sample was only 4.8 wt.%. This is due to the very high solubility of fructose in water, indicated by the high amount of sugar detected in the aqueous phase (73 wt.%). The sugar content in the other samples was also considerable (> 40 wt.%). Of course, this is due to the experimental design, as it is likely not necessary to add as much sugar to cause acceptable phase separation. The relationship between sugar content in the aqueous phase and water content in the organic phase should be investigated in further research.

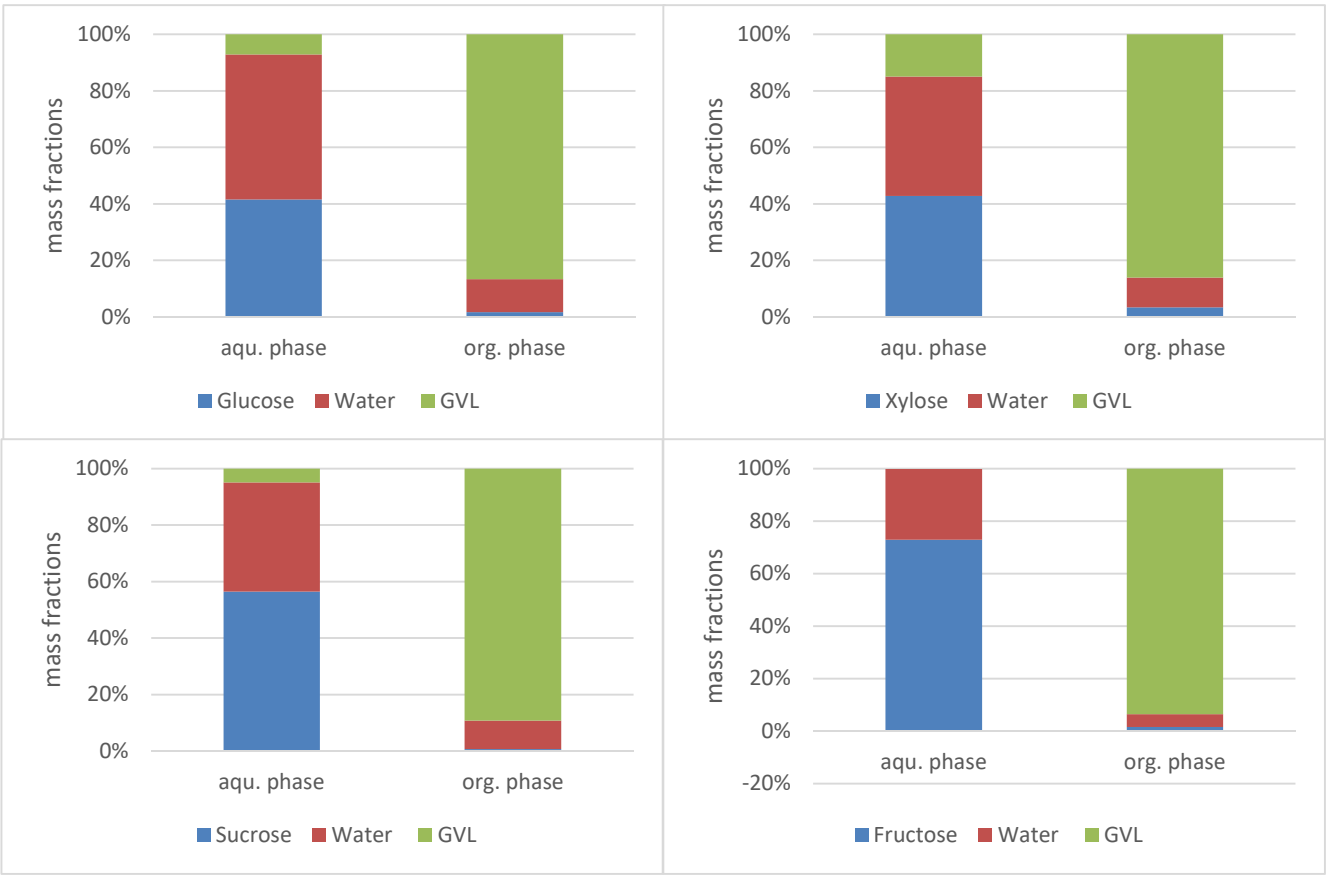

Figure 3 Resulting phase compositions based on mass balances after adding final amounts of sugars and separation of phases for GVL/water-mixtures (80:20, v/v%)

Summary

The addition of four out of the five investigated sugars (glucose, fructose, sucrose, xylose) caused the formation of a second liquid phase in systems of 80 % (v/v) GVL and 20 % (v/v) water. The sugaring out potential of the investigated sugars correlated with the number of hydroxy groups, as higher numbers of hydroxy groups increase the sugar's ability to from hydrogen bonds. Analysis of the organic phase revealed water contents of around 10 wt.%. The sugar content in the organic phases was low, highlighting the potential of this technique in the separation of GVL from water. However, further research is necessary to establish correlations between sugar content in the aqueous phase and the water content in the organic phase to reduce the amount of sugar.

References

1. Alonso, D. M.; Wettstein, S. G.; Dumesic, J. A. Gamma-valerolactone, a sustainable platform molecule derived from lignocellulosic biomass. *Green Chem.* **2013,** *15* (3), 584. DOI: 10.1039/c3gc37065h.

2. Fu, C.; Li, Z.; Sun, Z.; Xie, S. A review of salting-out effect and sugaring-out effect: driving forces for novel liquid-liquid extraction of biofuels and biochemicals. *Front. Chem. Sci. Eng.* **2021,** *15* (4), 854–871. DOI: 10.1007/s11705-020-1980-3.
3. Sadeghi, R.; Coutinho, J. A. Sugaring-out assisted organic-aqueous biphasic systems: Characteristics, mechanisms and applications. *Separation and Purification Technology* **2024,** *350*, 127919. DOI: 10.1016/j.seppur.2024.127919.
4. Grover, P. K.; Ryall, R. L. Critical appraisal of salting-out and its implications for chemical and biological sciences. *Chemical reviews* **2005,** *105* (1), 1–10. DOI: 10.1021/cr030454p.
5. Shoushtari, B. A.; Pazuki, G.; Shahrouzi, J. R.; Shahriari, S.; Hadidi, N. Separation of erythromycin using aqueous two-phase system based on acetonitrile and carbohydrates. *Fluid Phase Equilibria* **2020,** *505*, 112360. DOI: 10.1016/j.fluid.2019.112360.
6. Ebrahimi, N.; Sadeghi, R.; Ameen, B. A. Thermodynamics of clouding process in 1-butanol + water mixtures in the presence and absence of sugars. *Journal of Molecular Liquids* **2019,** *278*, 164–174. DOI: 10.1016/j.molliq.2019.01.011.
7. Sousa, K. M.; Maciel, G. E.; Buarque, F. S.; Santos, A. J.; Marques, M. N.; Cavalcanti, E. B.; Soares, C. M. F.; Lima, Á. S. Novel phase diagrams of aqueous two-phase systems based on tetrahydrofuran + carbohydrates + water: Equilibrium data and partitioning experiments. *Fluid Phase Equilibria* **2017,** *433*, 1–9. DOI: 10.1016/j.fluid.2016.11.001.

Ultrafast Hydrolysis of Grape Pomace in Hydrothermal Conditions: An Intensified Process for the Eco-Efficient Recovery of Lignin

Iván Briongos-Merino, Luis Vaquerizo

Institute of Bioeconomy, PressTech Group, Department of Chemical Engineering and Environmental Technology, University of Valladolid, Dr Mergelina s/n, 47011, Valladolid, Spain, luis.vaquerizo@uva.es

Introduction

In the current energy transition context, it is necessary to move forward in replacing products derived from fossil fuels with more sustainable and environmentally friendly alternatives that are available in our regions (Arai et al., 2009). In this regard, Spain has a large supply of lignocellulosic biomass that can be used for this purpose. Lignocellulosic biomass, consisting primarily of cellulose, hemicellulose, and lignin, is an abundant and renewable raw material (Cocero et al., 2018). While cellulose and hemicellulose are easily exploited due to their relative simplicity to be transformed into sugars and chemical compounds of interest, the valorization of lignin is more complex (Shorey et al., 2021).

Among the various processes available for lignin valorization, hydrolysis using sub- or supercritical water stands out due to the drastic change in the physical properties of water under these operating conditions (low viscosity, high diffusivity, low dielectric constant, and an easily adjustable ionic product), which allow for an easy solubilization of lignin, and a tunable reaction pathway, as depending on the operating conditions selected, either the ionic or the radical reactions are favored (Cantero et al., 2015;Abad-Fernández et al., 2019). During hydrothermal hydrolysis, the polymeric chains that make up lignin are broken into monomers of great industrial interest (Jiang et al., 2016). However, the resulting monomers repolymerize, so the total yield of monomers obtained at the end of the process remains at relatively low values (Adamovic et al., 2021; Wahyudiono et al., 2008), obtaining a final solid with a high lignin content (Adamovic et al., 2022; Yong & Matsumura, 2012).

This research work aims to recover high-lignin-content solids from the hydrolysis of grape pomace, a byproduct from the wine production industry widely available in Castilla y León, our region. Grape pomace features a high lignin content, ranging from 11.6% to 41.3% according to (Šelo et al., 2021), or from 32.5% to 56.7% for insoluble lignin, as reported

by (Rodrigues et al., 2022). To achieve this, the process utilizes hydrothermal treatments to recover lignin in a single-step process.

In this context, two specific goals have been defined: (i) to design an optimal pretreatment process that minimizes handling issues, particularly those related to pumping grape pomace; and (ii) to determine the optimal hydrolysis conditions that maximize both the solid recovery yield and its lignin content. These solids will be further used in the synthesis of novel biomaterials.

Experimental

Experimental setup and operating conditions: for the pretreatment phase, grape pomace is first dried in a Thermo Scientific™ Heratherm™ General Protocol Oven at 105ºC for 24-48h to remove water before milling for 5 minutes in a Cutting Mill SM 100 knife mill from Retsch. Because of the high oil content in the grape seeds, the grape pomace cannot be directly milled to sizes under 0.250 mm, so it must first be milled to 0.500 mm and dried again before being milled to sizes under 0.25 mm. For the hydrolysis process, tubular type reactors are used in the pilot plant “PHUn-1” of our research group, which is shown in Figure 1.

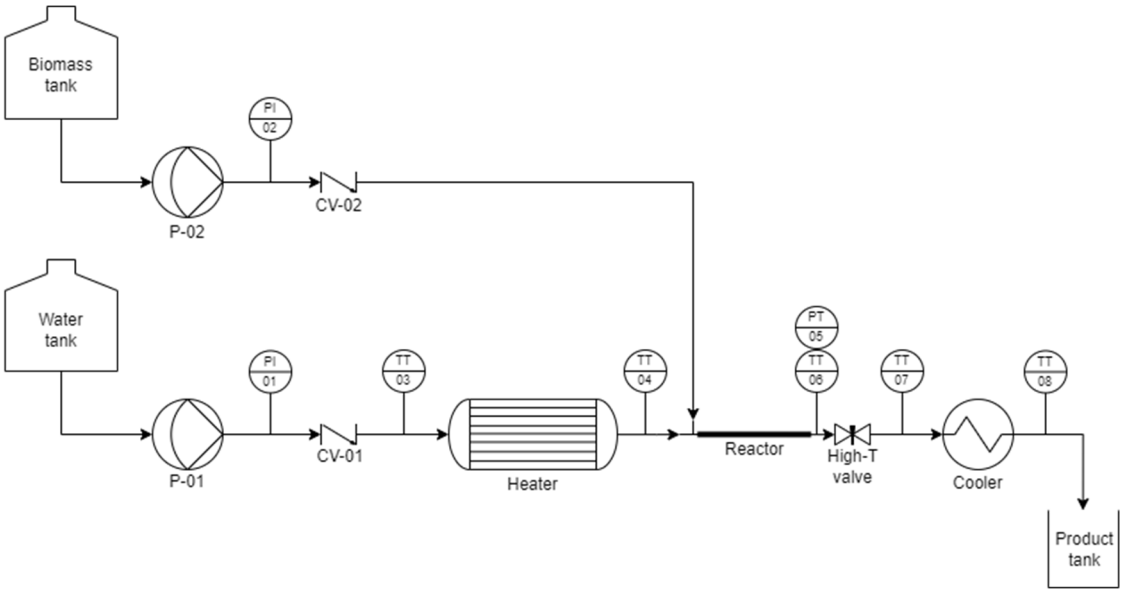

Fig. 1.: Scheme of the hydrothermal hydrolysis plant

Operational variables: the pilot plant allows for operating with biomass flows up to 30 kg/h, pressures ranging from 20 MPa to 26 MPa, temperatures from 300ºC to 420ºC, concentrations up to 20% w/w (depending on the biomass), and reaction times from less than 1s up to 30s.

Analysis: the initial solid composition is characterized using the Laboratory Analytical Procedure (LAP) of the National Renewable Energy Laboratory (NREL), specifically the protocol for structural carbohydrates and lignin in biomass (Sluiter et al., 2008). After hydrolysis, the resulting suspension was centrifuged, analyzing separately the solid and liquid fractions. FTIR spectroscopy was used to follow structural changes in the solid phase, while UV-Vis spectroscopy was employed to quantify soluble lignin. In addition, HPLC was used to identify and quantify soluble compounds in the liquid fraction. SEM analysis was performed to observe morphological changes, and DSC was used to determine degradation points of various compounds, including the glass transition temperature of lignin, which is important for assessing its potential applications.

The experiments were carried out using an aqueous suspension of grape pomace at 2% w/w concentration. The operating pressure was maintained at 260 bar, testing two different temperatures: 380ºC and 400ºC. Reaction times ranged from 65 milliseconds to 1 second, corresponding to biomass flows between 0.7 kg/h and 2.2 kg/h. The experiments also involved different reactor lengths, all with a constant water flow of 3.9 kg/h.

The initial biomass suspension is shown in Figure 2, where it can be observed that grape pomace tends to settle down if the slurry is not continuously agitated. This behaviour highlights the challenges in pumping such mixtures, which justifies the choice of a low biomass concentration (2% w/w) to minimize operational issues.

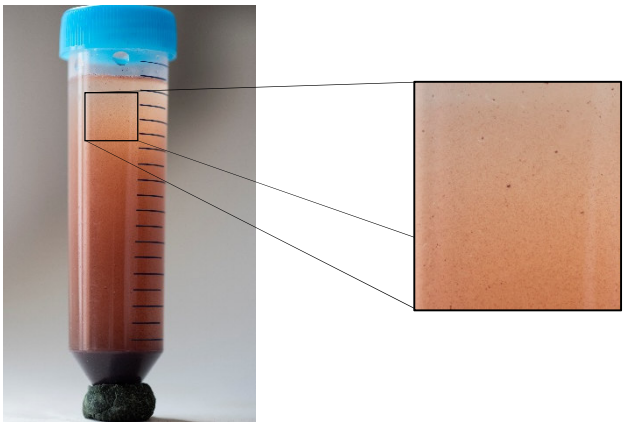

Fig. 2.: Initial biomass suspension: grape pomace in water at 2% w/w concentration partially sedimented

Regarding the hydrolysis products, there is a noticeable difference in the sample colour and solid concentration, which depends on the hydrolysis conditions (Figure 3). While the initial biomass suspension is a heterogeneous slurry, the hydrolysis products seem more homogeneous, although they still contain some undissolved solids. The apparent

homogeneity of the samples observed in Figure 3 is a consequence of the hydrolysis of various grape pomace components, especially polysaccharides, which leads to the formation of soluble sugars. As the temperature increases, hydrolysis becomes more extensive, producing more soluble compounds and thereby reducing the amount of suspended solids, which results in a more uniform liquid phase. The colour differences observed in the samples shown in Figure 3a, 3b, and 3c are primarily related to differences in reaction temperature, which affect the extent of cellulose and hemicellulose hydrolysis. The lighter colour in Figure 3b, corresponding to the highest temperature (400 °C), suggests a higher conversion of structural carbohydrates into soluble sugars, resulting in a more homogeneous and transparent liquid phase.

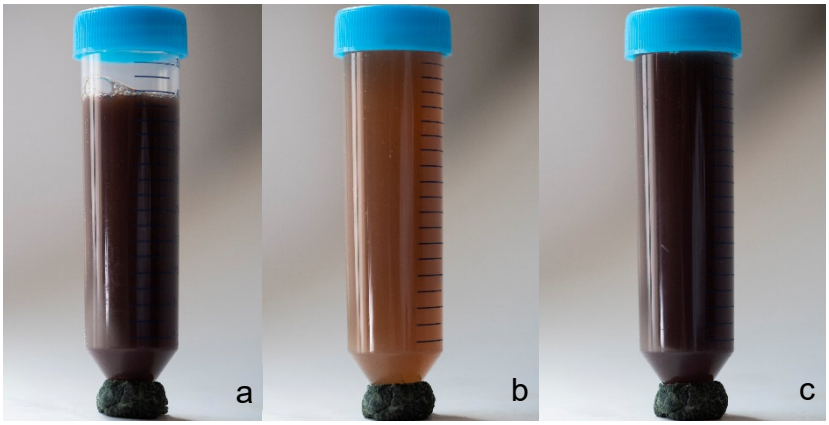

Fig. 3.: Hydrolysis product of grape pomace at: a) T=380ºC, p=260 bar, 66 ms reaction time, 0.72% w/w on reactor; b) T=400ºC, p=260 bar, 172 ms reaction time, 0.33% w/w on reactor; c) T=380ºC, p=260 bar, 378 ms reaction time, 0.57% w/w on reactor

In light of the results, the samples shown in Figures 3a and 3c appear visually similar in colour and turbidity, despite differing in residence time. This suggests that the reaction temperature of 380 °C may not have been high enough to achieve extensive hydrolysis under the tested conditions, or alternatively, that the residence times of 66 ms and 378 ms were still too short to fully break down the structural carbohydrates. These observations indicate a possible threshold effect in the hydrolysis kinetics, where either higher temperatures or longer reaction times are required to significantly increase the yield of soluble sugars.

Summary

This work is focused on the valorization of grape pomace, a widely available byproduct from the wine industry, by recovering lignin through hydrothermal processing. First, a pretreatment method was developed to solve the handling and pumping problems of grape pomace. It consisted of an initial drying step to remove moisture, followed by grinding to a particle size of below 0.500 mm. A second drying step was then carried out to eliminate the oil released during the first grinding, which caused clumping of the material and prevented single-step milling. Finally, the grape pomace was ground again to achieve a particle size below 0.250 mm. Then, different hydrolysis conditions using supercritical water were tested in order to identify the optimal combination of solid yield and lignin content. Results showed that operating at 400 °C leads to a lighter-coloured liquid and a lower amount of solid residue, suggesting more extensive hydrolysis. In contrast, at 380 °C, longer reaction times appear to be necessary to achieve comparable results.

Acknowledgment

The authors thank the support of the Spanish Ministry of Education through the Collaboration Scholarship Program for the year 2024-2025.

References

Abad-Fernández, N., Pérez, E., & Cocero, M. J. (2019). Aromatics from lignin through ultrafast reactions in water. *Green Chemistry*, *21*(6), 1351–1360. https://doi.org/10.1039/c8gc03989e

Adamovic, T., Tarasov, D., Demirkaya, E., Balakshin, M., & Cocero, M. J. (2021). A feasibility study on green biorefinery of high lignin content agro-food industry waste through supercritical water treatment. *Journal of Cleaner Production*, *323*. https://doi.org/10.1016/j.jclepro.2021.129110

Adamovic, T., Zhu, X., Perez, E., Balakshin, M., & Cocero, M. J. (2022). Understanding sulfonated kraft lignin re-polymerization by ultrafast reactions in supercritical water. *Journal of Supercritical Fluids*, *191*. https://doi.org/10.1016/j.supflu.2022.105768

Arai, K., Smith, R. L., & Aida, T. M. (2009). Decentralized chemical processes with supercritical fluid technology for sustainable society. In *Journal of Supercritical Fluids* (Vol. 47, Issue 3, pp. 628–636). https://doi.org/10.1016/j.supflu.2008.11.008

Cantero, D. A., Sánchez Tapia, Á., Bermejo, M. D., & Cocero, M. J. (2015). Pressure and temperature effect on cellulose hydrolysis in pressurized water. *Chemical Engineering Journal*, *276*, 145–154. https://doi.org/10.1016/j.cej.2015.04.076

Cocero, M. J., Cabeza, Á., Abad, N., Adamovic, T., Vaquerizo, L., Martínez, C. M., & Pazo-Cepeda, M. V. (2018). Understanding biomass fractionation in subcritical & supercritical water. In *Journal of Supercritical Fluids* (Vol. 133, pp. 550–565). Elsevier B.V. https://doi.org/10.1016/j.supflu.2017.08.012

Jiang, W., Lyu, G., Wu, S., Lucia, L. A., Yang, G., & Liu, Y. (2016). Supercritical H2O & lignin. In *BioResources* (Vol. 11, Issue 3).

Rodrigues, R. P., Gando-Ferreira, L. M., & Quina, M. J. (2022). Increasing Value of Winery Residues through Integrated Biorefinery Processes: A Review. In *Molecules* (Vol. 27, Issue 15). MDPI. https://doi.org/10.3390/molecules27154709

Šelo, G., Planinić, M., Tišma, M., Tomas, S., Koceva Komlenić, D., & Bucić-Kojić, A. (2021). A comprehensive review on valorization of agro-food industrial residues by solid-state fermentation. In *Foods* (Vol. 10, Issue 5). MDPI AG. https://doi.org/10.3390/foods10050927

Shorey, R., Gupta, A., & Mekonnen, T. H. (2021). Hydrophobic modification of lignin for rubber composites. *Industrial Crops and Products*, *174*. https://doi.org/10.1016/j.indcrop.2021.114189

Sluiter, A., Hames, B., Ruiz, R., Scarlata, C., Sluiter, J., Templeton, D., & Crocker, D. (2008). *Determination of Structural Carbohydrates and Lignin in Biomass: Laboratory Analytical Procedure (LAP) (Revised July 2011)*. http://www.nrel.gov/biomass/analytical_procedures.html

Wahyudiono, Sasaki, M., & Goto, M. (2008). Recovery of phenolic compounds through the decomposition of lignin in near and supercritical water. *Chemical Engineering and Processing: Process Intensification*, *47*(9–10), 1609–1619. https://doi.org/10.1016/j.cep.2007.09.001

Yong, T. L. K., & Matsumura, Y. (2012). Reaction kinetics of the lignin conversion in supercritical water. *Industrial and Engineering Chemistry Research*, *51*(37), 11975–11988. https://doi.org/10.1021/ie300921d

Antioxidative Activity of Flavonoids from *Thymus Vulgaris* and *Thymus Serpyllum*

Mina Miličič[1], Urban Bren[1,2,3,*], Veronika Furlan[1,*]

[1]Faculty of Chemistry and Chemical Engineering, University of Maribor, Smetanova ulica 17, SI-2000 Maribor, Slovenia,

[2]Faculty of Mathematics, Natural Science and Information Technologies, University of Primorska, Glagoljaška ulica 8, SI-6000 Koper, Slovenia

[3] Institute of Environmental Protection and Sensors, Beloruska ulica 7, SI-2000 Maribor, Slovenia

[*]Correspondence: urban.bren@um.si and veronika.furlan@um.si

Introduction

An imbalance in free radicals, caused by UV radiation, air pollution, alcohol, and tobacco in the human body, can lead to various damage to cellular compounds such as DNA, lipids, and proteins [1, 2]. Diet plays a crucial role in reducing the presence of radical species in the human body due to various natural antioxidants in different foods and herbs. In recent years, food and pharmaceutical industries have shown increasing interest in medicinal plants (MAPs) due to their beneficial health effects and high content of antioxidants. Among MAPs, members of the *Thymus* genus (*Lamiaceae* family), such as *Thymus vulgaris* and *Thymus serpyllum*, have attracted significant interest in recent years [3, 4]. Both species contain high levels of bioactive compounds, possessing a variety of bioactivities, such as antioxidative [5], anti-inflammatory [6], and anticancerogenic [5] activities. The main chemical groups present in *T. vulgaris* and *T. serpyllum* extracts are polyphenolic acids and flavonoids. In *T. vulgaris* extracts, apigenin (up to 7.6 mg/g) [7] and quercetin (up to 3.98 mg/g) were identified as major flavonoids [8]. In *T. serpyllum* extracts, apigenin (124.44 µg/g dry herb) and quercetin (1.29 µg/g dry herb), were also reposted as the main flavonoids [9]. The antioxidant activity of *T. vulgaris* and *T. serpyllum* extracts can be attributed to the high presence of polyphenolic acids, such as rosmarinic acid, as well as flavonoids apigenin and quercetin. These species have shown antioxidative activity in various assays, such as DPPH, ABTS, and FRAP [10].

Quercetin (2-(3,4-dihydroxyphenyl)-3,5,7-trihydroxychromen-4-one) belongs to the flavonoid class and is found in various food sources, such as caper, black chokeberry, lettuce, onion, tomato as well as *T. vulgaris* and *T. serpyllum*. This flavonoid contains five hydroxyl groups distributed across two benzene rings (A and B) and a pyrene ring (C), as

it is represented in Fig. 1 (A). Due to its specific structure, quercetin possess good antioxidative properties [11]. Quercetin has demonstrated antioxidative properties in several anitoxidative assays, including ABTS, DPPH, and FRAP [10]. However, further thermodynamic and kinetic investigations are necessary to improve our understanding of the molecular mechanisms of the antioxidative activity of quercetin against various biological free radicals. To clarify antioxidative mechanisms of quercetin, quantum-chemical methods were used to simulate hydrogen atom transfer (HAT), radical adduct formation (RAF), sequential proton loss electron transfer (SPLET), and sequential electron proton transfer (SET) reactions of quercetin with hydroxyl ($OH^{\bullet}$) radical under physiological conditions (pH = 7.40 in aqueous solution). The optimized structure of quercetin at physiological conditions is represented in Fig. 1 (B).

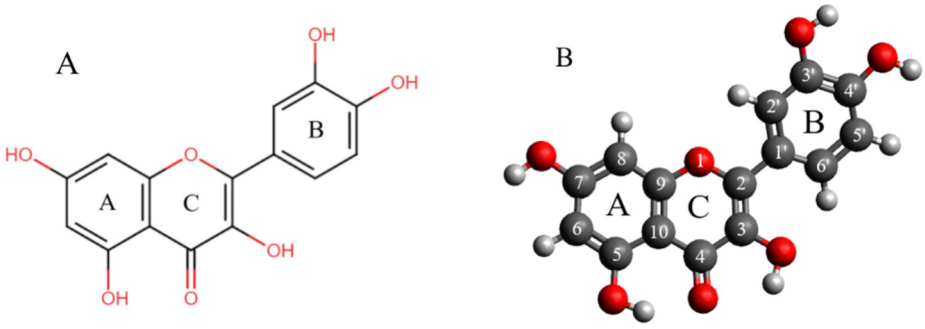

Fig 1. (A) Structural formula of quercetin; (B) Quercetin structure optimized with functional M06-2X in combination with flexible basis set 6-311++G(d,p) in aqueous solution. Carbon atoms are represented in gray, oxygen atoms in red, and hydrogen atoms in white.

Experimental

Computational Methods

Geometry optimization and frequency calculations were performed by applying Density Functional Theory (DFT) functional M06-2X in combination with the 6-311++G(d,p) flexible basis set and Solvation Model Density (SMD) in the Gaussian 16 software package on the server Elixir, located at UM FKKT [12]. Recently, functional M06-2X revealed good performance in the simulation of reactions between polyphenols and various free radicals [13, 14]. By analyzing the frequency calculation, the nature of stationaly point can be confirmed. Only real frequencies indicate an equilibrium geometry (local minima), while exactly one identified imaginary frequency, corresponding to the studied reaction coordinate, represents a transition state (TS).

Quantum mechanics-based test for overall free radical scavenging activity (QM-ORSA)

According to the QM-ORSA methodology, several antioxidative mechanisms are involved in the free radical scavenging activity of chemical compounds, namely HAT (eqn (1)), SET (eqn (2)), RAF (eqn (3)), SPLET (eqn (3) and eqn (4)), and sequential electron proton transfer (SEPT, eqn (6)) mechanisms [2].

$$H_5Q + R^{\bullet} \rightarrow H_4Q^{\bullet} + RH \quad (1)$$

$$H_5Q + R^{\bullet} \rightarrow [H_5Q - R]^{\bullet} \quad (2)$$

$$H_5Q + R^{\bullet} \rightarrow H_5Q^{\bullet+} + R^{-} \quad (3)$$

$$H_5Q + HO^{-} \rightarrow H_4Q^{-} + H_2O \quad (4)$$

$$H_4Q^{-} + R^{\bullet} \rightarrow H_4Q^{\bullet} + R^{-} \quad (5)$$

$$H_5Q + R^{\bullet} \rightarrow H_5Q^{\bullet+} + R^{-} \overset{-H^{+}}{\rightleftharpoons} H_4Q^{\bullet} + R^{-} \quad (6)$$

Thermodynamic calculations

Before the kinetic investigation of quercetin's antioxidative activity in aqueous solution, the Gibbs free energies (ΔGr) were calculated for all possible molecular mechanisms described above. All reactive centers on quercetin were thermodynamically investigated for the corresponding molecular mechanisms, and all forms of quercetin at pH 7.40 were included. For further kinetic investigations, only the exerogenic (ΔGr < 0) and isorgenic (ΔGr ≈ 0) reaction paths were considered.

Kinetic calculations

In all mechanisms, namely HAT, RAF, SET, and SPLET, the reaction rate constants were calculated by applying the transition state theory (TST):

$$k = \frac{k_B T}{h} e^{-(\Delta G^{\neq})/RT} \quad (7)$$

where k_B and h represent Boltzmann and Planck's constants, respectively, $\Delta G^{\neq}$ is the Gibbs free energy of activation, while T stands for temperature (K). After calculating the k for all thermodynamically favorable antioxidative mechanisms, the total rate coefficient (k_{tot}, eqn (8)) of quercetin were calculated.

$$k_{tot} = k^{HAT} + k^{RAF} + k^{SET} + k^{SPLET} \quad (8)$$

At pH 7.40 in aqueous solution, quercetin is present in three different acid-base forms, namely neutral (H_5Q), mono-anionic (H_4Q^-), and dianionic (H_3Q^{2-}) forms, as presented inFig. 2.

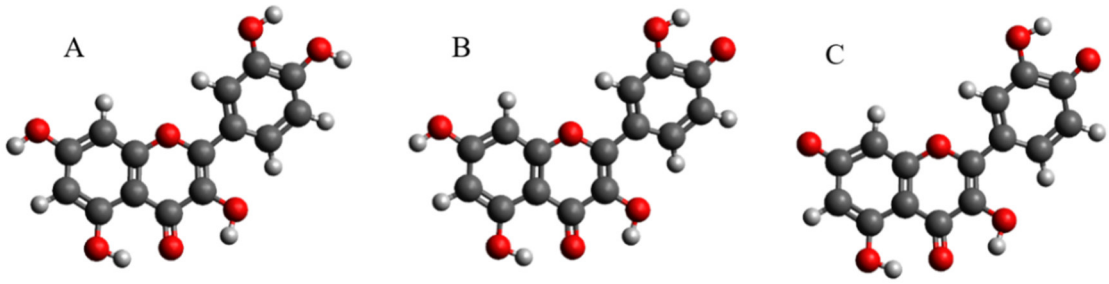

Fig. 2. Optimized neutral (A), monoanionic (B), and dianionic (C) structure of quercetin obtainedby applying M06-2X/6-311++G(d,p) level of theory and SMD solvation model.

Consequently, it is necessary to calculate the overall rate coefficient ($k_{overall}$) (eqn (9)). The molar fractions of quercetin at pH = 7.40 are *f* [H_5Q] = 0.06856, *f* [H_4Q^-] = 0.6702, *f* [H_3Q^{2-}] = 0.2608, and *f* [H_2Q^{3-}] = 4.231 x10^{-4} [15]. Therefore, $k_{overall}$ for quercetin in aqueous solution at pH = 7.40 represents the sum of k_{tot} multiplied by the corresponding molar fraction (*f*) for all acid-based species andcan be calculated in the following way:

$$k_{overall} = f(H_5Q)k_{tot}^{H_2Q} + f(H_4Q^-)k_{tot}^{H_4Q^-} + f(H_3Q^{2-})k_{tot}^{H_3Q^{2-}} \quad (9)$$

An example of the optimized geometry of the reactants (A), transition state (B), and product (C) for RAF mechanisms is shown in Fig. 3. The optimizations of geometries and frequency calculations were perferomed at M06-2X/6-311++G(d,p) level of theory in combination with SMD solvation model, and results confirmed that the geometries of both reactants and products are indeed local minima. The real frequencies for reactants and products were 30.260 cm^{-1} and 35.200 cm^{-1}, respectively. The TS geometry revealed exactly one imaginary frequency, with a value of -410.190 cm^{-1}, which corresponds to the reaction coordinate for the RAF mechanism.

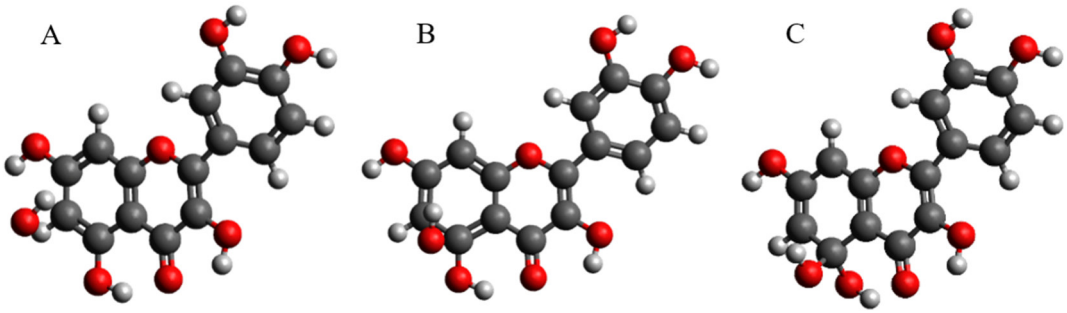

Fig. 3. Optimized geometries of reactants (A), transition state (B), and product (C) for the RAF reaction mechanism of quercetin and hydroxyl radical ($OH^•$) on reactive center 5 by applying M06-2X/6-311++G(d,p) level of theory and SMD solvation model.

Summary

Thymus vulgaris and *Thymus serpyllum* extracts exhibit different bioactivities due to the presence of various bioactive compounds, including polyphenolic acids, namely rosmarinic acid, and flavonoids, such as quercetin and apigenin. Numerous studies reported the antioxidative activity of quercetion and its importance in promoting human health. To fully understand its antioxidant activity, it is necessary to understand molecular mechanisms of reactions between quercetin and free radicals. Therefore, thermodynamic and kinetic investigations of the reactions between quercetin and hydroxyl radical were performed at the M06-2X/6-311++G(d,p) level of theory in combination with SMD solvent model at physiological conditions.

References

[1] Fifen, J.J.; Nsangou, M.; Dhaouadi, Z.; Motapon, O.; Jaidane, N. Solvent effects on the antioxidant activity of 3,4-dihydroxyphenylpyruvic acid : DFT and TD-DFT studies. Computational and Theoretical Chemistry. 2011, 966, 232-243.

[2] Galano, A.; Alvarez-Idaboy, J.R. A computational methodology for accurate predictions of rate constants in solution: Application to the assessment of primary antioxidant activity. J. Comput. Chem. 2013, 34, 2430–2445.

[3] Silva, A.S.; Tewari, D.; Sureda, A.; Suntar, I.; Belwal, T.; Battino, M.; Nabavi, S.M.; Nabavi, S.F. The evidence of health benefits and food applications of Thymus vulgaris L. Trends in Food Science & Technology. 2021, 117, 2018-227.

[4] Kosakowska, O.; Bączek, K.; Przybył, J.L.; Pawełczak, A.; Rolewska, K.; Węglarz, Z. Morphological and chemical traits as quality determinants of common thyme (Thymus vulgaris L.), on the example of 'Standard Winter' cultivar. Agronomy. *2020, 10,* 909.

[6] Amarowicz, R.; Żegarska, Z.; Rafałowski, R.; Pegg, R.B.; Karamać, M.; Kosińska, A. Antioxidant activity and free radical-scavenging capacity of ethanolic extracts of thyme, oregano, and marjoram. Eur. J. Lipid Sci. Technol. 2009, 111, 1053-1168.

[7] Kindl, M.; Bucar, F.; Jelić, D.; Brajša, K.; Blažeković, B.; Knežević, S.V. Comparative study of polyphenolic composition and anti-inflammatory activity of Thymus species. European Food Research and Technology. 2019, 245, 1951-1962.

[8] Gavarić, N.; Kladar, N.; Mišan, A.; Nikolić, A.; Samojlik, I.; Mimica-Dukić, N.; Božin, B. Postdistillation waste material of thyme (Thymus vulgaris L., Lamiaceae) as a potential source of biologically active compounds. Industrial Crops and Products. 2015, 74, 457-464.

[9] Palmieri, S.; Pellegrini, M.; Ricci, A.; Compagnone, D.; Lo Sterzo, C. Chemical Composition and Antioxidant Activity of Thyme, Hemp and Coriander Extracts: A Comparison Study of Maceration, Soxhlet, UAE and RSLDE Techniques. Foods. 2020, 9, 1221.

[10] Boros, B.; Jakabová, S.; Dörnyei, Á.; Horváth, G.; Pluhár, Z.; Kilár, F.; Felinger, A. Determination of polyphenolic compounds by liquid chromatography-mass spectrometry in Thymus species. Journal of Chromatography A. 2010, 1217, 792-7980.

[11] Tian, C.; Liu, X.; Chang, Y.; Wang, R.; Lv, T.; Cui, C.; Liu, M. Investigation of the anti-inflammatory and antioxidant activities of luteolin, kaempferol, apigenin and quercetin. South African Journal Botany. 2021, 137, 257-264.

[12] Wang, W.; Sun, C.; Mao, L.; Ma, P.; Liu, P.; Yang, J.; Gao, Y. The biological activities, chemical stability, metabolism and delivery systems of quercetin: A review. Trends in Food Science & Technology. 2016, 56, 21-38.

[13] Zhao, Y.; Truhlar, D.G. The M06 Suite of Density Functionals for Main Group Thermochemistry, Thermochemical Kinetics, Noncovalent Interactions, Excited States, and Transition Elements: Two New Functionals and Systematic Testing of Four M06-class Functionals and 12 Other Function. Theor. Chem. Acc. 2008, 120, 215–241.

[14] Tošović, J.; Bren, U. Antioxidative Action of Ellagic Acid—A Kinetic DFT Study. Antioxidants. 2020, 9, 587.

[15] Tošović, J.; Kolenc, Z.; Hostnik, G.; Bren, U.; Exploring antioxidative properties of xanthohumol and isoxanthohumol: An integrated experimental and computational approach with isoxanthohumol pKa determination. Food Chemistry. 2025, 463, 141377.

[17] Amić, A.; Mastiľák Cagardová, D. A DFT Study on the Kinetics of $HOO^{\bullet}$, $CH_3OO^{\bullet}$, and $O_2^{\bullet-}$ Scavenging by Quercetin and Flavonoid Catecholic Metabolites. Antioxidants. 2023, 12, 1154.

Deterministic Modeling of the High-Pressure Process for Ethene-Vinyl Acetate-Vinyl Neodecanoate Terpolymerization

Adil Boukhalaf, Anne Rott, Markus Busch

Ernst-Berl-Institute, Technical University Darmstadt, adil.boukhalaf@pre.tu-darmstadt.de

Introduction

To improve the accuracy of simulated molecular weight distributions, a deterministic model for the terpolymerization of ethene, vinyl acetate and vinyl neodecanoate (E-VA-VeoVA10) established by Anne Rott and Elisabeth Nowottny was adjusted [1] [2]. A schematic depiction of the model design is shown in Fig.1 and describes the terpolymerization as three simultaneously occurring copolymerizations. Improvement of the accuracy of the simulations was realized by the implementation of a conversion-dependent correlation for the transfer to polymer kinetic coefficient of VeoVA10 based on a correlation established by Thomas Herrmann for LDPE [3].

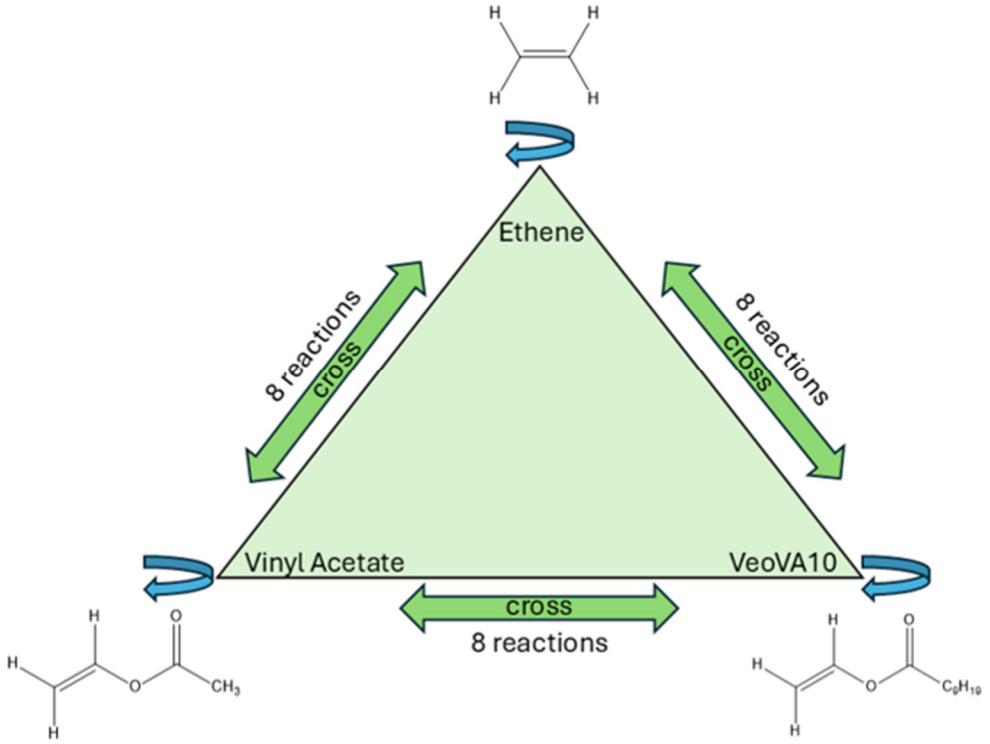

Fig.1: Schematic depiction of the terpolymerization model. This design assumes that the terpolymerization can be described by three copolymerizations occurring simultaneously

Existing literature provides kinetic parameters for VeoVA10 based on emulsion polymerizations under ambient conditions or adapted by kinetic parameters of vinyl acetate. Using these parameters for a model that is designed to describe high-pressure

co- and terpolymerization processes results into discrepancies which were investigated in this work.

Experimental

Accurate characterization of polymer samples is essential to identify discrepancies between simulated and experimental molecular weight distributions (MWDs). These discrepancies were addressed via parameter estimations, which heavily rely on the input data. At first, it was determined what type of detector is used for the characterization of the MWDs. The high branching density of the polymer samples result into systematically underestimated MWDs when evaluating the gel permeation chromatography with an infrared detector (GPC-IR). In this work, molecular weight distributions were determined via GPC-light scattering (GPC-LS). To ensure accurate results, the refractive index increments of each sample were determined individually with measurements conducted via a high-temperature differential refractometer.

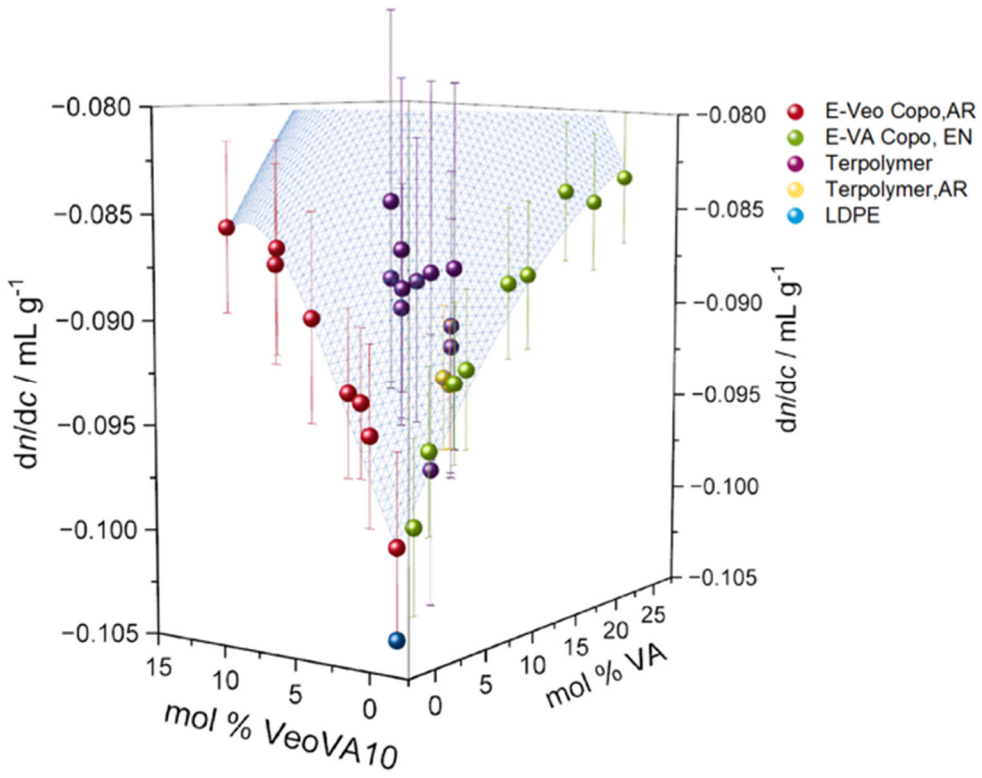

Fig.2: Refractive index increments determined for the copolymers E-VA by Elisabeth Nowottny (EN [1], green), E-VeoVA10 by Anne Rott (AR [2], red). Terpolymers measured by Anne Rott are depicted in yellow [2] while LDPE in blue serves as the point of origin.

Residual monomer significantly changes determined refractive index increments which is why each sample is dried with either the rotary evaporator, a heating oven or via

precipitation. The least residual monomer was achieved with the precipitation method [4]. The then measured refractive index increments depicted in Fig. 2 lay in the surface spanned by the copolymer data measured by the working group. [1] [2].

To correctly assign the refractive index increments, polymer compositions were determined via ^{1}H-NMR spectroscopy. After sufficient data was collected, the MWDs were characterized. There one may observe significant differences between the simulations and the experimental MWDs as depicted in Fig.3 It can be observed that the overall shapes of the MWDs do match but the simulations underestimate the results significantly.

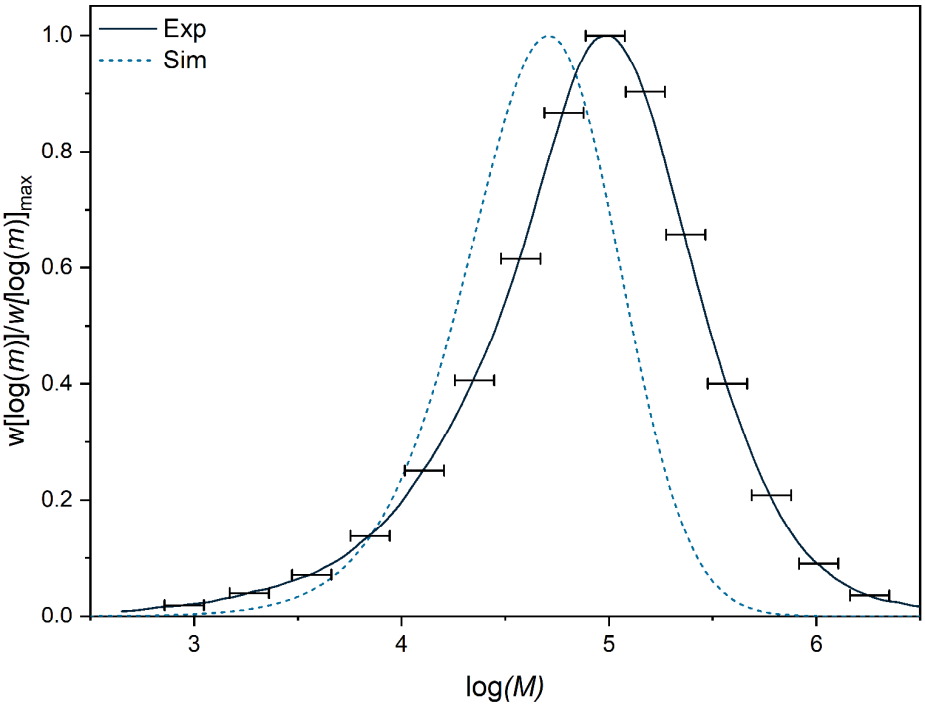

Fig.3: Comparison between the simulated (dashed blue line) and experimental molecular weight distributions of a sample.

With parameter estimations conducted via Predici [5] by CiT, a mathematical model is fitted in such a way that the simulated MWD reproduces the experimental data. The mathematical model, which are the kinetic coefficients θ, describes the time dependent behavior of the system. They serve as a set of ordinary differential equations (ODEs). In case of this work the kinetic network, specifically the transfer to polymer steps of VeoVA10 was adjusted to reproduce the position of the peak as closely as possible. At first, sensitivity studies were performed to investigate the feasibility of the parameter estimations and to reduce computation times by identifying the range in which the system is sensitive towards changes of $k_{tr,P,VeoVA}$.[6]

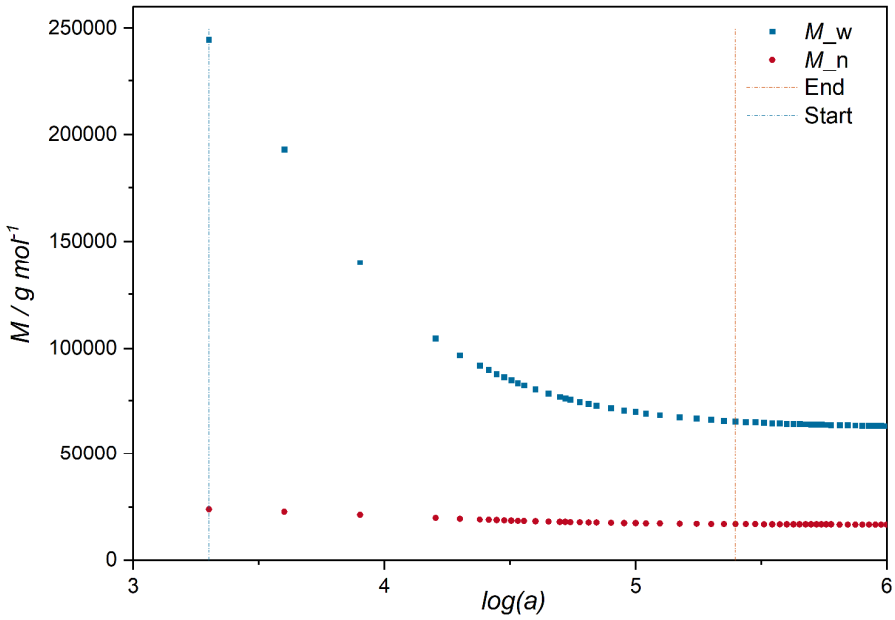

Fig.4: Sensitivity studies performed to investigate the boundaries in which a change in factor *a* impacts the weight and number average molecular weights of the system.

After confirming the feasibility and identifying the boundaries of the parameter estimations the parameter estimations were conducted. A factor *a* was introduced to be adjusted. This is achieved by solving the ODEs numerically via the Gauss-Newton method.[6] To ensure reliable results, parameter estimations for each sample were conducted separately while confirmation estimations were performed at different initial values. The results converged to the same solution for *a*. By comparing the new simulated and experimental molecular weight distributions depicted in Fig. 5 it can be observed that the molecular weight distributions lie within the error bars. In Fig. 6 one may observe that the implemented conversion dependency is now able to differentiate between two samples produced at identical process conditions but at varying conversions. Additionally, it can be observed that samples which were produced at identical process conditions result into significantly different molecular weight distributions, confirming the assumption that the conversion does influence the MWDs significantly.

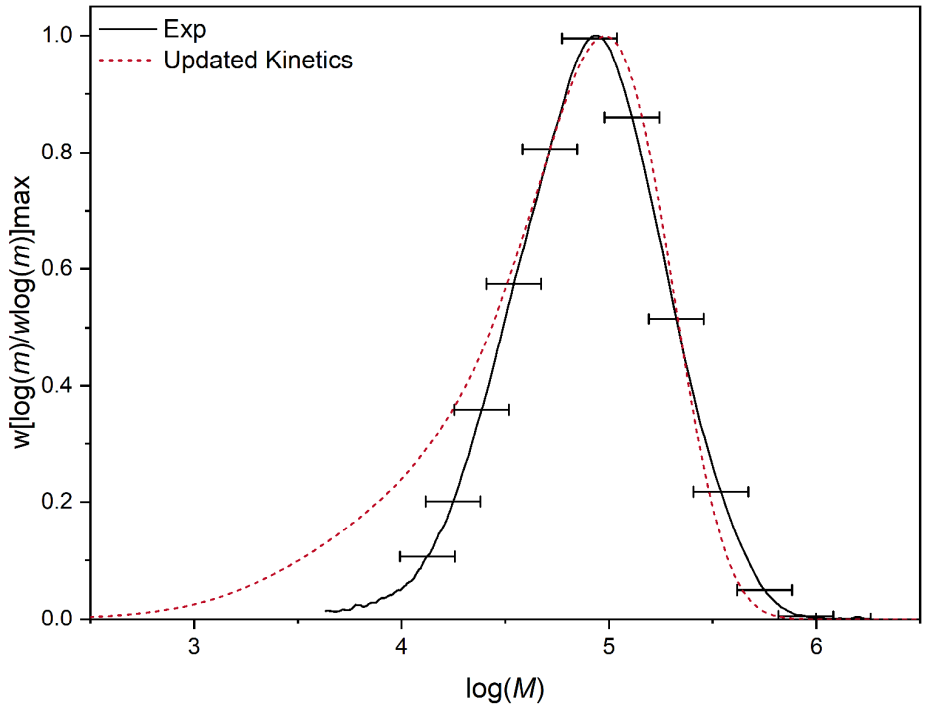

Fig. 5: Comparison between the experimental MWD in black and the simulated MWD in red (dashed line) of the same sample with the new correlation.

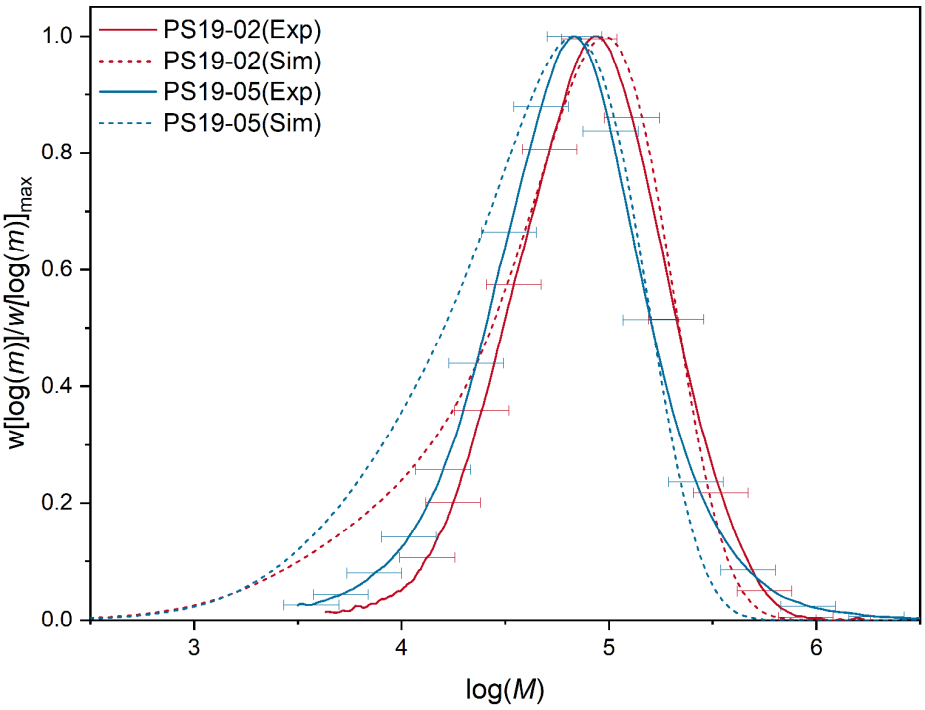

Fig. 6: Simulated (dashed lines) and experimental molecular weight distributions of two samples which were produced at identical process conditions but with varying conversions.

Summary

A deterministic terpolymerization model was adjusted to improve accuracy of simulated molecular weight distributions (MWDs). A key modification was the introduction of a conversion dependent correlation for the transfer to polymer steps of VeoVA10, considering inaccuracies resulting from literature data being derived under ambient conditions. Experimental MWDs were determined using GPC-LS. Accurate refractive index increments were ensured via drying methods which validated by NMR.[4] Discrepancies between simulation and experiment were addressed through parameter estimations using the Gauss-Newton method, optimizing factor *a* to align simulated and experimental MWD peaks. The improved model, which was validated across samples and initial values, reproduces MWDs within experimental error bars and can distinguish samples produced at equal conditions but with different conversions. Conformation simulations of samples not included in the parameter estimations were performed, confirming the ability of describing the polymerization behavior of the system.

References

[1] E. Nowottny, Dissertation, Technische Universität Darmstadt, 2024.

[2] A. Rott, Dissertation, Technische Universität Darmstadt, unpublished.

[3] T. Herrmann, Dissertation, Technische Universität Darmstadt, 2011.

[4] S.Hintenlang, Dissertation, Technische Universität Darmstadt, unpublished.

[5] M. Wulkow, *Macromolecular Reaction Engineering*., 2008, 2, 461-494.

[6] Hendricus C.M. van Boxtel, Dissertation, Georg-August-Universität Göttingen, 2000.

Ammonia Production

Megara Körmöczi
Department of Chemical Engineering Masters
Budapest University of Technology and Economics
megara.kormoczi98@gmail.com

I. Abstract

Our thesis task was to design a plant with a capacity of 250 000 t/year and outline its advantages and disadvantages. Nowadays, ammonia is increasingly recognised for its beneficial properties and could even represent a major step forward in the solution of growing energy needs. In this thesis, alternative ammonia production technologies were investigated with the above mentioned capacity throughout a detailed analysis. Besides, the five technologies were studied aiming to select which is the most economical and the most integrable process based on the environmental and energetical point of view. As the most common solution for ammonia production Haber-Bosch sytnhesis was used as a baiss for comparison. In addition, the different feedstock production alternatives in order to be able to summarise and draw conclusions were investigated. After the selection, the process was designed step by step from raw material to product, besides the material and energy balances were calculated, moreover cost estimation for the whole technologywas made. The simulation of the technology was carried out using Aspen Plus V11 software package, from which the key parameters and properties were determined for detailed sizing and design.

During our thesis project, we worked as a group of five; however, I will primarily focus on the parts I personally conducted and contributed to.

II. Introduction

Ammonia (NH_3) is a crucial compound in industrial processes, particularly in the agricultural and chemical industries. Its primary applications include the production of fertilizers and refrigerants, but it is also widely used in other sectors, such as animal feed additives and as a component in cleaning agents. Large-scale ammonia production is predominantly carried out using the Haber-Bosch process, an established and well-known technology. This method involves high-pressure and high-temperature reactions between

nitrogen (N_2) and hydrogen (H_2) gases to produce ammonia gas. Catalysts are used in this process to increase efficiency. Ammonia production is vital to agriculture, as it serves as a key raw material in fertilizers, providing essential nutrients for plant growth. In addition, ammonia is used in various other fields, including as a reducing agent in steel manufacturing, in the production of refrigerants, and in cosmetic and household cleaning products. Therefore, ammonia and its industrial synthesis play a fundamental role in modern industrial processes and agricultural productivity.

Ammonia is a naturally occurring compound that appears as a colorless gas or liquid. It is present in the atmosphere, soil, mineral waters, as well as in both plant and animal organisms. Ammonia plays a crucial role in numerous biological processes and serves as a fundamental building block for the synthesis of amino acids and nucleotides. In the environment, ammonia is part of the nitrogen cycle and is produced in the soil through bacterial activity. Naturally, ammonia behaves as a base and partially dissociates in aqueous solutions. Ammonia gas is easily compressible and, under pressure, forms a clear liquid, which is the preferred form for storage and transport. The molecule has a trigonal pyramidal geometry and is polar. Multiple ammonia molecules can form hydrogen bonds with each other. The formation of ammonia involves three hydrogen atoms covalently bonded to a nitrogen atom. The nitrogen atom possesses a lone pair of electrons that contributes to the formation of strong hydrogen bonds with other ammonia molecules [1]. The reaction is exothermic, and its stoichiometry is represented by Equation 1.

$$N_2+3H_2=2NH_3 \qquad (1)$$

The physical and chemical properties of the raw materials and the product are summarized in Table 1.1.

Table 1.1: Key properties of ammonia and its raw materials [2,3]

Property	Hydrogen	Nitrogen	Ammonia
Molar mass (g/mol)	2.02	28.01	17.03
Color	Colorless	Colorless	Colorless
Odor	Odorless	Odorless	Pungent, irritating
Physical state at 20 °C	Gas	Gas	Gas
Melting point (°C)	-259	-210	-77.7
Boiling point (°C)	-252.8	-195.8	-33.35
Density (gas, g/dm³)	0.084	0.807	0.771
Density(liquid, g/cm³)	0.071	1.251	0.6818
Critical temperature (°C)	-239.95	-146.9	132.4
Critical pressure (bar)	12.97	33.94	112.8
Standard enthalpy of formation (kJ/mol)	0	0	-46.11

Ammonia plays a major role in fertilizer production. It can be used directly, or more commonly, as a primary raw material in the manufacture of nitrogen-based fertilizers.In addition to its agricultural importance, ammonia is also used as a disinfectant, in the production of explosives, and as a refrigerant. However, the majority of its global use remains in agriculture. Annually, approximately 230 million tonnes of ammonia are produced worldwide, and this number is steadily increasing due to the rapidly growing global population and the corresponding rise in both energy and food demand [4].

III. Green ammonia

In 2021, the green ammonia market was valued at USD 44 million, with a projected CAGR of 127.9% by 2030. This growth is primarily driven by increasing awareness of clean energy production and the need to reduce carbon footprints, which is expected to significantly boost demand in the coming years. Green ammonia is being explored for use as a marine fuel, in the transportation of renewable energy, and in power generation, due to its carbon-free emissions profile [5].

Its production requires green hydrogen, which is most commonly obtained through the following methods:

- Solid oxide electrolysis,
- Proton exchange membrane (PEM) electrolysis,
- Alkaline water electrolysis.

Among these, solid oxide electrolysis is expected to see the most significant growth in the coming period, as it produces green hydrogen using electricity generated from renewable sources. PEM electrolysis is currently the most widely used technology due to its high efficiency (up to 90%), high current density, and low operating voltage. Alkaline electrolysis is a more conventional method and considered the simplest and most cost-effective approach to producing green hydrogen among the three.

IV. Technology Overview

As part of our thesis project, we designed five alternative technologies and evaluated which ones best met economic, equipment-related, and environmental criteria. During the decision-making process, we aimed to stick to widely used, well-known technologies while integrating modern and innovative thinking to explore which established technologies are still worth developing further. Due to the limited length of this essay, the tables used for the comparison are not included.

The annual raw material quantities used in the different processes are detailed in the tables. These figures enabled us to calculate the raw material costs. Apart from electrolysis, the other technologies use natural gas and nitrogen. One advantage of electrolysis is that it does not require natural gas; instead, it uses nitrogen and water as the main feedstocks. To minimize potential expenses, we also considered that the gas exiting the methanation reactor must be dried to remove excess steam that does not participate in further reactions. Since water is required for electrolysis, we analyzed whether the recovered water could partially cover this need. Based on our material balances, the excess water from natural gas decomposition can be reused—after proper purification and potassium hydroxide dosing—to cover part of the water demand of the electrolyzer cell. The amount of water exiting the technology is 1569.2 kg/h, which can be partially reused. The cost analysis reveals that the annual raw material

cost for an electrolyzer cell is the lowest among all the technologies. Another critical factor is the energy performance of the electrolyzer. A cell designed for 100% hydrogen production has a high energy consumption. Currently, there are no known industrial-scale hydrogen production systems based solely on electrolysis that are used for ammonia production. Furthermore, the high energy demand of the electrolyzer presents a major challenge, which leads to additional issues that need to be addressed. Therefore, our group concluded that we should develop a hybrid technology. We based it on the well-established Haber-Bosch process, into which we integrated a water electrolysis unit. We believe this hybrid technology could offer viable solutions to several key questions and, with further research and development, could become a practical option for the future. The electricity required for the cell will be supplied by solar panels. We determined the scale of solar panel deployment based on CO_2 emissions and raw material cost. To find the optimal configuration, we iteratively analyzed the ideal ratio of electrolysis to Haber-Bosch operation. This ratio is shown in Figure 2 below.

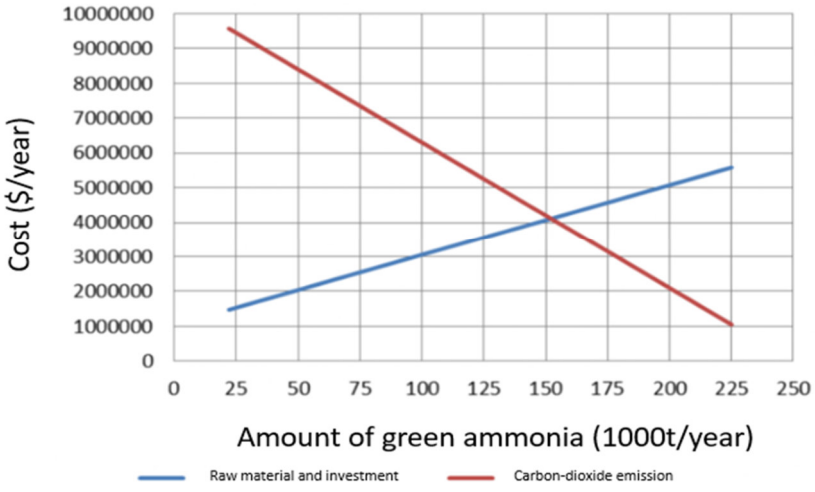

Figure 2: Intigrated technology optimalisation

Using graphical analysis, we determined the point at which the two curves intersect: 61% of the required hydrogen will be produced via electrolysis, and 39% from natural gas reforming.We took into account the European Union's goal of achieving net-zero carbon emissions by 2050 [6]. As a result, CO_2 quota prices will continue to rise. In 2023, the price of emitting one ton of CO_2 was $43. Based on this trend, we calculated the future costs of continuing 100% Haber-Bosch production. According to the material balance, annual CO_2 emissions would be 255,455 t/year. Given the allowable limit of 10,000 t/year, the excess

emissions would incur a cost of $10,505,450 annually.Because CO_2 regulations are expected to tighten and quotas become more expensive, using hydrogen from water electrolysis allows us to reduce emissions and associated costs. The savings from avoided CO_2 costs can be reinvested into solar panels, capital investments, and maintenance. With the chosen ratio, the hybrid plant will produce 152,000 t/year of ammonia via electrolysis and 98,000 t/year using the Haber-Bosch process.Water electrolysis can be powered by renewable energy sources such as solar and wind power, enabling truly green hydrogen production. The electrolyzer's electricity demand would require an area of about 6,500 m^2 for solar panels, operating for approximately 12 hours daily during summer [7]. Based on all these comparison points, we decided on the hybrid green ammonia technology. It is environmentally friendly, its feedstock generation involves significantly lower CO_2 emissions, and the required materials are cheap and sustainably available. Hydrogen produced by electrolysis can be integrated into the Haber-Bosch process, leveraging its lower capital and operational costs. The main drawback of green ammonia technology is its high energy demand. However, since no natural gas is needed, purification steps are eliminated, as water electrolysis provides clean hydrogen.Overall, water electrolysis is a versatile and environmentally friendly method for hydrogen production. It offers numerous industrial and ecological benefits. Advanced technologies and new energy solutions support its proliferation as a key component of clean and sustainable energy systems.

Once we outlined our technology and determined the ratio of green to grey hydrogen production, we proceeded to design the plant's operating units and ran a simulation using Aspen Plus V11 to ensure the process runs smoothly. To carry out this design project, we calculated the mass and energy balances of the technology, sized the operating units, and performed a comprehensive economic analysis to evaluate the cost-effectiveness of the new production process. The figure below shows the completed simulation of our technology. I was in charge of designing the electrolysis cell, including its sizing, operational characteristics, and integration into the overall process.

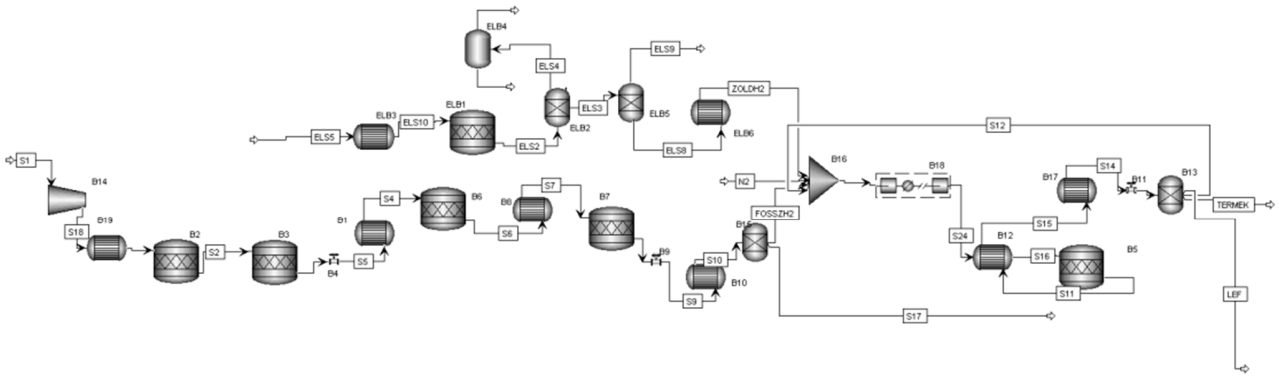

V. Acknowledgment

I would like to express my sincere gratitude to our supervisor, Dr. Norbert Miskolczi, and our consultant, Viktória Zsinka, whose dedicated work and professional guidance were essential to the completion of this thesis. I am deeply thankful for the expertise, support, and valuable advice they shared with us throughout the past year. I would also like to thank my friends and family for their unwavering support during the preparation of this work.

VI. References

[1] The Facts About Ammonia, 2005. The Facts About Ammonia

[2] WORTHINGTON, E. A., DATIN, R. C. and SCHUTZ, D. P., 1952. Physical Properties of Ammonia Solutions. Ammonium Nitrate-Ammonia-Water and Urea-Ammonia-Water. Industrial & Engineering Chemistry, April 1952. Vol.44, no.4, p.910–913. doi:10.1021/ie50508a054.

[3] NIST chemistry WebBook, 2004. Choice Reviews Online [online]. Vol.41, no.12, p.41 Sup:0257. DOI 10.5860/choice.41sup-0257

[4] https://www.statista.com/statistics/1065865/ammonia-production-capacity-globally/

[5] Industry analysis : Green ammonia market report, Grand view research

[6] European Climate Law. Climate Action

[7] Raman, M., & Darcy, M. Solar Panel Calculator

Ultrasound –Assisted Extraction of Phenolic Compounds from Grape Pomace Variety Pinot Noir

Krunoslav Aladić, Klara Opačak

Faculty of Food Technology Osijek, Josip Juraj Strossmayer University of Osijek,

kaladic@ptfos.hr, kopacak@ptfos.hr

Introduction

Pomace is a solid substance that remains after pressing grapes in wine production, making up 75% of the solid waste generated during winemaking and 20-30% of the initial mass of grapes. Pomace consists of 55 - 75% water, 30% polysaccharides and 6-15% lipids, proteins, unsaturated fatty acids and sugars. During wine production, 70% of the total bioactive compounds remain in the pomace, making it a very valuable by-product. Due to the bioactive compounds found in pomace, its further processing and application in the pharmaceutical, food and other industries is increasingly being used in order to maximize the use of by-products and enrich new products with bioactive components (Figure 1).

The primary goal of this work was to investigate the possibility of using the by-products that arise during the production of Pinot noir wine, with a special emphasis on the grape seed and skin. An innovative ultrasound-assisted extraction technique and different extraction conditions (solvent, amplitude and impulse) were applied. The obtained extracts were analysed for the content of total phenols (by Folin-Ciocalteu method), antioxidant activity (by DPPH method) and individual phenols (by HPLC analysis).

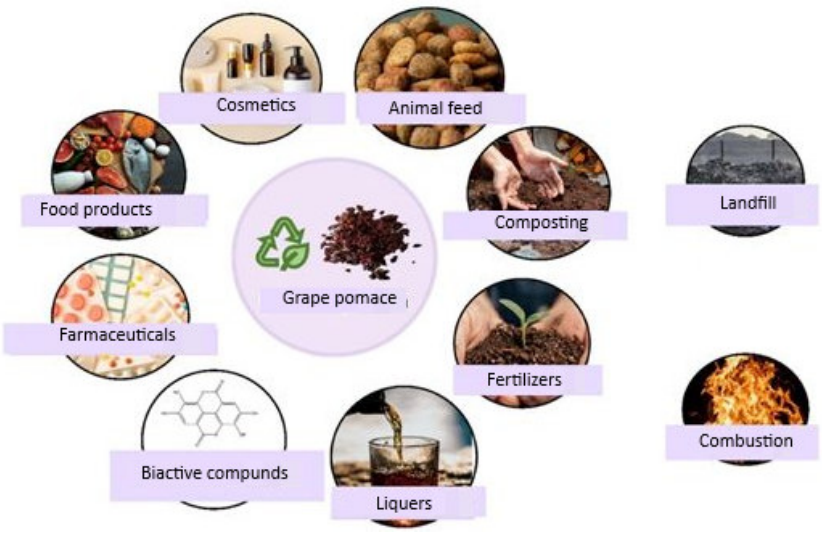

Fig 1. Different possibilities of using grape pomace (Source: Author)

Experimental

The objectives of this work were to perform ultrasonic extraction on samples of seeds and skins of Pinot Noir grapes using sonde (Hielscher Ultrasonicator UP400St), determine how different ultrasonic extraction parameters affect antioxidant activity and phenol content in the obtained extracts, determine antioxidant activity in the obtained extracts, the proportion of total phenols in the obtained extracts, identify and quantify individual phenols using high-performance liquid chromatography (HPLC-DAD) in extracts and optimize the ultrasonic extraction process using the response surface methodology (RSM).

Grape seeds and skins (Figure 2) were subjected to ultrasound-assisted extraction according to the following RSM experiment shown in Table 1.

Fig. 2 Grape skins and grape seeds Pinot noir (Source: Author)

Table 1. Process parameters for ultrasonic extraction

Sample number	Solvent [% EtOH]	Amplitude [%]	Impuls [%]
1	48	60	60
2	48	60	60
3	48	60	60
4	48	20	100
5	48	20	20
6	0	60	100
7	48	60	60
8	48	100	20
9	48	100	100
10	96	100	60
11	0	100	60
12	96	20	60
13	0	20	60
14	96	60	100
15	0	60	20
16	48	60	60
17	96	60	20

The extracts (Figures 3 and 4) were analysed by quantifying their total polyphenolic content (TPC) and antioxidant activity using DPPH method and results are shown in Table 2.

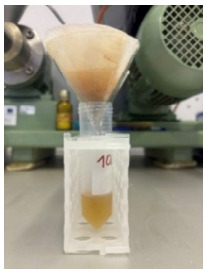

Fig. 3 Grape seed extract

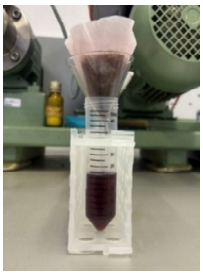

Fig. 4 Grape skin extract

Table 2. Total phenols content and antioxidant activity in grape seeds and skin extracts

Sample number	Solvent [% etOH]	Amplitude [%]	Impuls [%]	GAE [mg/L] Grape seeds	GAE [mg/L] Grape skin	%DPPH Grape seeds	% DPPH Grape skin
1	48	60	60	155.13	50.00	65.89	22.87
2	48	60	60	163.08	46.41	67.02	22.09
3	48	60	60	171.03	52.56	66.71	22.76
4	48	20	100	167.95	55.38	61.01	21.08
5	48	20	20	130.51	44.10	60.11	20.41
6	0	60	100	97.69	41.54	54.45	17.45
7	48	60	60	170.26	49.23	66.24	21.62
8	48	100	20	236.67	57.69	64.17	21.31
9	48	100	100	237.95	60.26	77.83	24.16
10	96	100	60	117.18	50.00	54.33	11.40
11	0	100	60	122.31	46.92	49.77	5.39
12	96	20	60	103.08	49.49	53.63	8.28
13	0	20	60	94.62	36.41	45.94	1.44
14	96	60	100	105.90	46.15	54.80	13.15
15	0	60	20	118.97	44.10	43.91	1.09
16	48	60	60	168.97	46.15	67.10	22.80
17	96	60	20	91.03	23.08	48.32	10.50

Selected graphs shown on Figures 5 and 6 show the influence of amplitude, impuls and solvents on TPC content in grape seeds.

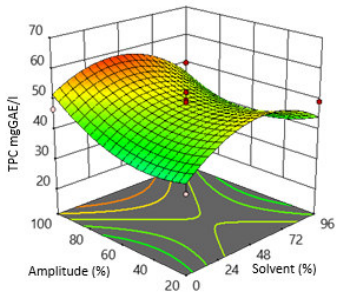

Fig. 5 3D graph of infuence of the amplitude and solvent on the content of TPC in the grape seeds

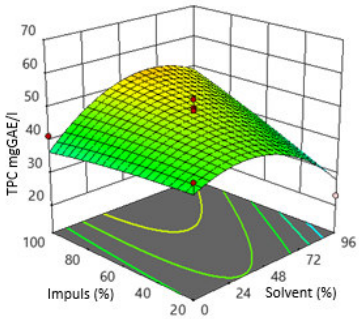

Fig. 6 3D graph of infuence of the impuls and solvent on the content of TPC in the grape seeds

HPLC analysis of grape seed samples revealed 11 compounds (Table 3.). Among the compounds identified in the highest concentrations are: epigallocatechin, catechin and epicatechin. Procyanidin B2 is present in lower concentrations, while sinapic acid and resveratrol are present in the lowest concentrations.

Table 3. Results of HPLC analysis of grape skin extracts according to BBD

RT	6.724	12.40	12.613	12.952	13.780	17.773	24.436	25.512	27.522	29.833	31.503
Sample	Galic acid	Epigalocatechin	Neochlorogenic acid	Catechin	Procyanidine B2	Epicatechin	7- hidroxy coumarine	Procyanidine A2	Sinapic acid	Bensoic acid	Resveratrol
	mg/l	mg/l	mg/l	mg/l	mg/l	mg/l	mg/l	mg/l	mg/l	mg/l	mg/l
1.	11.66	88.98	12.45	439.70	55.94	281.76	3.32	10.94	1.75	1.46	1.60
2.	11.53	91.52	12.77	423.28	54.13	271.66	21.27	9.55	1.80	1.54	1.58
3.	12.21	100.51	14.03	454.71	58.14	290.04	22.98	8.74	1.83	1.50	1.62
4.	12.07	90.76	12.74	419.62	52.59	263.10	27.58	11.75	13.46	2.63	1.80
5.	12.51	104.52	14.70	466.96	59.89	297.67	4.39	8.45	13.53	2.78	1.88
6.	10.83	82.80	12.80	284.59	50.71	180.28	12.99	9.06	0.88	4.05	-
7.	12.77	110.75	15.49	481.21	62.05	307.40	23.61	7.50	1.86	1.55	1.90
8.	13.89	120.09	16.86	530.51	67.11	333.94	123.49	9.16	15.60	2.94	1.94
9.	13.08	113.03	15.86	484.47	61.86	312.59	4.17	10.93	1.99	1.56	1.92
10.	5.26	42.04	1.50	315.52	21.22	174.46	-	11.12	9.22	9.47	1.50
11.	12.23	94.75	13.31	319.10	51.06	214.87	3.06	8.12	0.94	4.49	-
12.	4.04	19.83	1.20	242.22	16.01	130.13	9.66	11.97	0.75	2.17	1.40
13.	10.16	57.06	8.76	157.02	35.86	112.04	-	10.38	15.68	2.75	1.60
14.	5.29	25.61	1.47	308.00	20.89	172.40	-	9.69	0.87	2.85	1.40
15.	10.65	58.63	3.38	166.88	35.73	119.43	1.51	4.56	0.58	2.61	-
16.	12.58	107.01	15.03	464.09	59.14	294.05	111.85	8.92	1.83	1.59	1.61
17.	1.75	-	0.79	163.69	8.59	80.43	3.94	9.55	1.60	-	1.25

Summary

This study is focused on the valorization of waste generated in the wine production industry. The resulting waste represents a major burden on the environment if it is not adequately disposed of. In this way, this waste becomes a high-value raw material for the production of extracts with a high proportion of bioactive components that can be implemented in numerous functional products. Ultrasound-assisted extraction is an innovative technique that enables the isolation of valuable bioactive compounds from grape pomace. This technique improves extraction efficiency, allowing the pomace, rich in antioxidants, polyphenols, fiber and other beneficial components, to be used in the development of new functional products. This could optimize the food production process with maximum waste utilization, which is the goal of the transition from a linear to a circular economy model.

Acknowledgment

Research project of Osijek-Baranja County (Development of new products based on bioactive components obtained from grape seeds) , https://www.croris.hr/projekti/projekt/6867

References

Sušac, K. Ultrasound-assisted extraction of phenolic compounds from grape pomace variety pinot noir. Diploma thesis, University Josip Juraj Strossmayer Osijek, Faculty of Food Technology Osijek, 2024. urn:nbn:hr:109:051206.

https://zir.nsk.hr/islandora/object/ptfos:3007

Development of Antimicrobial Aerogels for Packaging

Gianluca Ricci, Alessandro Zambon

Department of Civil, Chemical, Environmental, and Materials Engineering (DICAM), University of Bologna

gianluca.ricci11@studio.unibo.it, alessandro.zambon2@unibo.it

Introduction

Recently, new forms of antimicrobial emitting materials (AEMs) have been developed, including aerogels that contain volatile components with antimicrobial properties. Aerogels are three-dimensional porous materials that possess exceptional properties such as low density, high specific surface area, and strong absorption capacity [1].

Antimicrobial aerogel materials (AAMs) are typically composed of an organic matrix made from starch and/or cellulose that hosts volatile substances (*e.g.* Essential Oils EOs) with antimicrobial properties. Starch is widely recognized as one of the most preferred biopolymers for food packaging due to its biodegradability, abundance, and renewability.

Several studies have investigated antimicrobial aerogels with volatile compounds like curcumin, hexanal, and thymol for active food packaging, highlighting essential oils as effective natural preservatives due to their ability to diffuse without direct food contact.

The main challenge lies in efficiently incorporating essential oils into the aerogel matrix and optimizing this process to develop high-performance antimicrobial materials. This project aims to analyze current production techniques to identify critical issues and enhance the properties of aerogels, with the goal of developing innovative processes to improve antimicrobial effectiveness and extend the shelf life of food products.

Experimental

The production of aerogels has become increasingly widespread and relatively standardized in recent years, with supercritical CO_2 ($scCO_2$) emerging as a reliable and widely used drying method. Building on this solid foundation, the scientific literature offers numerous production techniques that can be analyzed and compared. This work aims to examine these approaches, identify their strengths and limitations, and draw insights that can help improve current manufacturing processes and enhance the performance of antimicrobial aerogels.

Two key stages significantly influence the properties of antimicrobial aerogel materials (AAMs): the formation of the aerogel matrix and the impregnation of essential oils (EOs). Both phases determine the material's structure and its ability to efficiently release volatile antimicrobial agents.

The preparation of aerogels generally involves three main steps: sol-gel formation, gelation, and drying. Among these, drying plays a crucial role, especially in silica-based aerogels, as it directly affects the final porosity and mechanical integrity of the material.

Several drying methods are available, including ambient pressure drying (APD), freeze-drying (FD), and supercritical drying (SCD). However, APD is typically not recommended. Due to high capillary forces during evaporation, the gel structure tends to collapse, resulting in a dense and less porous material known as a xerogel. Freeze-drying offers an alternative by freezing the liquid within the pores and removing it via sublimation under vacuum. Nonetheless, the formation of ice crystals can damage the internal structure, making the material more fragile and leading to the creation of cryogels.

Supercritical drying with CO_2 presents a more effective solution. It replaces the pore liquid with $scCO_2$, avoiding liquid-vapor interfaces and thus eliminating capillary stresses. This process helps preserve the aerogel’s structure and results in a highly porous material, which is particularly important for loading and gradually releasing volatile substances [2].

Drying speed also affects porosity differently depending on the method used. In traditional methods like APD, fast drying can increase capillary forces and cause pore collapse. Even in FD, rapid sublimation may lead to non-uniform pore formation. In contrast, supercritical drying is less sensitive to drying rate because it avoids phase transitions that generate stress. The pore network remains largely intact even at faster rates. However, if pressure or temperature changes occur too abruptly, structural damage can still happen. For these reasons, $scCO_2$ drying remains the preferred option when producing aerogels that require high porosity for efficient encapsulation and controlled release of volatile compounds.

Volatile compounds can be incorporated into the aerogel matrix through several approaches, the most common being:

- Dry impregnation;
- Antisolvent methods;
- In situ synthesis techniques.

Among these, adsorption from supercritical CO_2 solutions has shown excellent results in terms of controlled release performance [3]. This technique benefits from the high diffusivity of active molecules—such as drugs and essential oils—in $scCO_2$, enabling efficient mass transfer. However, the success of this method largely depends on two key factors: the solubility of the substance in $scCO_2$ and its affinity for the aerogel surface.

When a compound has low or negligible solubility in $scCO_2$, an alternative strategy involves the solvent exchange phase. In this approach, alcogels—hydrogels obtained during gelation—are brought into contact with a solution containing the desired compound. Driven by a concentration gradient, the molecules diffuse into the liquid phase within the alcogel's pores. Once equilibrium is reached, supercritical drying is applied. This final step behaves similarly to a gas antisolvent (GAS) crystallization process, in which $scCO_2$ acts as an antisolvent, precipitating the compound inside the aerogel's pore structure [4].

This antisolvent technique was demonstrated effectively by Haimer et al., who loaded bacterial cellulose aerogels with bioactive compounds such as dexpanthenol and L-ascorbic acid. Importantly, their method does not rely on the chemical nature of the compound, making it versatile and broadly applicable [5].

On the other hand, Saini et al. adopted an in situ method by integrating cinnamon extract into a cellulose matrix during gel formation. This was achieved by dispersing cellulose fibers with charged cellulose nanocrystals, followed by mechanical homogenization and ultrasound treatment before freeze-drying. This process incorporates the active compound directly into the network during gelation, which can significantly influence the microstructure and release behaviour [6].

Similarly, Lehtonen et al. used an in situ approach to embed hexanal into hydrogels composed of galactoglucomannan and cellulose nanofibers. These were emulsified with sunflower oil and chemically cross-linked prior to freeze-drying. The resulting aerogels exhibited prolonged release of hexanal over several weeks, making them particularly suitable for active packaging applications [7].

Unlike supercritical CO_2 loading, which is applied to already-formed aerogels, in situ methods introduce bioactive compounds during gel synthesis. This fundamental difference influences not only the pore architecture but also the functional performance of the final material. Consequently, each method offers unique trade-offs in terms of loading efficiency and controlled release potential.

Table 1 summarize the main three, which have distinct advantages and challenges.

Table 1 : “Summarizing table of loading techniques”

Technique	**Advantages**	**Disadvantages**	**Potential Improvements**	**Reference**
Antisolvent crystallization with $scCO_2$ (post-formation loading)	Versatile; loading efficiency independent of compound’s chemical nature; preserves pore structure	Requires precise control of pressure and temperature; complex process	Optimization of operating parameters to enhance loading efficiency and uniformity	Haimer et al. [5]
In situ loading with extract dispersion and charged cellulose nanocrystals	Direct incorporation of bioactive compounds during gel formation; allows microstructure control	Possible alteration of gel structure; limited maximum loading capacity	Improve stability and uniform distribution of bioactive agents	Saini et al. [6]
In situ emulsification and cross-linking with volatile compounds	Enables sustained and controlled release; suitable for active packaging	Complex process; potential instability of volatile compounds over time	Pore size reduction and refined cross-linking control to prolong release duration	Lehtonen et al. [7]

Haimer et al. [5] utilized an antisolvent crystallization method with supercritical CO_2, which stands out for its post-formation loading approach. This technique is particularly versatile because it does not depend on the chemical nature of the compounds being loaded. Importantly, it preserves the original pore architecture of the aerogel, a critical factor for maintaining the material’s mechanical and functional properties. However, this method requires strict control over processing parameters such as pressure and temperature, which can complicate scale-up and industrial application. Its main strength lies in the ability to load a wide range of bioactives without compromising the aerogel’s microstructure.

In contrast, the in situ loading strategy presented by Saini et al. [6] involves the incorporation of bioactive extracts directly into the gel matrix during its formation. This technique is distinctive in allowing simultaneous control over the microstructure and the distribution of the active compounds within the material. While this can enhance interactions between the matrix and the bioactives—potentially improving functionality—it also risks altering the gel's structural integrity and limits the maximum achievable loading. The peculiarity of this method is its integrative nature, embedding bioactive agents within the forming network, which can tailor material properties but demands careful balance to avoid structural compromises.

Lehtonen et al. [7] advanced this concept further by employing an in-situ emulsification and chemical cross-linking technique to embed volatile compounds like hexanal within polysaccharide hydrogels before freeze-drying. This method is particularly notable for enabling controlled, sustained release of volatile substances, making it highly suitable for active packaging applications. Its complexity arises from the need to maintain stability of the volatile components and manage the cross-linking process, but it offers the distinct advantage of fine-tuning release kinetics through pore size and network density adjustments. This controlled release capability sets it apart from the other methods and directly addresses application-driven requirements for longevity and efficacy.

Summary

The selection of an impregnation technique for aerogels depends mainly on the application and the properties of the compound to be incorporated. Wet impregnation [5] works well for polar molecules, like phenolic compounds, which can be efficiently added during gel formation. However, it's less suitable for hydrophobic substances—such as essential oils—which may require extra steps like freeze-drying to preserve the aerogel's pore structure.

Post-drying impregnation using supercritical CO_2 [8] is ideal for non-polar compounds. It ensures good diffusion into the aerogel without damaging its structure. Still, it demands precise control during depressurization to avoid issues like precipitation or uneven loading.

In situ techniques [6,7] introduce active compounds during gel synthesis. These methods promote strong integration within the matrix and support long-lasting release, but they are more complex and require strict control of the gelation and drying stages to maintain stability.

A more recent alternative is the one-pot method [9], where the loading phase is combined with supercritical drying. By introducing essential oils in a compatible solvent during this step, the method ensures even distribution and better retention. It also reduces solvents and time, showing a promising impregnation efficiency of around 24%. Additionally, merging gelation, retrogradation, and drying may improve both structural and release properties.

Overall, while traditional methods each have their strengths, the one-pot approach offers a more efficient and potentially scalable solution for developing advanced, sustainable aerogel systems.

References

[1] D. Zhao, X. Zhang e Y. Zhang, «Recent advances in the fabrication, characterization and application of starch-based materials for active food packaging: hydrogels and aerogels,» *Sustainable Food Technol.,* vol. 2, pp. 615-634, 2024.

[2] C. García-González, M. Camino-Rey, M. Alnaief, C. Zetzl e I. Smirnova, «Supercritical drying of aerogels using CO 2: Effect of extraction time on the end material textural properties,» *The Journal of Supercritical Fluids,* 2012.

[3] I. Smirnova, J. Mamic e W. Arlt, «Adsorption of drugs on silica aerogels,» *Langmuir,* vol. 19, p. 8521, 2003.

[4] A. Weber, L. Yelash e T. Kraska, «Effect of the phase behaviour of the solvent-antisolvent systems on the gas-antisolvent-crystallisation of paracetamol,» *J. Supercrit. Fluids,* vol. 33, pp. 107-113, 2005.

[5] E. Haimer, M. Wendland, K. Schlufter, K. Frankenfeld, P. Miethe, A. Potthast, T. Rosenau e F. Liebner, «Loading of bacterial cellulose aerogels with bioactive compounds by antisolvent precipitation with supercritical carbon dioxide,» *Macromol. Symp.,* vol. 2, n. 294, pp. 64-74, 2010.

[6] A. Saini, Y. Chandravati e K. S. SethiBai-Liang, «Microdesigned Nanocellulose-Based Flexible Antibacterial Aerogel Architectures Impregnated with Bioactive Cinnamomum cassia,» *ACS Applied Materials & Interfaces,* vol. 13, n. 4, 2001.

[7] M. Lehtonen, S. Kekäläinen e I. Nikkilä, «Active food packaging through controlled in situ production and release of hexanal,» *Food Chemistry,* vol. 331, 2020.

[8] L. Manzocco, K. S.Mikkonen e C. A. García-González, «Aerogels as porous structures for food applications: Smart ingredients and novel packaging materials,» *Food Structure,* 2021.

[9] Y. Zhang, L. Gong e X. Xu, «Synthesis of carbon aerogels with controlled morphology and pore structure to modulate their bulk density and thermal conductivity via a quick one-pot preparation strategy,» *Carbon,* 2024.

Supercritical CO_2 Extraction from Bilberry Fruit

Jelena Martinović, Marko Stamenić

Department of Organic Chemical Technology, Faculty of Technology and Metallurgy, University of Belgrade, E-mail: 20243040@estudent.tmf.bg.ac.rs

Introduction

Bilberry (*Vaccinium myrtillus*) is a berry shrub belonging to the *Vaccinium g*enus. Like many other plants, berries have been consumed by people and used in traditional medicine for centuries or, perhaps, millenniums. Nowadays, with increasing interest in natural products for various applications, the positive effects of various berries on human health have been proved scientifically [1]. The constituents of berry fruits identified as main contributors to these positive effects are polyphenols, specifically anthocyanins [2, 3]. Among all *Vaccinium* species, bilberry was found to have the highest amount of phenolic compounds, including anthocyanins [4, 5].

One of the techniques for extraction of these valuable components from plant matrices is the supercritical fluid extraction (SFE), which implies using a supercritical fluid as a solvent. At supercritical state, i.e. at pressure and temperature above the critical values of these parameters, fluids possess a combination of liquid-like and gas-like properties which makes them suitable as solvents in the process of SFE. For example, the density of SCFs is relatively high, similar to liquid density, making them suitable solvents, while on the other hand, SCFs viscosity is comparable with viscosity of gases, so they can easily diffuse through solid matrices. In scientific and industrial practice supercritical carbon dioxide (SC CO_2) is predominantly used in the SFE process. It is a non-toxic, non-flammable and inexpensive compound with relatively low values of critical parameters (T_c = 31.1°C; P_c = 73.8 bar) which enable extraction at low temperatures, preventing thermo-degradation of heat-sensitive components. Moreover, by simple decompression at the end of the process, it is possible to obtain products without the traces of the solvent, which is favourable compared to the conventional solvent extraction [6].

In this work, the SFE form bilberry fruits is investigated. Several sets of process conditions are applied in order to examine the influence of some of the process parameters on the kinetics, total yield, antioxidant capability and composition of the extract.

Experimental

Experiments were conducted with bilberry seeds which were dried and ground in a coffee mill for 30 s before the extraction process. The material (20±0.1 g) was mixed with glass beads and placed into the stainless-steel tube, which was put in the extractor. . Extractions with SC CO_2 were performed in apparatus shown in Figure 1.

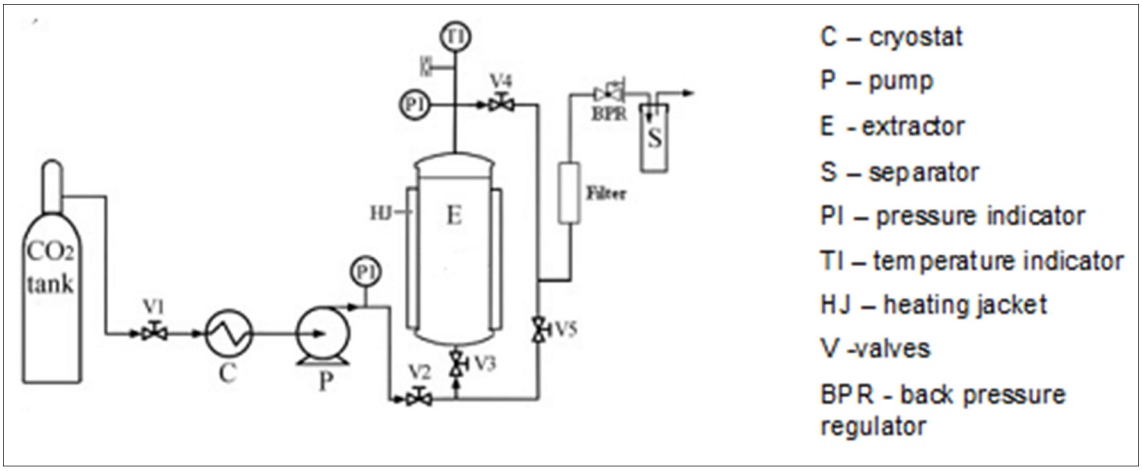

Fig. 1. Schematic of the apparatus for SFE used in experiments.

The temperature in all experiments was 70°C, while pressures of 15 and 30 MPa were applied. Additionally, every set of experimental conditions was replicated with the addition of ethanol as a cosolvent in the amount of 20wt%. Thus, a total of four sets of experimental conditions was analysed.

The influence of pressure on the rate and total yield of the SFE from bilberry fuit is depicted in Figure 2.

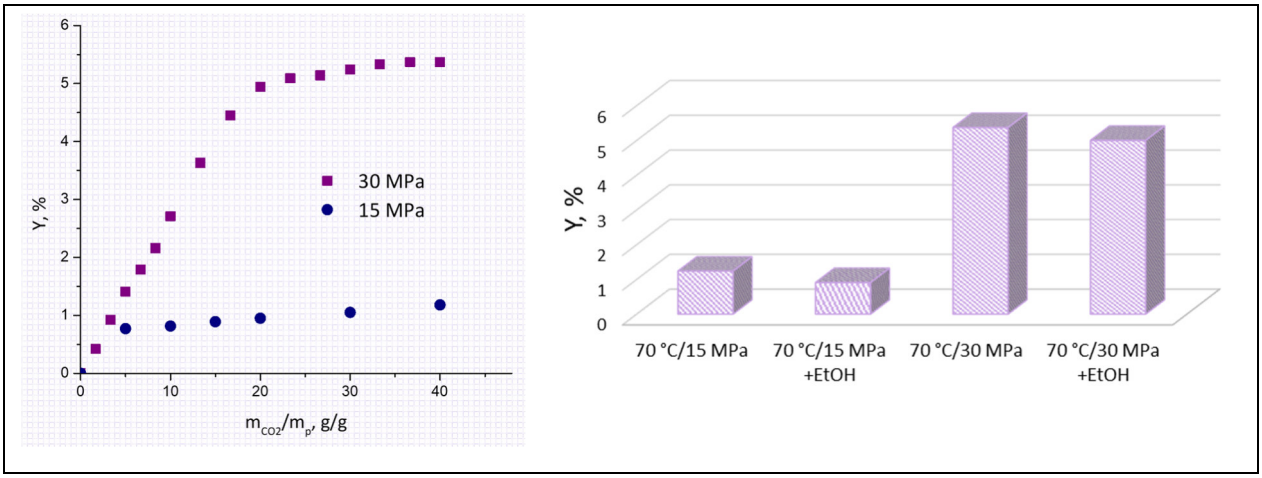

Fig.2. Results of the SFE from bilberry fruit: kinetics at different pressures (left), and the influence of pressure and cosolvent on the total yield (right).

As can be seen, increase in pressure led to the significant increase in total yield obtained in experiments. Specifically, at 15 MPa the yield was 1.24%, while at 30 MPa it was 5.37%, which is an almost 400% increase. This behaviour is actually expected as higher pressures imply higher densities, which leads to higher dissolving power of the SCF. On the other hand, the addition of ethanol as cosolvent did not positively affect the total yield of the SFE. Moreover, the influence was somewhat negative, as for both pressures applied a slight decrease in total yield was observed. This result implies that the extract is composed mainly of non-polar components, as the addition of polar ethanol is expected to positively affect the SFE of polar compounds.

The obtained extracts were further subjected to chemical analysis, in order to determine the total phenolic content (TPC) and composition. The results of these analyses are shown in Figure 3 and Table 1, respectively.

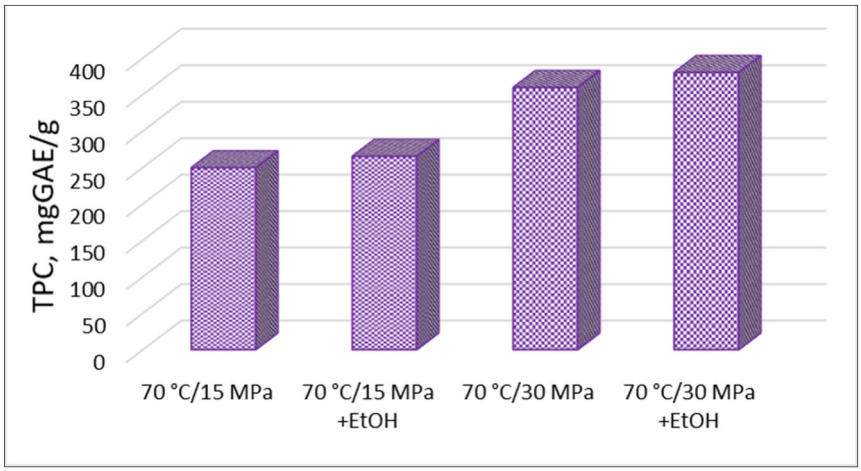

Fig. 3. Total phenolic content in obtained extracts of bilberry fruit.

From Figure 3 can be seen that an increase in pressure led to an increase in TPC values regardless of the addition of ethanol as cosolvent. Furthermore, the addition of cosolvent slightly increased the TPC values for both pressures applied.

HPLC analysis showed that the major constituent in all extracts was Procyanidin B1, a flavonoid belonging to the class of proanthocyanidins which was proven to have antioxidant, antibacterial, anti-inflammatory, antineoplastic and anti-allergic properties, among others [7].

Tab. 1.: Results of HPLC analyses of bilberry fruit extracts .

Name	70 °C/15 MPa	70 °C/15 MPa + EtOH	70 °C/30 MPa	70 °C/30 MPa + EtOH
		mg/g extract		
Gallic acid	0.020	0.062	0.018	0.100
Procyanidin B1	22.167	37.745	9.796	27.402
p-hydroxybenzoic acid	0.086	0.390	0.039	1.283
Vanillic acid	0.0200	0.062	0.014	0.092
Syringic acid	0.017	0.042	0.014	0.099
Procyanidin A2	/	0.702	/	/
trans-cinnamic acid	/	0.017	/	0.009
Hinokiflavone, di-apigenin	0.376	0.430	0.527	0.137

Summary

In this work the results of supercritical fluid extractions from bilberry fruit at different process conditions, as well as the analysis of the obtained extracts, are presented. Obtained results show that pressure drastically influence the total extraction yield - at 30 MPa the yield was 5.37%, while at 15 MPa it was only 1.24%. The addition of ethanol as cosolvent reduced the yield, but in a practically insignificant amount. On the other hand, ethanol positively influenced the extract properties, as TPC was slightly higher, and Procyanidin content was significantly higher in samples obtained with ethanol as cosolvent.

References

[1] Seeram, N. P. (2008). Berry Fruits: Compositional Elements, Biochemical Activities, and the Impact of Their Intake on Human Health, Performance, and Disease. *Journal of Agricultural and Food Chemistry*, *56*(3), 627–629. https://doi.org/10.1021/jf071988k

[2] Seeram, N. P. (2008). Berry Fruits for Cancer Prevention: Current Status and Future Prospects. *Journal of Agricultural and Food Chemistry*, *56*(3), 630–635. https://doi.org/10.1021/jf072504n

[3] Olsson, M. E., Gustavsson, K.-E., Andersson, S., Nilsson, Å., & Duan, R.-D. (2004). Inhibition of Cancer Cell Proliferation in Vitro by Fruit and Berry Extracts and Correlations with Antioxidant Levels. *Journal of Agricultural and Food Chemistry*, *52*(24), 7264–7271. https://doi.org/10.1021/jf030479p

[4] Giovanelli, G., & Buratti, S. (2009). Comparison of polyphenolic composition and antioxidant activity of wild Italian blueberries and some cultivated varieties. *Food Chemistry*, *112*(4), 903–908. https://doi.org/https://doi.org/10.1016/j.foodchem.2008.06.066

[5] Määttä-Riihinen, K. R., Kamal-Eldin, A., Mattila, P. H., González-Paramás, A. M., & Törrönen, R. (2004). Distribution and contents of phenolic compounds in eighteen scandinavian berry species. *Journal of Agricultural and Food Chemistry*, *52*(14), 4477–4486. https://doi.org/10.1021/jf049595y

[6] Reverchon, E., & de Marco, I. (2006). Supercritical fluid extraction and fractionation of natural matter. *The Journal of Supercritical Fluids*, *38*(2), 146–166. https://doi.org/https://doi.org/10.1016/j.supflu.2006.03.020

[7] Chen, H., Wang, W., Yu, S., Wang, H., Tian, Z., & Zhu, S. (2022). Procyanidins and Their Therapeutic Potential against Oral Diseases. *Molecules (Basel, Switzerland)*, *27*(9), 2932. https://doi.org/10.3390/molecules27092932

Fundamentals of Ammonothermal Growth of Nitride Crystals – Dissolution, Transport and Crystallization

V Y M Rajesh Chirala*, Saskia Schimmel

Chair of Electron Devices (LEB)

Friedrich-Alexander-Universität Erlangen-Nürnberg, Germany

*rajesh.chirala@fau.de

Introduction

The ammonothermal method is a solution-based crystal growth technique, analogous to the hydrothermal method but using supercritical ammonia (NH_3) instead of water as the solvent [1]. This method operates at moderate temperatures (400–900 °C) and is usually conducted at pressures between 100 and 300 MPa [2].

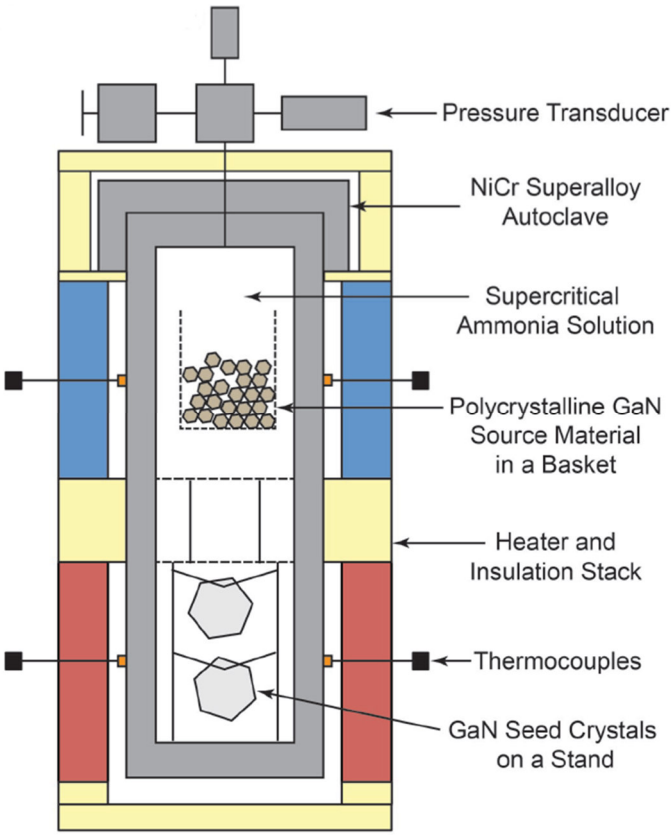

Fig. 1.: Schematic vertical cross-section of an ammonothermal autoclave inside a furnace for bulk GaN crystal growth illustrating key internal and external components. Reproduced from [3] with the permission from © 2017 WILEY-VCH Verlag GmbH & Co. KGaA, Weinheim

Material precursors are dissolved in supercritical ammonia, usually with mineralizers to enhance solubility. By manipulating temperature, pressure, or solvent removal, the solution is brought to a saturated or supersaturated state, prompting the formation of nitride crystals either spontaneously (nucleation) or on a seed crystal (as shown in Fig. 1) [4,5]. Specialized autoclaves are used to maintain the necessary temperature and pressure conditions, with careful control to avoid contamination and maintaining purity. Achieving high chemical purity and low point defect concentrations remains a technical challenge.There is also a need for pressures of few hundreds of MPa and oxygen-free environments, along with precise control over growth conditions, which complicates large-scale adoption [4,6].

Key features of the ammonothermal method include:

- High structural quality
- Self-nucleation and seed expansion
- Bypassing melt-growth limitations

This is largely due to the near-equilibrium nature of the process, which allows defects to be minimized during growth, resulting in crystals with superior mechanical and electronic properties compared to those produced by many alternative methods [4]. For example, threading dislocation densities as low as 10^2 - 10^4 cm^{-2} have been reported for ammonothermal GaN, which is critical for high-performance electronic and optoelectronic applications [6].

The process can start with either spontaneous nucleation (self-nucleation) or with a pre-existing seed crystal, allowing for the controlled enlargement of seed crystals over multiple growth runs [4,7]. This approach enables lateral and vertical expansion of the crystal, improving ideally both size and quality with each cycle. Seeded growth is particularly advantageous for producing large, high-quality crystals, as demonstrated by the successful enlargement of 2-inch-diameter GaN crystals using the acidic ammonothermal method [7].

This method circumvents the fundamental limitations of melt-growth techniques, which are often unsuitable for materials like nitrides due to their high decomposition temperatures and instability in the melt phase [4,8].

Instead, the ammonothermal process dissolves the source material in supercritical ammonia under high pressure and moderate temperature, enabling crystal growth from solution rather than melt [4]. This not only allows for the synthesis of materials that are difficult or impossible to grow from the melt, but also can provide greater control over impurity incorporation, defect formation, and overall crystal quality [9].

Experimental

Ammonothermal reactors are engineered to safely contain extremely high pressures (up to ~500 MPa) and temperatures (up to 600 °C or higher) while resisting corrosion in basic or acidic ammonia-rich environments. To meet these demands, load-bearing components are typically fabricated from nickel-based superalloys such as Inconel 718 and Rene 41, which offer a balance of high mechanical strength, creep resistance, and corrosion protection [10]. Molybdenum-based alloys are also used in some cases [11]. Inconel 718 is favored for its superior corrosion resistance and weldability, while Rene 41 excels in high-temperature strength and creep resistance, making it suitable for the most demanding thermal and mechanical conditions [12].

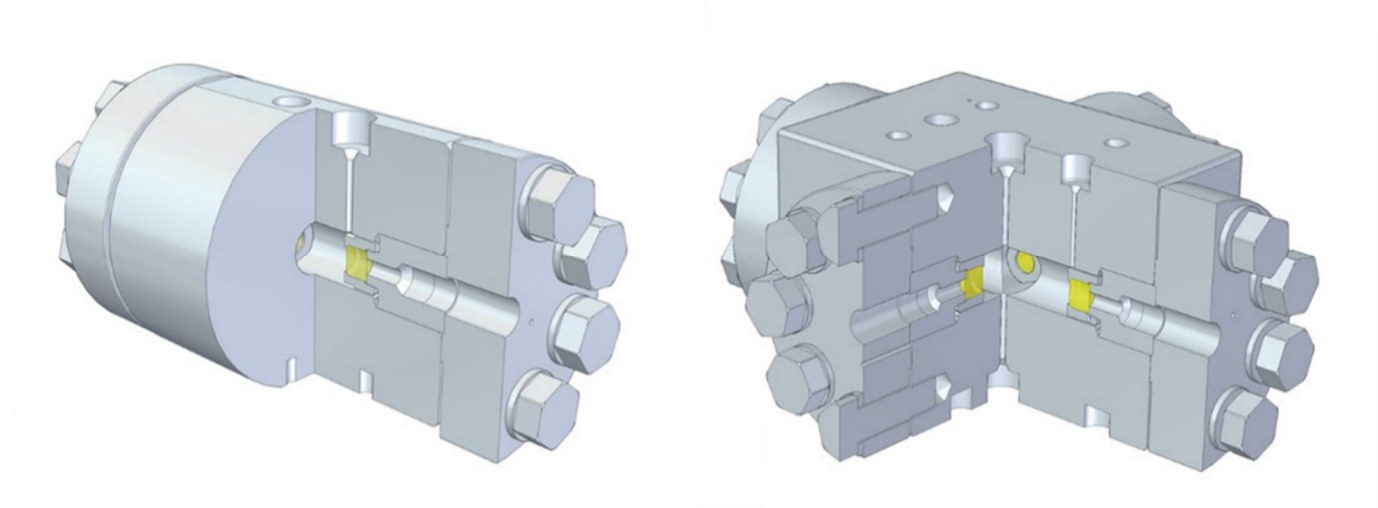

Fig. 2.: Visualization of the **(a)** uniaxial optical cell, (**b**) biaxial optical cell [14]

Reactor designs usually feature long, thin-walled tubular geometries to simplify manufacturing and enable controlled thermal gradients for crystal growth. More advanced designs now incorporate specialized optical cells in two variants such as uniaxial and biaxial (as shown in Fig. 2) with transparent and chemically stable window materials, such as sapphire and boron carbide to facilitate in situ optical and X-ray monitoring. These cells

may be configured horizontally (to suppress convection) or vertically (to enhance it), directly influencing fluid dynamics and temperature profiles.

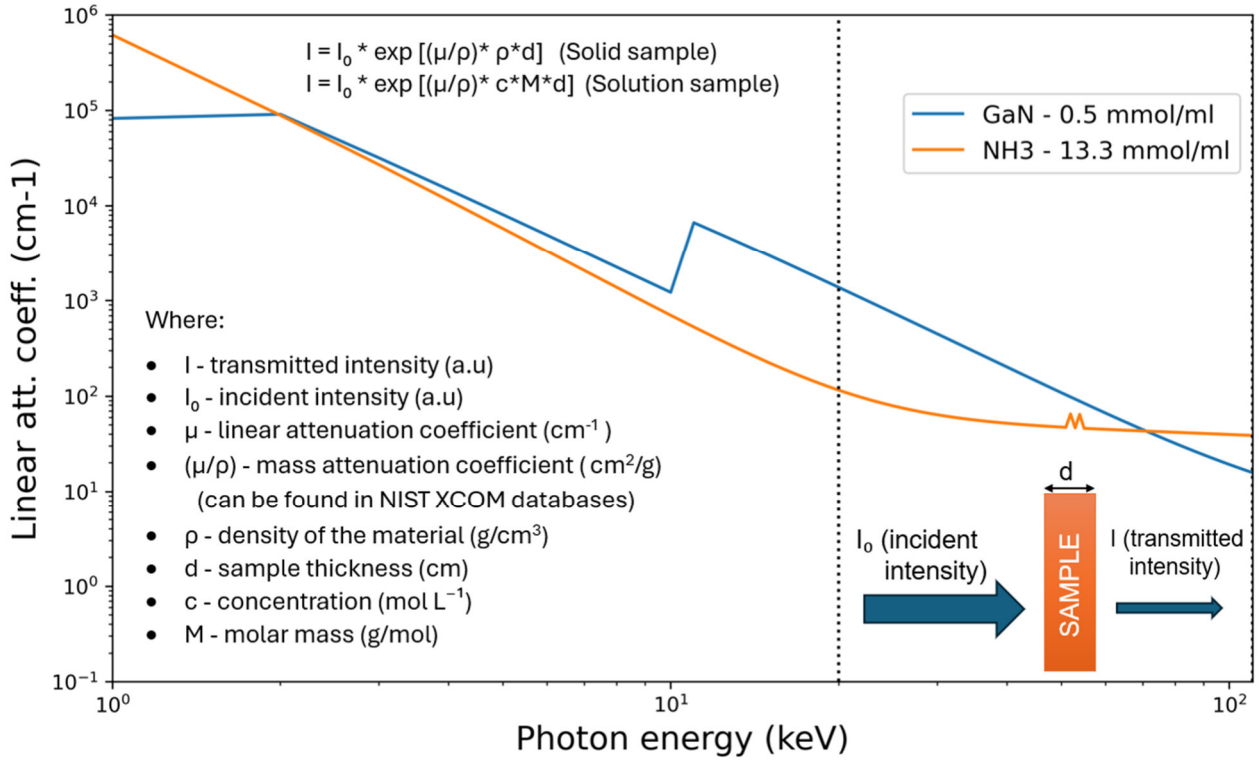

Fig. 3.: Linear attenuation coefficients (cm^{-1}) of GaN and supercritical ammonia (calculated using NIST XCOM database) plotted against photon energies (keV) showing distinctions in determining contrast in the range of photon energies used (20-110 KeV)

X-ray imaging is a powerful in situ technique for monitoring dissolution and growth in ammonothermal synthesis, especially for materials like GaN. X-rays provide clear contrast even in fluid phases based on differences in linear attenuation coefficients as illustrated in Fig. 3. This enables precise measurement of crystal growth kinetics and solubility, even in the presence of solutes. Window materials with low density and composed of light elements, such as sapphire and boron carbide, are preferred to minimize X-ray absorption, though their chemical and mechanical stability must be ensured. Diamond is ideal for chemical stability but is limited by cost and availability in suitable thicknesses [14].

Initial innovations include direct measurement of fluid X-ray absorption to determine solubility, eliminating errors from crystallization outside the field of view [15]. Enhanced X-ray setups with improved detectors can deliver better time and spatial resolution, which is

critical for capturing subtle changes in solubility and intermediate species formation apart from the possibility of detecting lighter elements in the reaction medium.

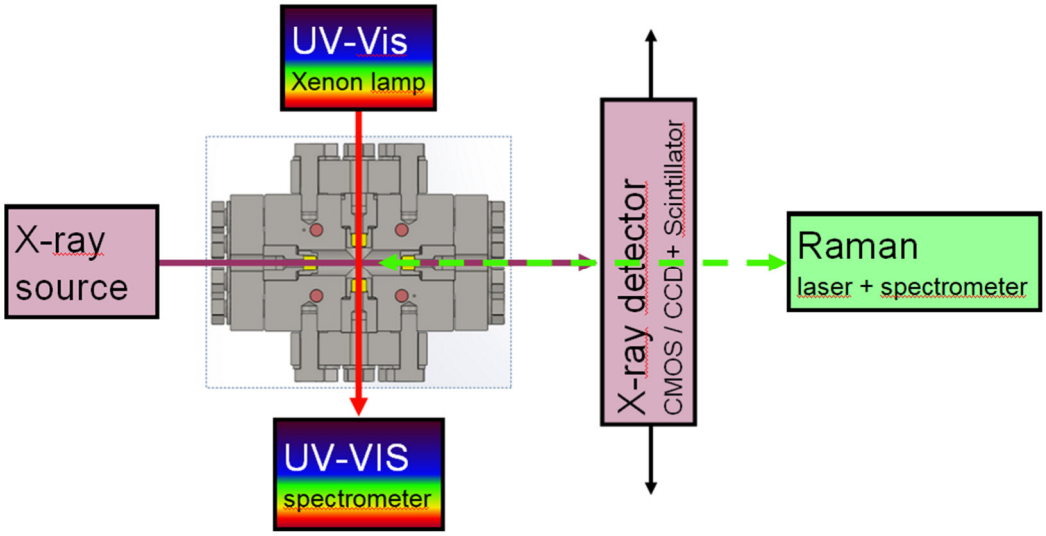

Fig. 4.: Schematic horizontal cross section showing in situ monitoring setup with devices for complementary measurement techniques to understand ammonothermal growth using a biaxial optical cell

Simultaneous or quasi-simultaneous optical (Raman, UV-Vis) and X-ray measurements, as conceptualized in Fig. 4 are also enabled by these advanced optical cells. Biaxial cell designs allow fully simultaneous transmission measurements, while uniaxial cells can accommodate Raman spectroscopy in backscattering geometry alongside X-ray imaging by alternating detector positions. This multi-modal approach provides comprehensive insight into the system, e.g. in the form of dimensional changes of the crystal as seen in 2D X-ray absorption imaging and characteristic vibrational frequencies of involved solvent and solutes indicating the presence of certain chemical species under the actual process conditions [4].

Summary

In situ monitoring with these advanced optical cells has the potential to transform ammonothermal crystal growth by providing real-time data on solubility, phase transitions, and the formation intermediate species.

The integration of X-ray and optical techniques allows researchers to:

- Directly observe and quantify dissolution and growth processes, supporting estimation of crystal size and volume changes over time.

- Characterize intermediate species and dynamic processes, informing the development of new materials and growth strategies.

These advances are not only supposed to deepen the fundamental understanding of ammonothermal processes but also are expected to pave way for practical improvements in crystal quality, process scalability, and the development of new nitride materials for electronic and optoelectronic applications.

Acknowledgment

This research is funded via the Emmy Noether Programme in the junior research group of Dr.-Ing. Saskia Schimmel by the Deutsche Forschungsgemeinschaft (DFG, German Research Foundation) under grant number 512083685. We are thankful for the funding provided by “Erasmus+ Staff mobility for training” program, which makes participation in ERASMUS+ BIP ESS-HPT 2025 possible.

References

[1] R. Dwilinski et al., Acta Phys. Pol. A **1995**, 88, 833-836

[2] D. Ehrentraut et al., J. Cryst. Growth **2008**, 310, 3902–3906

[3] S. Suihkonen et al., Adv. Electron. Mater. **2017**, 3, 1600496

[4] T. Wostatek et al., Materials **2024**, 17, 3104

[5] T. Richter et al., Inorganics **2014**, 2, 29–78

[6] S. Pimputkar et al ., Crystals **2023**, 13, 1004.

[7] K. Kurimoto et al., Appl. Phys. Express **2022**, 15, 055504.

[8] K. Grabianska et al., J.Cryst. Growth **2020**, 547, 125804

[9] A. Yoshikawa et al. J. Cryst. Growth **2004**, 260, 67–72

[10] S. Pimputkar et al. J. Supercrit. Fluids **2016**, 110, 193–229

[11] S. Pimputkar et al., J. Cryst. Growth **2016**, 456, 15–20

[12] S. Schimmel et al., Materials **2022**, 15(17), 6165

[13] S. Schimmel, Dissertation, FAU Erlangen-Nürnberg (**2018**)

[14] S. Schimmel et al., J. Cryst. Growth **2016**, 456, 33–42

[15] S. Schimmel et al., J. Cryst. Growth **2015**, 418, 64–69

Bioadhesives Production through Hydrothermal Treatment of Products with Suberin

Antonio Antón Rodríguez

BioEcouva, University of Valladolid, bailonan26@gmail.com

The most common adhesives include epoxies (strong and durable), polyurethanes (flexible and versatile), acrylics (fast-curing), cyanoacrylates (super glue) and phenol-formaldehyde (chemical stability and mechanical strength).

The importance of replacing different fossil-based feedstocks for structural adhesives synthesis is increasing, due to the high contaminant and health issues power attributed to them.

A good adhesive must have two main characteristics, strong adhesion (bonding to the substrate) and high cohesion (internal strength). Adhesion depends on surface energy, wetting ability, and compatibility with the material. Cohesion relies on the adhesive's molecular structure and mechanical integrity. Curing time is also an important factor to take into consideration.

Phenol-formaldehyde resins (PF) where selected as the most suitable ones to be replaced with the existing technology. These resins are widely used in the structural adhesion of wood structures, especially in furniture, whose requirements are good mechanical, thermal and moisture resistance, all of which are included in the mentioned composite.

The base for a PF resin is the use of a principal monomer consisting mainly on aromatic molecules like phenol and a cross-linker/binder agent similar to formaldehyde. When phenol reacts with formaldehyde under acidic or basic conditions, it forms methylene and ether bridges, creating a highly cross-linked, three-dimensional network, which requires high curing temperatures before application. Both types of phenol-formaldehyde resins are Novolac and Resol, whose main differences are the molar excess of formaldehyde for Resols and of phenol for Novolacs, in addition to the requirement of a hardener like hexamethylenetetramine for Novolacs (Fareez et al., 2021).

The idea is to look for a replacement of phenolic compounds without compromising the reactive nature of the formaldehyde with alcohol groups in the principal monomer. This objective is to obtain enough aromatics by hydrothermal depolymerization of the lignin contained by the cork, in addition, the use of suberin sub-products like carboxylic acids might function as partial binders. Using cork is a good idea because of the great cork

production of countries like Spain and Portugal, which together share the 78% of world production in this area, resulting in 146 million metric tons out of a 187 million metric tons industry (Mata & Dos-Santos, 2024). Suberin is the polymer in charge of confering hydrophobic properties to the cork whose structure is represented in Figure 1. The reason of the hydrophobic characteristic is the large apolar alquile chains of this compound (LAZAR, 2003).

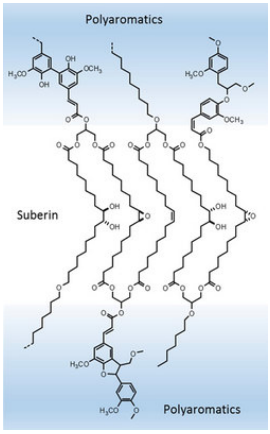

Figure 1. Suberin structure

The first step is pumping to pressurize the biomass mixed with water at 5%. The objective is to achieve cork biomass around the micron size. After this step, two different reactions where done in a plug-flow reactor: one with the addition of a strong base like NaOH to the hydrolyzed and another one with natural pH. The conditions in the reactor where of 380ºC and 250bar in both cases, reaching supercritical water conditions in the reactor. The hydrolyzed was then centrifuged for separation of the soluble from the non-soluble composites in the product. The results showed a higher depolymerization efficiency of the lignin and suberinic compounds when using high pH. This can be seen in Table 1, where the acid number of the product tend to increase as base concentration and time does (Rizhikovs et al., 2022).

It is well-known the reactive capacity of formaldehyde, due to its small size and exposed carbonyl group, which makes it the best bonding agent possible. What is more, the phenols used in the fossil-based adhesive is also an optimized reactant with the maximum efficiency possible. This is the reason why replacing the 100% of both of them looks challenging and why it was decided to create a mix between the non-renewable phenolic source and the less-reactant cork-based aromatics. The commercial formaldehyde solution is diluted down to 37% and the option of stabilizing it with methanol is very

common, however, for this investigation, the most reactive one was considered to be the best option.

Table 1. Properties of the SA-based adhesive depending on the depolymerization conditions.

KOH (%)	pH	Time (h)	Acid NR (mg KOH·g^{-1})
2	1	0,5	26,7±0,6
4	1	0,5	58,4±0,4
2	3	0,5	19,2±0,3
4	3	0,5	41,5±0,4
2	1	1,5	38,1±0,6
4	1	1,5	83,4±0,7
2	3	1,5	30,7±0,4
4	3	1,5	68,3±0,3
3	2	1,0	48,0±1,4

Different proportion reactions have been carried out and are shown in Table 2, with the reminder that the goal is to maximize the use of bio-based reactants, without compromising the desired crosslinking between monomers by replacing the high-reactive compounds:

Table 2. Formula optimization experiments varying proportions of reactants

Formula	Phenol	Formaldehyde	Centrifuged byproduct
1	60%	40%	0%
2	45%	30%	25%
3	36%	24%	40%
4	30%	20%	50%

Different analysis have been carried out for characterization and quantification, such as TGA, DCS, HPLC, GC.

For application specially in plywood of this type of adhesives, it is compulsory to apply temperatures up to 248ºC and 6.55 min. In addition, different additives are useful specially for maintaining cohesion properties and cheapening the process (Less adhesive is required). The most common method is replacing 80% of the adhesive with dust coming from the feedstock biomass, in this case cork dust. (Makars et al., 2022)

Summary

Bioadhesives are in constant evolution, searching for eco- and health- friendliness formulations that replace the existing ones.

Using cork as a initial biomass for hydrothermal treatment with supercritical water has proved to be a feasible alternative. Addying basic reactants like NaOH to the reactor enhances suberin depolymerization, which is crucial for obtaining a good interaction with the bonding agent.

References

Fareez, I. M., Jasni, A. H., & Norrrahim, M. N. F. (2021). Nanofibrillated Cellulose Based Bio-phenolic Composites. In *Phenolic Polymers Based Composite Materials* (pp. 139–151). Springer Singapore. https://doi.org/10.1007/978-981-15-8932-4_9

LAZAR, T. (2003). Taiz, L. and Zeiger, E. Plant physiology. 3rd edn. *Annals of Botany*, *91*(6), 750–751. https://doi.org/10.1093/aob/mcg079

Makars, R., Rizikovs, J., Godina, D., Paze, A., & Merijs-Meri, R. (2022). Utilization of Suberinic Acids Containing Residue as an Adhesive for Particle Boards. *Polymers*, *14*(11). https://doi.org/10.3390/polym14112304

Mata, F., & Dos-Santos, M. (2024). Modeling Cork Yield, Thickness, Price, and Gross Income in the Portuguese Cork Oak Montado. *Forests*, *15*(12). https://doi.org/10.3390/f15122163

Rizhikovs, J., Brazdausks, P., Paze, A., Tupciauskas, R., Grinins, J., Puke, M., Plavniece, A., Andzs, M., Godina, D., & Makars, R. (2022). Characterization of suberinic acids from birch outer bark as bio-based adhesive in wood composites. *International Journal of Adhesion and Adhesives*, *112*. https://doi.org/10.1016/j.ijadhadh.2021.102989

Investigation of 3D-printed Stirrers in a Model of a High-Pressure Autoclave

Christopher Schilling, Kristina Zentel*

Ernst-Berl-Institute of Technical and Macromolecular Chemistry, Technical University of Darmstadt, 64287 Darmstadt/Germany, *e-mail: kristina.zentel@pre.tu-darmstadt.de

Introduction

Emulsion polymerization is a polymerization process, where the liquid monomer is usually dispersed in water, and the polymerization occurs in confined particles in the nanometer scale, often stabilized by surfactants. Exceptionally effective heat dissipation as well as the non-toxic solvent drastically increase the safety of this process compared to polymerization in bulk or in organic solvents. The resulting polymer nanoparticle dispersions can be directly used, for example as coatings, paints or adhesives.[1] Usually, liquid monomers are employed in this type of polymerization, but also gaseous monomers like ethene can be polymerized this way.[2] Sufficient mixing has to be present, to achieve a uniform distribution of the added liquid monomer or initiator during a semi-batch process, in order to achieve defined growth of the polymer particles.[3] In addition, a gaseous monomer has to have a maximized interface area with the aqueous phase, to ensure a rapid diffusion into the water and to avoid having a mass transport limitation, which reduces to possible rate of polymerization.[4] For this purpose, a polymethyl methacrylate (PMMA) model of a high-pressure steel autoclave has been manufactured, to mimic the inner dimensions of the reactor, which is used in the polymerization mini-plant. Multiple types of stirrers were created with CAD software and were 3D-printed, to investigate their suitability for the use in emulsion polymerizations with and without gaseous monomers.

Experimental

The reactor in which the polymerizations are carried out, is a high-pressure steel autoclave from *Büchi*. The vessel has an inner volume of 0.56 l, with a diameter of 84 mm and a height of 105 mm. The system can be operated up to a pressure of 300 bar and a temperature of 250°C. The inner dimensions of the vessel were measured and implemented as a model in the CAD software *Autodesk Inventor Professional 2024*. A PMMA model has been manufactured by the mechanical workshop of the TU Darmstadt, which was used for the stirrer investigations (Fig. 1.).

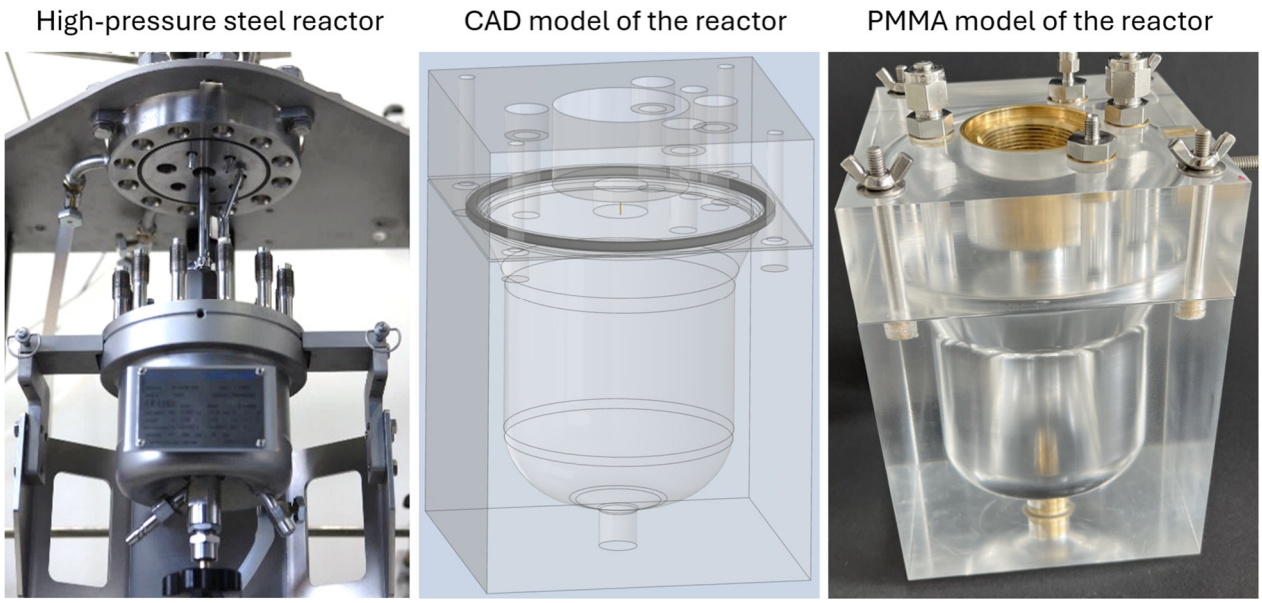

Fig. 1.: The high-pressure steel reactor, the derived CAD model of the reactor and the manufactured PMMA model.

The different stirrer types, which were used in the mixing-time investigations were designed in the CAD program and 3D-printed via stereolithography. All the designed stirrers, their abbreviations and diameters are summarized in Tab. 1.

Tab. 1.: Descriptions, abbreviations and diameters of the stirrers used for investigations.

Stirrer	Short	Diameter /mm
impeller	Imp	40
propeller	P	53
propeller – wide base	PW	53
pitched blade small	PBS	34,5
pitched blade large	PBL	74
pitched blade 30°	PB30	45
pitched blade 45°	PB45	44
pitched blade – 6 blades	6PB	43
flat blade turbine	FB	35

The two stirrers, Imp and PBS were stirrers supplied by the reactor manufacturer. The stirrers PBL, PB30 and PB45 are pitched blade stirrers, which exist as steel variants for the reactor and have also been used for reactions in the past. 6PB is a pitched blade stirrer with 6 smaller blades at 45° blade angle. P and PW are propeller stirrers, where

PW has a wider base. FB is a Rushton turbine like flat blade stirrer. The stirrers are depicted in Fig. 1Fig. 2 below.

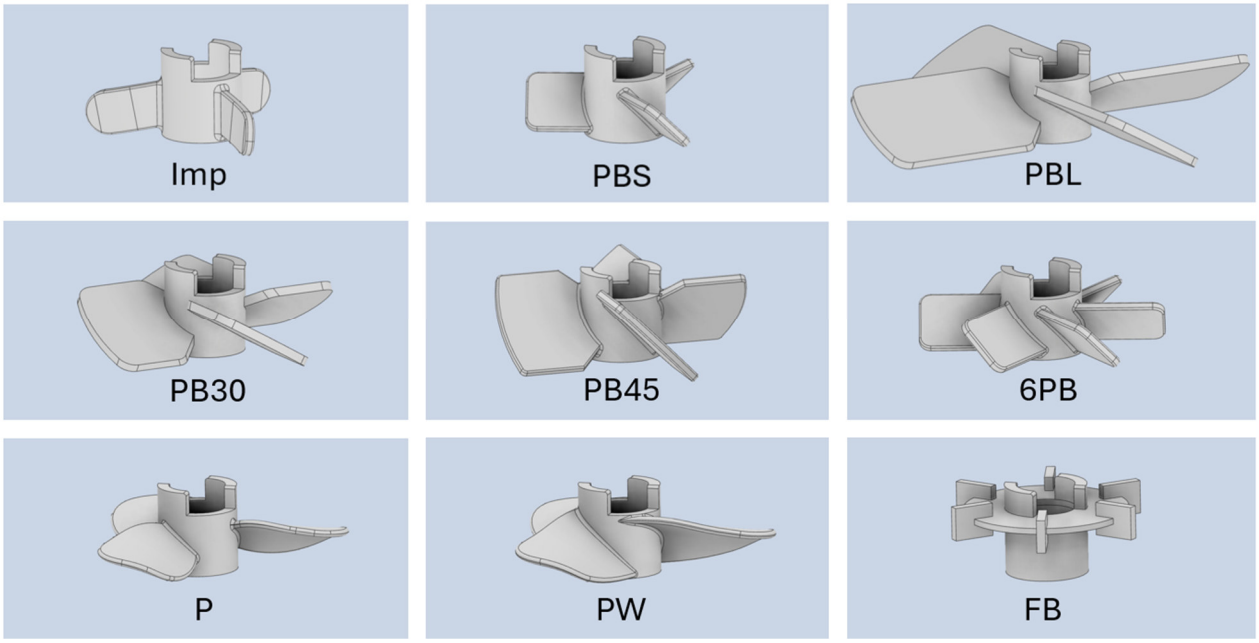

Fig. 2.: CAD models of all stirrers used for the investigations.

For the determination of mixing times at 250 and 500 rpm of the stirrer, the reactor model was filled with 250 ml of water, and 50 µl of blue ink were injected with a syringe as a pulse. This process was captured with a camera, and the mixing time was determined by viewing the resulting video frame by frame until homogeneity in the vessel was reached. In Fig. 3, the mixing process is depicted for the PB30 stirrer for 250 and 500 rpm without a baffle after certain amounts of time.

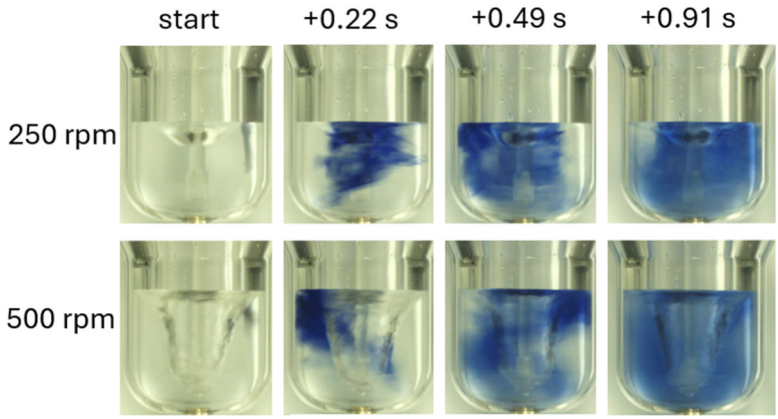

Fig. 3.: Ink distribution in the reactor model during mixing with the PB30 stirrer for 250 and 500 rpm and different amounts of time after injection.

The reactor can be equipped with a baffle, which is equally possible in the reactor model. It was also investigated whether this baffle has an influence on the mixing time. The determined mixing times τ of each stirrer at 250 and 500 rpm, with and without a baffle are depicted in Fig. 4. The stirrers with small diameters exhibit the worst mixing behavior. The large stirrer PBL provides good mixing but due to its large diameter, high shear forces are generated, which is unfavorable for emulsion polymerization, since this can lead to particle coagulation. The medium-sized pitched blade stirrers all showed good mixing performance, where the 6PB had slightly lower mixing times than the other models.

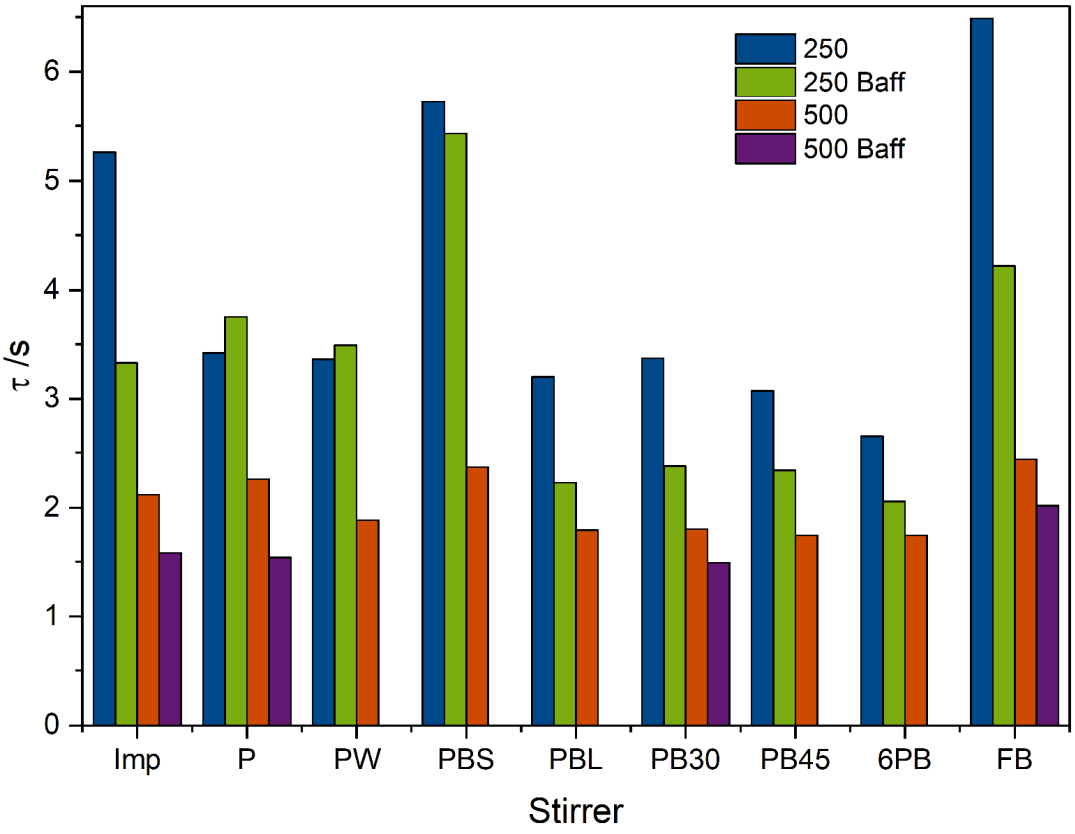

Fig. 4.: Measured mixing times for all designed stirrer types. Measurements were conducted at 250 and 500 rpm stirring speed and with or without a baffle (Baff).

Summary

Different types of stirrers have been designed and 3D-printed. Among them were stirrers from the reactor manufacturer and other pitched blade stirrers that have been used for reactions in the past. Since the mixing and gas dissipation capabilities could not be accessed in the steel reactor, a PMMA model of it was manufactured. With water as a model substance – what is suitable for the low viscosities in emulsion polymerization – the stirrers were tested at 250 and 500 rpm stir rate, under baffled and unbaffled conditions.

Overall, the pitched blade stirrers 6PB gave the best combination of mixing and acceptable shear. But even the mixing time of the small stirrers is still in a range, where reaction times are larger in comparison, and no retardation of the reaction due to poor mixing is to be expected.

References

[1] P. A. Lovell, F. J. Schork, *Biomacromolecules* **2020**, *21*, 4396.

[2] G. Billuart, E. Bourgeat-Lami, M. Lansalot, V. Monteil, *Macromolecules* **2014**, *47*, 6591.

[3] S. Fathi Roudsari, R. Dhib, F. Ein-Mozaffari, *J of Applied Polymer Sci* **2014**, *131*.

[4] A. C. M. Ecoscia, N. Sheibat-Othman, T. F. L. McKenna, *Can J Chem Eng* **2022**, *100*, 654.

Selective Recognition of Corticosteroids: Development and Characterization of Molecularly Imprinted Polymers for Hydrocortisone Extraction

Bartosz Poszwald[1], Joanna Wolska[1], Anna Jakubiak-Marcinkowska[1]

[1]Department of Process Engineering and Technology of Polymer and Carbon Materials, Wroclaw University of Science and Technology,

bartosz.poszwald@pwr.edu.pl

Introduction

Corticosteroids are essential steroid hormones that regulate critical physiological processes including metabolism, immune function, and stress response [1]. While synthetic corticosteroids like hydrocortisone and dexamethasone are widely used to treat inflammatory conditions, their prolonged use can cause serious side effects including hyperglycemia, osteoporosis, and adrenal suppression [2]. This creates an urgent need for reliable monitoring methods in both clinical and environmental settings.

Molecularly imprinted polymers (MIPs) have emerged as promising synthetic receptors for steroid detection, offering advantages over biological recognition elements in terms of stability, cost, and reusability [3]. These polymers create specific binding cavities through template-directed synthesis, enabling selective recognition of target molecules. Recent advancements in MIP technology have demonstrated remarkable sensitivity, with gold nanoparticle-enhanced sensors achieving cortisol detection limits as low as 0.036 nM [4].

The development of MIP-based sensors for corticosteroids has gained significant attention, particularly for therapeutic drug monitoring and point-of-care diagnostics [5]. Various transducer platforms, including electrochemical and optical systems, have been successfully integrated with MIP recognition elements to create robust sensing devices. However, challenges remain in optimizing binding affinity, selectivity, and reproducibility for environmental applications.

This study focuses on developing optimized MIP formulations for corticosteroid detection, with particular emphasis on hydrocortisone (HC) as a model analyte. We investigate the relationship between polymer composition and binding performance, aiming to establish design principles for high-performance MIP sensors.

Experimental

Materials and Reagents

Acrylic acid (AA) and ethylene glycol dimethacrylate (EGDMA) were purchased from Sigma-Aldrich as functional and crosslinker monomer, respectively. The polymerization initiator 2,2′-azobisisobutyronitrile (AIBN) was obtained from Merck Schuchardt. Hydrocortisone (HC) used as the template molecule was supplied by Pol-Aura, while ethanol (analytical grade) was acquired from POCH. All chemicals were used as received without further purification

Synthesis of Molecularly Imprinted Polymers (MIPs)

Molecularly imprinted polymers (MIPs) were prepared via bulk polymerization using acrylic acid (AA) as the functional monomer and ethylene glycol dimethacrylate (EGDMA) as crosslinker at three molar ratios (50:50, 40:60, 30:70). Hydrocortisone (HC) served as template at 1%, 2%, or 5% molar concentrations relative to monomers. Each mixture containing AA, EGDMA, HC, and 1% AIBN initiator (w/w) was dissolved in water:ethanol (1:1 v/v), purged with nitrogen for 10 min, and polymerized at 60°C for 24 h. The resulting polymers were crushed and Soxhlet-extracted with ethanol to remove template and impurities. NIPs were prepared with the same procedure as MIPs but without the addition of HC molecule. These polymers served as controls to evaluate the specificity and selectivity of the MIPs. Synthetized products are shown in the table (Tab. 1.).

Interaction Between Functional Monomer and Template

The interaction between AA and hydrocortisone is primarily governed by non-covalent interactions, notably hydrogen bonding [6]. The carboxylic acid group of AA can form hydrogen bonds with the hydroxyl and carbonyl groups present in the HC molecule. Such interactions are crucial for the formation of specific binding sites within the polymer matrix. Studies have demonstrated that the strength and specificity of these interactions significantly influence the binding affinity and selectivity of the resulting MIPs [7]. Reaction scheme is show on the figure (Fig. 1.)

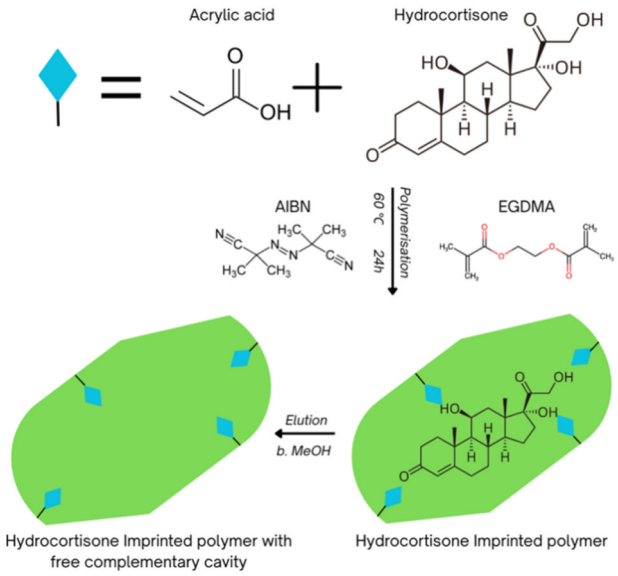

Fig. 1. Schematic reaction of hydrocortisone imprinted polymers synthesis

Sorption characteristics

The adsorption experiments were conducted at room temperature (~22–25 °C) to evaluate the binding performance of the synthesized MIPs and NIPs toward hydrocortisone. To determine the optimum MIP composition batch adsorption tests were carried out, by incubating 50 mg of polymer in 50 mL of HC aqueous solutions with initial concentration of 25 mg/L. The mixtures were shaken for 24 hours to ensure equilibrium was reached. The residual concentration of HC in the solution was determined using UV-Vis spectrophotometry at 269 nm. Based on the measurements of standard solutions in the range of 5-50 mg/L, calibration curve was constructed with coefficient of determination R^2 = 0.998. The equilibrium concentration (C_t, mg/L) was a concentration of HC after 24 h of sorption. The amount of adsorbed analyte (q_e, mg/g) was calculated by the difference between the initial and equilibrium concentrations, considering the solution volume and polymer mass (Eq. 1.).

$$q_e = \frac{(C_0 - C_t) \cdot V}{m} \qquad \text{Eq. 1}$$

where C_0 is the initial concentration of HC (mg/L) in pre-absorption solution, C_t is the concentration of HC after the sorption (mg/L), V (L) is the volume of HC solution and m (g) is a mass of sorbent used for the absorption tests. To determine which of the synthetized MIPs has a highest HC uptake an imprinting factor (IF, -) was calculated (Eq. 2.)

$$\mathrm{IF} = \frac{K_{\mathrm{MIP}}}{K_{\mathrm{NIP}}} \qquad \text{Eq. 2}$$

where, K_{MIP} and K_{NIP} (-) are partition coefficients of the MIP and NIP, respectively, calculated from the equation (Eq. 3.):

$$K = \frac{q \cdot \rho}{C} \qquad \text{Eq. 3.}$$

where q (mg/g) is the HC uptake by the polymer sorbent, ρ stands for solution density, that equals 1000 g/L and C (mg/L) is the equilibrium concentration of the solution.

Results

As the NIPs and MIPs were synthetized by bulk polymerization the rustling polymers were white solids. They had to be crushed in order to obtain any workable grain. The yielding of synthesis are shown in Tab. 1.

Tab. 1. Synthesis parameters and sorption parameters

Sample	Synthesis parameters			Sorption parameters		
	AA:EGDMA ratio	HC amount	Yield	C_t	q_e	K
	-	%	%	mg/L	mg/g	-
MIP 1	50:50	1	77.9%	15.08	8.62	572
MIP 2	50:50	2	69.1%	14.45	12.31	852
MIP 3	50:50	5	93.9%	16.76	9.94	593
MIP 4	40:60	1	93.2%	16.29	10.58	650
MIP 5	40:60	2	94.8%	16.05	10.63	662
MIP 6	40:60	5	72.2%	17.75	8.64	487
MIP 7	30:70	1	93.7%	13.52	11.32	837
MIP 8	30:70	2	91.5%	14.66	12.19	832
MIP 9	30:70	5	37.8%	12.40	13.82	1115
NIP 1	50:50	0	87.5%	12.27	13.58	1107
NIP 2	40:60	0	89.8%	18.64	8.13	436
NIP 3	30:70	0	86.0%	19.02	7.44	391

While most MIP samples (77.9-94.8%) showed higher synthesis yields than NIP controls (86.0-89.8%), three MIPs (2,6,9) underperformed (<80%). It was due to the exothermic events during bulk polymerisation, related to the amount of AA in polymerisation mixture, that made it unstable. The 30:70 and 40:60 AA:EGDMA ratios

achieved optimal yields (MIPs 3-5,7-8 >90%), demonstrating improved stability versus 50:50 formulations.

To evaluate different MIP formulations and identify the optimal composition for hydrocortisone (HC) adsorption, binding capacity (q_e) and imprinting factor (IF) were analyzed, comparing MIPs with NIPs. The results (Fig. 2.) highlight key structure-performance relationships. The adsorption capacity (q_e) of the synthesized molecularly imprinted polymers (MIPs) varied between 8.62 and 13.82 mg/g, with the highest binding observed for MIP 9 (q_e = 13.82 ± 0.61 mg/g). In contrast, non-imprinted polymers (NIPs) exhibited usually lower adsorption (q_e = 7.44–13.58 mg/g), confirming the role of imprinting in enhancing HC recognition. The imprinting factor (IF), which quantifies MIP selectivity over NIPs, ranged from 0.92 to 7.78 with MIP 9 again showing the highest selectivity. Notably, MIPs 7–9 demonstrated IF values >2.1, suggesting superior template affinity due to optimized monomer-crosslinker ratio.

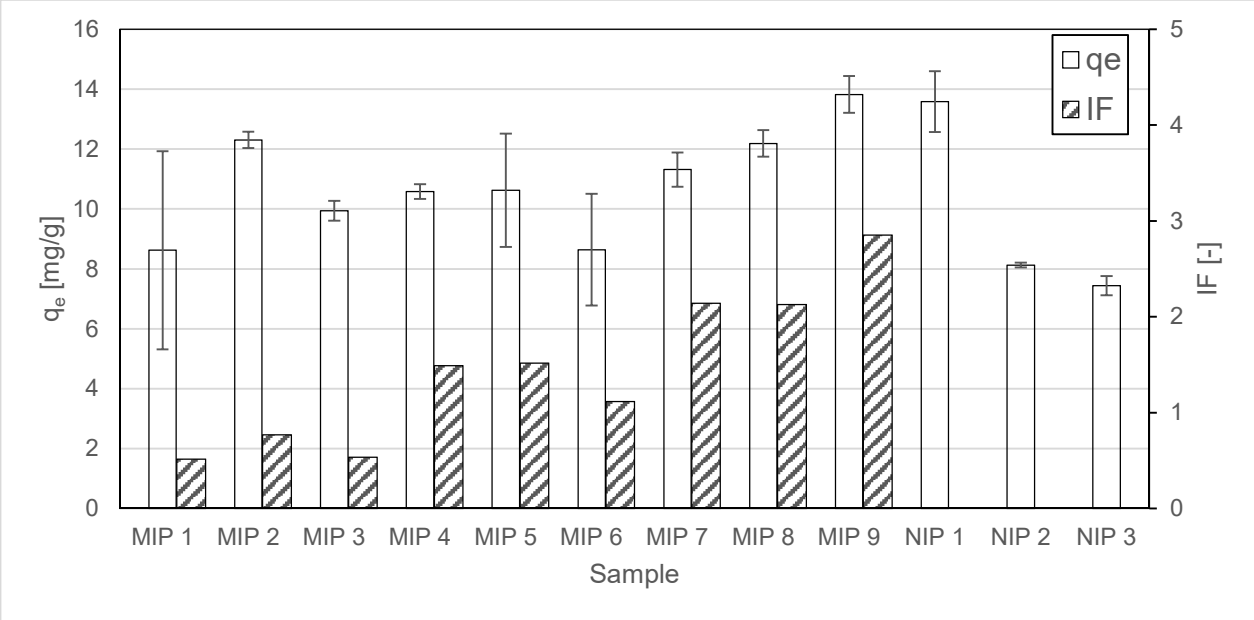

Fig. 2. Calculated results of HC uptake (q_e) and imprinting factor (IF) of polymers

Summary

This study developed molecularly imprinted polymers (MIPs) for selective hydrocortisone (HC) recognition through free-radical polymerization using acrylic acid (AA) and ethylene glycol dimethacrylate (EGDMA) at varying ratios (50:50 to 30:70) and template concentrations (1-5% HC). The optimal MIP (9) demonstrated exceptional binding capacity (13.82 ± 0.61 mg/g) and selectivity (IF = 2.85), attributed to its 30:70 monomer ratio and 5% HC content. This q_e higher than reported MIPs for steroids:

9.2 mg/g for cortisol using gold-doped MIPs [4] and 7.8 mg/g for dexamethasone [3]. Control experiments with NIPs confirmed the critical role of imprinting, showing around 2 times lower adsorption. While most syntheses achieved >90% yield, exothermic events during polymerisation affected some 50:50 ratio polymers.

The developed MIPs represent a robust platform for environmental corticosteroid monitoring, combining high selectivity (IF >2.1 for 30:70 ratio) and reproducible synthesis. This work provides a foundation for designing MIP-based sensors to detect trace corticosteroids in complex environmental matrices.

Acknowledgements

The research was supported by Wroclaw University of Science and Technology as part of the Academia Professorum Iuniorum.

References

[1] Kumar, R., et al. (2022). Corticosteroid pharmacology: Mechanisms and clinical applications. Endocrine Reviews, 43(3), 466-487. https://doi.org/10.1210/endrev/bnab037

[2] Stratakis, C. A. (2023). Adrenal steroids and their metabolic effects: New insights. Nature Reviews Endocrinology, 19(2), 89-102. https://doi.org/10.1038/s41574-022-00753-9

[3] Poma, A., et al. (2020). Advances in molecularly imprinted polymers as drug delivery systems. Chemical Society Reviews, 49(6), 1791-1811. https://doi.org/10.1039/C9CS00632F

[4] Zhang, Y., et al. (2021). Ultrasensitive cortisol detection using plasmonic MIP sensors. Biosensors & Bioelectronics, 181, 113148. https://doi.org/10.1016/j.bios.2021.113148

[5] Ansari, S., et al. (2023). Electropolymerized molecularly imprinted polymers for dexamethasone sensing. ACS Sensors, 8(3), 1024-1033. https://doi.org/10.1021/acssensors.2c02561

[6] Feás, X., Fente, C. A., Hosseini, S. V., Seijas, J. A., Vázquez, B. I., Franco, C. M., & Cepeda, A. (2009). Use of acrylic acid in the synthesis of molecularly imprinted polymers for the analysis of cyproheptadine. Materials Science and Engineering: C, 29(2), 398–404. https://doi.org/10.1016/j.msec.2008.08.011

[7] Takeuchi, T., & Hishiya, T. (2008). Molecular imprinting of proteins emerging as a tool for protein recognition. Organic & Biomolecular Chemistry, 6(18), 3325–3331. https://doi.org/10.1039/b804034j

On the Use of Biopolymer-Based Carbon Aerogels in the HER

Mathis Kirstein, Irina Smirnova, Baldur Schroeter

Institute of Thermal Separation Processes, Hamburg University of Technology,
mathis.kirstein@tuhh.de

Introduction

A key component of the sustainability strategies of Germany and the European Union is the development of a hydrogen economy based on green hydrogen. Green hydrogen serves as both a feedstock for industrial processes - such as fertilizer and steel production - and as a long-term energy carrier or fuel for high energy density applications. Its production requires efficient yet cost-effective electrolysers. The high capital costs of electrolysers are mainly due to the use of scarce and expensive materials in both the membrane–electrocatalyst assembly and the structural components of the electrolyser.

This study investigates the use of biopolymer-derived carbon aerogels as a support matrix for platinum nanoparticle (PtNP) catalysts in the hydrogen evolution reaction (HER). Specifically, it explores the influence of the aerogel's pore structure and the platinum deposition method on the stability and catalytic performance of the resulting electrocatalysts (ECs).

Commercial ECs for the hydrogen evolution reaction typically consist of platinum nanoparticles dispersed on a carbon black support. Carbon blacks form a macroporous structure composed of agglomerated carbon spheres but lack sufficient meso- and microporosity to effectively stabilize PtNPs, which limits platinum utilization. As a result, high platinum loadings are often required in commercial catalysts to achieve low overpotentials over extended periods [1].

In prior work by Alsuhile et al. [1], electrocatalysts produced using supercritical CO_2 deposition (SCD) on cellulose- and chitosan-based carbon aerogels (CAs) demonstrated superior performance compared to both commercial ECs and those made from carbon blacks using SCD.

The improved stability aligns with findings by Meier et al. [2], who showed that small mesopores can effectively stabilize PtNPs of similar dimensions.

The current study examines how the pore structure of carbon supports influences EC stability and overpotential. It also compares various platinum loading techniques for their effectiveness in forming well-dispersed, reaction-suitable PtNPs. Electrochemical performance and durability are assessed using a rotating disk electrode (RDE) setup.

Experimental

Carbon aerogels can be synthesized from various (bio-)polymers via pyrolysis. The resulting pore structure depends on the synthesis route, polymer system, crosslinkers, and additives used. The extent to which the original aerogel's pore structure is preserved during pyrolysis depends on the thermal stability of the polymer and the pyrolysis conditions, especially the heating rate. Lower heating rates promote mesopore retention, whereas micropores form primarily as a function of the maximum process temperature.

Three different loading methods for EC production were selected for the comparison of different deposition methods:

- Supercritical CO2 deposition (SCD)
- Cold plasma deposition (PD)
- Wet impregnation (WI) at the hydrogel or alcogel stage (i.e., pre-pyrolysis)

This current work focusses more on the WI and PD, since SCD was already investigated by Alsuhile et al.

In a proof-of-concept experiment, WI was applied to a chitosan-based gel, yielding an electrocatalyst with approximately 50 wt.% platinum. This catalyst demonstrated comparable HER performance to a commercial EC containing 40 wt.% platinum as shown on the left in Figure 1. On the right the surface of a primary catalyst particle before grinding is shown. Large (~100-200 nm) to small (~4-10 nm) platinum particles have formed on the surface during pyrolysis.

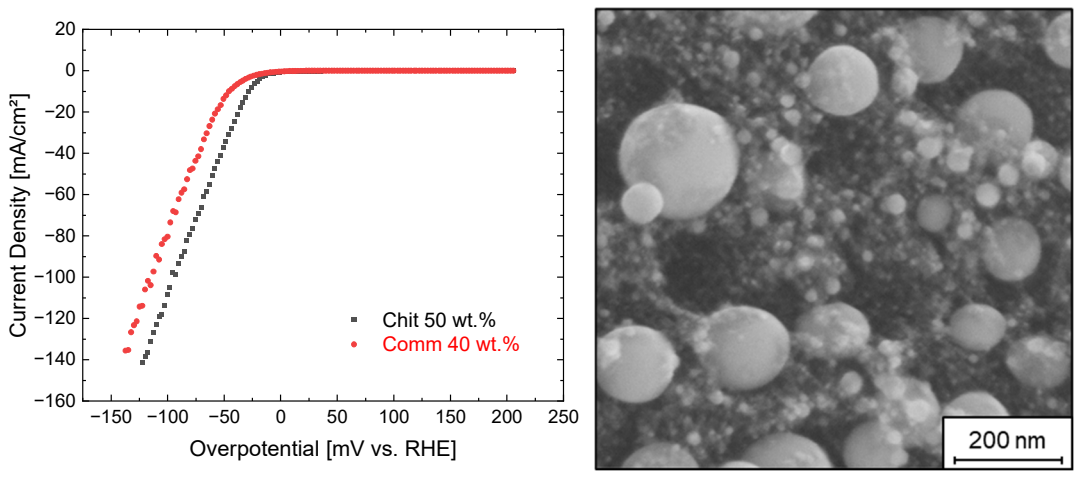

Figure 1: Linear sweep voltammetry (LSV) comparison between a commercial EC (40 wt.% Pt) and a WI-derived EC (50 wt.% Pt) (left) and a SEM image of the surface of a catalyst particle (right).

For better comparability with SCD-produced catalysts, the platinum content in WI samples will be reduced to the 1–10 wt.% Pt range typical for SCD. This reduction may also alleviate the mass transport limitations often observed in RDE-based electrochemical testing [3].

To study the influence of the platinum ions on the gel structure three more different Pt loadings were prepared via WI and analysed using gas physisorption analysis. The results are shown in Table 1. A general observation is that the weigh specific surface area decreases with increasing platinum content. For the other properties no trends are apparent. Pre-pyrolysis samples were studied using the BJH method, while post-pyrolysis samples use a DFT-Method.

Table 1: Comparison of the pore structure in dependence of the platinum content.

Pt-content	Pre-pyrolysis			Post-pyrolysis		
	Surface area [m²/g]	Pore width [nm]	Pore volume [cm³/g]	Surface area [m²/g]	Pore width [nm]	Pore volume [cm³/g]
Low	1060	14.0	4.23	1250	12.7	1.77
Medium	820	27.3	4.31	770	15.1	1.13
High	890	27.5	5.55	610	15.1	1.27

Cold plasma deposition (PD) was also explored in preliminary experiments and yielded ECs with platinum loadings between 0.3 wt.% and 3 wt.%. However, these results could not be replicated with the currently available equipment with a lower power density. So far only lower loadings of 0.02-0.04 wt.% Pt were achieved. Although not relevant for industrial applications these samples might be suitable to study degradation mechanisms and the kinetics of the electrochemical reaction, which is typically limited by mass transport [3].

Summary

This study highlights the potential of biopolymer-derived carbon aerogels, particularly chitosan-based gels, as adaptable support materials for PtNP catalysts in the hydrogen evolution reaction. Wet impregnation prior to pyrolysis produced electrocatalysts with performance comparable to commercial benchmarks. Future work will focus on optimizing platinum content and improving the reproducibility of cold plasma deposition.

Acknowledgment

A heartfelt thanks to Baldur Schroeter for the extensive support in all fields and to Sinem Akyldiz for the tremendous lab work. The author thanks the Federal Ministry for Economic Affairs and Climate Action for funding this project with No. KK5440301ZG1

References

[1] A. Alsuhile et al. Adv. Energy Sustainability Res., Wiley-VCH, 2025

[2] J. C. Meier et al. Beilstein J. Nanotechnol. 2014

[3] J. N. Hansen, et al. ACS Energy Lett., ACS, 2021

Accelerated Mineral Carbonation of Industrial Alkaline Residues: Influence of Water Content and CO_2 Pressure

G. P. Sorrentino;[1] R. Guimarães;[2] B. Valentim;[2] E. Bontempi;[3] T. E. Müller[1]

[1] Ruhr-Universität Bochum, Carbon Sources and Conversion

[2] University of Porto, Earth Science Institute – Porto Pole

[3] University of Brescia, Chemistry for Technologies Laboratory

Corresponding author: giampiero.sorrentino@ruhr-uni-bochum.de

Introduction

Human activities, primarily fossil fuel combustion, deforestation, land-use change, and resource-intensive industries, have driven atmospheric CO_2 from ~280 ppm in pre-industrial times to 420 ppm today, with projections reaching up to 550 ppm by 2050 [1]. This rise underpins global warming, intensifies extreme weather events, accelerates sea-level rise, and risks displacing vulnerable populations [1–4]. Limiting temperature increases, currently forecast at 1.8–4 °C by 2100 without decisive action [1], requires a rapid shift to renewable energy and efficiency gains, the deployment of zero-emission and carbon-removal technologies, and a transition to sustainable raw materials.

Carbon capture utilization and storage (CCUS) offers a critical bridge: it can cut industrial CO_2 emissions and mitigate up to 55 % of cumulative warming by the end of the century [5]. Among CCUS options, mineral carbonation converts CO_2 into stable carbonate minerals *via* exothermic reactions with calcium- (Ca) and magnesium- (Mg) bearing solids, processes that require no external heat and are thermodynamically favoured at high pH [6,7]. Rather than mining ultramafic ores, which entails economic, environmental, and energy-intensive pretreatment challenges [8,9], industrial alkaline residues provide abundant, reactive Ca/Mg sources at low cost and with minimal processing [6,9–11].

Municipal solid waste incineration fly ash (MSWI FA), for instance, can contain more than 50 wt.% free CaO, yet it is often landfilled due to hazardous leachates and heavy metals [12,13]. Although many studies have examined carbonation of single industrial residues, frequently requiring chemical additives or pretreatments [14,15], the synergistic blending of multiple residues remains underexplored. Recent work demonstrates that mixtures of MSWI FA, MSWI bottom ash (MSWI BA), coal fly ash (CFA), and flue gas desulfurization residues (FGD) can naturally stabilize heavy metals and sequester CO_2 over weeks [16], and that pressurized accelerated carbonation can capture > 90 wt.% CO_2 within days [17].

Building on these findings, the influence of residue properties, water content, and CO_2 pressure on accelerated carbonation performance is systematically investigated. Blends of MSWI ashes, CFA, and FGD, locally sourced to minimize transport and eliminate the need for commercial chemicals, are tested at liquid-to-solid (L/S) ratios of 0.7–1.2 and under CO_2 pressures of 15 bar. The effects of these variables on carbonation yield and reaction kinetics are assessed.

Experimental

The residues were provided by the waste-to-energy plant and the coal-fired power plant in Brescia (Italy), both operated by A2A S.p.A. Carbonation tests were performed according to a patented protocol [17], adapted as described below. A mixture consisting of MSWI FA (59 wt.%), ground MSWI BA (< 2 mm, 9 wt.%), CFA (14 wt.%), and FGD (18 wt.%) was prepared. The materials were combined with ultrapure water at liquid-to-solid (L/S) ratios of 0.7, 0.9, and 1.2 $L \cdot kg^{-1}$ and mixed for 10 minutes to ensure homogeneity. Carbonation was then carried out under two conditions:

Table 1: Summary of accelerated (AC) and natural carbonation (NC) trials conducted on the residue mixture under varying durations, liquid-to-solid (L/S) ratios, and CO_2 pressure.

Samples ID	Carbonation Type	Time	L/S Ratio	Reactor Volume	Initial Total Pressure
AC_0.7	Accelerated	17 h	0.7	150 mL	15 bar
AC_0.9		72 h	0.9	150 mL	15 bar
AC_0.9bis		12 d	0.9	150 mL	15 bar (const.)
AC_1.2		51 h	1.2	150 mL	15 bar
NC1_0.7	Natural	1 mth	0.7	-	Ambient Condition
NC1_0.9		1 mth	0.9	-	
NC2_0.9		2 mths	0.9	-	
NC1_1.2		1 mth	1.2	-	

- **Accelerated Carbonation (AC)**: Mixtures were exposed to high-purity CO_2 gas (99.99%) at 15 bar in a 150 mL reactor at ambient temperature. Reactions proceeded until a pressure plateau was observed. For the L/S ratio of 0.9, one trial was conducted under constant CO_2 pressure.
- **Natural Carbonation (NC)**: Mixtures were stored at ambient conditions for 1 month, with weekly mild remixing. For the L/S ratio of 0.9, one trial was extended to 2 months.

Afterwards, all samples were dried at 105 °C to constant weight, manually milled, and subjected to characterization. An overview of the trials is shown in Table 1.

The AC experimental setup included a single sample cylinder (SC, 150 mL), made of stainless steel (AISI 316L) from Swagelok, equipped with two needle valves (V-1, V-2) for CO_2 inlet, venting, and pressure control. A pressure transducer (PT, ±0.125%) and an externally mounted thermocouple (TC, ±1.5 °C) were used for monitoring. The system was evacuated using a vacuum pump (VP), and high-purity CO_2 (99.99%) was supplied by SOL Group (Monza, Italy). Pressure and temperature data were recorded every 5 s using a data acquisition system (DAQ/PC) and processed in LabVIEW®. A schematic of the setup is shown in Figure 1 [18].

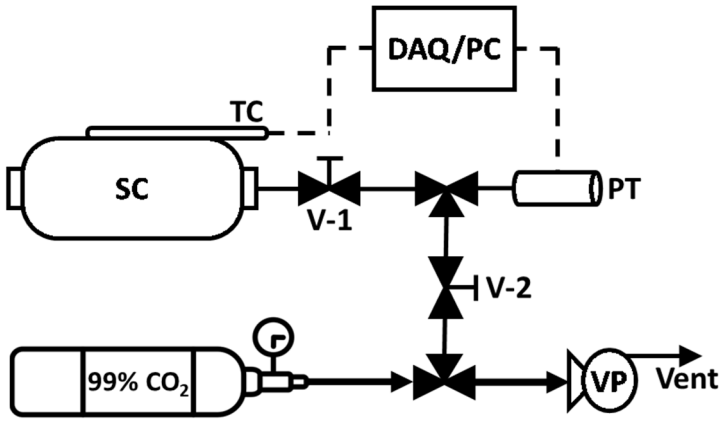

Figure 1: Schematic layout of the experimental apparatus. Sample cylinder (SC); thermocouple (TC); pressure transmitter (PT); needle valves (V-1 and V-2); vacuum pump (VP); 99.99 % CO_2; data acquisition system (DAQ/PC).

The carbonated samples were analysed by loss on ignition (LOI), X-ray diffraction with Rietveld refinement (XRD-Rietveld), and scanning electron microscopy with energy-dispersive X-ray spectroscopy (SEM-EDS).

Results and Discussion

A clear correlation was observed between CO_2 uptake and both the liquid-to-solid (L/S) ratio and CO_2 pressure during the AC trials. Higher L/S ratios enhanced CO_2 dissolution and permeability within the mixtures, resulting in increased uptake, reaching a maximum of 166 kg CO_2 per ton of MSWI FA at L/S = 1.2. In contrast, the NC trials did not follow this trend, with CO_2 sequestration values of 193, 208, and 181 kg CO_2 per ton MSWI FA for L/S ratios of 0.7, 0.9, and 1.2, respectively. These findings emphasize the critical role

of water content in AC processes, where increased moisture facilitates gas–liquid–solid interactions. Incorporating a continuous stirring system could further improve mass transfer and enhance carbonation efficiency.

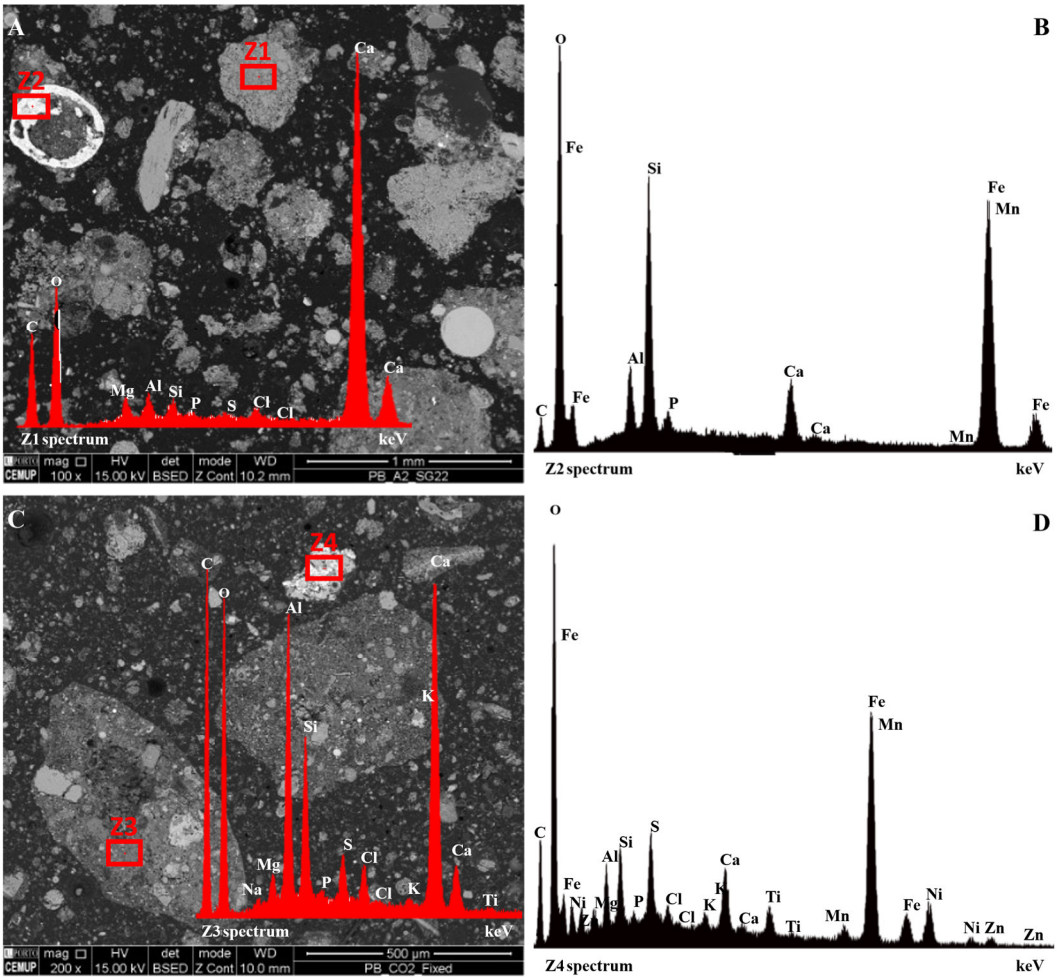

Figure 2: SEM Micrographs (polished blocks) and EDS spectra (Intensity [Arb. Units]) of AC_0.9bis (A, B) and NC2_0.9 (C, D) [18].

The trial conducted under constant CO_2 pressure (15 bar) yielded the highest uptake in the AC tests, at 170 kg CO_2 per ton MSWI FA, confirming the benefit of maintaining steady reaction conditions. Overall, the results demonstrate that blending different industrial alkaline residues can significantly improve CO_2 sequestration compared to MSWI FA alone, achieving uptake levels beyond those typically reported in the literature.

SEM-EDS analyses of the carbonated products revealed the formation of calcium carbonate agglomerates and calcium aluminosilicate phases encapsulating other particles, indicating possible heavy metal stabilization (Figure 2). These observations support the potential of AC not only for rapid and effective CO_2 capture but also for residue valorization.

Conclusions

In conclusion, the AC process presents a promising pathway for enhanced CO_2 sequestration, particularly when optimized for both moisture content and pressure conditions. Utilizing industrial by-products leverages synergies across sectors, reduces transportation and disposal burdens, and minimizes the need for chemical additives. Additionally, the exothermic nature of the reaction may further reduce external energy demands. The resulting carbonated materials hold potential for various circular applications, including construction materials, fire-resistant products, and pollutant immobilization.

Acknowledgments

The authors thank Paolo Iora, Costante Mario Invernizzi, Gioele Di Marcoberardino, and Modestino Savoia for their support in the accelerated carbonation tests.

References

1. IPCC, 2023: Climate Change 2023: Synthesis Report. Contribution of Working Groups I, II and III to the Sixth Assessment Report of the Intergovernmental Panel on Climate Change [Core Writing Team, H. Lee and J. Romero (Eds.)]. *IPCC, Geneva, Switzerland* **2023**, 1–184, doi:10.59327/IPCC/AR6-9789291691647.
2. Shayanmehr, S.; Rastegari Henneberry, S.; Sabouhi Sabouni, M.; Shahnoushi Foroushani, N. Climate Change and Sustainability of Crop Yield in Dry Regions Food Insecurity. *Sustainability* **2020**, *12*, 9890, doi:10.3390/su12239890.
3. Carleton, T.A.; Hsiang, S.M. Social and Economic Impacts of Climate. *Science (1979)* **2016**, *353*, doi:10.1126/science.aad9837.
4. Berchin, I.I.; Valduga, I.B.; Garcia, J.; de Andrade Guerra, J.B.S.O. Climate Change and Forced Migrations: An Effort towards Recognizing Climate Refugees. *Geoforum* **2017**, *84*, 147–150, doi:10.1016/j.geoforum.2017.06.022.
5. Chiang, P.-C.; Pan, S.-Y. Introduction. In *Carbon Dioxide Mineralization and Utilization*; Springer Singapore: Singapore, 2017; pp. 1–6.
6. Olajire, A.A. A Review of Mineral Carbonation Technology in Sequestration of CO_2. *J Pet Sci Eng* **2013**, *109*, 364–392, doi:10.1016/j.petrol.2013.03.013.
7. Sanna, A.; Uibu, M.; Caramanna, G.; Kuusik, R.; Maroto-Valer, M.M. A Review of Mineral Carbonation Technologies to Sequester CO_2. *Chem. Soc. Rev.* **2014**, *43*, 8049–8080, doi:10.1039/C4CS00035H.
8. Labande, A.; Debono, N.; Sournia-Saquet, A.; Daran, J.-C.; Poli, R. Oxidation-Promoted Activation of a Ferrocene C–H Bond by a Rhodium Complex. *Dalton Transactions* **2013**, *42*, 6531, doi:10.1039/c3dt50240f.

9. Ji, L.; Yu, H.; Zhang, R.; French, D.; Grigore, M.; Yu, B.; Wang, X.; Yu, J.; Zhao, S. Effects of Fly Ash Properties on Carbonation Efficiency in CO_2 Mineralisation. *Fuel Processing Technology* **2019**, *188*, 79–88, doi:10.1016/j.fuproc.2019.01.015.
10. Gomes, H.I.; Mayes, W.M.; Rogerson, M.; Stewart, D.I.; Burke, I.T. Alkaline Residues and the Environment: A Review of Impacts, Management Practices and Opportunities. *J Clean Prod* **2016**, *112*, 3571–3582, doi:10.1016/j.jclepro.2015.09.111.
11. Chiang, P.-C.; Pan, S.-Y. *Carbon Dioxide Mineralization and Utilization*; Springer Singapore: Singapore, 2017; ISBN 978-981-10-3267-7.
12. Assi, A.; Bilo, F.; Zanoletti, A.; Ponti, J.; Valsesia, A.; La Spina, R.; Zacco, A.; Bontempi, E. Zero-Waste Approach in Municipal Solid Waste Incineration: Reuse of Bottom Ash to Stabilize Fly Ash. *J Clean Prod* **2019**, *245*, 118779, doi:10.1016/j.jclepro.2019.118779.
13. Quina, M.J.; Bontempi, E.; Bogush, A.; Schlumberger, S.; Weibel, G.; Braga, R.; Funari, V.; Hyks, J.; Rasmussen, E.; Lederer, J. Technologies for the Management of MSW Incineration Ashes from Gas Cleaning: New Perspectives on Recovery of Secondary Raw Materials and Circular Economy. *Science of The Total Environment* **2018**, *635*, 526–542, doi:10.1016/j.scitotenv.2018.04.150.
14. McKelvy, M.J.; Chizmeshya, A.V.G.; Diefenbacher, J.; Béarat, H.; Wolf, G. Exploration of the Role of Heat Activation in Enhancing Serpentine Carbon Sequestration Reactions. *Environ Sci Technol* **2004**, *38*, 6897–6903, doi:10.1021/es049473m.
15. Munz, I.A.; Kihle, J.; Brandvoll, Ø.; Machenbach, I.; Carey, J.W.; Haug, T.A.; Johansen, H.; Eldrup, N. A Continuous Process for Manufacture of Magnesite and Silica from Olivine, CO2 and H2O. *Energy Procedia* **2009**, *1*, 4891–4898, doi:10.1016/j.egypro.2009.02.319.
16. Assi, A.; Federici, S.; Bilo, F.; Zacco, A.; Depero, L.E.; Bontempi, E. Increased Sustainability of Carbon Dioxide Mineral Sequestration by a Technology Involving Fly Ash Stabilization. *Materials* **2019**, *12*, 2714, doi:10.3390/ma12172714.
17. Sorrentino, G.P.; Zanoletti, A.; Ducoli, S.; Zacco, A.; Iora, P.; Invernizzi, C.M.; Di Marcoberardino, G.; Depero, L.E.; Bontempi, E. Accelerated and Natural Carbonation of a Municipal Solid Waste Incineration (MSWI) Fly Ash Mixture: Basic Strategies for Higher Carbon Dioxide Sequestration and Reliable Mass Quantification. *Environ Res* **2022**, 114805, doi:10.1016/j.envres.2022.114805.
18. Sorrentino, G.P. Carbon Capture through Accelerated Carbonation and Enhanced Stabilization of Industrial Alkaline Residues. Doctoral Dissertation, University of Brescia, Italy: Brescia, 2025.

Registered Teachers

Country	University / Company	Name	Email
AT	Graz	Prof. Thomas Gamse	thomas.gamse@tugraz.at
AT	Natex	DI Martin Sova	m.sova@natex.at
AT	Natex	Dr. Eduard Lack	e.lack@natex.at
AT	INNOWELD	Maximilian Schrittwieser	m.schrittwieser@innoweld.at
CZ	Prag	Dr. Helena Sovova	helsov@seznam.cz
DE	Bochum	Prof. Marcus Petermann	petermann@fvt.ruhr-uni-bochum.de
DE	Bochum	Prof. Thomas Müller	thomas.mueller@ls-csc.ruhr-uni-bochum.de
DE	Darmstadt	Prof. Markus Busch	markus.busch@pre.tu-darmstadt.de
DE	Erlangen	Prof. Eberhard Schlücker	eberhard.schluecker@fau.de
DE	Erlangen	Dr. Detlef Freitag	detlef.freitag@fau.de
DE	Freising	Prof. Sabine Grüner-Lempart	sabine.gruener-lempart@hswt.de
DE	Hamburg	Dr. Carsten Zetzl	zetzl@tu-harburg.de
DE	Hamburg	Prof. Pavel Gurikov	pavel.gurikov@tuhh.de
ES	Valladolid	Prof. Maria Cocero	mariajose.cocero.alonso@uva.es
ES	Valladolid	Prof. Angel Martin	angel.martin.martinez@uva.es
FR	Albi	Dr. Martial Sauceau	martial.sauceau@mines-albi.fr
HR	Osijek	Prof. Stela Jokic	Stela.Jokic@ptfos.hr
HU	Budapest	Prof. Edit Szekely	edit.szekely@edu.bme.hu
HU	Budapest	Dr. Erika Vagi	vagierikamaria@gmail.com
IT	Bologna	Prof. Alessandro Zambon	alessandro.zambon2@unibo.it
PL	Wroclaw	Prof. Irena Zizovic	irena.zizovic@pwr.edu.pl
PT	Lisbon	Dr. Ana V.M. Nunes	avn07929@fct.unl.pt
RS	Belgrade	Prof. Marko Stamenic	stamena@tmf.bg.ac.rs
SI	Maribor	Prof. Urban Bren	urban.bren@um.si
SI	Maribor	Prof. Zeljko Knez	zeljko.knez@um.si
SI	Maribor	Dr. Maša Knez-Marevci	masa.knez@um.si
SI	Maribor	Dr. Amra Perva	amra.perva@um.si

Registered Students

	University / Company	First Name	Family Name	Sex	Nationality
AT	Graz	Sebastian	Sandner	m	Austria
AT	Graz	Christoph	Weinzettl	m	Austria
AT	Tulln	Barbora	Benetková	f	Czech Republic
AT	Tulln	Lara	Dumschat	f	Germany
DE	Bochum	Iván Gonzalo	Navarro Cárdenas	m	Chile
DE	Bochum	Giampiero Pasquale	Sorrentino	m	Italy
DE	Darmstadt	Jarne	Berning	m	Germany
DE	Darmstadt	Adil	Boukhalaf	m	Germany
DE	Darmstadt	Ferel	Issa	f	Germany
DE	Darmstadt	Alexander	Keßler	m	Germany
DE	Darmstadt	Erik	Prenzel	m	Germany
DE	Darmstadt	Christopher	Schilling	m	Germany
DE	Erlangen	V Y M Rajesh	Chirala	m	India
DE	Freiberg	Tom	Goldberg	m	Germany
DE	Hamburg	Juan Sebastian	Castillo Gonzalez	m	Colombia
DE	Hamburg	Mathis	Kirstein	m	Germany
ES	Valladolid	Antonio	Antón Rodríguez	m	Spain
ES	Valladolid	German Rodrigo	Araujo Barahona	m	El Salvador
ES	Valladolid	Iván	Briongos Merino	m	Spain
ES	Valladolid	Beatriz	Martín Gómez	f	Spain
HR	Osijek	Krunoslav	Aladic	m	Croatia
HR	Osijek	Klara	Opačak	f	Croatia
HR	Osijek	Kristina	Perišić	f	Croatia
HU	Budapest	Mihály	Hegyi	m	Hungary
HU	Budapest	Megara	Körmöczi	f	Hungary
IT	Bologna	Davide	Bonaldo	m	Italy
IT	Bologna	Gianluca	Ricci	m	Italy
PL	Wroclaw	Katarzyna	Gajewska	f	Poland
PL	Wroclaw	Aneta	Krawiec	f	Poland
PL	Wroclaw	Bartosz	Poszwald	m	Poland
PT	Lisbon	Ricardo	Hipólito	m	Portugal
PT	Lisbon	Beatriz	Monteiro	f	Portugal
PT	Lisbon	Inês	S. Fernandes	f	Portugal
RS	Belgrade	Jelena	Martinović	f	Serbia
RS	Belgrade	Jana	Stamenović	f	Serbia
SI	Maribor	Adela	Avdičević	f	Slovenia
SI	Maribor	Miha	Fermišek	m	Slovenia
SI	Maribor	David	Hvalec	m	Slovenia
SI	Maribor	Mina	Miličić	f	Serbia